1-1-2016

Toward A Better Estimation Of Shear Capacity And Structural Reliability Of Prestressed Concrete Girders

Alaa Ibrahim Chehab
Wayne State University,

TOWARD A BETTER ESTIMATION OF SHEAR CAPACITY AND STRUCTURAL RELIABILITY OF PRESTRESSED CONCRETE GIRDERS

by

ALAA IBRAHIM CHEHAB

DISSERTATION

Submitted to the Graduate School

of Wayne State University,

Detroit, Michigan

in partial fulfillment of the requirements

for the degree of

DOCTOR OF PHILOSOPHY

2016

MAJOR: CIVIL ENGINEERING (Structural)

Approved By:

_____

Advisor Date

_____

_____

_____

DEDICATION

To my parents, for their limitless love and support

ACKNOWLEDGMENTS

I take immense pleasure in thanking Dr. Christopher D. Eamon, Associate Professor at the Department of Civil and Environmental Engineering at Wayne State University, for his guidance, support and professional academic supervision, which assisted me in completing this Ph.D. dissertation.

I am grateful to Dr. Christopher D. Eamon, Dr. Hwai-Chung Wu, Dr. John J. Gruber, from the Department of Civil and Environmental Engineering at Wayne State University, and Dr. Gustavo J. Parra-Montesinos, from the Department of Civil and Environmental Engineering at the University of Wisconsin-Madison, for their time and effort serving as my Dissertation Committee Members.

Finally, I would like to thank Emira Rista from Wayne State University for her assistance, and Thai Dam, Bob Spencer and Dr. James Wight from the University of Michigan, Ann Arbor, for their support with the lab testing.

PREFACE

TOWARD A BETTER ESTIMATION OF SHEAR CAPACITY AND STRUCTURAL RELIABILITY OF PRESTRESSED CONCRETE GIRDERS

The main research objectives of this study are to determine the most accurate and consistent method for predicting shear capacity of MDOT PC bridge girders, determine the reliability of PC bridge girders in shear, develop an optimal shear design expression for MDOT PC bridge girders, and recalibrate the AASHTO LRFD code for shear as necessary, such that PC bridge girders will have consistent and adequate level of reliability for shear.

Keywords: Prestressed concrete girder; Shear strength; FEA; AASHTO LRFD; Structural reliability.

TABLE OF CONTENTS

LIST OF TABLES

LIST OF FIGURES

CHAPTER 1: INTRODUCTION AND LITERATUR REVIEW

1.1 Introduction

In the last several decades, various models to estimate the shear capacity of prestressed concrete girders were proposed. Some of these developments can be tracked through periodic revisions in the American Association of State Highway and Transportation Officials (AASHTO) Bridge Design Specifications (AASHTO 1973-2014). These changes include how the shear strength contributions attributed to the concrete and transverse steel are calculated, as well as limits on the maximum allowable shear stress. For example, in 1983, the 12th edition of the AASHTO Standard Specifications (AASHTO 1983) presented a significantly revised shear design method for prestressed concrete (PC) bridges from that previously found in the 1979 Interim Specifications (AASHTO 1979). Revisions included a new method for calculating the concrete shear strength that explicitly accounts for web-shear cracking and flexural-shear cracking; a change in location of the critical shear section near supports; and a reduction of 50% in the calculated shear strength contribution from the transverse reinforcement, as compared to the 1979 Interim Specifications. These 1983 shear provisions have remained unchanged up to the latest, 17th edition of the Standard Specifications, which were last published in 2002 (AASHTO 2002). A second significant change in shear design was presented in the 1st edition of the AASHTO Load and Resistance Factor Design (LRFD) Specifications, released in 1994 (AASHTO LRFD 1994). Based on the Modified Compression Field Theory, the shear design provisions in the AASHTO LRFD Specifications are significantly more complex than those in the Standard Specifications, with major changes in calculation of the concrete shear strength contribution, horizontal projection of diagonal cracks, and maximum allowable shear stress. Although some revisions have been made, the 1994 LRFD

shear design approach is essentially the same method presented in the 6th edition of AASHTO LRFD, published in 2014 (AASHTO LRFD 2014).

Despite these new developments and code advancements, it is not clear which methods are practically most accurate when predicting the shear capacity of prestressed concrete bridge girders. This concern arises as a number of Michigan Department of Transportation (MDOT) bridges designed with AASHTO code procedures were recently found to have shear cracks, which may indicate inadequacy in the shear design provisions (Eamon et al., 2014).

A larger concern is that the AASHTO LRFD Code was probabilistically calibrated for shear design essentially using the 1994 AASHTO LRFD shear model, which, as noted above, may not be as accurate as previously believed (NCHRP 368). Thus, the appropriate resistance factor for design may have been determined using an inaccurate model, which can result in inconsistent or inadequate levels of shear reliability for bridge girders.

1.2 Objective and Scope

The main research objectives of this study are to: 1) assess the adequacy of the current AASHTO PC shear design methods, 2) determine the reliability of I-shaped PC bridge girders in shear based on the current LRFD General Procedure, 3) determine the most accurate and consistent method for predicting shear capacity of AASHTO “I” shape PC bridge girders, 4) recalibrate the AASHTO LRFD code for shear design as necessary, such that PC bridge girders will have a more consistent and minimum target of reliability for shear, and 5) compute load rating analysis based on the HL-93 and MI live loads for PC bridges designed in accordance to the General LRFD Procedure for shear.

1.3 Literature Review

1.3.1 AASHTO 1979 Interim Design Specifications

In the 1979 Interim provisions, contrary to the AASHTO Standard and LRFD Specifications, the "concrete" contribution to shear strength V_c was assumed to be linearly related to concrete compressive strength and was taken equal to $0.06\,f'_c$. This contribution, however, was limited to 180 psi, which in practice governed the design value of V_c for all prestressed concrete (PC) girders, since this limit was reached with an f'_c of only 3000 psi ($3.3\sqrt{f_c'}$). For comparison, for concrete compressive strengths of 4000 and 10000 psi, this shear stress limit corresponds to $2.8\sqrt{f_c'}$ and $1.8\sqrt{f_c'}$ (psi), respectively. In the 1979 Interim provisions for PC, the shear strength contribution of the transverse steel reinforcement is given as:

$$V_s = 2A_v f_y \frac{jd}{s} \tag{1.1}$$

Where A_v is the area of transverse steel reinforcement spaced at a distance s, f_y is the yield strength of the transverse steel reinforcement, and jd is the distance between the resultant normal tension and compression force couple in the section (i.e. truss depth).

Although the angle of inclination for the diagonal elements to be used in the truss analogy was not explicitly specified, the number of layers of steel transverse reinforcement assumed to be crossed by a diagonal crack in equation 1.1 is effectively $2jd/s$, which leads to a truss angle of 29.1 degrees. This significantly shallower design angle compared to the typical 45 degree angle used in reinforced concrete was due to the effect of the prestressing force in PC beams, which lowers the principal compression angle. However, this beneficial effect is not accounted for in the 1983 nor the latest 2002 AASHTO Standard Specifications. Other important provisions of the 1979 Interim Specifications are a minimum shear transverse reinforcement requirement to provide a shear stress

contribution of at least 100 psi, while maximum stirrup spacing was limited to ¾ of the member height. It should be noted that the 1979 Interim Specifications did not limit the maximum shear strength contribution that could be assigned to the steel transverse reinforcement. That is, no explicit provisions were provided to prevent web-crushing failures.

Another aspect of the 1979 Interim Specifications that deserves attention is the critical section used for design near the supports. In the case of simply supported beams, the shear calculated at a quarter of the span length from the support is used as the maximum shear design value; i.e. higher shear forces closer to the support are neglected.

1.3.2 AASHTO Standard Specifications

The shear design provisions in the 1973-2002 AASHTO Standard Specifications are based on research conducted at the University of Illinois (MacGregor 1960; MacGregor et al. 1965). In these provisions, the "concrete" shear strength is calculated as the smaller of the shear force associated with flexural shear cracking and the shear force that causes web-shear cracking. Flexural shear cracking will govern in sections with high moment and low shear, while web-shear cracking will govern in sections subjected to high shear and low moment.

Section 9.20.1 (General) in the 2002 AASHTO Standard Specifications states that prestressed concrete flexural members shall be reinforced for shear and diagonal tension stresses. Shear reinforcement may be omitted if the factored shear force, $V_{u,}$ is less than half the shear strength provided by the concrete.

Web reinforcement shall consist of stirrups perpendicular to the axis of the member or welded wire fabric with wire located perpendicular to the axis of the member. Web reinforcement shall extend to a distance "d" from the extreme compression fiber and shall be carried as close to the compression and tension surfaces of the member as cover requirements and the proximity of other

reinforcement permit. Web reinforcement shall be anchored at both ends for its design yield strength in accordance with the provisions of Article 8.27. Members subjected to shear shall be designed so that:

$$V_u = \phi(V_c + V_s) \tag{1.2}$$

Where V_u is the factored shear force at the section considered, V_c is the nominal shear strength provided by the concrete, and V_s is the nominal shear strength provided by web reinforcement.

When the reaction to the applied loads introduces compression into the end regions of the member, sections located at a distance less than h/2 from the face of the support may be designed for the same shear V_u as that computed at a distance h/2.

In the case of flexural-shear cracking, the shear strength is calculated as the sum of the shear corresponding to flexural cracking and the shear required to turn a flexural crack such that it becomes a flexural-shear crack.

Section 9.20.2 (Shear Strength Provided by Concrete) in the 2002 AASHTO Standard Specifications states that the shear strength provided by concrete, V_c, shall be taken as the lesser of the values V_{ci} or V_{cw}. The shear strength, V_{ci}, shall be computed by the following equation:

$$V_{ci} = 0.6\sqrt{f_c'}b_v d + V_d + \frac{V_i M_{cr}}{M_{max}} \tag{1.3}$$

However, V_{ci} need not be less than $1.7\sqrt{f_c'}b'd$, and d need not be taken less than 0.8h. Here, b_v is the web width, d is the member effective depth, V_d is the shear force due to unfactored dead load, V_i, is the factored shear that occurs simultaneously with the maximum factored moment at the section (M_{max}), while M_{cr} is the cracking moment due to external loads. The last term in equation 1.3 represents the factored shear due to external loads (in addition to dead load) that leads to flexural cracking in the section. For sections subjected to low moment, equation 1.3 will lead to very large shear strength values (infinity at points where $M_{max} = 0$). In these cases, design shear

strength is governed by the shear corresponding to web-shear cracking. The shear strength V_{cw} is computed by assuming that the section is uncracked in flexure and that first diagonal cracking will develop on the member web when the principal tensile stress in the concrete, calculated including the effect of prestressing, reaches the assumed concrete tensile strength of $3.5\sqrt{f_c'}$ (psi). This shear force, combined with the vertical component of the prestressing force, V_p, is then taken as the web shear strength, V_{cw}:

$$V_{cw} = \left(3.5\sqrt{f_c'} + 0.3f_{pc}\right)b_v d + V_p \tag{1.4}$$

Where f_{pc} is the stress due to prestressing at the centroid of the cross section or at the web-flange interface when the centroid is in the flange. But d need not be taken less than 0.8h.

Section 9.20.3 (Shear Strength Provided by Web Reinforcement) in the 2002 AASHTO Standard Specifications states that the shear strength provided by web reinforcement shall be takes as:

$$V_s = \frac{A_v f_{sy} d}{s} \tag{1.5}$$

Where A_v is the area of web reinforcement within a distance s. V_s shall not be taken greater than $8\sqrt{f_c'}b_v d$, and d need not be taken less than 0.8h. The spacing of web reinforcing is not to exceed 0.75h or 24 inches. When V_s exceeds $4f_c'b'd$, this minimum spacing shall be reduced by 50%. The minimum area of web reinforcement shall be determined as follows:

$$A_v = \frac{50b's}{f_{sy}} \tag{1.6}$$

Where b' and s are in inches, and f_{sy} (the design yield strength of web reinforcement) is in psi and shall not exceed 60,000psi.

1.3.3 AASHTO LRFD Design Specifications

The General Sectional Method for shear design in the AASHTO LRFD Specifications represents a significant departure from the traditional shear design methods applied to reinforced and prestressed concrete members in other design codes (e.g. ACI Building Code, AASHTO Standard Specifications). Based on the Modified Compression Field Theory (MCFT) developed at the University of Toronto in the late 1970s and early 1980s (Vecchio and Collins, 1986), this shear design method relies on the use of equilibrium, strain compatibility, and material constitutive relations to determine the "concrete" and steel reinforcement contributions to shear strength. In compression, the concrete behavior is assumed to "soften" (or become weaker) due to the presence of transverse tensile strains. Moreover, on average terms, concrete is assumed to carry some tension beyond cracking to account for tension stiffening (i.e. the tension carried by the concrete between cracks).

The shear resistance of a concrete member may be separated into a component, V_c that relies on tensile stresses in the concrete, a component V_s, that relies on tensile stresses in the transverse reinforcement, and a component V_p, that is the vertical component of the prestressing force.

Section 5.8.3.3 (Nominal Shear Resistance) in the 2012 AASHTO LRFD states that the nominal shear resistance, V_n, shall be determined as the lesser of:

$$V_n = V_c + V_s + V_p \tag{1.7}$$

$$V_n = 0.25 f_c' b_v d_v + V_p \tag{1.8}$$

In which:

$$V_c = 0.0316 \beta \sqrt{f_c'} b_v d_v \tag{1.9}$$

Where b_v is the effective web width taken as the minimum web width, measured parallel to the neutral axis, between the resultants of the tensile and compressive forces due to flexure (in), d_v

is the effective shear depth taken as the distance, measured perpendicular to the neutral axis, between the resultants of the tensile and compressive forces due to flexure (and need not be taken less than the greater of $0.9d_e$ or $0.72h$), s is the spacing of transverse reinforcement measured in a direction parallel to the longitudinal reinforcement, β is a factor indicating the ability of diagonally cracked concrete to transmit tension and shear, θ is the angle of inclination of diagonal compressive stresses, and α is the angle of inclination transverse reinforcement to longitudinal axis. The concrete contribution is controlled by the value of the coefficient β. The value of 0.0316 is and is used to convert the relationship for V_c from psi to ksi units. Note that V_c is taken as the lesser of V_{ci} and V_{cw} if the procedures of Article 5.8.3.4.3 (Simplified Procedure) are used. V_s is in general given as:

$$V_s = \frac{A_v f_y d_v (cot\theta + \cot\alpha) sin\alpha}{s} \tag{1.10}$$

When α = 90 degrees (shear reinforcement placed vertically), Eq.14 reduces to:

$$V_s = \frac{A_v f_y d_v \cot(\theta)}{s} \tag{1.11}$$

The expressions V_c and V_s apply to both prestressed and non-prestressed sections, with the terms β and θ depending on the applied loading and the properties of the section. The upper limit of V_n given by Eq. 8 is intended to ensure that the concrete in the web of the beam will not crush prior to yield of the transverse reinforcement. A variable angle truss model is used to calculate the contribution of the shear reinforcement. The angle of the field of diagonal compression, θ, is used in calculating how many stirrups, $[d_v\cot(\theta)/s]$, are included in the transverse tie of the idealized truss. The parameters β and θ may be determined either by the General Procedure or the Simplified Procedure.

The actual section is represented by an idealized section consisting of a flexural tension flange, a flexural compression flange, and a web. After diagonal cracks have formed in the web, the shear force applied to the web concrete, (V_u -V_p) will primarily be carried by diagonal compressive stresses in the web concrete. These diagonal compressive stresses will result in a longitudinal compressive force in the web concrete of (V_u -V_p)cot θ. Equilibrium requires that this longitudinal compressive force in the web be balanced by tensile forces in the two flanges, with half the force, that is 0.5(V_u -V_p)cot θ, being taken by each flange. For simplicity, 0.5cot θ may be taken as 2.0 and the longitudinal demand due to shear in the longitudinal tension reinforcement becomes (V_u – V_p), without significant loss of accuracy. After the required axial forces in the two flanges are calculated, the resulting axial strains ε_t and ε_c can be calculated based on the axial force-axial strain relationship.

For the General Procedure, for sections containing at least the minimum amount of transverse reinforcement specified in Article 5.8.2.5, the value of β is taken as:

$$\beta = \frac{4.8}{(1 + 750\varepsilon_s)} \tag{1.12}$$

When sections do not contain at least the minimum amount of shear reinforcement, the value of β is taken as:

$$\beta = \frac{4.8}{(1 + 750\varepsilon_s)} \frac{51}{(39 + s_{xe})} \tag{1.13}$$

The value of θ in both cases is:

$$\theta = 29 + 3500\varepsilon_s \tag{1.14}$$

where ε_s is the net longitudinal tensile strain in the section at the centroid of the tension reinforcement:

$$\epsilon_s = \frac{\left(\frac{M_u}{d_v} + 0.5N_u + 0.5\left|V_u - V_p\right| - A_{ps}f_{po}\right)}{\left(E_sA_s + E_pA_{ps}\right)} \quad (1.15)$$

The crack spacing parameter s_{xe} , is:

$$s_{xe} = s_x\frac{1.38}{a_g + 0.63} \quad (1.16)$$

Where 12.0 in $\leq s_{xe} \leq$ 80.0 in., A_c is the area of concrete on the flexural tension side of the member, A_{ps} is the area of prestressing steel on the flexural tension side of the member, A_s is the area of non-prestressed steel on the flexural tension side of the member at the section under consideration, a_g is the maximum aggregate size, f_{po} is a parameter taken as modulus of elasticity of prestressing tendons multiplied by the locked-in difference in strain between the prestressing tendons and the surrounding concrete. For the usual level of prestressing, a value of $0.7f_{pu}$ will be appropriate for both pretensioned and post-tensioned members, N_u is the factored axial force, taken as positive if tensile and negative if compressive, $\left|M_u\right|$ is the factored moment, s_x is the lesser of either d_v or the maximum distance between layers of longitudinal crack control reinforcement, where the area of the reinforcement in each layer is not less than $0.003b_vs_x$, and V_u is the factored shear force.

In using the General Procedure, some additional considerations are:

- $\left|M_u\right|$ shall not to be taken less than $\left|V_u - V_p\right| d_v$
- In calculating A_s and A_{ps}, the area of bars or tendons terminated less than their development length from the section under consideration should be reduced in proportion to their lack of full development.

- If the value of ε_s is negative, it should be taken as zero or the value should be calculated using $\left(E_s A_s + E_p A_{ps} + E_c A_{ct}\right)$ as the denominator. However, ε_s should not be taken less than -0.40x10^{-3}.
- For sections closer than d_v to the face of the support, the value of ε_s calculated at d_v from the face of the support may be used in evaluating β and θ.
- If the axial tension is large enough to crack the flexural compression face of the section, the value calculated by the denominator for ε_s should be doubled.
- It is permissible to determine β and θ using a greater value of ε_s than calculated by the equation above, however, ε_s should not be taken greater than 6.0x10^{-3}.

The relationships for evaluating β and θ in the previous equations are based on calculating the stresses that can be transmitted across diagonally cracked concrete. As the cracks become wider, the stress that can be transmitted decreases. For members containing at least the minimum amount of transverse reinforcement, it is assumed that the diagonal cracks will be spaced about 12.0 in apart. For members without transverse reinforcement, the spacing of diagonal cracks inclined at θ degrees to the longitudinal reinforcement is assumed to be $s_x/\sin\theta$. Hence, deeper members having larger values of s_x are calculated to have more widely spaced cracks and hence, cannot transmit such high shear stresses. The ability of the crack surfaces to transmit shear stresses is influenced by the aggregate size of the concrete. Members made from concretes that have a smaller maximum aggregate size will have a larger value of s_{xe} and hence, if there is no transverse reinforcement, will have smaller shear strength.

As an alternative to the General Procedure, a Simplified Procedure may be used in some cases. The Simplified Procedure is based on the recommendations of NCHRP Report 549. These concepts are compatible with ACI 318-11 and the AASHTO Standard Specifications for Highway

Bridges (2002) for evaluation of the shear resistance of concrete members. For nonprestressed sections, Section 5.8.3.4.1 (Simplified Procedure) states that for concrete sections not subjected to axial tension and containing at least the minimum amount of transverse reinforcement, or having an overall depth of less than 16 in, β can be taken as 2.0 and θ can be taken as 45°. Section 5.8.3.4.3 (Simplified Procedure) addresses prestressed sections as well. Here, for concrete beams not subject to significant axial tension, prestressed or non-prestressed, and containing at least the minimum amount of transverse reinforcement, V_n may be determined with V_p taken as zero and V_c taken as the lesser of V_{ci} and V_{cw}, where V_{ci} is the nominal shear resistance provided by the concrete when inclined cracking results from combined shear and moment, and V_{cw} is the nominal shear resistance provided by the concrete when inclined cracking results from excessive principal tension in web. In this case, V_{ci} shall be determined as:

$$V_{ci} = 0.02\sqrt{f_c'}b_v d_v + V_d + \frac{V_i M_{cre}}{M_{max}} \geq 0.06\sqrt{f_c'}b_v d_v \tag{1.17}$$

Where V_d is the shear force at the section due to the unfactored dead load and includes both DC and DW, V_i is the factored shear force at section due to externally applied loads occurring simultaneously with M_{max}, M_{cre} is the moment causing flexural cracking at section due to externally applied loads, and M_{max} is the maximum factored moment at section due to externally applied loads. M_{cre} hall be determined as:

$$M_{cre} = S_c\left(f_r + f_{cpe} - \frac{M_{dnc}}{S_{nc}}\right) \tag{1.18}$$

Where f_{cpe} is the compressive stress in the concrete due to the effective prestress forces only at the extreme fiber or section where tensile stress is caused by externally applied loads, M_{dnc} is the total unfactored dead load moment acting on the monolithic or noncomposite section, S_c is the section modulus for the extreme fiber of the composite section where tensile stress is caused by

externally applied loads, and S_{nc} is the section modulus for the extreme fiber of the monolithic or noncomposite section where tensile stress is caused by externally applied loads. V_{cw} shall be determined as:

$$V_{cw} = \left(0.06\sqrt{f_c'} + 0.30 f_{pc}\right) b_v d_v + V_p \quad (1.19)$$

Where f_{pc} is the compressive stress in the concrete at the centroid of the cross section resisting the externally applied loads or at the junction of the web and flange when the centroid lies within the flange.

For the simplified procedure, the angle θ used to calculate V_s can be determined as follows:

When $V_{ci} < V_{cw}$: $\cot\theta = 1.0$

When $V_{ci} > V_{cw}$: $\cot\theta = 1.0 + 3\left(\frac{f_{pc}}{\sqrt{f_c'}}\right) \leq 1.8$ (1.20)

Transverse reinforcement is required in all regions where there is a significant chance of diagonal cracking. A minimum amount of transverse reinforcement is required to restrain the growth of diagonal cracking and to increase the ductility of the section. A larger amount of transverse reinforcement is required to control cracking as the concrete strength is increased. According to the 2014 AASHTO LRFD Code (Section 5.8.2.4; Regions Requiring Transverse Reinforcement), for beams, transverse reinforcement shall be provided where:

$$V_u > 0.5\phi\left(V_c + V_p\right) \quad (1.21)$$

Here, V_u is the factored shear force, V_c is the nominal shear resistance of the concrete, V_p is the component of prestressing force in direction of the shear force (V_p = 0 when the simplified method of Section 5.8.3.4.3 is used), and Φ is the resistance factor specified in Article 5.5.4.2. For shear (normal weight concrete), Φ is taken as 0.90, but for compression in strut-and-tie models, Φ is taken as 0.70.

Section 5.8.2.5 (Minimum Transverse Reinforcement) states that the area of steel shall satisfy:

$$A_v \geq 0.0316\sqrt{f_c'}\frac{b_v s}{f_y} \quad (1.22)$$

Where A_v is the area of transverse reinforcement within distance s, b_v is the width of web adjusted for the presence of ducts, s is the spacing of transverse reinforcement, and f_y is the yield strength of transverse reinforcement. Section 5.8.2.7 (Maximum Spacing of Transverse Reinforcement) states that the spacing of the transverse reinforcement shall not exceed the maximum permitted spacing, s_{max}, determined as:

If $v_u < 0.125f_c'$, then $s_{max} = 0.8d_v \leq 24.0$ in (1.23)

If $v_u > 0.125f_c'$, then $s_{max} = 0.4d_v \leq 12.0$ in (1.24)

Where v_u is the shear stress calculated in accordance with 5.8.2.9, and d_v is the effective shear depth. Section 5.8.3.2 (Sections near Supports) states that where the reaction force in the direction of the applied shear introduces compression into the end region of a member, the location of the critical section for shear shall be taken as d_v from the internal face at the support.

When a beam is loaded on top and its end is not built integrally into the support, all the shear funnels down into the end bearing. Where the beam has a thin web so that the shear stress in the beam exceeds $0.18f_c'$, there is a possibility of a local diagonal compression or horizontal shear failure along the interface between the web and the lower flange of the beam. Here strut-and-tie models are useful for analysis.

1.3.4 ACI 318-11

The calculation for nominal shear capacity in ACI 318-11 is similar to previous versions (1983 to 2002) of the AASHTO Standard Specifications for Highway Bridges. ACI 318-11 divides the

nominal shear strength into contributions from concrete and steel transverse reinforcement. They are computed using the following equations:

$$V_{ci} = 0.6\sqrt{f_c'}b_w d_p + V_d + \frac{V_i M_{cre}}{M_{max}} \quad (1.25)$$

$$V_{cw} = \left(3.5\sqrt{f_c'} + 0.3f_{pc}\right)b_w d_p + V_p \quad (1.26)$$

$$V_s = \frac{A_v f_y d_v}{s} \quad (1.27)$$

Where V_{ci} is the concrete shear capacity when cracking results from combined shear and moment, V_{cw} is the concrete shear capacity when cracking results from high principal tensile stress, V_s is the shear capacity of steel web reinforcement, M_{cre} is the moment causing flexural cracking at the section due to externally applied loads, V_d is the unfactored shear due to dead load, V_i is the factored shear at the section due to externally applied loads, M_{max} is the factored moment at the section due to externally applied loads, f'c is the concrete compressive strength (psi), f_{pc} is the compressive stress in the concrete at the centroid of the gross section resisting externally applied loads including effective prestressing force, b_w is the width of the web adjusted for ducts, d_v is the effective shear depth (in), A_v is the total area of shear stirrups, f_y is the yield stress of the web reinforcement, s is the spacing of shear stirrups, and V_p is the vertical component of prestressing force.

The nominal shear resistance of concrete is taken as the lesser of V_{ci} or V_{cw}. Typically, V_{cw} will control near the supports and V_{ci} will control closer to midspan. The effective prestressing force is included directly in the equation for V_{cw} as the vertical contribution of prestressing force and in the term f_{pc} which includes only the uniform axial compression due to the effective prestressing force. It is important to note that, although not shown explicitly in the equations above, the effective prestressing force is used in V_{ci} as it must be considered when determining M_{cre}.

The minimum shear reinforcement area is determined as follows:

$$A_v \geq \frac{0.75\sqrt{f_c'}b_w s}{f_{yt}} \tag{1.28}$$

Where f_c' is the compressive strength of concrete, b_w is the effective width of the web, *s* is the spacing of shear reinforcement, and f_{yt} is the tensile strength of shear reinforcement.

1.3.5 Strut and Tie Modeling

Both AASHTO and ACI allow strut and tie models. Strut and tie models can be used when beam theory is not applicable, such as in D-regions. Here, the girder is modeled as a truss where concrete struts take the compressive loads and steel ties take the tension loads (Kuchma et al. 2008). A proper truss model should show how forces are distributed throughout the girder. Schlaich et al. (1987) states that the model producing the least strain energy is the most appropriate. In almost all cases where a point load is applied with a shear span to depth ratio less than 2.0, the least strain energy occurs when a compressive strut connects the load and support (Brown and Bayrak, 2008). Nominal strut and tie capacities for AASHTO LRFD are determined as follows, respectively:

$$P_n = f_{cu}A_{cs} \tag{1.29}$$

$$P_n = f_y A_{st} + A_{ps}\left(f_{pe} + f_y\right) \tag{1.30}$$

Nominal strut and tie capacities for ACI 318 are determined by the following equations:

$$F_{ns} = f_{ce}A_{cs} \tag{1.31}$$

$$F_{nt} = f_y A_{ts} + A_{tp}\left(f_{se} + \Delta f_p\right) \tag{1.32}$$

These equations are very similar as both codes use a limiting stress for the concrete strut capacity and include both conventional steel reinforcement and prestressing strands in the calculation of tie capacity. The development of stress in the steel ties must be considered in

evaluating the tie capacity and the main difference between the codes is how the limiting stress of the concrete struts is calculated. For AASHTO LRFD, limiting concrete strengths are given as:

$$f_{cu} = \frac{f_c'}{0.8 + 170\varepsilon_1} \leq 0.85 f_c' \tag{1.33}$$

$$f_{ce} = 0.85\beta_s f_c' \tag{1.34}$$

$$\varepsilon_1 = \varepsilon_s + (\varepsilon_s + 0.002)cot^2\alpha \tag{1.35}$$

The value for ε_1 is based on the tensile strain in the strut due to the adjoining tie and the angle between the strut and tie. The ε_s factor is determined by the type of strut. When the width of a strut is allowed to increase at its midsection, it is called bottle shaped. For a bottle shaped strut the ε_s factor is taken as 0.6 or 0.75 depending on whether the minimum transverse reinforcement requirement is met. The strength of nodal regions is also considered. AASHTO LRFD applies a factor of 0.85, 0.75 and 0.65 to f_c' for nodes containing no ties, ties in one direction and ties in more than one direction, respectively. ACI uses similar equations.

1.3.6 Shear Models

Most traditional shear design procedures are generally derived from a parallel chord truss model by Ritter (1899) and Mörsch (1920 and 1922). In this model, for any member under shear forces, there are four unknowns (diagonal compressive stress, stress in stirrups, stress in longitudinal reinforcement, and the angle of the diagonal compression), but only three equations of statics to determine the unknowns. The determination of the final condition required for solution is what makes for the largest difference between design codes. The angle of the diagonal compression strut is an important factor in deciding the shear reinforcement contribution to shear resistance. In early parallel chord truss models, θ was taken as 45 degrees. However, it was determined by various researchers that this angle often poorly estimated capacity, and thus over the past several decades, the use of a truss analogy with angles shallower than 45 degrees has been

explored (Ramirez and Breen, 1991; Vecchio and Collins, 1986; Hsu, 1988). Reducing this angle implies a higher efficiency of the transverse reinforcement (as geometrically, more stirrups will cross a shear crack with a lower angle) and thus results in less shear reinforcement required for the same shear demand. The concrete shear strength contribution can be considered as well, and in early formulations, it was based on a limiting shear stress. Later it was taken to be the diagonal cracking strength (i.e. the concrete contribution at ultimate, based on test data). Code provisions such as those of ACI 318 and the AASHTO Standard Specifications take into account the effect of flexure, axial force, and prestressing into the diagonal cracking strength. However, they also make the assumption that the concrete shear strength contribution is independent of shear reinforcement. In contrast, some European design methods take θ as the angle defined by a plasticity-based model and different equations can result in values as low as 21.8 degrees. However, the concrete shear strength contribution depends on the shear reinforcement and is calculated by different expressions used that are based on shear-friction models. In AASHTO LRFD, the angle θ is often taken between 20 and 25 degrees, consequently providing a larger shear strength contribution from the shear reinforcement than that found from a 45 degree model. The concrete shear strength contribution is defined as the ability of the cracked concrete to carry diagonal tension in the web of the member, and it depends on the longitudinal strain, the reserve capacity of the longitudinal reinforcement at a crack location, and the shear-slip resistance of concrete. The Tureyen and Frosch (2003) model takes the angle θ as 45 degrees and bases the concrete strength contribution on the limiting capacity of the uncracked section (Kuchma and Hawkins 2008).

Traditional provisions for shear capacity such as those of the ACI code do not explicitly take into account shear friction as a contributor to shear strength; they rather lump it together with other

contributors such as the dowel effect and the shear strength capacity of the compression zone of the beam. This term is referred to as the concrete contribution to shear strength V_c. In the last 20 years, more rational methods for shear strength calculation (such as AASHTO LRFD and the Canadian Code CSA) have been able to explicitly account for the contribution of shear friction across cracks in resisting shear, by referring to concepts of the Modified Compression Field Theory (MCFT). The MCFT also provides a way to study the softening of concrete (effect of tensile stress in lowering the compressive strength of concrete below its uniaxial strength).

The MCFT (Vecchio and Collins, 1986) is a rational theory that satisfies the equilibrium of forces and moments, compatibility of displacements, and stress-strain relationship of concrete and steel to predict the shear strength of RC and PC beams. The assumption MCFT makes is that the principal direction of stress and strain coincide. The shear strength is given by the sum of the steel reinforcement contribution (based on the angle θ truss model) and the concrete contribution (shear resisted by the tensile stresses in the diagonally cracked concrete). While some researchers (Richart, 1927; Bresler and Pister, 1958; Tureyen and Frosch, 2003) have argued that most of the "concrete" contribution to beam shear strength is provided by shear carried in the beam compression zone, others (Vecchio and Collins, 1986) have claimed that most of this shear is resisted by the member web through aggregate interlock, which is the approach followed by MCFT. After the transverse reinforcement yields, the transfer of tension across the cracks requires local shear stresses τ along the stress. The ability of the crack interface to transmit shear stresses τ depends on the crack width w. According to MCFT,

$$V = V_s + V_c = \frac{A_v f_v}{s} jd\ cot\theta + f_{c1} b_w jd \cot\theta \tag{1.36}$$

$$\frac{\tau}{\tau_{max}} = 0.18 + 1.64\frac{\sigma}{\tau_{max}} - 0.82(\frac{\sigma}{\tau_{max}})^2 \tag{1.37}$$

$$\tau_{max} = \frac{\sqrt{f_c'}}{0.3 + \frac{24w}{c + 16}} \tag{1.38}$$

Where σ is the compressive normal stresses across the cracks, c is the maximum aggregate size, and f_c' is the compressive strength of concrete.

Another expression developed later by Collins and Mitchell (1991) for τ is:

$$\tau = 0.18\tau_{max} \tag{1.39}$$

MCFT assumes a parabolic relationship between stress and strain of concrete in compression:

$$\frac{f_{c2}}{f_{c2max}} = 2\left(\frac{\varepsilon_2}{\varepsilon_0}\right) - \left(\frac{\varepsilon_2}{\varepsilon_0}\right)^2 \tag{1.40}$$

Where ε_0 is the strain at peak uniaxial stress, and f_{c2max} is the compressive strength of concrete panels in biaxial tension-compression and depends on the transverse tensile strain ε_1. A softening parameter was derived from tests with a mean value of 0.98 and coefficient of variation of 0.16. and f_{c2} is then a function of the principal compressive strain ε_2 and the principal tensile strain ε_1.

$$\beta = \frac{f_{c2max}}{f_c'} = \frac{1}{0.80 + \frac{0.34\varepsilon_1}{\varepsilon_0}} \leq 1.0 \tag{1.41}$$

For ε_0=0.002,

$$\beta = \frac{1}{0.80 + 170\varepsilon_1} \tag{1.42}$$

Two major research directions for the shear behavior in reinforced concrete are the characterization of shear friction, which controls the transfer of shear force across a crack, and the

characterization of softening, which reduces the compressive strength of concrete when in a state of bi-axial compression and tension. Work related to shear friction is discussed first.

Walraven and Reinhardt (1981) and Walraven (1981) developed early equations for predicting the normal and shear stresses in cracked concrete. They based their expressions on experimental investigations of shear friction. The experiments consisted of internally and externally beam sections loaded in direct shear. It was observed that the behavior of the externally reinforced beams was different from that of the internally reinforced ones; the shape of the crack width vs. crack slip curve was more sensitive for the externally reinforced beams. However, the authors used the same model for aggregate interlock for both types of beams. This model involved two components, a rigid plastic mortar component and a rigid spherical aggregate component. When the crack faces open and slide against one another, the portion of mortar in contact with the aggregates is assumed to yield and therefore creates normal and shear stresses that are related by a coefficient μ. Walraven and Reinhardt's equation for normal and shear stresses are given as:

$$\sigma = \sigma_{pu}(A_x - \mu A_y) \quad and \quad \tau = \sigma_{pu}(A_y - \mu A_x) \tag{1.43}$$

Where A_x and A_y are the nondimensionalized sums of a_x and a_y (contact areas), and depends on crack width w, crack slip v, the maximum particle diameter, and the total aggregate volume per unit volume of concrete. The coefficient μ and strength of mortar σ_{pu} were found by fitting curves to experimental results:

$$\mu = 0.40 \quad and \quad \sigma_{pu} = 6.39(f_{cc})^{0.56} \tag{1.44}$$

The authors developed an empirical expression for shear friction capacity of internally reinforced cracks as a function of concrete strength and amount of reinforcement:

$$\tau_{max} = C_1(\rho_v f_y) \tag{1.45}$$

Where $C_1 = 0.822(f_{cc})^{0.406}$ and $C_2 = 0.159(f_{cc})^{0.303}$, ρ_v and f_y are the cross sectional area and yield strength of the steel reinforcement, respectively, and f_{cc} is the compressive strength of a concrete test cube.

Walraven and Reinhardt's expressions gave good approximations to their experimental data for a linear range. However, the equations require a limit so that shear and normal stresses do not increase indefinitely as the crack slip increases. Other researchers did work on the same topic and derived expressions for the shear cracking capacity. Mau and Hsu (1988) derived an expression that works well for normal strength RC:

$$\frac{\tau_{max}}{f_c'} = 0.66\sqrt{w} < 0.3 \ \ with \quad w = \frac{\rho_v f_y}{f_c'} \tag{1.46}$$

It was found that the cracks are smoother in High Strength Concrete (HSC) because the cracks go through the aggregates (as opposed to NSC where the cracks go around the aggregates), then shear friction decreases as concrete strength increases. It has been shown that shear friction at a crack slip of HSC is reduced by 35% of its value for NSC for externally reinforced specimens, and between 55-75% of its value for internally reinforced specimens. The expressions for stresses for the model cracks then became:

$$\sigma = k\sigma_{pu}(A_x - \mu A_y) \ \ and \ \ \tau = k\sigma_{pu}(A_y - \mu A_x) \tag{1.47}$$

Where k = 0.35 or 0.65 for externally reinforced and internally reinforced concrete specimens, respectively.

Other authors derived expressions based on the experimental results of Walraven. Reineck (1982, 1991) used the following expressions for the friction of shear faces:

$$\tau = \tau_{f0} + 1.7\sigma = \tau_{f0}({}^{v - 0.24w}/_{0.096w + 0.01mm}) \tag{1.48}$$

The cohesion friction stress τ_{f0} is the limiting value of shear strength without the normal stress σ on the crack face and is found as:

$$\tau_{f0} = 0.45 f_t \left(1 - \frac{w}{0.9mm}\right) \tag{1.49}$$

Where f_t is the concrete tensile strength.

Reineck's expressions also needed a limit for stresses. The expressions worked well for w = 0.5 mm, but lost accuracy when w = 0.8 mm. Kupfer and Bulicek (1992) used the following relationships based on Walraven and Reinhardt's (1981) work:

$$\tau_{max} = -\frac{f_{cc}}{30} + (1.8(w)^{-0.8} + (0.234(w)^{-0.707} - 0.20) f_{cc}) v \geq 0 \tag{1.50}$$

$$\sigma = \frac{f_{cc}}{20} - (1.35(w)^{-0.63} + 0.191(w)^{-0.552} - 0.15) f_{cc}) v \leq 0 \tag{1.51}$$

Earlier, Kupfer, Mang, and Karavesyroglou (1983) had used:

$$\frac{\tau}{f_c'} = 0.117 - 0.085v \; for \; Case \; A: v = w \tag{1.52}$$

$$\frac{\tau}{f_c'} = 0.117 + 0.1\frac{v}{w} - 0.085v \; for \; Case \; B: v \neq w \tag{1.53}$$

These expressions were derived based on earlier work from Walraven, which considered concrete with strength of 25 MPa and v > 0.20 mm. However, the relationships established Kupfer et al. (1983) were based on weaker concrete and did not agree well with Walraven's original experimental data. Dei Poli, Prisco, and Gambarova (1990) used a rough crack model to describe aggregate interlock stress as:

$$\sigma = 0.62 \frac{r\sqrt{w\tau}}{(1 + r^2)^{0.25}} \tag{1.54}$$

$$\tau = 0.25 f_c' \left(1 - \sqrt{\frac{2w}{c}}\right) r \frac{a_3 + a_4 |r|^3}{1 + a_4 r^4} \tag{1.55}$$

Here: $a_3 = 9.8/f_c'$, $a_4 = 2.44 - 39/f_c'$, and $r = \frac{v}{w}$

Various researchers have also explored the effect of concrete softening. The web in a reinforced concrete beam in flexure and shear is in a biaxial state of tension-compression. The existence of transverse tensile strains leads to a weakening of the cracked concrete compressive strength, or 'softening'. Different researchers derived softening expressions based on models and test panels. Vecchio and Collins (1993) expressed a softening parameter β as a function of the ratio of the principal strains:

$$\beta = \frac{1}{0.85 - 0.27\, {\varepsilon_1}/{\varepsilon_2}} \tag{1.56}$$

Where ε_1 is the principal tensile strain averaged over several cracks. They used a parabola for the uniaxial compressive stress-strain curve of concrete and multiplied both f_c' and its associated strain ε_0 by β. They found good agreement with 178 experimental data points.

Kollegger and Mehlhorn (1987, 1990) determined that the effective compressive strength did not reduce beyond $0.8 f_c'$ and that the primary influencing factor was the tensile stress f_{c1} rather than the tensile strain ε_1. They determined the following for calculating β:

For $0 \le f_{c1} / f_t \le 0.25$, then $\beta = 1.0$

For $0.25 < f_{c1} / f_t \le 0.75$, then $\beta = 1.1 - 0.4\, ({f_{c1}}/{f_t})$ (1.57)

For $0.75 < f_{c1} / f_t \le 1.0$, then $\beta = 0.8$

The tests were based on panels where the tension-compression loads were applied parallel to the reinforcement, and some on a 45 degree angle. Miyahara et al (1988) Proposed a softening model based on tensile strains, but predicted lesser degree of softening than the model by Vecchio and Collins:

For $\varepsilon_1 \leq 0.0012,\ \beta = 1.0$

For $0.0012 < \varepsilon_1 < 0.0044,\ \beta = 1.15 - 125\varepsilon_1$ (1.58)

For $0.0044 \leq \varepsilon_1,\ \beta = 0.60$

Shirai and Noguchi (1989) and Mikame et al. (1991) proposed the following expression for the softening parameter:

$$\beta = \frac{1}{0.27 + 0.96(\varepsilon_1/\varepsilon_0)^{0.167}} \tag{1.59}$$

It was noted that the softening is greater for HSC than for NSC. Ueda et al. (1991) proposed the following high strength concrete softening parameter:

$$\beta = \frac{1}{0.8 + 0.6(1000\varepsilon_1 + 0.2)^{0.39}} \tag{1.60}$$

Later, Vecchio and Collins updated the model that they had previously developed by basing the uniaxial stress-strain curve on Thorenfeldt's curve, which provided better linear correlation for HSC:

$$f_{c2base} = -f_p \frac{n\left(-\varepsilon_2/\varepsilon_p\right)}{n - 1 + \left(-\varepsilon_2/\varepsilon_p\right)^{nk}} \tag{1.61}$$

Where,

$$n = 0.80 + {}^{f_p}/_{17} \tag{1.62}$$

$$k = 1.0 \; for - \varepsilon_p < \varepsilon_2 < 0;$$

$$k = 0.67 + {}^{f_p}/_{62} \; for \;\; \varepsilon_2 < -\varepsilon_p \tag{1.63}$$

Here, f_p = maximum compressive stress for softened concrete. In these equations, $f_p = \beta f_c'$ and $\varepsilon_p = \varepsilon_0$ = strain in uniaxial compression at peak stress f_c'. Modifications to the base stress-strain curve were explored using two models. Model A used strength and strain softening (both peak stress and its appropriate strain decrease):

$$\beta = \frac{1}{1.0 + K_c K_f} \tag{1.64}$$

$$K_c = 0.35\left(\frac{-\varepsilon_1}{\varepsilon_2} - 0.28\right)^{0.80} \geq 1.0 \; for \; \varepsilon_1 < \varepsilon_{1L} \tag{1.65}$$

$$K_f = 0.1825\sqrt{f_c'} \geq 1.0 \tag{1.66}$$

Where, ε_{1L} is the limiting tensile strain at which the reinforcement at a crack yields and the concrete experiences slight additional cracking. The curve was divided into 3 parts depending on:

Prepeak: $For - \varepsilon_2 < \beta\varepsilon_0 \, , f_{c2} \; is \; calculated \; from \; f_p = \beta f_c' \; and \; \varepsilon_p = \beta\varepsilon_0$

Peak: $For \; \beta\varepsilon_0 \leq -\varepsilon_2 \leq \varepsilon_0, f_{c2} = f_p = \beta f_c'$

Postpeak: $For - \varepsilon_2 > \varepsilon_0, f_{c2} = \beta f_{c2base}$

Note: $K_f \geq 1.0$ when $f_c' \geq 30$ MPa and $K_c \geq 1.0$ when $-\varepsilon_t / \varepsilon_2 \geq 4$

Model B uses strength softening only:

$$\beta = \frac{1}{1 + K_c} \tag{1.67}$$

$$K_c = 0.27\left(\frac{\varepsilon_1}{\varepsilon_0} - 0.37\right) \tag{1.68}$$

$$K_f = 2.55 - 0.2629\sqrt{f_c'} \leq 1.11 \tag{1.69}$$

Vecchio and Collins repeated experiments with other panels reinforced with a reinforcement grid at a 45 degree angle and both models agreed well with the experimental data. It was also found that the compression-softening formulation worked well for NSC as well as HSC.

Belarbi and Hsu (1991) used Hognestad's parabola but suggested one softening parameter for stress and another for strain:

$$\beta_\sigma = \frac{0.9}{\sqrt{1 + K_\sigma \varepsilon_1}} \tag{1.70}$$

$$\beta_\varepsilon = \frac{1.0}{\sqrt{1 + K_\varepsilon \varepsilon_1}} \tag{1.71}$$

Where K_σ and K_ε depend on the orientation ϕ of the cracks to the reinforcement and the type of loading:

Table 1.1. Values for K for Belarbi and Hsu's Model, 1991

	Proportional Loading		Sequential Loading	
ϕ	$K\sigma$	$K\varepsilon$	$K\sigma$	$K\varepsilon$
45 deg	400	160	400	160
90 deg	400	550	250	0

Later, after experimental testing, Belarbi and Hsu (1995) derived the following expressions for softening:

$$For\ \varepsilon_2 \leq \beta\varepsilon_0 \qquad f_{c2} = \beta f_c'\left[2\left(\frac{\varepsilon_2}{\beta\varepsilon_0}\right) - \left(\frac{\varepsilon_2}{\beta\varepsilon_0}\right)^2\right] \tag{1.72}$$

$$For\ \varepsilon_2 > \beta\varepsilon_0 \quad f_{c2} = \beta f_c' \left[1 - \left(\frac{\frac{\varepsilon_2}{\beta\varepsilon_0} - 1}{\frac{2}{\beta} - 1}\right)^2\right] \tag{1.73}$$

$$\beta = \frac{0.9}{\sqrt{1 + K_\sigma \varepsilon_1}} \tag{1.74}$$

Where K_σ = 400 for proportional loading, and K_σ = 250 for sequential loading with some tension release immediately prior to failure.

The softening expression provided by Belarbi and Hsu is less severe than the one by Vecchio and Collins. This might be due to the angle of reinforcement (45 degrees in the case of Vecchio and Collins and parallel in the case of Belarbi and Hsu). Therefore, even the amount of reinforcement is different between the two studies.

Based on measurements of reinforced cylindrical specimens under axial compression and internal pressure, Okamura and Maekawa (1987) developed the following expression for softening:

$$\beta = 1.0\ for\ \varepsilon_1 < \varepsilon_a$$

$$\beta = 1.0 - 0.4\frac{\varepsilon_1 - \varepsilon_a}{\varepsilon_b - \varepsilon_a}\ for\ \varepsilon_a \leq \varepsilon_1 \leq \varepsilon_b \tag{1.75}$$

$$\beta = 0.6\ for\ \varepsilon_b < \varepsilon_1$$

Take $\varepsilon_a = 0.0012\ and\ \varepsilon_b = 0.0044$.

Shirai (1989) performed tests on small reinforced panels and derived the following:

$$\beta_1 = -\left(\frac{0.31}{\pi}\right) tan^{-1}(4820\varepsilon_1 - 11.82) + 0.84 \tag{1.76}$$

$$\beta_2 = -5.9 - \frac{\sigma_1}{f_c'} + 1.0 \tag{1.77}$$

$$\beta = \beta_1 \times \beta_2 \tag{1.78}$$

Kupfer and Bulicek (1992) opted for a constant softening factor (0.85) coupled with a sustained load factor of 0.80:

$$f_{c2} = 0.80 \times 0.85 \times f_c' \approx \frac{2}{3} f_c' \tag{1.79}$$

They also considered the following expression with a constant softening factor:

$$f_{c2} = f_c' \times 0.85 \times 0.75 \left(1 - \frac{f_c'}{250}\right) \tag{1.80}$$

Where, 0.85 is the factor for sustained load, 0.75 is the factor for irregular crack trajectory, and $1 - \frac{f_c'}{250}$ is the difference between cylinder strength and uncracked concrete prism strength.

Reineck (1991) also proposed that the strength of the web struts be taken no lower than f_{cw}.

$$f_{cw} = 0.80 f_c' \tag{1.81}$$

To account for the effects of transverse reinforcement in tension, Prisco and Gambarova (1995) proposed that the concrete strength be reduced by:

$$f_c = 0.75 f_c' \ \ or \ f_c = \frac{0.90 f_c'}{\sqrt{1 + 600\varepsilon_1}} \geq \frac{f_c'}{2} \tag{1.82}$$

Due to the presence of so many formulations for shear friction and concrete softening, a parametric study was performed by Duthinh (1999) to examine the effect that shear friction and concrete softening have on concrete shear strength according to the Modified Compression Field Theory. The results showed that:

1) The ratio of reinforcement is in inverse proportion with the shear friction: as the reinforcement ratio decreases, the effect of shear friction increases.

2) The effects of stresses normal to the interface (σ) were negligible regardless of which method was used.
3) Failure by concrete crushing was predicted to happen for very wide cracks, much higher than Walraven's experimental data ($v \leq 2mm$, $w \leq 1.5mm$)
4) The models of Kollegger, Okamura, Miyahara, and Shirai demonstrate significant postlinear strength and no concrete crushing. The models by Ueda and Noguchi also demonstrate concrete crushing after significant postlinear strength and wide cracks.
5) The models presented by Vecchio, Collins, and Hsu show no significant postlinear strength gained.

Depending on the method of estimation, the shear strength of beams with low shear reinforcement could be decreased by 15-25% if a decrease in shear friction occurs (according to MCFT). This has been experimentally observed in HSC beams.

A similar study was conducted by Suthinh (1997) in which a comparison was presented of the various relationships that have been proposed to represent the shear friction behavior of cracked reinforced concrete. A decrease in shear friction within the range of experimental data, as found for example in high strength concrete, can lower the shear strength of beams with minimum shear reinforcement by 15 percent to 25 percent, according to the MCFT. In addition, a comparison was presented of different relationships used to represent the biaxial compression-tension strength of reinforced concrete for RC and PC beams. Some theories of biaxial softening of concrete did not predict concrete crushing even for very high deformations, but rather showed significant shear force gain after stirrup yielding and crack slipping. For the RC beam example, some theories predict shear tension failure while others predict diagonal compression failure. However, the first peaks of shear load, which occur close to stirrup yielding and crack slipping, are within 10 percent

of one another for the various theories and within 10 percent of the test values for the PC beams considered.

Kuchma and Hawkins (2008) provide a summary of the results from the National Cooperative Highway Research Program Report 549, "Simplified Shear Design of Structural Concrete Members". The report sought to provide some simplifying provisions to the existing Sectional Design Method in AASHTO LRFD. These changes were suggested after consideration of provisions existing in various other design codes. Note that the changes proposed are currently implemented in AASHTO LRFD.

Prior to the implemented changes, AASHTO LRFD used a shear design procedure based on (and derived from) MCFT (Modified Compression Field Theory), in which the values for the critical parameters β and θ were obtained from tables. Note that the shear strength calculated using the AASHTO LRFD Sectional Design Method does not provide the same shear strength calculated by MCFT. An interesting observation was made by the authors regarding the minimum transverse reinforcement, in that it was specified in AASHTO LRFD as 50% more than the minimum required reinforcement by the AASHTO Standard Specifications.

Several design procedures that were used in design practice were studied and compared by the authors: ACI 318-02, AASHTO Standard Specifications (2002), AASHTO 1979 Interim Specifications, Canadian Standard Association (CSA) Design of Concrete Structures (2004), AASHTO LRFD Specifications, Eurocode 2 (2004), German code DIN 1045-1 (2001), the Japanese specifications for design and construction of concrete structures (2007), and the shear design approach by Tureyen and Frosch (2003). Some results from evaluation and comparison of these codes were:

1) Most design procedures (Canadian Standard Association (CSA) Design of Concrete Structures 1994 & 2004, AASHTO 1979 Interim Specifications, AASHTO LRFD Specifications, Eurocode 1 and 2, and the German code) permit designers to use the angle θ as less than 45 degrees when calculating shear strength by shear reinforcement.
2) AASHTO LRFD Specifications, Eurocode 1&2, and the German code allow the design of members that support much larger shear stresses than permitted in the traditional design approach. An important observation was made that the AASHTO Standard Specifications place a limit on the shear stress that can be supported by the concrete as $8\sqrt{f_c'}b_v d$ to prevent diagonal crushing of the concrete before the yielding of the reinforcement. However, MCFT has determined that such failures do not occur until shear stresses reach a level of 0.25 f'_c. This makes a difference when it comes to cast concrete with 10 ksi compressive strength.
3) Basing concrete contribution at ultimate on the diagonal cracking strength enables designers to determine whether a member will crack in shear under service loads, which helps assessing the condition of structures in the field.
4) Some design procedures were simple and depended only on a few variables, while others were more complex. Such a case is that of AASHTO LRFD Specifications shear design which is an iterative process; to determine β and θ, a designer needs to calculate mid-depth strain, which on the other hand depends on θ itself. Furthermore, the mid-depth strain, β, and θ all depend on V_u.
5) Different codes take different approaches when considering the effect shear has on longitudinal reinforcement. The influence is directly described in the parallel chord and truss model, but other codes have specific rules to handle this influence. This influence is particularly of interest at the ends of simply supported prestressed members.

Kuchma and Hawkins (2008) assembled a large experimental database and evaluated the accuracy of the different design methods to determine the shear-strength ratio (V_{test}/V_{code}). A total of 1359 beams were tested from which 878 were RC beams and 481 were PC beams. The majority of the PC beams were T-shaped and I-shaped and had depths less than 20 in, simply supported on bearings, and only 160 of them were reinforced. Most members were subjected to four-point loading and there was a clear shear span length. The results of the experiment were tabulated and some of the findings were summarized below:

1) From all methods evaluated, the CSA and the AASHTO LRFD methods provided the most accurate estimates for the shear strength ratio. The means were consistent and the COV (coefficient of variation) values were low. These two methods would be expected to result in conservative design.
2) Based on the close mean and COV values for the CSA and AASHTO LRFD methods, it was determined that these methods would yield similar designs and therefore the design equations of CSA 2004 for β and θ could be adopted for the AASHTO LRFD method.
3) For members with shear reinforcement close to the minimum required by the ACI code, the shear strength ratios were often under 1.0, which emphasizes the fact that the higher minimum shear reinforcement imposed by AASHTO LRFD method is necessary.
4) Beams with a large amount of reinforcement were able to support high shear stresses (up to $0.25f'_c$), which means that the upper shear strength limit imposed by the ACI code is conservative compared with the higher strength limit in the AASHTO LRFD specifications.

These findings resulted in two main changes to the LRFD Design Specifications as follows:

1) The Simplified Method. The simplified provisions differed from the existing AASHTO LRFD specifications in the expressions for web shear cracking, the angle θ of diagonal compression

in the parallel chord truss model, the maximum allowed shear stress, the minimum required amount of reinforcement, the evaluation of shear depth, and the requirements for the amount of longitudinal reinforcement that must be developed at the face of the support.

New equations were developed for the web shear component V_w and the flexure shear strength V_{ci}. The shear strength contribution of concrete V_c was taken to be the smaller of the two. Therefore the new provisions present the V_c as the lower bound of the possible concrete shear strength at ultimate state. During this state the concrete shear strength contribution is comprised of the shear carried in the compression zone, shear carried along diagonal cracks due to shear friction (aggregate interlock), direct tension across diagonal cracks, dowel action, and arch action. However, accounting for all of these factors would complicate the procedure. Therefore, the simplified provisions accounted for the lower bound estimate of the diagonal cracking load that when summed with the stirrup contribution to shear resistance, resulted in a conservative estimate of the capacity.

2) Equations to calculate β and θ values. The second significant change involved using the expressions for calculating β and θ present in CSA method. This would eliminate the iterative aspect of the shear design in the AASHTO LRFD specifications. In addition, a new equation for the mid-depth strain was developed which assumed θ was 30 degrees when evaluating the influence of shear on longitudinal strain. The equations for these changes were presented in the AASHTO LRFD Bridge Design Specifications summary in Part 1 of this review.

Other researchers have conducted code comparisons for shear design of prestressed concrete girders as well, and the general opinion appears to be that relative to LRFD, shear design by the Standard Specifications are generally less conservative (in terms of ultimate strength) as girder spacing increases and span decreases. These differences are detailed in NCHRP Report 368

(Nowak 1999) and must be considered along with capacity to assess differences and problems among the design approaches. Kuchma, Hawkins, and Kang (2008) also recommend using the LRFD Sectional Design Model for high strength prestressed concrete girders.

Additional research has been conducted to develop new approaches to shear design in RC and PC beams. These approaches were mainly based on the MCFT method (on which AASHTO LRFD or the Canadian Code CSA were based) or the Strut and Tie model.

Ramirez and Breen (1991) proposed a modified truss model with a variable angle of inclination diagonals and a concrete contribution for beams with web reinforcement. The model includes a diminished concrete contribution to account for the variable angle truss model. For PC beams, the model utilizes a constant concrete contribution, but limits the compressive strength to $30\sqrt{f_c'}$, and lowered the angle of inclination from 30 degrees for RC beams to 25 degrees for PC beams. The provisions were compared with a large number of test results and were found satisfactory.

Shahawy and Cui (1999) worked to develop a tied-arch model for the shear design of PC beams. This model was applied to predict the failure load and to study the interaction between the tie, the shear reinforcement, and the struts. Iteration is required to solve the equations and a few critical assumptions must be made. Experimental testing was conducted on 25 full scale AASHTO girders, and the proposed model was used to rate the girder capacities and compared to the AASHTO Standard Specifications and the AASHTO LRFD values. The girders were found to be overdesigned in shear to achieve flexural failure. The authors recommended use of the model due to its consistency. They also suggest, in the case of deep beams and beam ends, to include the contribution of shear reinforcement which is usually ignored in typical strut-and-tie models.

Wang and Meng (2008) developed a modified strut-and-tie model which is useful for the design of simply supported deep beams. The effects of prestressing are modeled with equivalent externally applied loads. The effect of concrete softening is taken into account (the model is based on the Kupfer-Gerstle biaxial tension-compression criterion) by adding a factor k which is determined from consideration of force and moment equilibrium. The model was validated using the experimental results of 56 simply supported PC deep beams and found to be accurate, consistent, and conservative.

Ning and Tan (2007) worked to develop a modified strut-and-tie model for determining the shear strength of reinforced concrete deep beams based on the Mohr Coulomb failure criterion. More recently, Tuchscherer, Birrcher, and Bayrak (2011) also proposed a modified strut-and-tie model based on experimental data from a database of 868 deep beam tests. The procedure was proposed for the strength design of deep-beam regions.

Cladera and Mari (2006) provide a revision of a previously proposed tension-shear model (intended for the shear design of reinforced concrete beams) and applied it to the design of PC beams with or without web reinforcement. For the beams with web reinforcement, the design procedure was based on a truss model with variable angle of inclination of the struts and a concrete strength contribution. The model was based on the MCFT method, where the angle of inclination is obtained by compatibility. The model includes the interaction of axial loads and bending moment. The procedure takes into account the influence of compressive strength on the size effect and limits the strength of beams without stirrups to 60 MPa. It also accounts for the non-linear relationship between the amount of shear reinforcement and shear strength. The procedure was found satisfactory for all tests done, and it appeared to correlate well with the ACI procedures. However, it provides only one formulation for both RC and PC beams.

Esfandiari and Adebar (2009) present a shear strength evaluation procedure similar to the AASHTO LRFD method (2008) without the need for iteration. The approach considers the failure modes of stirrup yielding, diagonal concrete crushing, and longitudinal reinforcement yielding. The approach was compared to the traditional MCFT model of a beam under uniform shear as well as to numerical models of beams under combined shear and bending. For validation, the shear strength predictions were compared to shear strength results from experimental results and provisions by ACI 318 and AASHTO LRFD.

Laskar, Hsu, and Mo (2010) present a simple shear design equation that was experimentally developed. They tested five full scale PC beams and observed three variables: shear span-depth ratio (a/d), transverse steel ratio (ρ_t), and the presence of harped strands in the web and flexural shear capacity. The expression is a function of shear span to depth ratio (a/d), concrete compressive strength $\sqrt{f_c'}$, the web area $b_w d$, and the transverse steel ratio ρ_t. It was also shown that the prestressing force and the angle of failure crack had no effect on shear strength. The authors also derived a formula for the maximum shear strength to guarantee prevention of web crushing prior to reinforcement yielding. The proposed method was evaluated by comparing it to the provisions of the ACI 318 code and AASHTO LRFD 2007 Specifications.

Most recently, Yang, Ashour, and Lee (2011) proposed a mechanism analysis based on the upper-bound theorem of concrete plasticity to predict the critical failure plane and corresponding shear capacity of reinforced concrete dapped-end beams. Failure modes observed in physical tests of reinforced concrete dapped-end beams were idealized as an assemblage of two moving blocks separated by a failure surface of displacement discontinuity. The developed mechanism analysis represented the effect of different parameters on failure modes, and the predicted shear capacity was in good agreement with test results. Furthermore, it was observed that empirical equations

specified by PCI as well as strut-and-tie model based on ACI 318-05 highly underestimated test results.

1.3.7 Experimental Results

Early results include Mast (1964), who considered some of the most common girder shapes and analyzed them for shear and flexure according to the provisions of the ACI 318-63 code. The height-to-span ratio was found to be the crucial parameter in determining whether the member was controlled by shear or flexure. This provided a rapid way to determine whether shear analysis was even necessary.

Nazir and Wilby (1964) tested the behavior and strength in shear of uniformly loaded, post-tensioned prestressed concrete beams without web reinforcement. Comparisons were made with tests on similar beams under different load configurations and the results indicated that the shear strength was influenced by the type of loading. Beams with uniformly distributed loading failed at higher ultimate shears than similar beams tested under concentrated loadings.

Gustafson and Bruce (1966) present the results from tests conducted on eight PC beams and five smaller RC beams simply supported and equally loaded at third points of the span. The main variable of the test was shear reinforcement (including vertical, inclined and prestressed reinforcement—bonded or unbonded). Seven of the beams failed in shear and one had a transitional failure. The results were compared with the AASHTO and ACI codes. The study determined that the shear strength of full size PC girders can be predicted with reasonable accuracy from tests on smaller laboratory specimens. It was also observed that if failure occurred from flexure shear cracking, prestressing the web reinforcement did not add to the ultimate strength of the member. The inclination of the web stirrups also did not add to the ultimate shear strength, but it did better control the opening of inclined cracks than the vertical stirrups.

Bennett and Mlingwa (1980) conducted tests on twenty-eight PC beams with prestressed web reinforcement and stirrups of mild steel or high strength steel. The results served to derive a formula to calculate the width of inclined cracks and the ultimate shear capacity of beams with vertical prestress. It was observed that the prestressing part of the web reinforcement increased the inclined shear and ultimate shear.

Fenwick and Paulay (1968) examined the nature of shear resistance of reinforced concrete beams. It was observed that shear may be resisted by beam and arch action. At diagonal cracking load of shear span, the beam action breaks down. Unless beams contain prestressed reinforcement, arch action cannot develop to a significant extent prior to diagonal cracking. It was also demonstrated that the shear strength of beam action strongly depends on the mechanism of shear transfer across crack; by interlocking of aggregate particles and to a lesser extent, by dowel action of the reinforcement.

Hanson and Hulsbos (1969) conducted laboratory fatigue tests on six prestressed concrete I-beams to determine their shear strength. Each beam was loaded statically to almost 80% of its ultimate flexural capacity and later subjected to repeated loads varying in magnitude between 20-45% of its flexural capacity for about 2,000,000 cycles. The load range was increased and the beams continued to be subjected to it until failure was attained. The tests demonstrated that the prestressed concrete beams have a remarkable shear fatigue resistance. In addition, shear fatigue failures do not occur suddenly, but gave considerable warning with increasing deflection and shear crack widths before failure.

More recently, Pei, Martin, Sandburg, and Kang (2008), as reported in (FHWA OK-08-08), conducted analytical and experimental studies of shear capacities of prestressed concrete bridges in Oklahoma. The concern was to determine if older structures were adequate in shear. The study

focused on precast pretensioned prestressed concrete girders, mainly AASHTO Type II girders, designed according to AASHTO Standard Specifications prior to the 1979 Interim provisions.

In the study, actual girders removed from the I-244 Bridge and the Wild Horse Creek Bridge were tested. Camber measurements were taken to estimate the prestressing stress as well as flexural stiffness, as according to Sandburg (2007), the prestressing stress has a significant influence on shear carrying capacity; as prestress increases, so does the shear capacity.

The results obtained from the tests were then compared to the performance standards provided by different design codes. Three different code provisions were compared on the basis of minimum shear reinforcement; shear demand, nominal shear strength, and margin of safety. The latter was defined as the ratio of the factored nominal shear capacity to design shear demand considering all loads and reduction factors. It was found that the actual tested capacity of the bridge girders exceeded the nominal capacity of each code.

A similar study as the one previously described was conducted by Runzell, Shield, and French (2007) for the Minnesota Department of Transportation. The scope of the study was to determine whether bridge girders designed according to the 1979 Interim provisions were under designed for shear under the current code provisions (such as AASHTO LRFD code). Two shear capacity tests were performed on opposite ends of a bridge girder removed from a highway bridge in Minnesota, which was designed according to the 1979 Interim shear provisions. The results from the shear tests indicated the girder was capable of holding the required shear demand because the applied shear at failure for both tests was larger than the factored shear strength required by the 2004 LRFD HL-93 and 2002 Standard HS20-44 loads. The results of a parametric study, however, showed that some girders designed using the 1979 Interim Specifications would most likely be under designed

for shear near the support. The girders most likely to be under designed in this region had smaller length to girder spacing ratios.

Moreover, girders most likely to be under designed for shear between $0.1L$ (where L is the girder span length) and the support. In this region, the $\frac{\phi V_n}{V_u}$ ratio for the girders varied between 0.73 and 1.09, and was proportional to the $\frac{L}{S_g}$ ration where S_g is the girder spacing. Girders with a length-to-spacing ratio of more than 10 we determined to be safe while those with ratios under 8.5 were determined to be under designed in shear.

Ross, Ansley, and Hamilton (2011) evaluated the structural condition of prestressed concrete girders salved from a bridge in the Gulf of Mexico in Florida. The four salvaged girders were AASHTO type III from a bridge built in 1979. The girders were originally designed using the 1973 edition of the AASHTO Standard Specifications. Girders were tested using a three-point loading scheme with five different *a*/*d* (shear span-to-depth) ratios ranging from 1.2 to 5.4. The results were presented according to the *a*/*d* used and the corresponding modes of failure: bond-shear failure, shear-compression failure, or flexural failure. Experimental results were compared to code calculated strengths, as shown in Table 1.2.

Table 1.2. Shear test results (Ross et al., 2011)

Specimen #	Design Code	V_{pred} (kips)	V_{test} (kips)	V_{test}/V_{pred}
Specimen I (with bridge deck)	2004 LRFD	259	392	1.51
	2002 Standard	316		1.24
	1979 Interim	189		2.07
	Strut and Tie	281		1.4
Specimen II (with no bridge deck)	2004 LRFD	204	392	1.61
	2002 Standard	238		1.38
	1979 Interim	157		2.09
	Strut and Tie	146		1.34

Each of the three girders tested at an *a*/*d* of 3 or less (G1, G2, and G3) demonstrated bond-shear failure. Bond-shear failure was identified by the formation of flexural cracks in the strand development length and by slipping of the strands. Results of the tests indicate that capacity of the prestressing strands was limited by slipping and that additional capacity beyond this slip point might be possible with the use of vertical and horizontal mild steel reinforcement. Two girders were tested with a (*a*/*d)* of 4.1 (G4-1 and G4-2). Girder G4-1 failed in a shear-compression mode, whereas girder G4-2 failed in a bond-shear mode. Although the girders failed differently, their shear versus displacement behavior was similar. One girder was tested with a (*a*/*d)* of 5, and the failure was categorized as flexural. Overall, the 30-year-old girders performed well in the load tests. Comparison of calculated shear capacity with experimental results is shown in Table 1.3. The full-scale testing gave no indication of reduced capacity or performance as a result of exposure or use. Testing confirmed visual ratings made during inspections before demolition.

Table 1.3. Comparison of calculated shear capacity with experimental results (Ross et al. 2011)

a/d	Test	*Vexp*	MCFT		STM		ACI detailed		Modified end region	
			Vn	*Vexp/Vn*	*Vn*	*Vexp/Vn*	*Vn*	*Vexp/Vn*	*Vner*	*Vexp/Vn*
1.2	G1	344	211	1.63	159	2.16	268	1.28	252	1.37
2.1	G2	255	231	1.10	108	2.36	243	1.05	255	1.00
3.1	G3	207	193	1.07	n.a.	n.a.	227	0.91	222	0.93
4.2	G4-1	180	181	0.99	n.a.	n.a.	181	0.99	n.a.	n.a.
4.2	G4-2	198	181	1.09	n.a.	n.a.	181	1.09	n.a.	n.a.
5.4	G5	158	167	0.95	n.a.	n.a.	160	0.99	n.a.	n.a.

Note: units in kips. *a/d*=shear span-to-depth ratio; MCFT=modified compression field theory; STM=strut-and-tie method; *Vexp* = experimental shear capacity; *Vn* = nominal shear capacity; *Vner* = nominal shear capacity of the end region.

Idriss and Liang (2010) measured in-service shear and moment girder distribution factors in simple-span prestressed concrete girders with a built-in optical fiber sensor system. This system was built into the I-25 Bridge in New Mexico during construction. The bridge is composed of six simple-span, high-performance prestressed concrete girders. Sensors were installed along the top

and bottom flanges and at midspan and quarter spans. Pairs of crossed sensors in a rosette configuration were also embedded in the webs at the supports. The bridge was monitored for two years, from transfer of the prestressing force through service. The sensor data were analyzed to evaluate shear and moment girder distribution factors, in situ material properties, prestress losses, camber, dynamic load allowance, and bridge performance under traffic loads. Shear and moment girder distribution factors were obtained from a finite element model, sensor measurements under a live load test, as well as regular traffic loading and compared with the values specified by the AASHTO standard specifications (2002) and the AASHTO load and resistance factor design specifications (2007).

Hartmann, Breen, and Kreger (1988) evaluated the adequacy of code provisions for shear capacity when applied to high strength prestressed concrete girders. The results of shear testing of ten pretensioned girders made from concrete with compressive strength ranging from 10,800 psi-13,160 psi were summarized. Existing design approaches were found to be acceptable for concrete ranging to at least 12,000 psi. It was observed that three design methods studies showed little variation from conservatism as a function of concrete strength. It was also shown that the maximum shear reinforcement limits could be significantly increased.

Cumming, French, and Shield (1998) performed four shear tests on high-strength concrete prestressed girders. The shear test results were compared with predicted results from the ACI 318-95 Simplified Method, the ACI 318-95 Detailed Method (AASHTO 1989), the Modified ACI 318-95 Procedure, Modified Compression Field Theory (AASHTO LRFD 1994), the Modified Truss Theory, Truss Theory, Horizontal Shear Design (AASHTO 1989), and the Shear Friction approach (AASHTO LRFD 1994). The calculated shear capacities were in all cases conservative compared to the actual shear capacity.

Fagundo, Lybas, Basu, Shaw, and White (1995) studied the effects that the shear span-to-depth ratio and moment-to-shear ratio have on the interaction between bond and shear forces in prestressed concrete girders. The study was also focused on identifying parameters that affect the transfer lengths of the prestressing strands and evaluating the current code provisions. Two sets of four simply supported beams were tested. The beams tested at 2D tended to fail in a brittle manner. The failure was governed by strut and tie action due to the presence of the disturbed regions. The beams tested at LD tended to fail in a more ductile manner. These beams had a shear span to depth ratios greater than 2.5. The modified compression field theory provided a reasonable method of analysis for prestressed concrete members with shear span to depth ratios greater than 2.5. It was found that the presence of shear cracks deteriorated the bond between the tendons and the surrounding concrete. As the shear cracks formed, there were sudden increases in tendon slip in every case. The shear and bond forces did appear to be related, but premature shear failures due to excessive loss of bond were not experienced.

Llanos, Ross, Hamilton (2009) tested three types of concrete bridge girders: AASHTO Type IV, AASHTO Type III, and circa 1950's Post-Tensioned Girders. Testing generally focused on shear capacity and behavior under shear load. For the AASHTO Type IV girders, it was found that capacity was not controlled by the typical shear failure mechanisms, but rather was due to cracking and separation of the bottom bulb flange of the girder. This was a result of the unusual debonding pattern that placed the fully bonded strands out in the bulb flange and the debonded strands under the web. A carbon fiber-reinforced plastic (CFRP) fabric strengthening possibility was tested to alleviate issues associated with the strand debonding pattern. The bonded CFRP reinforcement provided an increase in capacity of 9 and 21 percent for shear span-to-depth (a/d) ratios of one and three, respectively. The AASHTO Type III girders were tested at a/d ratios

ranging from one to five. For a/d ratios of three or less, the failure mode was strand slip, which was precipitated by the formation of cracks in the strand development length zone. While these cracks resulted in strand slip, transverse and longitudinal mild steel reinforcement at the girder end was engaged, which improved the capacity and ductility beyond the first strand slip. Post-Tensioned test girders were constructed to replicate a circa 1950s bridge design. Unique features included a presence of both straight and parabolic post-tension bars, and lack of shear reinforcement away from the end block. The girder tested with direct bearing on concrete displayed a 7% larger capacity and nearly half the displacement of a similar girder tested on a neoprene bearing pad.

Oh and Kim (2004) experimentally explored the shear behavior of post-tensioned prestressed concrete girders. Large-scale post-tensioned prestressed concrete girders were fabricated using medium-high and high-strength concrete. The girders were tested to failure while deflections, steel stirrup strains, cracking pattern, and average strains in the web were monitored. The stirrup strains showed a sudden increase immediately after cracking and continued to grow as the load increases. It was found that the angle of principal strain direction decreased as the applied load increased and that it approached approximately 23 to 25 degrees at the ultimate load stage. The concept of average strains and the change of principal direction investigated in this study might be used for a more accurate shear analysis of post-tensioned prestressed concrete girders.

Libby and Konzack (1985) discussed the shortcomings of using ACI code provisions for the shear design of PC beams. An issue that complicates the shear design of PC bridges is that, based on the results of NCHRP Report 322, The Design of Precast, Prestressed Bridge Girders Made Continuous (Oesterle et al. 1989), depending on the construction sequence and reinforcement detailing, some continuous PC bridges have been flexurally-designed as if they were simply

supported spans under some load conditions, potentially resulting in under-design in some instances.

Maruyama and Rizkalla (1988) studied the influence of slippage of prestressing strands on the beam behavior of pretensioned prestressed concrete T-beams, when tested to failure. The effect of various shear reinforcement configurations, crack behavior, overall deformation, and mode of failure are discussed. Based on the test results, a proposed mechanism is introduced to describe the overall behavior of such beams, and design recommendations are presented.

Ranasinghe, Mutsuyoshi, and Ashraf (2001) described the effect of bond between the reinforcement and concrete on the shear behavior of reinforced and prestressed concrete beams. Seven beams with different bond conditions were tested up to failure, while stress-slip relationships for these specimens were obtained from a parallel series of simple pullout tests. A numerical analysis was also conducted to simulate the beams tested. It was found that the bond condition of steel bars and prestressing bars highly influences the shear strength and failure mode of RC and PC beams. A reasonably good correlation was observed between the experimental and analytical results.

Hegger, Sherif, and Görtz (2004) used laser-interferometry and photogrammetry devices to attempt to gain insight to the shear resistance mechanism of PC beams by studying pre- and post-cracking behavior. For studying the precracking behavior, the laser-interferometry was applied. It was found that a nonlinear stress distribution was evident before the formation of visible cracks, thereby influencing the cracking angle. Photogrammetry was used to study the postcracking behavior. Here, measured displacement components of the crack edges were used to estimate shear transferred across the cracks by shear friction. It was also shown that for beams with low or

high shear reinforcement ratios, the amount of shear force transferred across cracks by shear friction was negligible.

De Silva, Mutsuyoshi, and Witchukreangkrai (2007) experimentally explored the shear cracking behavior of prestressed reinforced concrete girders. Tests were conducted on three I-shaped RC beams and four I-shaped PC beams. The variables of interest were the prestressing force, side concrete cover, stirrup spacing, bond characteristics of the stirrups, and amount of longitudinal reinforcement. The influence on shear crack width from each of these parameters was observed. The study determined that the prestressing force significantly reduced the shear crack width in PC beams compared to RC beams. Furthermore, an equation was proposed to calculate the shear crack width of PC beams.

Aboutaha and Burns (1991) studied how the mode of failure of prestressed composite flexural member could be changed from a sudden shear failure to a ductile flexural failure by utilizing external prestressing bars. This research studied the behavior of retrofitted prestressed composite beams that originally lacked shear reinforcement. Before retrofitting, these beams experienced sudden horizontal shear failures. However, ductile flexural failures occurred after the sections were retrofitted with external prestressing bars.

Cederwall (2006) summarized the results of experimental investigations of the shear capacity of composite prestressed concrete I-beams. On the basis of the test results, the relevance of the equation in the Swedish Code (BBK-79) for shear capacity of homogeneous prestressed concrete beams is discussed, if applied to composite beams. The test series indicate a slight overestimation of the beneficial influence of prestressing, which was greater for homogeneous beams than for composite beams.

Ma and Hu (2008) developed formulas that could determine the diagonal section strength of composite prestressed concrete beams (such as those where reaction powder concrete is applied in the unbonded prestressed composite beams without stirrups). The new formulas were found to be less conservative than the existing ones.

Saqan, Frosch (2009) investigated the shear strength and behavior of partially prestressed reinforced concrete rectangular beams with prestressing strands and reinforcing bars, but without transverse reinforcement. Tests were conducted on nine large-scale beams, and the prestressing force was kept constant. The test variables were the amount of prestressing steel and the amount of mild steel. A strong correlation was found between the flexural reinforcement and shear strength of PC beams (increasing the cross sectional area of prestressing steel can increase the shear strength of the beam). In general, the total amount of reinforcement controls the behavior and strength of the member until the first shear crack occurs.

Similar work was done by Recupero, D'Aveni, and Ghersi (2005), who attempted to generalize a model for evaluating the shear strength of prestressed beams that was previously proposed for box and I-shaped reinforced concrete cross sections. After being modified, the model included the effect of prestressing tendons, and took into consideration variable-depth stress fields applied to the cross section. The reliability of the method was validated by comparing its numerical results to the strength provided by tests on reinforced concrete beams and on thin-webbed prestressed concrete beams. The method was used in the design of a pretensioned bridge beam to evaluate the additional reinforcement necessary in the flanges, as a function of the reinforcement provided to the web.

Lee, Cho, and Oh (2010) investigated the shear deformation of large-scale reinforced I-shaped girders and post-tensioned prestressed concrete girders with a small shear span-depth ratio of 2.5.

The test variables were the compressive strength of the concrete, the stirrup ratio, and the prestressing force. This large-scale experimental study enabled the investigation of diagonal cracking behavior, crack patterns, principal strain direction, and crack width, as well as ultimate shear capacity. From the experimental results, it was shown that the ultimate shear capacity of concrete girders increased with an increase in the concrete compressive strength, the stirrup ratio, and the prestressing force. The effect of concrete strength in the girders with stirrups and prestressing force, however, was not as much as in those without stirrups and prestress. It was also shown that the stirrup was highly effective for controlling diagonal crack width, whereas the prestressing force is only effective at delaying cracking load. It was found that the presence of stirrups was the dominant factor contributing to the arching action of a beam member with a short shear span-depth ratio.

Yoshitake et al. (2011) emphasized the difficulty of evaluating shear cracking load when many factors influence the behavior of RC and PC flexural members, when evaluating the shear strength of plain concrete through testing. The results showed that reinforcement had little influence on the shear cracking strength. On the other hand, tensile strength and Poisson ratio were strongly related to shear cracking strength.

1.3.8 Numerical Modeling

Few studies in the technical literature are specifically focused on the numerical modeling of prestresssed concrete girder shear behavior. However, some examples of numerical modeling-focused research are given below.

Laskar, Howser, Mo, and Hsu (2010) discussed the development of the Cyclic Softened Membrane Model (CSMM), which has been efficiently used to predict the behavior of RC and PC beams critical in shear. CSMM has been implemented into the OpenSees (Open System for

Earthquake Engineering Simulation) finite element framework, and is being implemented in the finite element program Simulation of Concrete Structures (SCS). To create SCS, five full scale prestressed girders were tested to study their behavior in web shear and flexure shear. The failure plane on each of the girders occurred at an angle of approximately 45 degrees, which was inconsistent with the provisions of AASHTO and ACI 318 codes (where angles of failure planes ranged from 22.3-35.7 degrees for AASHTO and 37.5 degrees for ACI code). To confirm the failure angle, the researchers used SCS. It was found that SCS was capable of well-predicting the shear behavior of beams under vertical loading.

Mahesh and Surinder (2011) predicted the shear strength of RC and PC deep beams by using Support Vector Regression. Here, a back-propagation neural network and three empirical relations were used to model reinforced concrete deep beams. For prestressed deep beams, one empirical relation was used. Results suggest an improved performance could be obtained by use of SVR in terms of prediction capabilities in comparison to the existing empirical relations and the back propagation neural network. Parametric studies with SVR suggest the importance of concrete cylinder strength and ratio of shear span to effective depth when predicting the strength of deep beams. The SVR model was also used to perform parametric studies, which suggest that the shear strength of deep beams is in direct proportion with the concrete strength and inversely proportional to the shear span-to-depth ratio. However, it was found that the shear strength of deep beams is not affected by the variation in horizontal web reinforcement for a span-to-depth ratio greater than 1. The results of the parametric studies using SVR were in agreement with previous work.

Liu, Wu, and Xu (2012) discussed a method that uses inner transverse prestressing bars to enhance the shear capacity of concrete beams. Four transversely prestressed concrete beams and one ordinary reinforced concrete beam were modeled using a nonlinear finite element method. A

parametric study was carried out to analyze the behavior of the PC beams. It was found that the transverse prestressing bars can increase the shear capacity and failure load of the reinforced concrete beam, where the increase in prestressing force directly increases the shear capacity of reinforced beams. It was found that bars with smaller diameters and smaller spacing can be more efficient in enhancing the shear capacity of transversely prestressed concrete beams.

1.3.9 NCHRP Reports

The NCHRP Report findings most relevant to the shear design and behavior of PC beams of interest to this research were discussed earlier in this report (NCHRP 322; 368; and 549), when the literature review from technical journal papers was presented. However, a summary of additional report information is provided below.

The objective of NCHRP 368, *Calibration of LRFD Bridge Design Code* (Nowak 1999) was to develop the reliability-based calibration for the Load Resistance Factor Design bridge design code. Load and resistance factors were derived so that the reliability of bridges designed using the proposed provisions will be at the predefined target level. The report describes the calibration procedure and reviews proposed changes to load and resistance models. It was found that the AASHTO Standard Specifications resulted in PC beam designs in shear that generally had reliability indices lower than the target proposed for the AASHTO LRFD Specification, with least-reliable beams being in the longer span ranges.

The code calibration procedure in the NCHRP 368 project was formulated including the following steps:

1) Selection of representative bridges:

   About 200 structures were selected from various geographical regions of the United States. The selection was based on structural type, material, and geographical location. Bridges

were grouped by material (steel, reinforced concrete, prestressed concrete and wood), span (simple and continuous) and structural type (slab, beam, box, truss, arch). Current and future trends were considered. The selected set also included representative existing bridges. For each selected bridge, load effects (moments, shears, tensions and compressions) are calculated for various components. Load carrying capacities were also evaluated .State DOT's were requested to provide the drawings and other relevant information.

2) Establishing the statistical data base for load and resistance parameters:

The available data on load components, including results of surveys and other measurements, was gathered. Truck survey and weigh-in-motion (WIM) data were used for modeling live load. There was little field data available for dynamic load therefore a numerical procedure was developed for simulation of the dynamic bridge behavior. Statistical data for resistance included material tests, component tests and field measurements. Numerical procedures were developed for simulation of behavior of large structural components and systems.

3) Development of load and resistance models:

Load and resistance parameters were treated as random variables. Their variation was described by cumulative distribution functions (CDF) and correlations. For loads, the CDFs were derived using the available statistical data base (Step 2). The live load model included the presence of multiple trucks in one lane and in adjacent lanes. Multilane reduction factors were calculated for wider bridges. Dynamic load was modeled for single trucks and two tucks side-by-side. Moreover, resistance models were developed for girder bridges. The variation of the ultimate strength was determined by simulations. In this study

the reliability analysis was performed using the Rackwitz and Fiessler procedure, Monte Carlo simulations and special sampling techniques.

4) Development of the reliability analysis procedure:

Structural performance was measured in terms of reliability. Limit states were defined as mathematical formulas describing the state (safe or failure). Reliability was measured in terms of the reliability index, β. Reliability index is calculated the Rackwitz and Fiessler procedure. The developed load and resistance models (step 3) were part of the reliability analysis procedure.

5) Selection of the target reliability index:

Reliability indices are calculated for a wide spectrum of bridges designed according to the 1989 AASHTO Standard Specifications. The target reliability index, β_T, was selected to provide a consistent and uniform safety margin for all structures.

6) Calculation of load and resistance factors:

Load (ϒ) and resistance (Q) factors were calculated so that the structural reliability of all bridges is close to the target value, β_T.

NCHRP 454, *Calibration of Load Factors for LRFR Bridge Evaluation* (Moses 2001) presented the derivation of live load factors and associated checking criteria incorporated in the proposed *Manual for Condition Evaluation and Load and Resistance Factor Rating of Highway Bridges* prepared for NCHRP Project 12-46. A major goal in the study was to unify the reliability analyses and corresponding database used in the load and resistance factor rating (LRFR) and the recommendations for the Evaluation Manual compatible with the AASHTO LRFD bridge design specifications. Although the report considers all types of bridges, it provides no particular insight for the shear design or behavior of prestressed concrete bridges.

NCHRP 485, *Bridge Software-Validation Guidelines and Examples* (Baker et al. 2003) developed a process for bridge design and analysis software validation. The study has resulted in a test-bed of bridges with well-defined parametric inputs and outputs. This test-bed (or portions thereof) is readily usable by developers, end users, and others, and is available on CD-ROM. Using project 12-50 results, two or more software analysis packages and/or hand calculations with the same data set may be compared in tabular and/or graphical format. Project 12-50 permits drilling-down in the results to show how computations were performed and to clearly reveal differences between processes clearly. Various prestressed concrete sections were considered in the test-bed, and errors in some existing software for computing the shear in prestressed concrete girders were identified.

The objective of NCHRP 517, *Extending Span Ranges of Precast Prestressed Concrete Girders* (Castrodale and White 2004) was to address the limitations caused by the infrequent use of precast prestressed concrete girders for spans longer than 160 ft. The authors address this issue by extending the practical use of prestressed concrete girders to longer spans and to applications not normally associated with precast prestressed concrete girder construction. The major goal of the research was to provide a design procedure for long span precast, prestressed girders. Suggested design details and examples are presented. Particular attention was given to the effects of splicing long girders on shear and shear transfer through joints, with the interface shear at bent caps of interest.

NCHRP 549, *Simplified Shear Design of Structural Concrete Members* (Hawkins et al. 2005) developed simplified shear design provisions for the AASHTO LRFD Bridge Design Specifications that attempted would overcome perceived difficulties with using the previous shear

design provisions, which were the provisions of the Sectional Design Model. The detailed provisions recommended by this project were described earlier in this report.

NCHRP 579, *Application of LRFD Bridge Design Specifications to High-Strength Structural Concrete: Shear Provisions* (Hawkins and Kuchma 2007), proposed guidelines to allow the use of concrete strengths greater than 10 ksi, up to 18 ksi, for shear design. It addressed the compression angle θ; the proper concrete strength contribution to shear strength; minimum shear reinforcement; and maximum shear limits. It was found that the existing LRFD values for θ, β, and minimum shear reinforcement were safe to use for high strength concrete, but the maximum shear stress limit requires restriction.

In report NCHRP 654, *Evaluation and Repair Procedures for Precast/Prestressed Concrete Girders with Longitudinal Cracking in the Web* (Tadros et al. 2010), a user's manual was established for the acceptance, repair, or rejection of precast/ prestressed concrete girders with longitudinal web cracking. The cracks of concern occur in the end zone as a result of prestress transfer, and may result in debonding and increased corrosion. Experimental tests determined that girder shear capacities were larger than estimated by code design procedures even with the longitudinal cracks present. The report proposes revisions to the AASHTO LRFD Bridge Design Specifications and provides recommendations to develop improved crack control reinforcement details for use in new girders. To achieve this objective, guidelines were established for various cracking categories such as: cracks that are not required to be repaired, cracks that are required to be repaired, including the methods and materials of repair, and cracks that cause structural capacity to be compromised and thus may cause the girders to be rejected.

Additional objectives were to propose revisions to the AASHTO LRFD Bridge Design Specifications as warranted, and to develop improved crack control reinforcement details for use in new girders.

NCHRP 678, *Design of FRP Systems for Strengthening Concrete Girders in Shear* (Belarbi et al. 2011) develops recommendations for a design method that can be used to strengthening concrete girders in shear using externally bonded FRP systems. It was found that beams with existing shear cracks displayed stirrup yield at a lower shear force than beams that did not have cracks, and limiting stirrup stress to the yield stress will avoid fatigue failures in the girder.

NCHRP 700, *A Comparison of AASHTO Bridge Load Rating Methods* (Mlynarski et al. 2011) compared the load factor rating to load and resistance factor ratings for various design vehicles. It provides proposals for changes to the AASHTO *Manual for Bridge Evaluation* through the extensive data analysis of 1,500 bridges of varying material types and structure configurations. The bridges were analyzed using the AASHTO Ware Virtis software (Thompson, 1999). It was found that a significant number of the girders analyzed achieved favorable LFR ratings but had LRFR ratings less than 1.0. This occurred because LRFR included evaluation criteria not covered by LFR that in fact governed the rating, though these criteria did not include prestressed concrete girder shear strength checks. However, for concrete structures, the suggested evaluation provisions include a check for shear capacity when the factored load effects from the permit load exceed the factored load effects from the design load, which was not previously included under LFR. Concrete bridges that show no visible signs of shear problems need not be checked for shear when rating for design or legal loads, however. Revisions to load factors for permit vehicles were suggested to increase the target reliability index to 3.5

CHAPTER 2: EXPERIMENTAL STUDY

2.1 Lap Testing Setup

Two full-scale AASHTO Type II girders were tested in controlled conditions under various load configurations. The objective of this testing was to collect the experimental information necessary for development of a reliable numerical model (see Chapter 3). Each girder was approximately 36 ft long, and was tested three times at three different locations of the span by adjusting support locations, to generate data for different critical shear span-to-depth ratios and stirrup spacings. For each girder, the portion of the span which was to be preserved for subsequent testing was externally clamped with vertical steel bars to prevent shear damage in this region during the prior tests as shown in Figure 2.1.

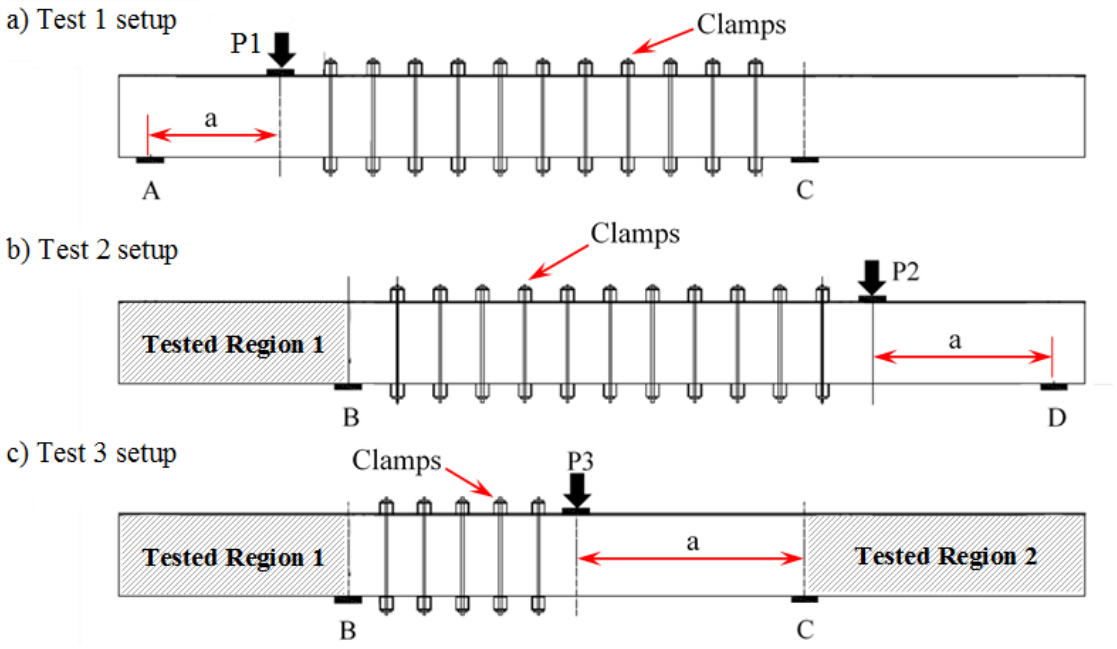

Figure 2.1. Tested spans for each girder

The tested Girders were instrumented with strain gages on transverse steel stirrups, an Optotrack marker grid for measuring displacements on the Girder exterior in the critical shear

region, as well as potentiometers at supports and near the load location at the bottom of the girder, as shown in Figure 2.2.

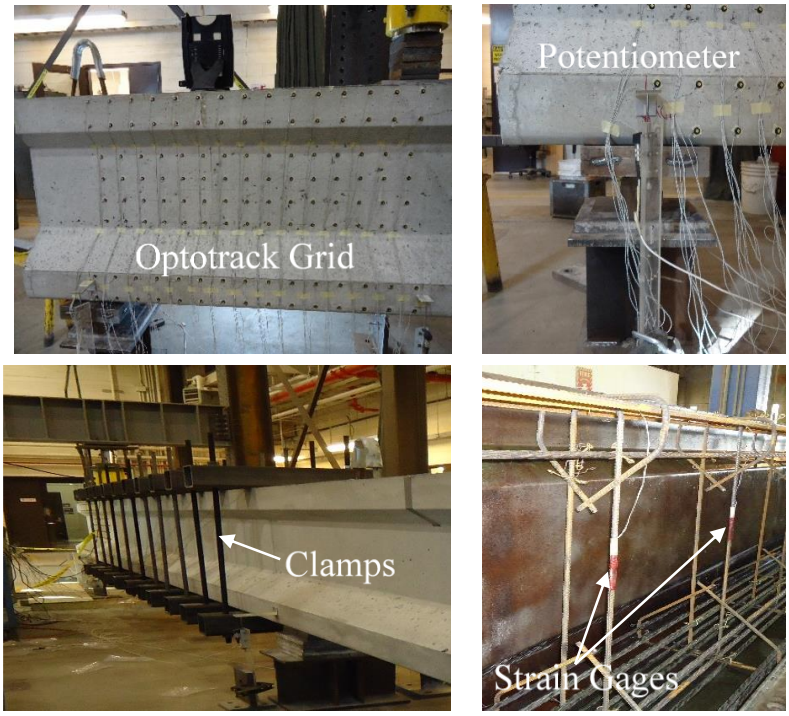

Figure 2.2. Lab test instrumentation

During the testing of each girder, a monotonic point load was applied using a hydraulic actuator resting on a 6 inch long steel plate centered at a distance "a" from the support. Initially, load was applied at 20 kip increments until cracks were observed. After major cracks developed, the load was slowly increased until failure. A summary of the critical girders' parameters is given in Table 2.1, where "a" is the load location measured from the support, "d*"* is the effective strand depth, and "S*"* is the stirrups spacing.

Table 2.1. Summary of the tested girders parameters

	Test	*S* (in)	*a/d*
Girder 1	1	8.0	2.8
	2	8.0	3.4
	3	21.0	3.4
Girder 2	1	21.0	2.0
	2	21.0	2.8
	3	21.0	3.5

2.2 Girder 1

The first Girder was cast at Stress-Con Industries (Kalamazoo, MI), and transported to the University of Michigan Civil and Environmental Engineering Structures Lab for testing. The casting specification sheet is given in Appendix A. The layout for Girder 1 is shown in Figure 2.3, where the load (*P1, P2, P3*) and support (*A, B, C, D*) positions for each test are summarized, as well as stirrup spacing and location of strain gages.

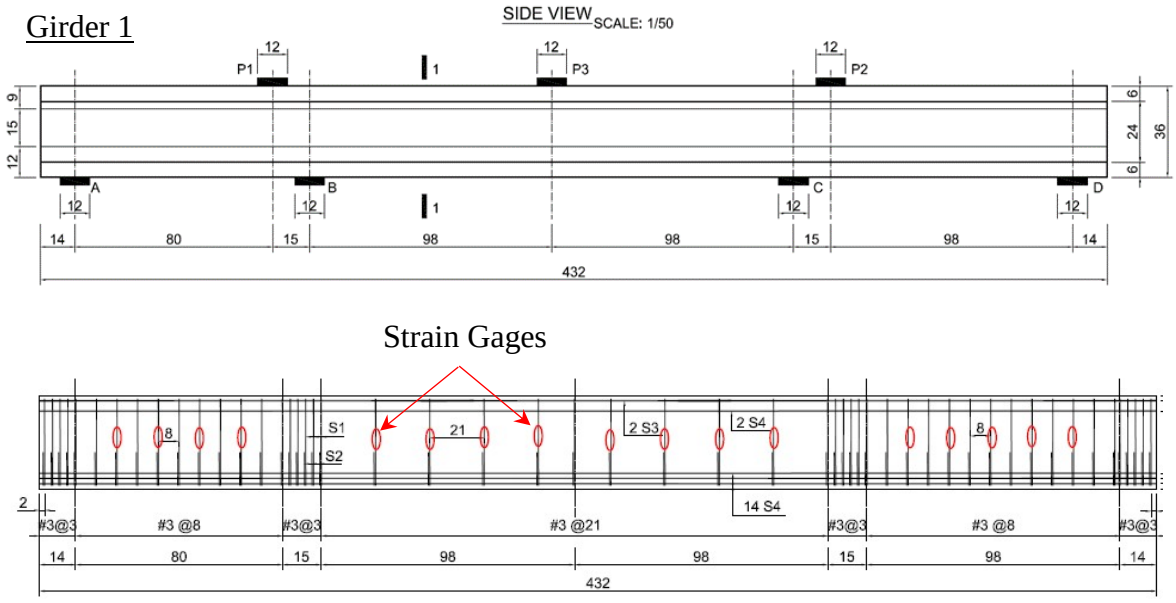

Figure 2.3. Girder 1 layout and strain gage location (dimensions in inches)

Reinforcement details, as well as cross section of Girder 1 are shown in Figure 2.4. Pre-stressed steel reinforcement consisted of sixteen 1/2 in. dia., seven-wire, Grade 270, low-relaxation strands with a total area of 2.4 in^2 (labeled as S4). Mild steel reinforcement consisted of two Grade 60 bars (labeled as S3) with a total area of 0.4 in^2 at the top flanges of Girder. Transverse reinforcement consisted of #3 double leg stirrups with an area of 0.22 in^2 (labeled as S1). Concrete had an average compressive strength of approximately 8 ksi with a coarse aggregate having a maximum-size of 0.75 in.

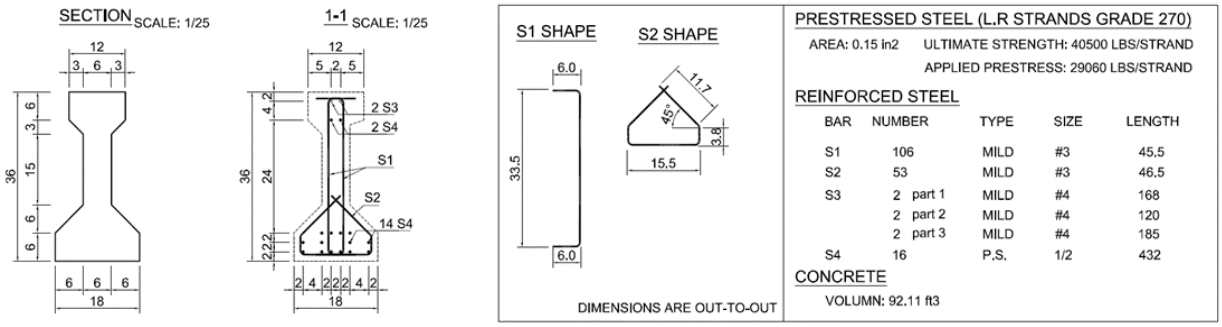

Figure 2.4. Girder 1 cross section (dimensions in inches)

Girder 1-Test 1

For test 1, the girder was supported and loaded as shown in Figure 2.5.

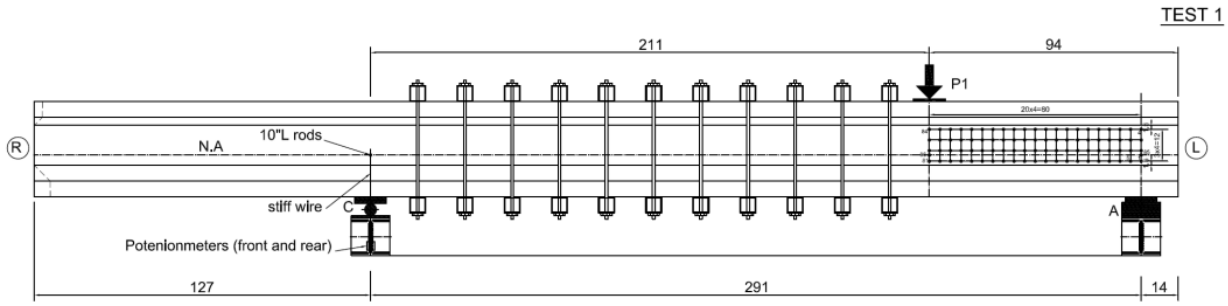

Figure 2.5. Girder 1-Test 1 Configuration (dimensions in inches)

Five concrete cylinders were tested on test day, with results shown in Table 2.2. Note that the mean strength (7.6 ksi) is substantially higher than the 5.5 ksi as specified in the design.

Table 2.2. Girder 1-Test 1 cylinder compressive strength tests

Cylinder	Failure	Stress (psi)	% from Mean
1	76.1	6057	-20.8
2	115.9	9222	20.6
3	88.9	7072	-7.5
4	109.0	8670	13.4
5	90.7	7219	-5.6
Mean	96.1	7648	-

The test results are summarized in Figures A1-A4 (Appendix A). The first cracking load occurred at approximately 180 kips (Figure A1); flexural cracks appeared at approximately 280 kips (Figure A2); and failure occurred at approximately 300 kips (Figures A3 and A4).

Girder 1-Test 2

For test 2, the girder was supported and loaded as shown in Figure 2.6.

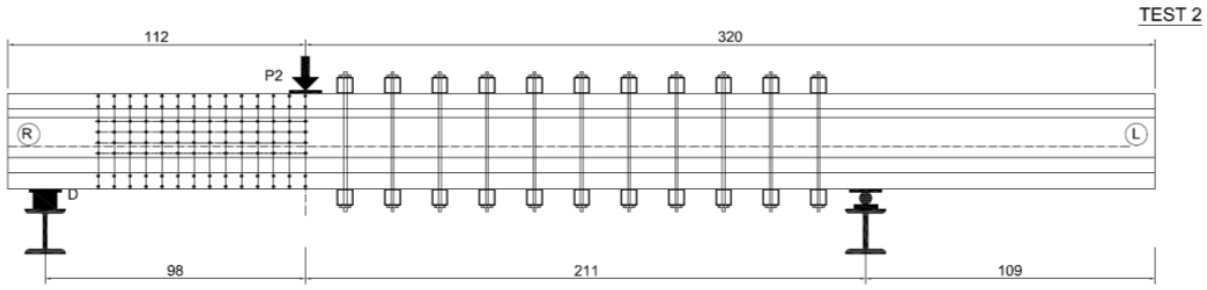

Figure 2.6. Girder 1-Test 2 configuration (dimensions in inches)

Concrete cylinder strength test results on the test date are given in Table 2.3.

Table 2.3. Girder 1-Test 2 cylinder compressive strength tests

Cylinder	Failure	Stress (psi)	% from Mean
1	81.5	6482	-17.7
2	120.3	9572	21.6
3	105.7	8414	6.9
4	86.3	6863	-12.8
5	101.0	8038	2.1
Mean	99	7874	-

The test results are summarized in Figures A5-A7 (Appendix A). First cracking load occurred at approximately 200 kips (Figure A5). Figure A6 shows the Girder response before failure, while failure occurred at approximately 265 kips (Figure A7).

Girder 1-Test 3

For test 3, the Girder was supported and loaded as shown in Figure 2.7.

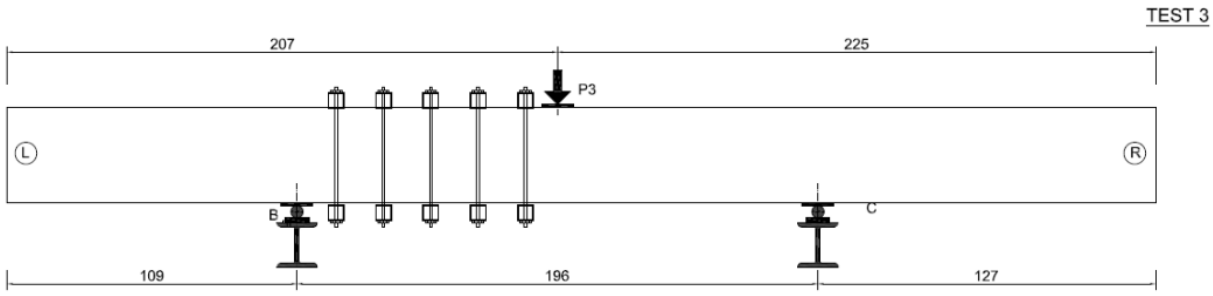

Figure 2.7. Girder 1-Test 3 configuration (dimensions in inches)

Concrete cylinder strength test results on the test date are given in Table 2.4.

Table 2.4. Girder 1-Test 3 cylinder compressive strength tests

Cylinder	Failure	Stress (psi)	% from Mean
1	106.3	8455	-1.9
2	112.3	8933	3.6
3	94.4	7513	-12.9
4	127.2	10125	17.4
5	101.6	8081	-6.3
Mean	108.3	8622	-

The test results are summarized in Figures A8-A10 (Appendix A). The first cracking load occurred at approximately 220 kips (Figure A8), while failure occurred at approximately 355 kips (Figures A9 and A10).

2.3 Girder 2

Girder 2 was similarly cast at Stress-Con Industries. The casting specification sheet is given in Appendix A. The layout, geometry, properties and instrumentation of Girder 2 are similar to those in Girder 1 as shown in Figure 2.8.

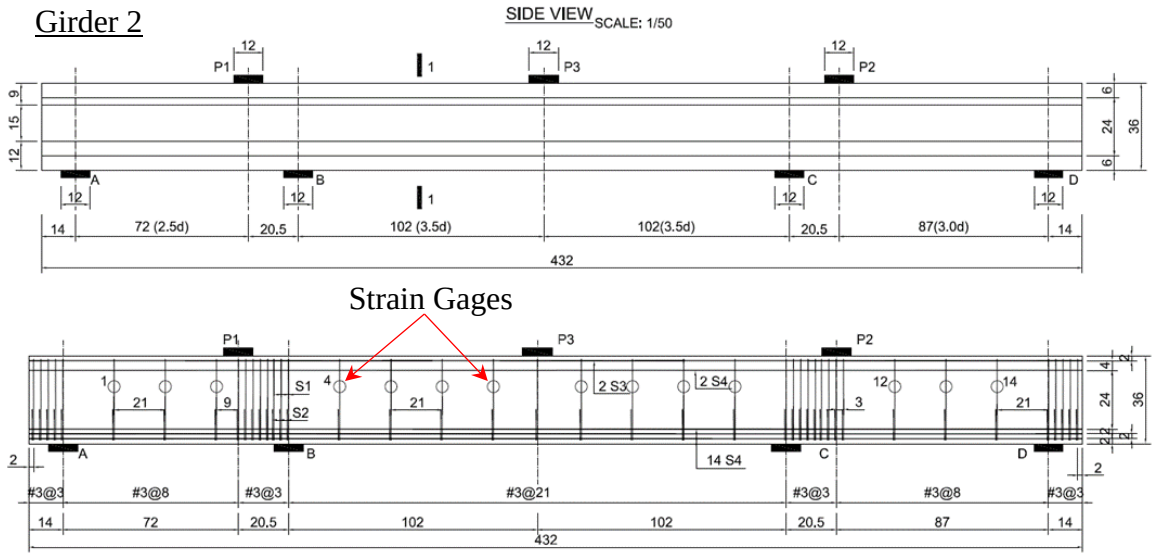

Figure 2.8. Girder 2 layout and strain gage locations (dimensions in inches)

Reinforcement details, as well as cross section of Girder 2 are shown in Figure 2.9. Pre-stressed steel reinforcement consisted of sixteen 1/2 in. dia., seven-wire, Grade 270, low-relaxation strands with a total area of 2.4 in^2 (labeled as S4). Mild steel reinforcement consisted of four #4 Grade 60 bars (labeled as S3) with a total area of 0.8 in^2 at the top flanges of Girder 2. Transverse reinforcement consisted of #3 double leg stirrups with an area of 0.22 in^2 (labeled as S1). Concrete had an average compressive strength of approximately 9.2 ksi with a coarse aggregate having a maximum-size of 0.75 in.

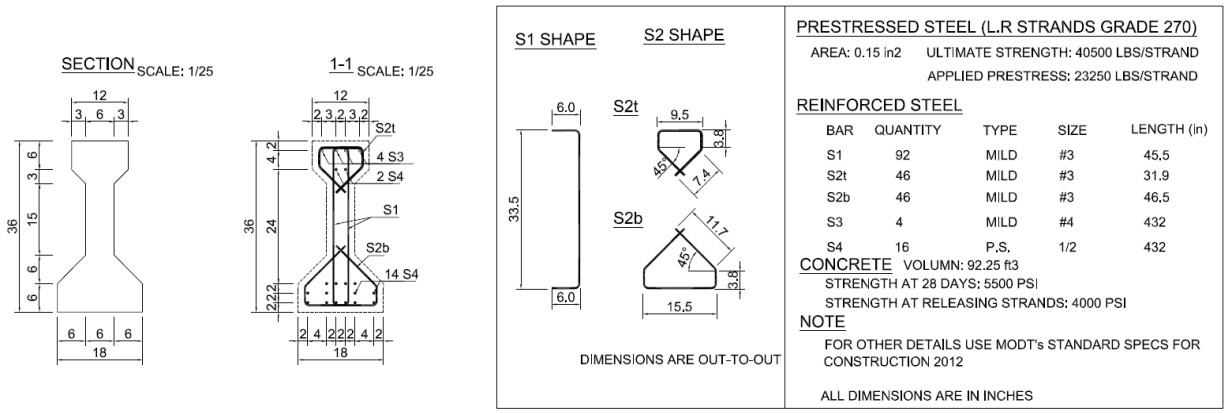

Figure 2.9. Girder 2 cross section details (dimensions in inches)

Girder 2- Test 1

For Test 2, the girder was supported and loaded as shown in Figure 2.10.

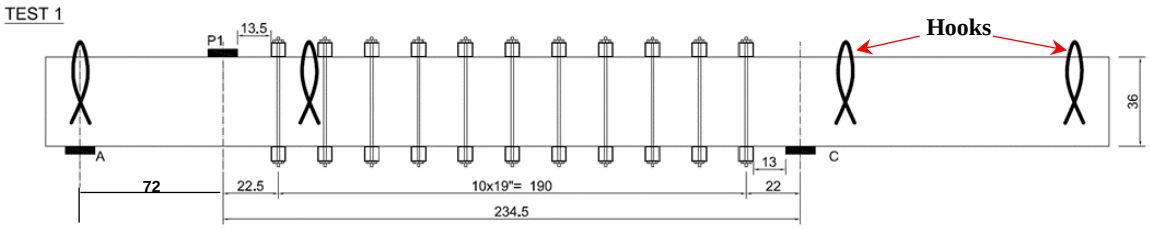

Figure 2.10. Girder 2 Test 1 configuration (dimensions in inches)

Five concrete cylinders were tested on test day, with result shown in Table 2.5.

Table 2.5. Girder 2-Test 1 cylinder compressive strength tests

Cylinder	Failure Load	Stress (psi)	% from Mean
1	120.4	9579.5	4.8
2	110.0	8754.2	-4.2
3	115.6	9196.0	0.8
4	123.0	9788.7	6.8
5	104.0	8274.5	-10.2
Mean	114.6	9118.6	-

The test results are summarized in Figures A11 and A12 (Appendix A). Similar to Girder 1-Test 1, first cracking load occurred at approximately 180 kips (Figure A11). For safety concerns,

the test was stopped at 294 kips, due to localized concrete crushing under the load point, indicating impending failure based on previous test results (Figure A12).

Girder 2-Test 2

For Test 2, the girder was supported and loaded as shown in Figure 2.11.

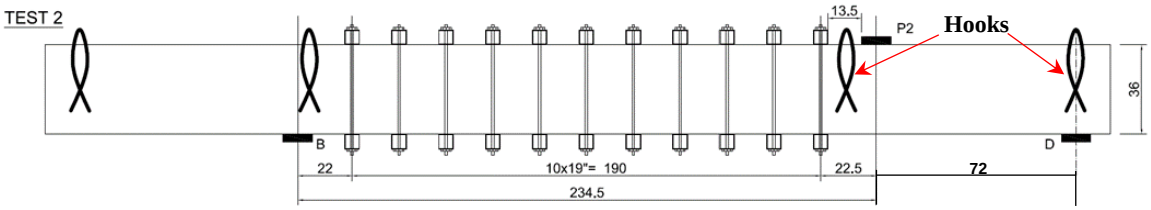

Figure 2.11. Girder 2-Test 2 configuration (dimensions in inches)

Concrete cylinder strength test results on the test date are given in Table 2.6.

Table 2.6. Girder 2-Test 2 cylinder compressive strength tests

Cylinder	Failure	Stress (psi)	% from Mean
1	126.5	10065	8.7
2	119.1	9475	3.0
3	101.2	8056	-14.0
4	130.6	10388	11.6
5	104.4	8307	-10.6
6	111.0	8835	-4.0
Mean	115	9188	-

The test results are summarized in Figures A13-A16. The first cracking load occurred at approximately 175 kips (Figure A13); flexural cracks appeared at approximately 200 kips (Figure A14); and failure occurred at approximately 267 kips (Figures A15 and A16).

Girder 2-Test 3

For Test 3, the girder was supported and loaded as shown in Figure 2.12, and three concrete cylinders were tested on test day, with results shown in Table 2.7.

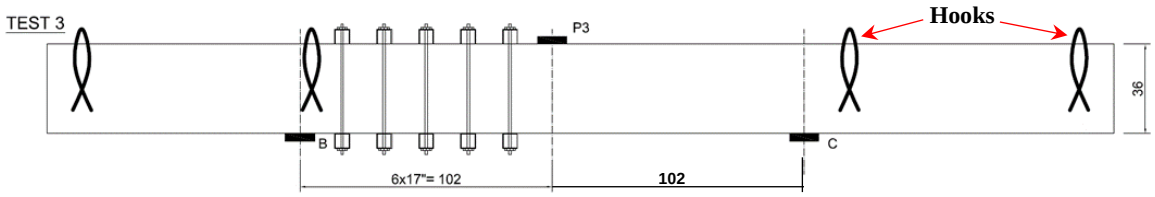

Figure 2.12. Girder 2-Test 3 configuration (dimensions in inches)

Table 2.7. Girder 2-Test 3 cylinder compressive strength tests

Cylinder	Failure Stress (psi)		% from Mean
1	126.6	10074	8.6
2	112.1	8921	-3.3
3	108.6	8639	-6.6
Mean	116.8	9211	-

The test results are summarized in Figures A17 and A18. The first cracking load occurred at approximately 220 kips. For safety concerns, the test was stopped near impending failure at 273 kips. A summary of all test results and the code-predicted capacity is given in Table 2.8. Note for the LRFD Code computation, the test failure load is taken as V_u. However, for comparison to the test girders, it was found that more accurate results can be obtained with the method by iterating until V_n=V_u. An example using this iterative method is provided in Appendix E.

Table 2.8. Summary of test results

	Test	S (in)	a/d	f'_c (ksi)	Failure Load	Standard	1979	LRFD
Girder 1	1	8.0	2.8	7.5	299	167	154	147
	2	8.0	3.4	7.8	262	168	157	148
	3	21.0	3.4	8.6	356	141	112	105
Girder 2	1	21.0	2.0	9.2	294	143	117	108
	2	21.0	2.8	9.2	271	143	117	108
	3	21.0	3.5	9.2	273	143	117	108

CHAPTER 3: FINITE ELEMENT MODELING OF SHEAR FAILURE

3.1 Methodology

In order to develop and test a tool that can accurately predict the shear capacity of pre-stressed concrete beams, a numerical model that is constructed based on reliable and precise experimental parameters was required. In this chapter, the development and validation of a FEA model to predict the shear capacity of prestressed concrete bridge girders are presented. Validation of the FEA model was achieved by comparing numerical results to the experimental results presented in Chapter 2, as well as a collection of independent beam tests documented in the technical literature. In this study, VecTor2 (Wong et al., 2013) FEA code was considered for modeling and computing the shear capacity of prestressed concrete girders presented in Chapter 2. This FEA code has been developed at the University of Toronto by researchers studying reinforced concrete behavior and applications of the finite element method. VecTor2 is a program based on the Modified Compression Field Theory (MCFT) (Vecchio and Collins, 1986) and the Disturbed Stress Field Model (DSFM) (Vecchio, 2000) for nonlinear finite element analysis of two-dimensional reinforced concrete membrane structures. Using VecTor2, finite element models with fine mesh can be constructed. The cracked concrete behavior can be modeled by VecTor2 as an orthotropic material with smeared rotating cracks. This methodology is applicable for reinforced and prestressed concrete structures that require a relatively fine mesh to model reinforcement details and local crack patterns.

3.1.1 Modified Compression Field Theory and Disturbed Stress Field Model:

The MCFT is an analytical model for predicting the load-deformation response of reinforced concrete membrane elements subjected to shear and normal stresses shown in Figure 3.1.

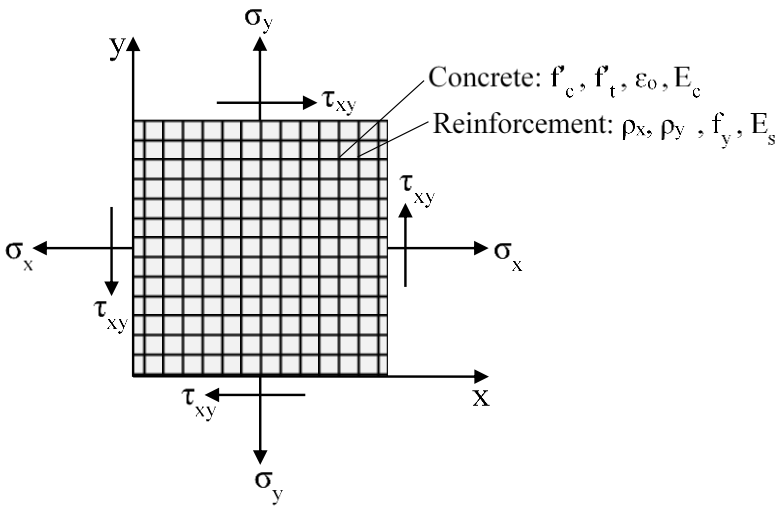

Figure 3.1. Reinforced concrete membrane element subject to in-plane stresses (Wong et al., 2013)

Using the MCFT, average and local strains and stresses of concrete and reinforcement, and the widths and orientation of cracks throughout the load-deformation response of the element are determined. Based on history of stresses, strains, and cracks, the failure mode of the element can be determined (Wong and Vecchio 2002).

The DSFM is conceptually similar to the MCFT, but extends the MCFT in several respects. Most importantly, the DSFM addresses systematic deficiencies of the MCFT in predicting the response of certain structures and loading scenarios. In lightly reinforced elements, where crack shear slip is significant, the rotation of the principal stress field tends to lag the greater rotation of the principal strain field. For such elements, the shear stiffness and strength is generally overestimated by the MCFT, which assumes the rotations are equal. Conversely, in elements that exhibit limited rotation of the principal stress and strain fields, the MCFT generally underestimates the shear stiffness and strength, partly because the concrete compression response calibrated for the MCFT is overly softened for the effect of principal tensile strains. The DSFM enhances the compatibility relationships of the MCFT to include crack shear slip deformations. The strains due to these deformations are distinguished from the strains of the concrete continuum due to stress.

As such, the DSFM unlocks the orientation of the principal stress field from that of the principal strain field, resulting in a smeared delayed rotating-crack model. Moreover, by explicitly calculating crack slip deformations, the DSFM eliminates the crack shear check as required by the MCFT (Wong and Vecchio 2002).

3.1.2 Material Models

The concrete model uses Hognestad's parabola for compressive pre-peak behavior, and modified Park-Kent relationship for post-peak as shown in Figure 3.2. Compression softening is governed by Vecchio's *e1/e2*-Form approach (Vecchio and Collins 1993) and a modified Bentz model for tension stiffening (Bentz 2000). Linear tension softening is assumed, while confined strength is described by Kupfer/Richart (Kupfer et al. 1969) and dilation by the variable Kupfer model (Kupfer and Gerstle 1973). Mohr-Coulomb failure criteria is used to determine cracking stress, with stress calculated from DSFM/MCFT. The crack slip calculation is according to the Walraven (monotonic) approach (Walraven 1981), while the crack width check is the *Agg*/2.5 Max Crack Width method, which reduces average compressive stresses when crack widths exceed a specified limit, and is useful for beams with minimal shear reinforcement (Vecchio, 2000). Concrete bond is given by Eligenhausen et al. (1983). Additional details can be found in Wong and Vecchio (2002).

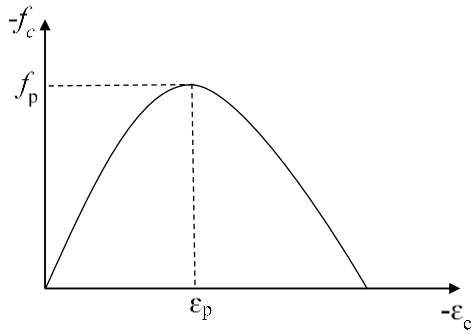

Figure 3.2. Hognestad parabolic pre-and post- peak concrete compression response (Wong et al., 2013)

The reinforcement steel constitutive models are illustrated in Figures 3.3 and 3.4. In the figures, ε_s is the reinforcement strain, ε_y is the yield strain, ε_{sh} is the strain at the onset of strain hardening, ε_u is the ultimate strain, E_s is the elastic modulus, E_{sh} is the strain hardening modulus, f_y is the yield strength, and f_u is the ultimate strength, where:

$$\varepsilon_u = \varepsilon_{sh} + \frac{(f_u - f_y)}{E_{sh}} \tag{3.1}$$

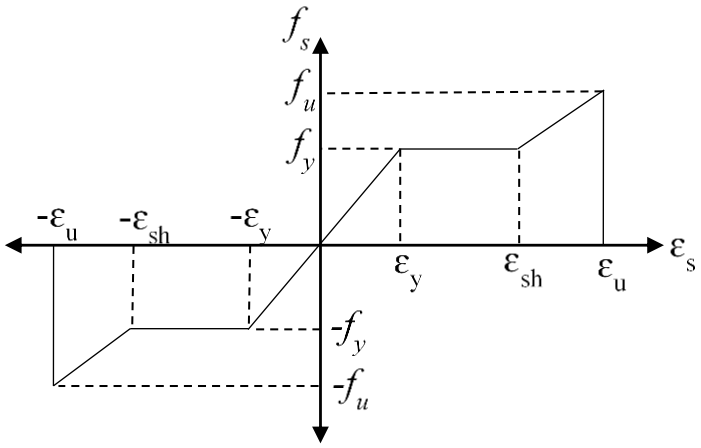

Figure 3.3. Ductile steel reinforcement stress-strain response (Wong et al., 2013)

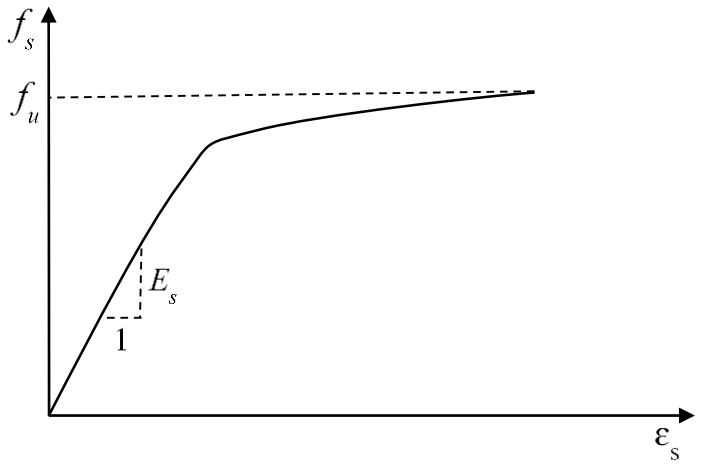

Figure 3.4. Prestressing steel reinforcement stress-strain response (Wong et al., 2013)

3.2 Verification Cases

The objective of these verification cases is to investigate the accuracy of VecTor2 in predicting the deformation and shear capacity of prestressed concrete beams.

3.2.1 Verification Data Set 1: Saqan and Frosch Tests

Very few prestressed beam shear tests were documented with sufficient detail that allows for model verification. One of the suitable sources describes a series of tests on prestressed concrete beams conducted and documented by Saqan and Frosch (2009). Three beam tests from the selected study were used for model verification; one beam included prestressed strands only, whereas the other two beams included prestressed strands and mild steel reinforcement. Beams, dimensions, and reinforcement details are summarized in Table 3.1 and Figure 3.5. Reinforcement consisted of ASTM A416, 1/2 in. (12 mm) dia., seven-wire, Grade 270, low-relaxation prestressing strands and ASTM A615, Grade 60 reinforcing bars, and with no transverse reinforcement. Concrete had compressive strength values of 7550-7750 psi (52.1-53.4 MPa). Cement was specified as ASTM C150, Type I, with a coarse aggregate maximum-size of 3/4 in. (20 mm). The effective prestress force applied to each beam was 480 kN (108 kips).

Table 3.1. Specimens Details (Saqan and Frosch, 2009)

		Mild reinforcement				
Beam ID	(#) Prestressed Strands (1/2 *in.*)	Bars	Area, $in.^2$	Width, *in.*	Effective depth of strands, $d_p, in.$	Effective depth of bars, $d, in.$
V-4-0	4	-	0	14.25	24	-
V-4-0.93	4	3 No.5	0.93	14.5	24	26.4
V-4-2.37	4	3 No.8	2.37	14.68	24	26.4

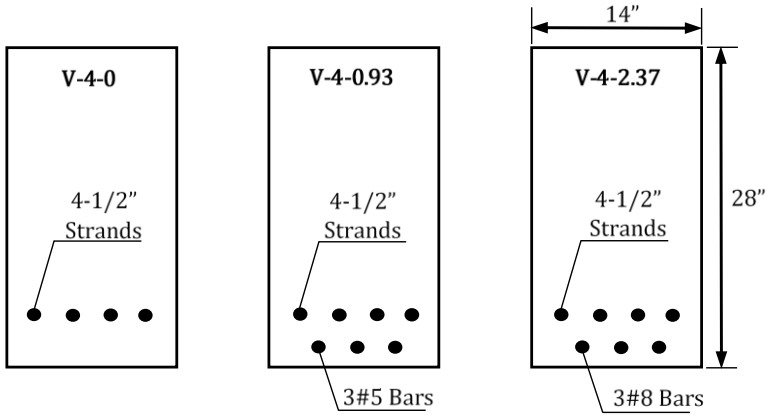

Figure 3.5. Beams cross section details (Saqan and Frosch, 2009)

The experimental test consisted of a simply supported beam with a concentrated load applied at mid-span. The beam span, loading and boundary conditions are the same for the three tests, shown in Figure 3.6.

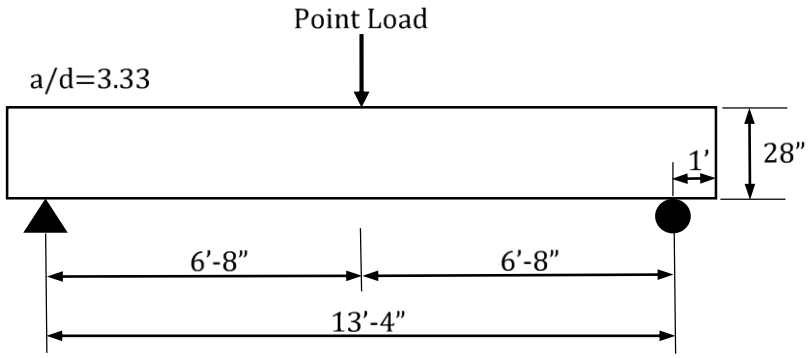

Figure 3.6. Test setup (Saqan and Frosch, 2009)

Since both, the beam loading and the boundary conditions, are symmetrical about mid-span, only half of each beam was modeled using VecTor2. The node at the support (left side) was restrained against the displacement in the transverse direction (Y direction) while the nodes at the mid span (right side) were restrained against the displacement in the longitudinal direction (X direction) as shown in Figure 3.7. Additional information on the FEA model materials and mesh details used for this verification set are presented in Appendix B.

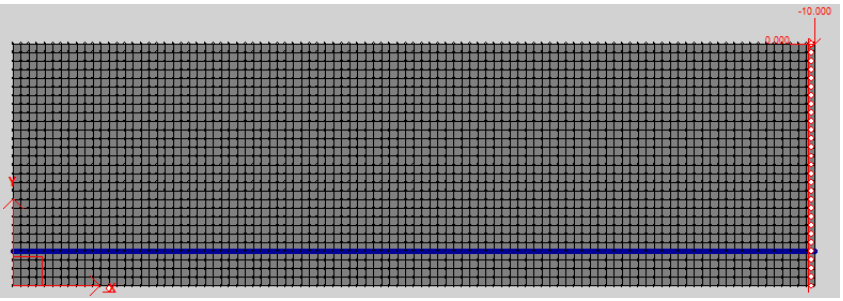

Figure 3.7. Boundary and loading conditions of the FEA model (beam V-4-0.93)

A monotonic concentrated load of 2.25 kips (10 kN) was applied at the mid-span top node (Figure 3.7) in the negative Y direction. The load was increased monotonically at a rate of 2.25 kips/step until the failure point was reached, as shown in Figures 3.8-3.10.

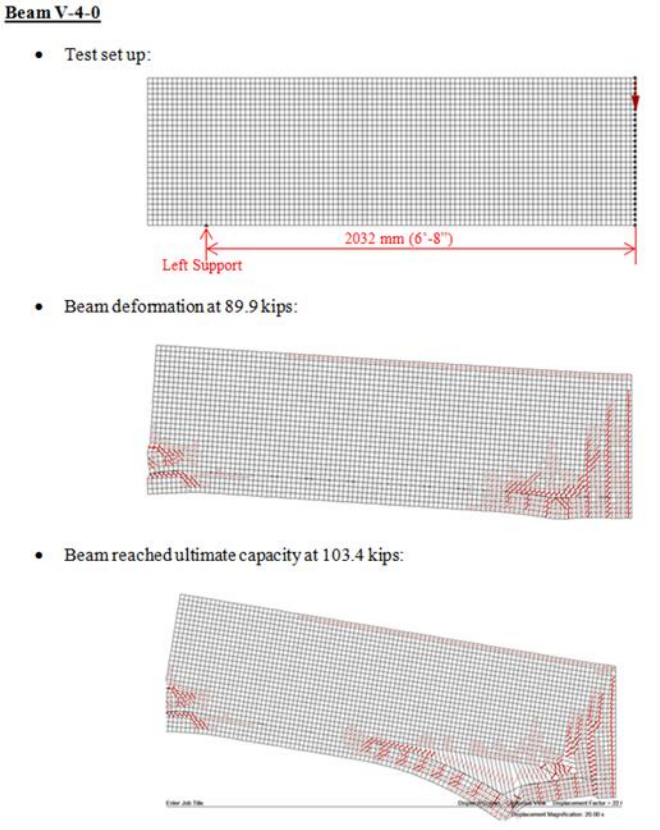

Figure 3.8. FEA model of beam V-4-0 at failure

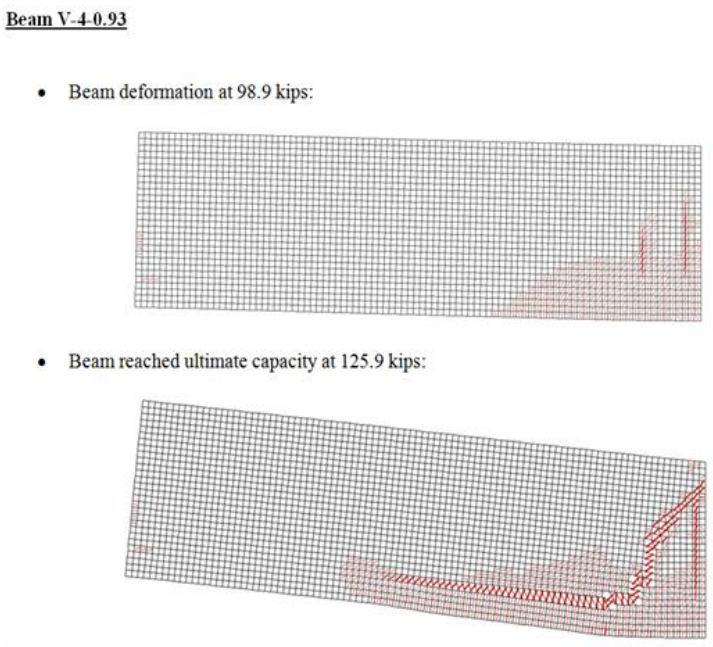

Figure 3.9. FEA model of beam V-4-0.93 at failure

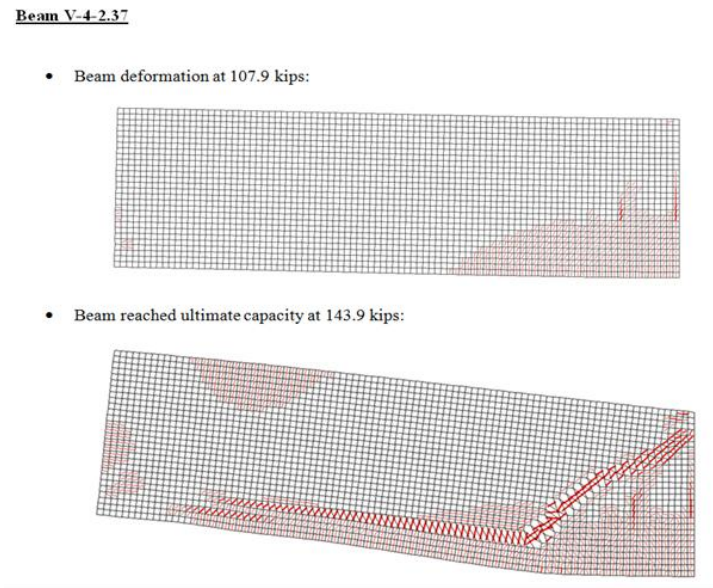

Figure 3.10. FEA model of beam V-4-2.37 at failure

Plots of the applied load vs. deflection at mid span of the experimental and the FEA models are presented in Figure 3.11, and a numerical summary is presented in Table 3.2.

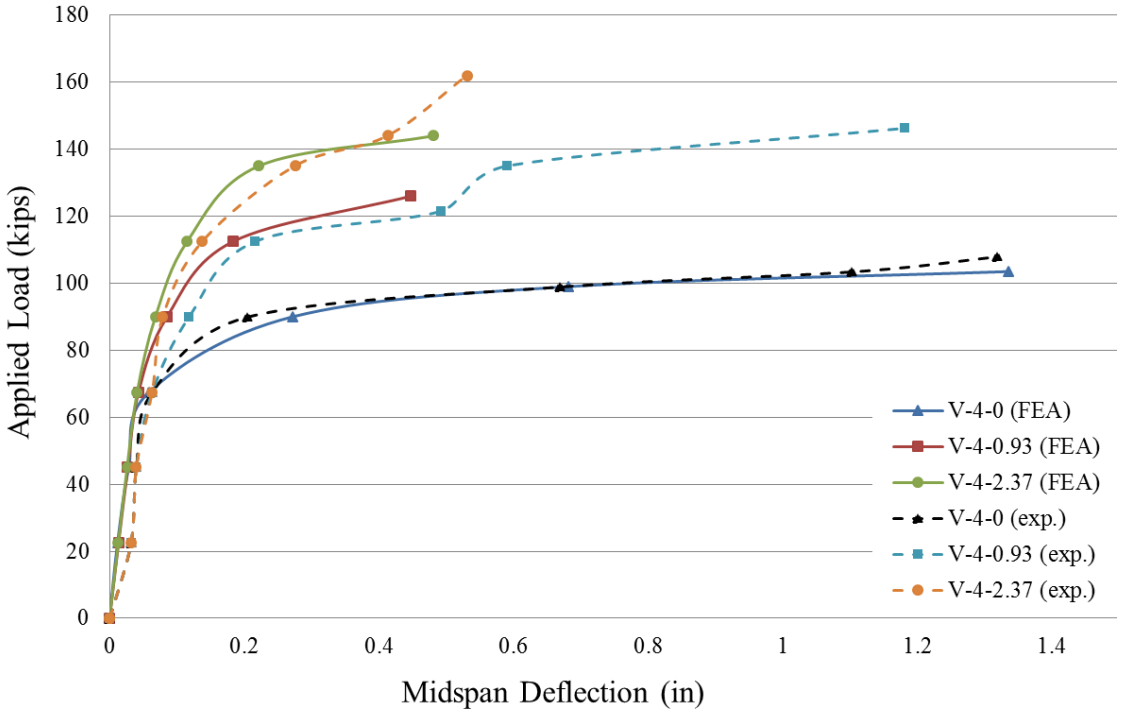

Figure 3.11. FEA vs. experimental results (Saqan and Frosch, 2009)

Table 3.2. Summary of FEA and Experimental Results

Beam #	FEA (kips)	Exp. (kips)	FEA/Exp.
V-4-0	103	110	0.94
V-4-0.93	126	150	0.84
V-4-2.37	144	165	0.87

As shown in the Figure 3.11, excellent results have been obtained for each of the three beam tests using the FEA models, with very close response throughout the load-deflection profile, as well as the ultimate capacity. The FEA model successfully predicted the ultimate capacity of the three tested beams with an average of 88% out of the actual capacity, with lowest accuracy of 84% and 87% for Beams V-4-0.93 and V-4-2.37, respectively. Since no transverse reinforcement was considered, such differences in the results are expected. Hence, for the beams modeled for this study, VecTor2 proved to be a reliable tool in predicting the failure behavior and the ultimate shear capacity of the pre-stressed concrete beams tested by Saqan and Frosch.

3.2.2 Verification Data Set 2: Lin et al. Tests

In the study conducted by Lin et al. (2012), 18 "T" shape prestressed concrete beams were tested in shear. Four beams out of the 18 were selected for FEA modeling using Vector2. The four selected beams were 400 mm (31 in.) deep, and contained mild and prestressed steel reinforcement, as shown in Figure 3.12. Concrete strength, prestressed force, and stirrups spacing of the four selected beams are shown in Table 3.3.

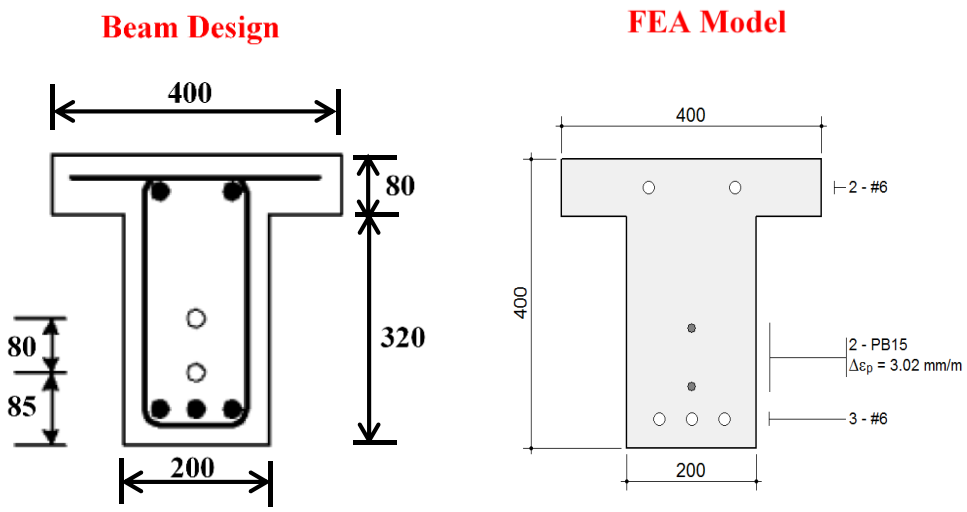

Figure 3.12. Beam cross section dimensions (mm); 1 in=25.4 mm (Lin et al., 2012)

Table 3.3. Beam Properties

Beam #	f'c (Mpa)	Pe (kN)	Concrete Stress (Mpa)	a/d	S (mm)
NC6	41.9	206	2.15	3.5	-
NC7	42.8	206.2	2.15	2.5	200
NC8	41.3	201.8	2.10	2.5	250
NC9	41.1	205.3	2.14	2.5	300

For each beam, a clear span length of 3800 mm (12'-6") was symmetrically loaded at two points as shown in Figure 3.13. The effective depth for all the beams was 275 mm (11 in.).

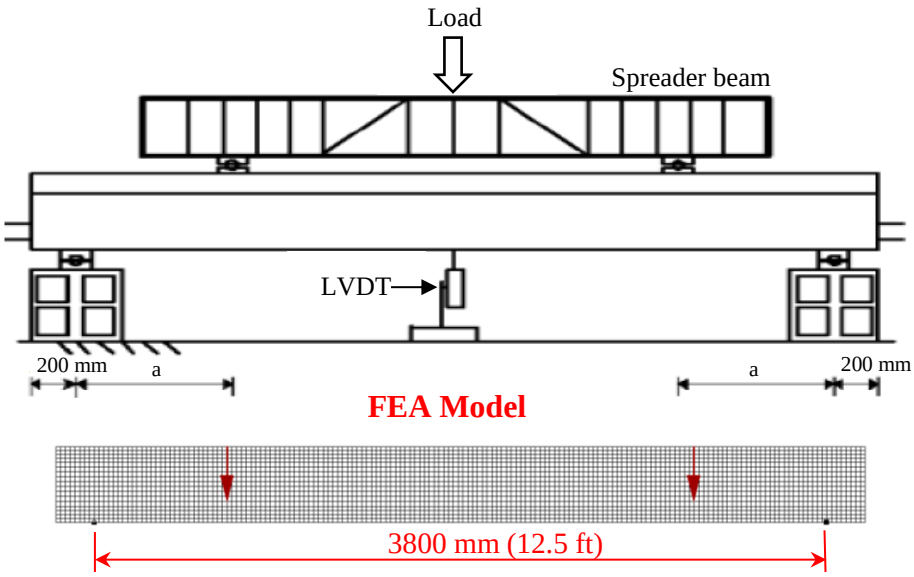

Figure 3.13. Test and FEA model setups (mm); 1 in=25.4 mm (Lin et al., 2012)

The four FEA models had a concrete strength of 41.1- 42.8 MPa (6000-6200 ksi) and a maximum aggregate size of 19 mm (¾ in.). Longitudinal reinforcement consisted of two 15 mm (0.6 in.) prestressed strands and five 19 mm (0.75 in.) mild steel bars. An average prestress force of 102.4 kN (23 kips) was applied to each strand. Transverse reinforcement consisted of 10 mm (0.39 in.) double leg mild steel stirrups spaced at 200-300 mm (8-12 in.). In this group, only beam NC6 did not contain transverse reinforcement. The yield strength, ultimate strength, and modulus of elasticity are taken as 409 MPa (60 ksi), 620 MPa (90 ksi) and 2105 MPa (30500 ksi) for the mild steel and as 1230 MPa (178 ksi), 196500 MPa (28500 ksi), and 200000 MPa (29000 ksi) for the prestressed strands, respectively. The FEA modeling technique used in the first verification set was used for modeling the beams for this study. The four beam models failed mainly in shear, and the failure shapes are shown in Figure 3.14.

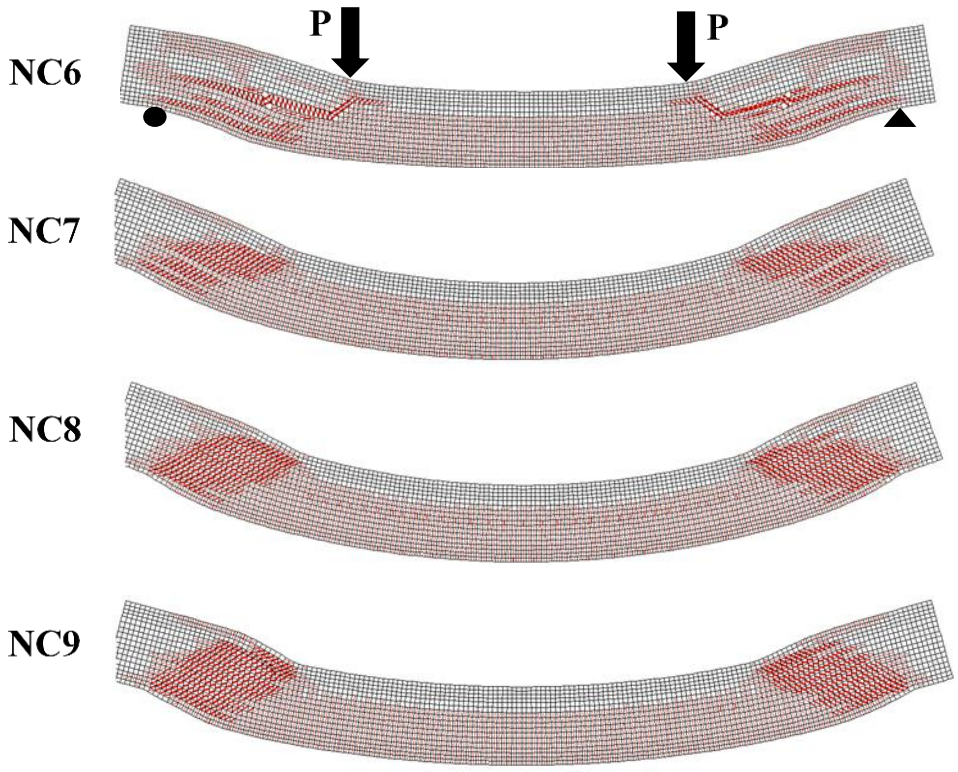

Figure 3.14. FEA models at failure

A comparison between the actual and FEA results of beam NC6 failure mode is shown if Figure 3.15. The comparison shows a very good agreement with regards to cracks propagation and failure mode.

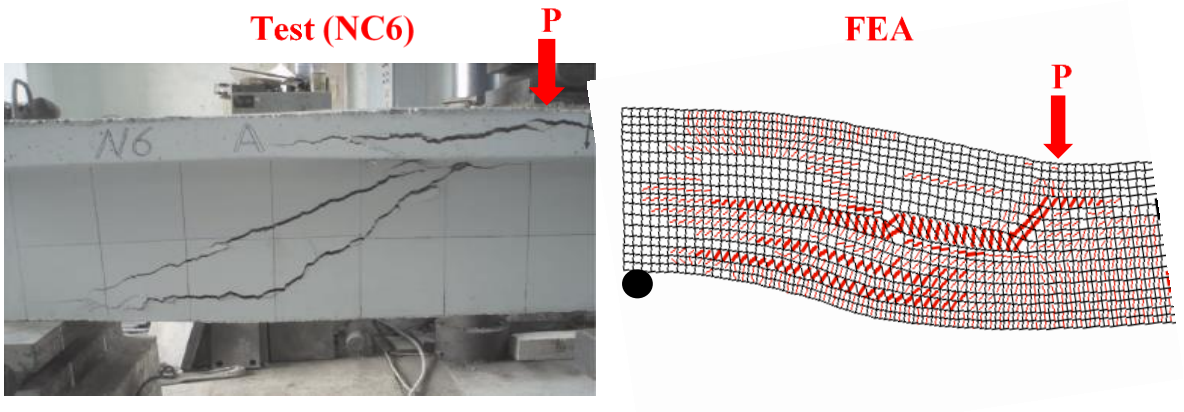

Figure 3.15. Comparison between experimental and FEA failure shapes for beam NC6 (Lin et al., 2012)

Overall, shear failure loads of the FEA and experimental results (FEA/Exp.) showed an excellent agreement with a mean value of 0.95 and a coefficient of variation (COV) of 0.036, as shown in Table 3.4. Based on results of this verification set, the developed FEA model showed to be consistent and conservative in predicting the shear capacity of T-shaped, prestressed concrete beams within an average of -5% of the actual tested capacity.

Table 3.4. Comparisons between FEA and experimental results

Beam	Shear Failure Load (kN)		
#	FEA	Exp.	FEA/Exp.
NC6	165	180	0.92
NC7	340	368	0.92
NC8	320	324	0.99
NC9	295	307	0.96
		Mean	0.95
		COV	0.036

3.2.3 Verification Data Set 3: Girder Lab Testing

Finite element models were developed and compared to the results of the two girder tests discussed in Chapter 2. For these FEA analyses two 36 feet long AASHTO Type II girders were considered for testing under various load configurations. Three tests were performed on each girder considering three different loadings (P1, P2 and P3) and three different simple span lengths. The three test setups (similar for both beams) are shown in Figure 3.16 with an illustration of the FEA model for Girder 1-Test 1.

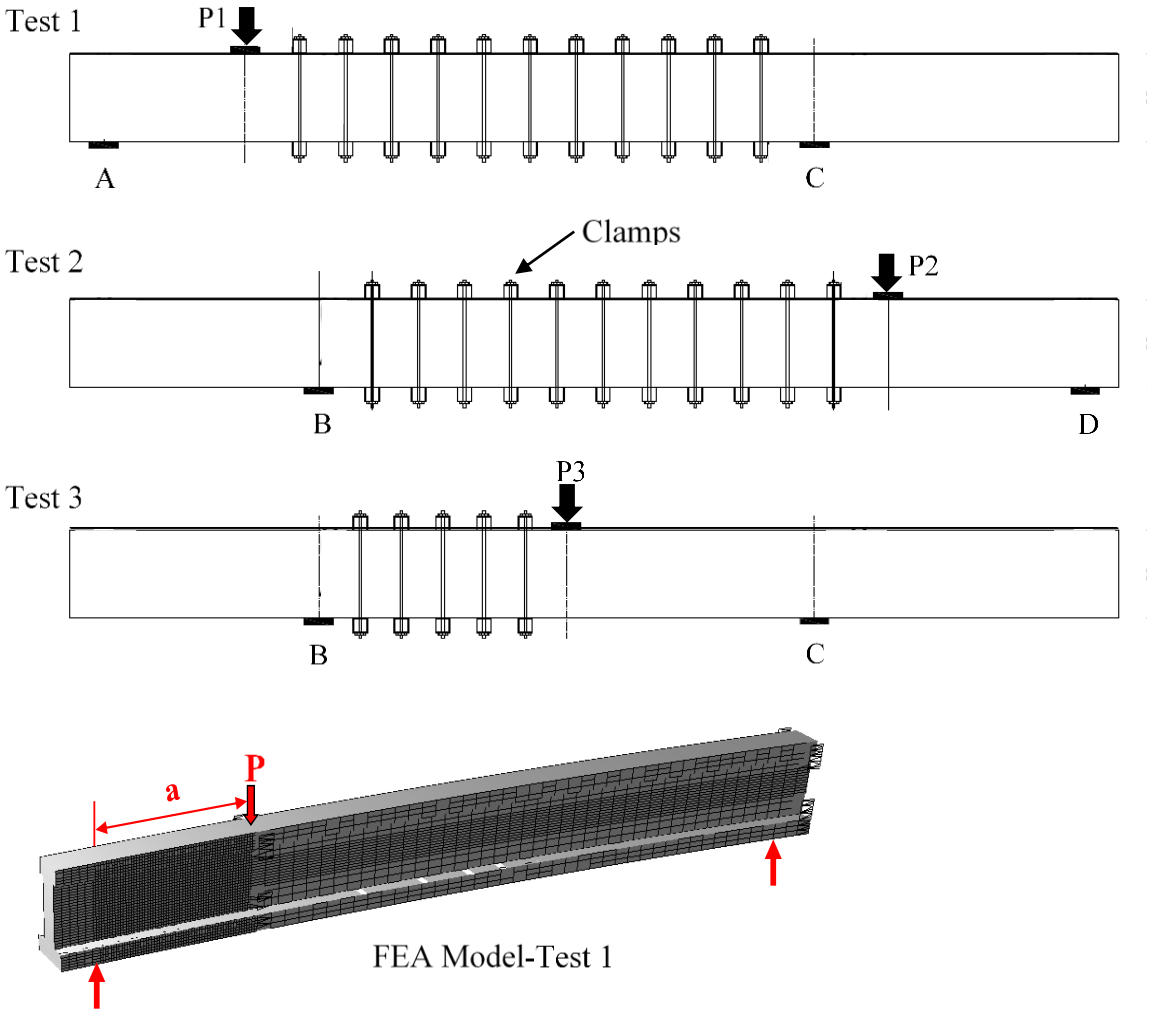

Figure 3.16. Finite element model set up

In Test 1, only the left portion of the full girder (between supports A and C) was modeled. The boundary conditions were modeled as a roller at support A, and as a pin at support C. No clamps were applied to the FEA model. Instead, the transverse reinforcement at the clamped section (Figure 3.16) was increased (approximately 3 times) to prevent any cracking along that section. Due to the elements limitation (6000 elements) in the current available version of Vector2 preprocessor (FormWorks, version 3.5), a fine mesh (1 in^2) was considered only at the section of interest where the critical shear cracks are most likely to occur. A monotonic concentrated load of 5 kN (1.1 kips) was applied along 6 inches at the P1 location (Figure 3.17) in the negative Y direction. The 5 kN was divided along the 6 inch length over7 nodes. The load was divided as follows: 2 kN (~0.5 kip) at the center node and 0.5 kN (~0.1 kip) at each of the other 6 nodes. The load was increased monotonically at a rate of 20 kN (5.5 kips)/step until the failure point was reached (the same loading scenario was used for the other two tests).

After running the analysis for the first time, the left face of the girder cracked immediately at the beginning of the analysis as shown in Figure 3.17(a). These cracks occurred as a result of the prestrain of the longitudinal reinforcement at that location. Hence, the prestress force was applied as prestrain to the longitudinal reinforcement. In order to prevent the left face from cracking, a coarse mesh with a greater concrete strength was applied at that section (beyond support). Increasing the element size at the left side of the beam greatly reduced the cracking, and resolved this issue, as shown in Figure 3.17(b).

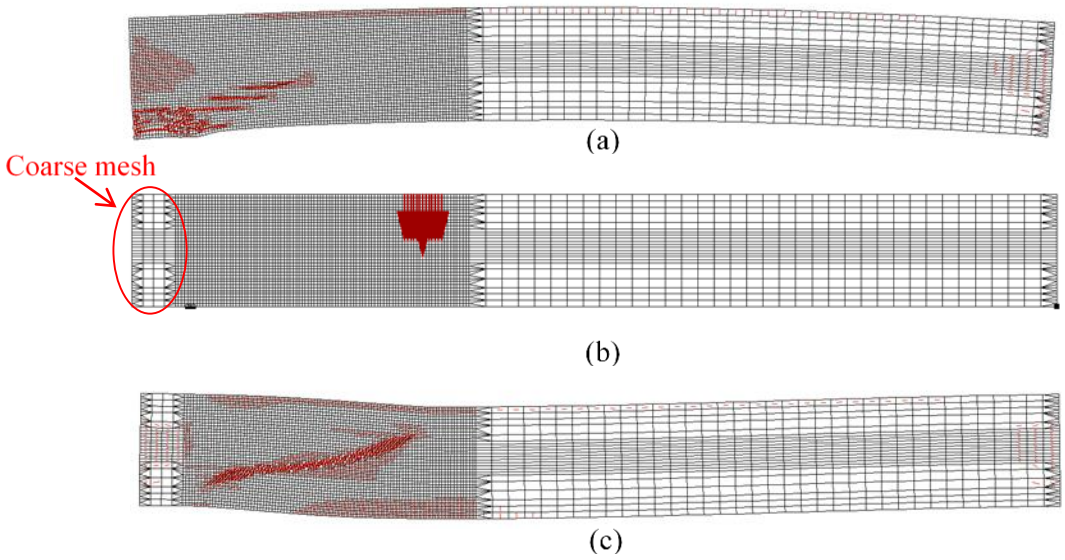

Figure 3.17. Girder 1-FEA 1 results: (a) fine mesh at the left face (b) coarse mesh at the left face (c) deformation shape at failure.

In Test 2, only the right span of the full girder (between supports B and D) was modeled as shown in Figure 3.18. The boundary conditions consisted of a pin at support B (left) and a roller at support D (right). The transverse reinforcement at the clamped section (Figure 3.16) was increased (approximately 3 times) to prevent any cracking along that section.

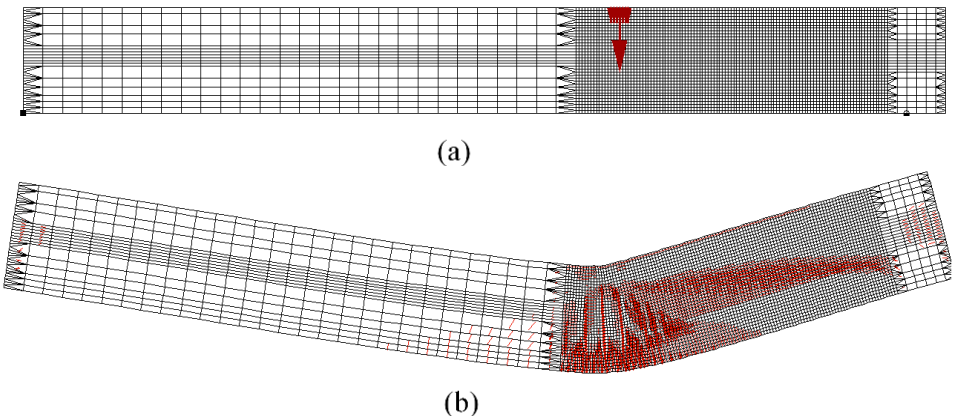

Figure 3.18. Girder 1-FEA 2 results: (a) Beam at rest (b) Deformation shape at failure

In Test 3, the portion of the girder between supports B and C was considered for analysis. After running the analysis and prior to failure, large horizontal cracks propagated around and above the right support location. These cracks greatly reduced the capacity of the girder as shown in Figure 3.19.

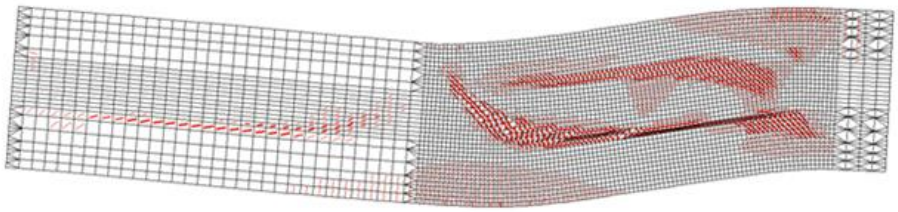

Figure 3.19. Girder 1-FEA 3 beam at failure at 279.9 kips

Based on the failure mode in Test 3, a modified cross section for the Type II girder was modeled. The purpose of this modification was to minimize the propagation of longitudinal cracks caused by the prestress force at the sloped areas of the girder. In the modefied model, the sloped cross sectional area of the web was distributed along the height of the web, resulting in a wider web section compared to the original model, as shown in Figure 3.20. The results of the new model showed a better agreement with the experimental results.

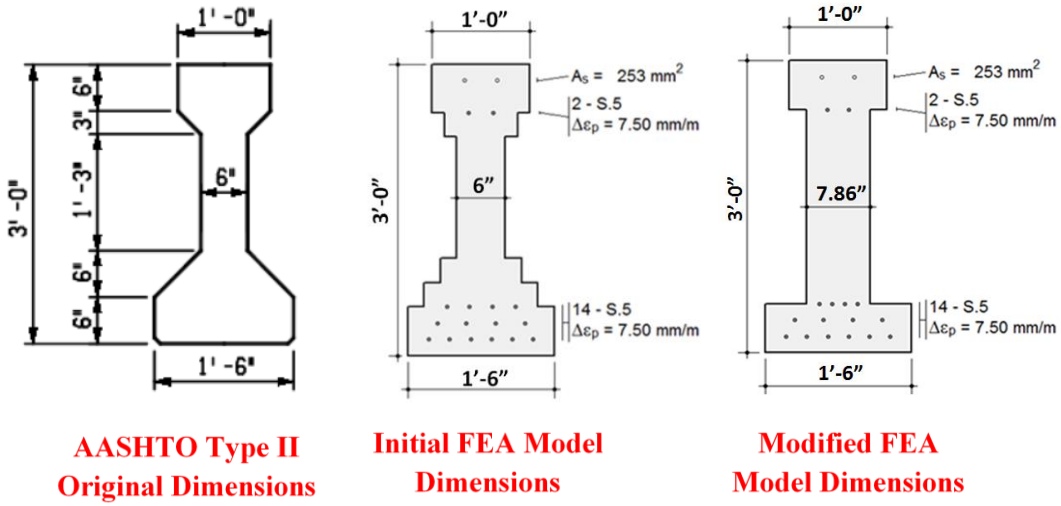

Figure 3.20. Girder Type II dimensions modification

FEA results for the modified beam section produced a better shear failure capacity prediction compared to the experimental results. Shear failure behaviors for the modified model for Girder 1 are shown in Figure 3.21.

Test 1-Modified Model (7.5 KSI):

Failure at 266.4 kips

Test 2 Modified Model (7.8 KSI):

Failure at 239.4 kips

Test 3 Modified Model (8.6 KSI):

Failure at 337.2 kips

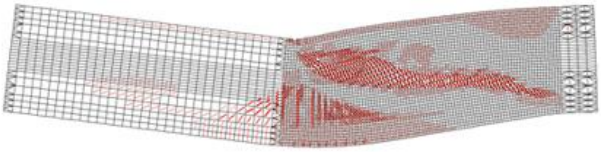

Figure 3.21. Girder 1 modified FEA models at failure

Using the same FEA technique developed, three tests for Girder 2 were conducted. Model details and results of the FEA models for both girders are given in Appendix B, and the results of the 6 tests are summarized in Table 3.5 and Figures 3.22 and 3.23.

Table 3.5. Summary of FEA model/experimental results

							Failure Load (kips)					
Girder ID	Test	f'c (ksi)	Stress (ksi)	Height (in)	S (in)	a/d	Original FEA	Modified FEA	Exp.	% (O/E)	% (M/E)	Failure Mode
1	1	7.5	1.39	36	8.0	2.8	265.3	266.4	298.9	-12.7	-12.2	S-C
1	1	9.2	1.39	36	8.0	2.8	277.6	278.8	298.9	-7.7	-7.2	S-C
1	2	7.8	1.39	36	8.0	3.4	239.4	239.4	262.4	-9.6	-9.6	S-C
1	2	9.5	1.39	36	8.0	3.4	245.1	243.9	262.4	-7.1	-7.6	S-C
1	3	8.6	1.39	36	21.0	3.4	279.9	337.2	355.7	-27.1	-5.5	S
1	3	10	1.39	36	21.0	3.4	299.0	352.9	355.7	-19.0	-0.8	S
2	1	9.2	1.01	36	21.0	2.0	223.7	260.8	294.0	-31.4	-12.7	S-C (stopped)
2	2	9.2	1.01	36	21.0	2.8	179.8	213.6	271.0	-50.7	-26.9	S
2	3	9.2	1.01	36	21.0	3.5	239.4	275.4	273.0	-14.0	0.9	S-C (stopped)
									Mean	-19.9	-9.1	

S=shear failure; S-C= shear-compression failure; Stopped=test was stopped once a significant crack occurred

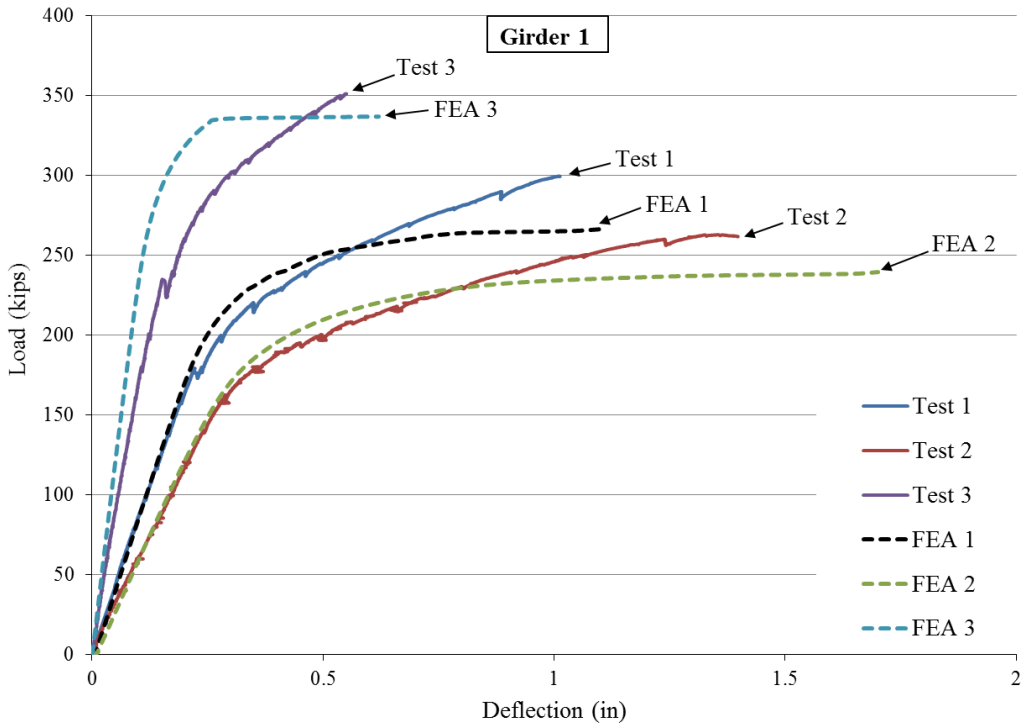

Figure 3.22. Comparison of load versus deflection results for Girder 1

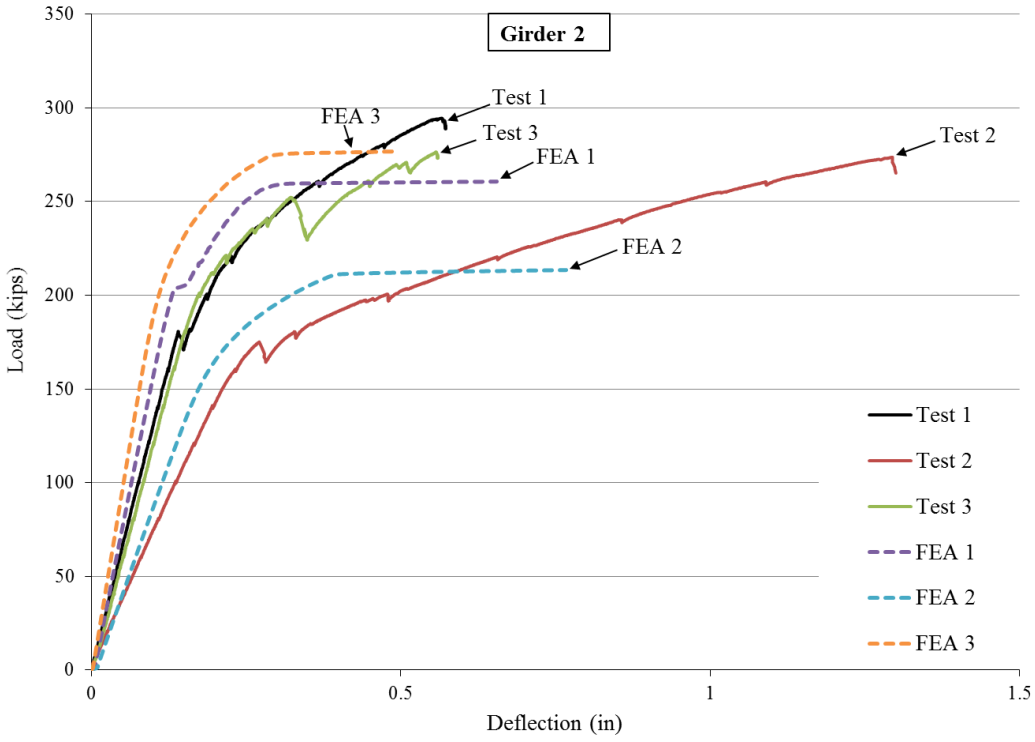

Figure 3.23. Comparison of load versus deflection results for Girder 2

3.3 Parametric Analysis

FEA Models Considered

A large collection of girder models were analyzed using the developed FEA technique in Sec. 3.2 to calculate the shear capacity ratio (V_{FEA}/V_{code}), where V_{FEA} is the FEA ultimate load to cause shear failure and V_{code} is the calculated shear capacity using the LRFD General Method. The analyses consisted of 324 prestressed concrete FEA models with different variables and loading locations. A simple span length of 20 ft under point load was considered for all the models. The selection of parameters considered is given in Table 3.6.

Table 3.6. FEA Model Parameters

Parameter	Values
Girder Type	II, III, IV
Load Position	h/2, LRFD, Worst position
Strand Geometry	Straight, Harped
Concrete Strength	5.5 ksi, 8.0 ksi
Section Axial Stress	0.5 ksi, 1.5 ksi, 2.5 ksi
Stirrup Spacing	3”, 12”, 24”
Long. Steel Reinf. Ratio	Tension control limit, 0.01

In the table, Girder Type refers to AASHTO Types II, III, and IV, respectively. Load position refers to the location from the support where a single point load was applied and increased until shear failure; “LRFD” refers to the critical section as specified by the AASHTO LRFD Sectional Method, while the “Worst position” is the position of the load which produces the smallest capacity from the FEA model, which was generally found to be near L/4 for the models considered (note that this position depends on the span/depth ratio of the girder, and is valid only for the girder depths and span length considered for this parametric analysis). The sectional axial stress is found by taking the total prestress force applied to the girder and dividing by the gross cross-sectional

area. Moreover, it was found that the LFRD approach becomes generally less conservative as the (longitudinal) reinforcement ratio increases. Two cases of relatively large reinforcement ratios were analyzed. The first case used a reinforcement ratio equal to the tension controlled limit, which was thought to be a reasonable upper limit used for most designs. The second case used a reinforcement ratio equal to 0.01, which is beyond the LRFD-specified tension controlled limit for the beams considered. The FEA models dimensions were modified from the original dimensions as shown in Figures 3.24-3.26. This modification was done by subtracting the triangular areas from the original cross section, and dividing them along the web height. A wider web resulted, but by keeping the same original cross sectional area.

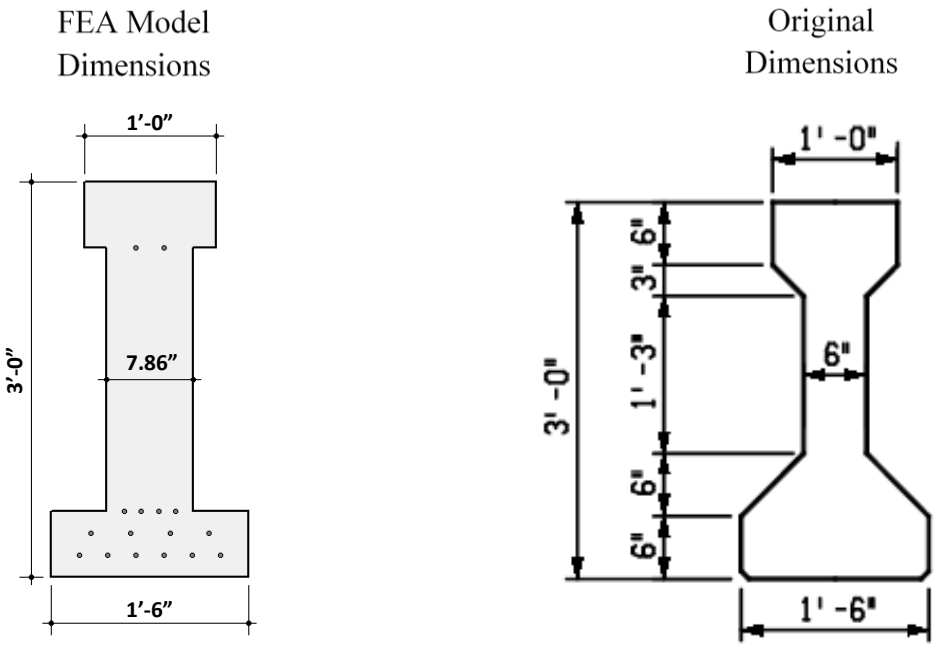

Figure 3.24. Girder Type II dimensions

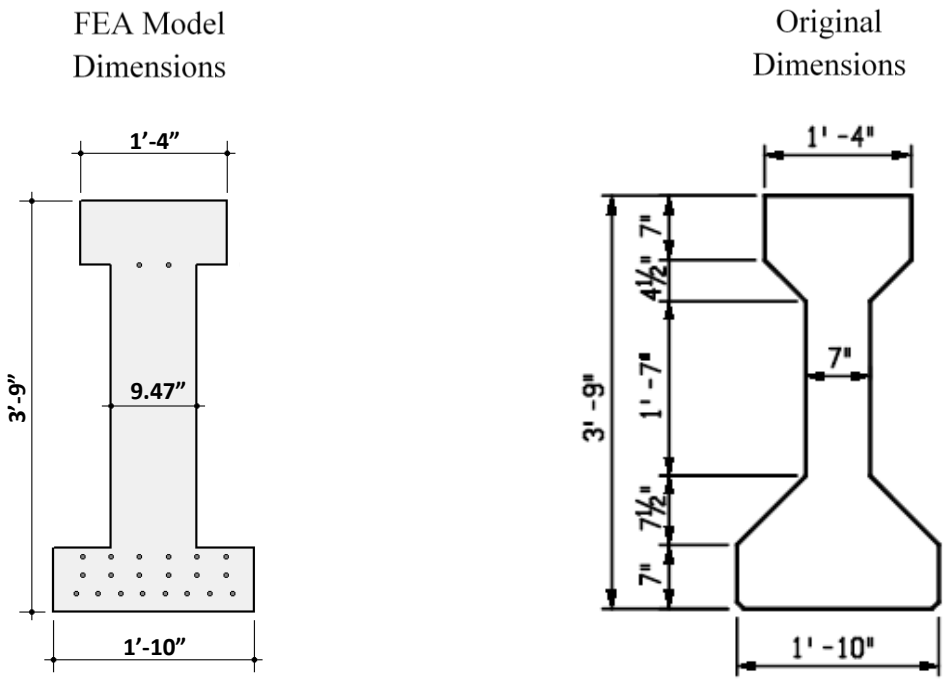

Figure 3.25. Girder Type III dimensions

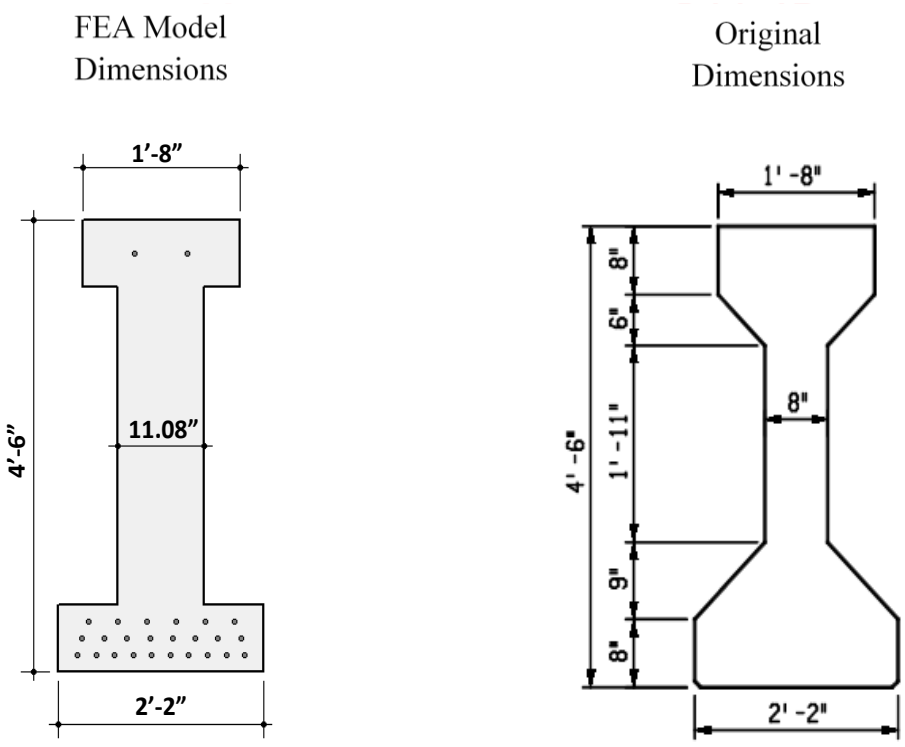

Figure 3.26. Girder Type IV dimensions

Specific parameter combinations considered are summarized in Appendix C, Tables C1 and C2, and results are presented in Tables C34-C180. FEA cases that produced the smallest shear capacities (L/4) were considered for regression analysis in Chapter 5. These results were the closest to the code predictions, and are considered to be the most conservative between all the cases. Thus, a total of 216 FEA model cases were used to develop the regression equations in chapter 5.

CHAPTER 4: RELIABILITY ANALYSIS

4.1 Methodology

In structural engineering, reliability analysis is necessary to establish accepted safety levels for various design cases covered by a code. These safety levels are usually expressed in terms of target reliability indexes which serve as a basis for development of design criteria (load and resistance factors). Reliability methods such as the first and second order reliability methods (FORM, SORM) are common choices for reliability analysis. The selection of target indexes is a multidisciplinary task that involves structural safety and economic analyses. In general, reliability indexes below the target value, β_T, are not accepted, except for some special cases to maintain the simplicity of the format. On the other hand, reliability indexes higher than β_T are practically inevitable. For example, a beam designed for flexure may have an index β for shear much larger than the target reliability index for shear. In the development of a new code, it is convenient to compare the new provisions to the old code. Selection of target reliability indices can be based on the indices for current codes, evaluation of performance of existing structures, experimental testing, and engineering judgment as described in Nowak et al. (2000).

One of the first steps in reliability analysis is to identify a limit state function which describes the boundaries between survival and failure. There are two major categories of limit states: ultimate limit states and serviceability limit states. Ultimate limit states (ULSs) are used to evaluate load carrying capacity, while serviceability limit state are mainly used to evaluate the serviceability of a structure, such as, deflection, deformation, cracking, etc.

When considering ULS, for example, a beam fails if the shear due to loads exceeds the shear capacity of the beam. Let R represent the resistance (shear capacity) and Q represent the load effect (total shear applied to the considered beam). Then the corresponding limit state function

(g) can be written as:

$g = R - Q$. If $g > 0$, the structure is safe, otherwise it fails. The probability of failure (P_F) is equal to:

$$P_F = P(R - Q < 0) = P(g < 0) \quad (4.1)$$

Let the probability density function (PDF) of R be f_R and PDF of Q be f_Q, then let $Z = R - Q$, where Z is a random variable that represents the safety margin, as shown in Figure 4.1.

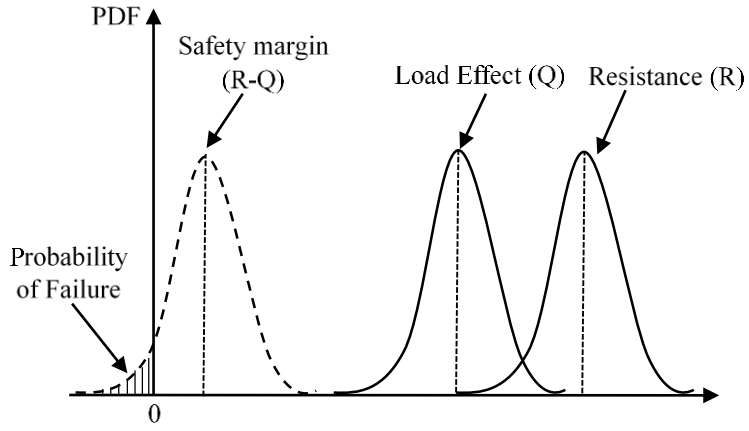

Figure 4.1. PDFs of resistance, load and safety margin (NCHRP 368)

4.2 Code Calibration

Code calibration is a process used to develop reliability-based design codes in the civil engineering field. The major steps in calibrating a code are as follows:

1- A variety of hypothetical structures based on the existing code procedures are designed, and reliability indices of these structures are calculated.

2- After the range of reliability is identified, an "average" reliability index is chosen within the range that is assumed to be adequate. This "average" is often taken as the reliability index of the most typical design. Here it is assumed that the most typical structure designed by current code procedures has a level of safety that is adequate.

3- By adjusting safety factors for the various kinds of loads (load factors), materials and failure mode types (resistance factors), as well as potential other aspects of the design procedure, the standard is adjusted such that a uniform level of reliability is provided for all designs.

An example of a previous code calibration is presented in Figure 4.2.

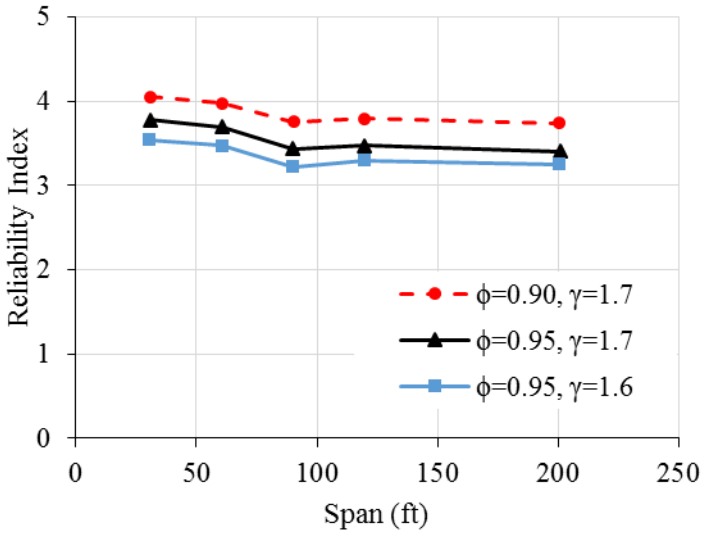

Figure 4.2. Reliability indices for LRFD code, simple span shears in prestressed concrete girders (NCHRP 368)

4.3 Reliability Analysis Methods

4.3.1 First Order Second Moment Methods (FOSM)

Such methods consider only linear limit state functions or linear approximations of them, where the first two moments of a random variable, the mean and the standard deviation, are considered. The third and fourth moments, skewness and kurtosis, are often unavailable and thus rarely used.

4.3.2 Rackwitz-Fiessler Procedure

The Rackwitz-Fiessler (RF) Procedure (Rackwitz and Fiessler 1978) is an iterative procedure used to calculate a reliability index that can account for the distributions of random variables by computing “equivalent normal” random variables from non-normal distributions evaluated at the

design point. Linear formulations of the limit state function can be computed using the following steps:

1- A design point $R^* = Q^*$ that is between the mean values of R and Q is first assumed.

2- A cumulative distribution function $\left(F_x(X^*)\right)$ and a PDF $\left(f_x\,(X^*)\right)$ of X is calculated at X^*, where X^* is Q^* or R^*.

3- The mean ($\bar{X}$) and standard deviation (σ_x) values of the approximating normal distributions of Q and R are calculated as follows:

$$\bar{X} = X^* - \sigma_x\left[\Phi^{-1}\left(F_x(X^*)\right)\right] \tag{4.2}$$

$$\sigma_x = \frac{\phi\left[\Phi^{-1}\left(F_x\,(X^*)\right)\right]}{f_x\,(X^*)} \tag{4.3}$$

4- Reliability index is computed:

$$\beta = \frac{\bar{R} - \bar{Q}}{\sqrt{{\sigma_R}^2 + {\sigma_Q}^2}} \tag{4.4}$$

5- A new design point $X^* = R^* = Q^*$ is calculated:

$$X^* = \bar{X} - \frac{\beta\,{\sigma_x}^2}{\sqrt{{\sigma_R}^2 + {\sigma_Q}^2}} \tag{4.5}$$

6- Steps 2-5 are repeated until the reliability index converges.

4.4 Design Loads

In this research, the procedure used to determine girder reliability in shear is as follows:

1- Girders are designed for shear in accordance to the LRFD Code Sectional Method (AASHTO LRFD 2014), considering the ultimate shear capacity limit state. Since the focus of this study is on the shear limit state only, other design limit states are ignored. Note, however, that neither

moment nor deflection will govern design at the shear critical section considered in this study (between 3 ft to 5 ft from the left support). The 2014 LRFD AASHTO Code strength I limit state is defined by the following expression:

$$\phi R_n \geq 1.25(DC) + 1.5(DW) + 1.75(DF)(LL + IM) \quad (4.6)$$

Here, DC and DW are the dead load of structural components and nonstructural attachments, and the dead load of wearing surfaces and utilities, respectively. LL and IM are the vehicular live load and vehicular dynamic load allowance, respectively, while DF is the girder distribution factor. Details of the dead and live loads considered for design in this study are shown in Appendix G. For shear, the resistance factor for prestressed concrete girders (ϕ) is taken as 0.9. Live load is taken as the HL-93 Design Load, which is equivalent to the HS20 Design truck as shown in Figure 4.3, with an additional 0.64 kip/ft uniformly distributed load along the span of the bridge. Axle loads of the design truck are multiplied by an impact factor of 1.33 to account for the dynamic (impact) load.

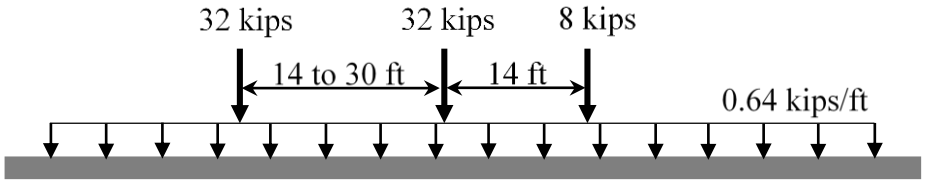

Figure 4.3. Characteristics of the HS20 design truck (AASHTO LRFD 2014)

The girder distribution factors for shear force (DFV) are taken as:

For one design lane loaded:

$$DFV = 0.36 + \frac{S}{25} \quad (4.7)$$

For two or more lanes loaded:

$$DFV = 0.2 + \left(\frac{S}{12}\right) - \left(\frac{S}{35}\right)^2 \quad (4.8)$$

While the girder distribution factors for moment force (DFM) are taken as:

For one design lane loaded:

$$DFM = 0.06 + \left(\frac{S}{14}\right)^{0.4} \left(\frac{S}{L}\right)^{0.3} \left(\frac{K_g}{12Lt_s^3}\right)^{0.1} \quad (4.9)$$

For two or more lanes loaded:

$$DFM = 0.075 + \left(\frac{S}{9.5}\right)^{0.6} \left(\frac{S}{L}\right)^{0.2} \left(\frac{K_g}{12Lt_s^3}\right)^{0.1} \quad (4.10)$$

Where,

DFM= distribution factor for moment for interior beam

S= girder spacing, ft

L= girder span, ft

t_s = depth of concrete slab, in.

K_g = longitudinal stiffness parameter = $n\left(I + A\, e_g^2\right)$, in.^{4}

A = cross sectional area of the girder (noncomposite section), in.^{2}

I = moment of inertia of the girder (noncomposite section), in.^{4}

$$n = \frac{E_{ci}(beam)}{E_{ci}(slab)}$$

e_g = distance between the centers of gravity of the girder and slab (in)

In all the design cases considered for this study, it was found that the GDFs for two or more lanes governed for both shear and moment.

2- Mean girder shear resistance (R) is calculated using Eq. 13 (Sec. 4.5), considering 13 different random variables. The random resistance parameters are given in Table 4.2.

3- Total shear load effect (Q) is determined by summing the individual load effects:

$$Q = Q_{DL} + Q_{LL} = (Q_g + Q_s + Q_b + Q_{ws}) + Q_{HL93} + Q_{IL} \quad (4.11)$$

Where dead loads (Q_{DL}): Q_g, Q_s, Q_b, Q_{ws} are due to girder, slab, barrier and wearing surface, respectively. While live loads (Q_{LL}), are due to the HL-93 design load (Q_{HL93}) and impact live load (Q_{IL}). The mean value of the total (nominal) load effect is determined by multiplying each load component by the appropriate bias factor as follows:

$$mQ_{DL} + mQ_{LL} = [(Q_g)(\lambda_1) + (Q_s + Q_b)(\lambda_2) + Q_{ws}(\lambda_3)] + [(Q_{HL93} + Q_{IL})(\lambda_4)] \quad (4.4.7)$$

Here, the bias factors $\lambda_1,\ \lambda_2,\ \lambda_3,\ \lambda_4$ are the appropriate bias factors, shown in Table 4.3.

4- Standard deviation (σ_x) of each load effect is determined by simply multiplying the mean value by the appropriate coefficient of variation (COV). COVs for load effect are shown in Table 4.3.

5- Reliability index is calculated using the Rackwitz-Fiessler Procedure described above, where resistance parameters and total load effect are taken as normal variables.

4.5 Design Cases

75 prestressed concrete AASHTO bridge girders were considered for shear design in accordance to the current LRFD General Method. AASHTO girder Types II, III and IV were

considered for design with five different span lengths of 30, 60, 90, 120 and 200 ft, and five different beam spacings of 4, 6, 8, 10 and 12 ft per span length. Span length and girder spacing combinations presented in the NCHRP 368 report are considered for design and reliability analysis in this study, as shown in Table 4.1.

Table 4.1. Bridge girder cases considered

Comb. #	Span (ft)	Spacing (ft)
1	30	4
2	30	6
3	30	8
4	30	10
5	30	12
6	60	4
7	60	6
8	60	8
9	60	10
10	60	12
11	90	4
12	90	6
13	90	8
14	90	10
15	90	12
16	120	4
17	120	6
18	120	8
19	120	10
20	120	12
21	200	4
22	200	6
23	200	8
24	200	10
25	200	12

In this study, reliability indices for the cases presented in the NCHRP 368 report (discussed in sec. 1.3.9) were computed using the RF procedure. This practically resulted in different bias factors and COVs for resistance parameters used in calculating the design shear capacity. This approach was not considered in the NCHRP 368, where the resistance model had one constant bias factor and one COV for all cases. Such simplification does not capture the differences in resistance parameters from one beam design to another. Where no clear steps are provided in the NCHRP

368 report on how the mean load and mean resistance values were computed, an example with calculations for a 90 ft span girder is presented in Appendix F. Resistance random variables considered in this study are shown in Table 4.2.

Table 4.2. Parameters of resistance model

RV	Bias Factor	COV
f'_c	1.38	0.120
b_v	1.01	0.040
d_e	1.00	0.025
A_v	1.00	0.015
f_y	1.145	0.050
s	1.00	0.040
f_{pu}	1.04	0.025
E_{ps}	1.00	0.010
A_{ps}	1.00	0.015
b_e	1.00	0.040
h	1.00	0.030
t_s	1.01	0.120
f'_{cs}	1.38	0.120

In Table 4.2, f'_c is the concrete compressive strength at 28 days, b_v is the web thickness, d_e is the effective depth, A_v is the area of stirrups, f_y is the yield strength of transverse steel, s is the stirrup spacing, f_{pu} is the ultimate strength of the prestressed strands, E_{ps} is the modulus of elasticity of the prestressed strands, A_{ps} is the area of the prestressed strands, b_e is the effective flange width, h is the height of the composite section, t_s is the slab thickness, and f'_{cs} is the concrete compressive strength of the slab. The statistical parameters for these RVs are taken as those used to calibrate the ACI 318 code for pre-tensioned, plant-cast PC beams, where distributions are reported as normal (Nowak, and Szerszen, 2003). In addition, a professional factor with a COV of 0.1 was applied to the resistance component in the reliability analysis (NCHRP 368). The professional factor is used to account for uncertainties in the ordinarily conservative

analysis models used to establish member strength. For example, assumptions that concrete crushes at a strain of 0.003, and that steel is elasto-plastic, etc (ACI 318-11).

For the load model, the same bias factors and COVs presented in NCHRP 368 were used in analysis, except for the shear live load (V_{LL}) bias factor (ratio of actual shear to AASHTO LRFD HL-93 design shear), which was taken as 1.0 (1.1 in the NCHRP 368). This bias factor was taken as 1.0 based on the recommended value for code calibration presented in the RC-1601 report (Eamon et al. 2014). Load bias factors and COVs considered in this study are shown in Table 4.3, where V_g, V_s, V_b, V_{ws}, V_{LL} are loads due to girder self-weight, slab, barrier, wearing surface, and total live load effect (including impact), respectively.

Table 4.3. Parameters of load model

RV	Bias Factor	COV
V_g (Q_g)	1.03	0.08
V_s (Q_s)	1.05	0.10
V_b (Q_s)	1.05	0.10
V_{ws} (Q_s)	1.00	0.25
V_{LL} (Q_s)	1.00	0.18

Reliability indices (β) of the shear capacity of AASHTO bridge girder Types II, III, and IV were determined from the General LRFD Method and computed using the Rackwitz-Fiessler Procedure described above. A RF algorithm implemented in FORTRAN was used to conduct that reliability analysis in this study. The algorithm used is provided in Appendix I, and a design example using the LRFD General Method for a typical PC bridge girder is presented in Appendix D.

Reliability indices were computed using two versions of Resistance calculation, the Original Resistance and Iterative Resistance. In the Original Resistance, the mean shear load value (V_u)

used in design was considered for reliability analysis, while in the Iterative Resistance, V_u was iteratively changed until $V_u = V_n$, where V_n is the nominal shear capacity of the PC girder at the critical section. This proposed change in computing the nominal resistance was found to produce closer values to actual capacity, based on the FEA and experimental results presented in Chapter 3.

This change in V_u mainly affected the calculation of ε_s , as shown in the design process below:

$$V_u = \left[1.25\left(V_g + V_s + V_b\right) + 1.5(V_{ws}) + 1.75(V_{HL93} + V_{IL})\right] = 0.9\, V_n \tag{4.12}$$

$$V_n = V_c + V_s + V_p = V_u;\ V_p = 0 \tag{4.13}$$

$$V_c = 0.0316\, \beta \sqrt{f_c'}\, b_v d_v \tag{4.14}$$

$$V_s = \frac{A_v f_y d_v (\cot\theta + \cot\alpha)\sin\alpha}{s} \tag{4.15}$$

Where $\alpha = 90^{\circ}$, V_s reduces to:

$$V_s = \frac{A_v f_y d_v (cot\,\theta)}{s} \tag{4.16}$$

$$\beta = \frac{(4.8)\ (51)}{(1 + 750\varepsilon_s)(39 + S_{xe})};\ S_{xe} = 12 \tag{4.17}$$

$$\theta = 29 + 3500\varepsilon_s \tag{4.18}$$

$$M_u = \left[1.25\left(M_g + M_s + M_b\right) + 1.5(M_{ws}) + 1.75(M_{HL93} + M_{IL})\right] \tag{4.19}$$

$$\varepsilon_s = \frac{|M_u/d_v| + 0.5N_u + \left|\left(V_u - V_p\right)\right| - A_{ps}f_{po}}{\left(E_s A_s + E_p A_{ps}\right)} \tag{4.20}$$

When ε_x is negative, it is taken as either zero or recalculated as the following:

$$\varepsilon_s = \frac{|M_u/d_v| + 0.5N_u + \left|\left(V_u - V_p\right)\right| - A_{ps}f_{po}}{\left(E_s A_s + E_p A_{ps} + E_c A_{ct}\right)} \tag{4.21}$$

Where V_c is the concrete shear capacity (kip); V_s is the shear capacity of steel web reinforcement (kip); V_p is the vertical component of pre-stressing force (kip); f'_c is the compressive strength in concrete (ksi); b_v is the effective web width (in.); d_v is the effective shear depth (in.); s is the spacing of transverse reinforcement (in.); A_v is the area of shear reinforcement (in^2) within a distance s; f_y is the yield stress of the transverse reinforcement (ksi); and α is the angle of stirrups inclination (α=90º); β is a factor indicating the ability of diagonally cracked concrete to transmit tension and shear; θ is the angle of inclination of diagonal compressive stresses; ε_s is the net longitudinal tensile strain in concrete at the centroid of the tension reinforcement; M_u is the total factored moment (kip-in.), not to be taken less than $\left|\left(V_u - V_p\right)\right| d_v$.

In design, only when the initial calculated ε_s value is negative, the LRFD code permits taking ε_s as zero or it may be recomputed (more accurate approach and less conservative) using an alternative equation. To compare the difference in the reliability index β when each approach was used (zero value or the equation), two sets of results for Type II girder were computed and compared. The first set of results was computed based on the alternative design equation of ε_s, while the second set is based on $\varepsilon_s = 0$. Results showed no significant difference in β when the equation or zero value for ε_s were used to compute V_n. The more accurate design approach (alternative ε_s equation) was considered for design and analysis in this study. This approach is more accurate as it evaluates ε_s based on the applied shear and moment forces at the critical section rather than assuming a constant level of stresses when the zero value is taken. Even though, the difference is small between the two approaches, it is more accurate to compute reliability indices based on the less conservative design approach (alternative ε_s equation).

Two sets of results were computed and compared to identify the best approach that would produce a consistence reliability index of the design cases considered. The first set was computed

using the Original Resistance Procedure (no Iteration) and showed discrepancies between the NCHRP 368 and the LRFD computed β values. As a beginning, a comparison was made to confirm that discrepancies between reliability indices presented in the NCHRP 368 report and those designed using the current LRFD General Method, and computed using the Original Resistance Procedure were not as a result of variances in mean load to mean resistance ratios. In this comparison, ratios of the mean shear load to the mean shear capacity were computed and plotted as shown in Figures 4.4-4.6. Plotted results showed a very close match between the ratios used in the NCHRP 368 and ratios used for design cases considered for reliability analysis, and therefore, discrepancies in reliability indices are not because of variances in mean load to mean resistance ratios. Note that over designed cases in the figures are plotted as hollow symbols.

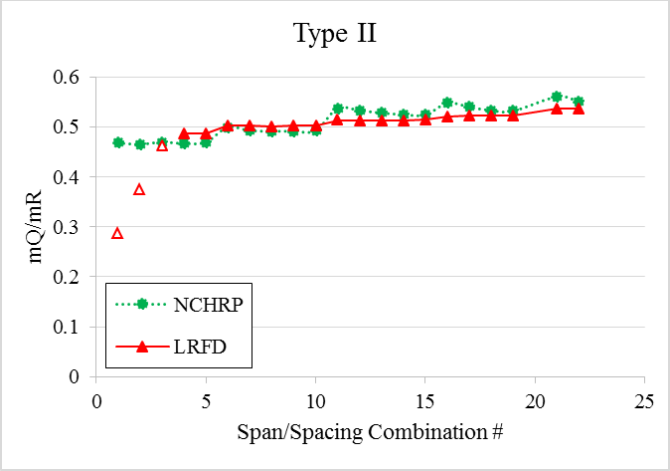

Figure 4.4. Ratios of mean shear load to mean shear capacity (Type II girder)

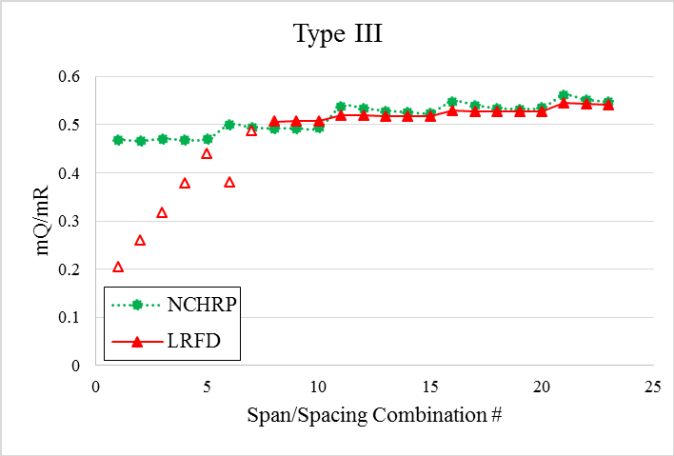

Figure 4.5. Ratios of mean shear load to mean shear capacity (Type III girder)

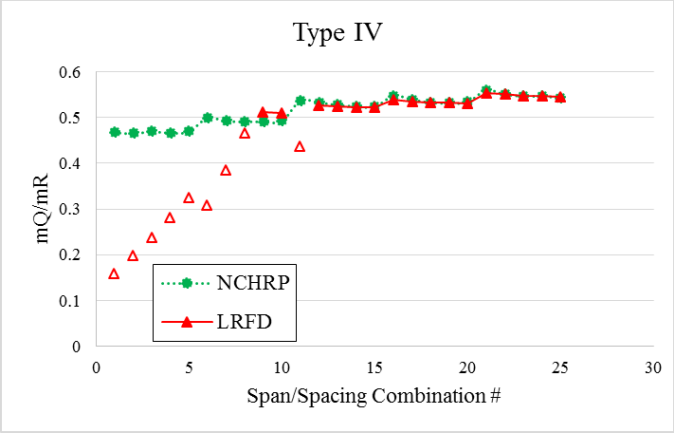

Figure 4.6. Ratios of mean shear load to mean shear capacity (Type IV girder)

By analyzing the data in Table 4.5, β values show consistency when the design values of ε_s are negative, but start to increase for the positive design values of ε_s. This increase in β is because all the computed ε_s values in reliability were negative compared to those in design (negative and positive), and thus the obtained value for V_n in analysis was greater than the calculated value for V_n in design. This is mainly due to the difference in the shear and moment forces used to compute ε_s in design and analysis, where factored values were used in design and mean values were used in analysis.

In design, as the increase in the applied shear and moment forces increases the stresses that can be transmitted across diagonally cracked concrete, the cracks become wider and the stress that can be transmitted decreases. The evaluation of β and θ from equations 4.17 and 4.18, respectively, is based on these transmitted stresses, and correspondingly, the calculation of V_c and V_s from equations 4.14 and 4.15, respectively. Since the same design procedure and parameters are used in both design and reliability analysis, β is expected to be consistent for all of the presented cases. This would be true if the shear load value (V_u) and the corresponding moment value (M_u) used to compute ε_s was the same in both design and analysis. Since the LRFD factored shear loads were used in design and the mean values in analysis, the calculated ε_s in design would be different from the corresponding ε_s in analysis. As shown in equation 4.20, the change in V_u and M_u (where M_u=V_u. d_v) would significantly affect the calculated value of ε_s. Such variation in the shear load values between design and analysis (higher in design) resulted in switching the sign of ε_s from positive to negative in analysis for the cases when β started to increase. And since either the original equation (for positive ε_s) or alternative equation (for negative ε_s) are used to compute ε_s, the switch in sign from positive to negative changed the computed value of ε_s in analysis, and as a result, the computed shear capacity.

In the second set of results, reliability indices showed more consistency when the Iterative Resistance Procedure was used for analysis and the LRFD code procedure for design (non-iterative), with a decrease when ε_s became positive as shown in Table 4.4. This iterative procedure was found to correspond more accurately to the experimental/FEA data than the original code method, as previously discussed in Chapter 2. Therefore, this procedure was considered for the remaining analysis in this study.

The Iterative Resistance Procedure produced reliability indices closer to the NCHRP values than using the non-iterative (General LRFD Procedure). The reason behind this alteration is that prior to the 2008 interim revisions, the General LRFD Procedure for shear design was iterative. It was derived from the Modified Compression Field Theory (MCFT, Vecchio and Collins, 1986), and required the use of tables for evaluation of β and θ. In the 2008 revisions and later, this design procedure was modified to be non-iterative, and equations 4.17 and 4.18 were introduced for the evaluation of β and θ. These two equations were also derived from the MCFT (Bentz et al. 2006), and were considered as appropriate for use in the AASHTO LRFD Bridge Design Specifications (Hawkins et al., 2005, 2007).

Table 4.4. Reliability indices using the Original Resistance Procedure*

#	Span (ft)	Spacing (ft)	Beta-NCHRP	Beta-II	Beta-III	Beta-IV
1	30	4	4.16	6.71	7.73	8.27
2	30	6	4.19	5.68	7.05	7.81
3	30	8	4.12	4.75	6.37	7.32
4	30	10	4.25	4.50	5.68	6.81
5	30	12	4.21	4.49	5.02	6.32
6	60	4	4.09	4.48	5.80	6.65
7	60	6	4.10	4.46	4.66	5.76
8	60	8	4.14	4.45	4.46	4.90
9	60	10	4.10	4.43	4.43	4.41
10	60	12	4.12	5.15	4.43	4.43
11	90	4	3.74	4.44	4.44	5.34
12	90	6	3.77	4.42	4.43	4.39
13	90	8	3.81	4.84	4.40	4.40
14	90	10	3.83	5.72	4.39	4.40
15	90	12	3.85	6.24	4.38	4.39
16	120	4	3.78	4.41	4.40	4.35
17	120	6	3.81	4.70	4.37	4.36
18	120	8	3.88	5.79	4.36	4.36
19	120	10	3.89	6.40	4.54	4.35
20	120	12	3.83	-	5.38	4.35
21	200	4	3.70	5.30	4.31	4.27
22	200	6	3.79	6.34	4.72	4.26
23	200	8	3.82	-	5.70	4.24
24	200	10	3.79	-	-	4.99
25	200	12	3.82	-	-	5.64

*Orange cells= over-designed cases using f`c=4 ksi and stirrups spacing of 24 in; Green cells= design cases with positive ε_s

Table 4.5. Reliability indices using the Iterative Resistance Procedure*

#	Span (ft)	Spacing (ft)	Beta-NCHRP	Beta-II	Beta-III	Beta-IV
1	30	4	4.16	6.29	7.39	8.00
2	30	6	4.19	5.24	6.66	7.47
3	30	8	4.12	4.34	5.94	6.95
4	30	10	4.25	4.10	5.25	6.41
5	30	12	4.21	4.13	4.61	5.90
6	60	4	4.09	4.09	5.38	6.24
7	60	6	4.10	4.08	4.25	5.33
8	60	8	4.14	4.09	4.07	4.47
9	60	10	4.10	3.85	4.06	4.04
10	60	12	4.12	3.62	4.07	4.05
11	90	4	3.74	4.09	4.05	4.92
12	90	6	3.77	4.08	4.06	4.01
13	90	8	3.81	3.57	4.05	4.03
14	90	10	3.83	3.58	4.04	4.04
15	90	12	3.85	3.57	3.69	4.04
16	120	4	3.78	4.07	4.04	3.98
17	120	6	3.81	3.54	4.03	4.01
18	120	8	3.88	3.56	4.08	4.01
19	120	10	3.89	3.53	3.48	4.02
20	120	12	3.83	-	3.52	4.03
21	200	4	3.70	3.51	3.96	3.93
22	200	6	3.79	3.46	3.44	3.92
23	200	8	3.82	-	3.46	3.60
24	200	10	3.79	-	-	3.41
25	200	12	3.82	-	-	3.42

*Orange cells= over-designed cases using f'c=4 ksi and stirrups spacing of 24 in; Green cells= design cases with positive ε_s

Reliability indices as a function of span and girder spacing using the Iterative Resistance Procedure are compared with the corresponding NCHRP 368 values as shown in Figures 4.7-4.9. Note that hollow symbols without connecting lines represent over designed cases (most of the 30 ft and some of the 60 ft span cases). Those cases have high reliability indices compared to the cases designed in accordance to the LRFD code, and show that the corresponding values presented in NCHRP 368 report are significantly under estimating the level of safety in shear.

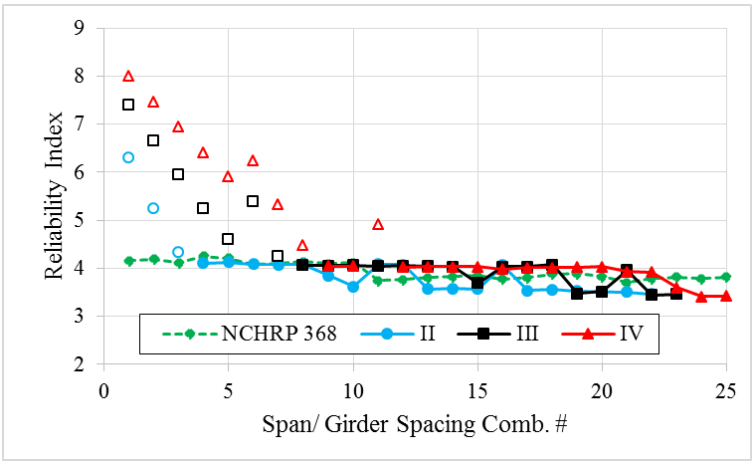

Figure 4.7. Comparison of Reliability Indices between NCHRP 368 and using the Iterative Resistance

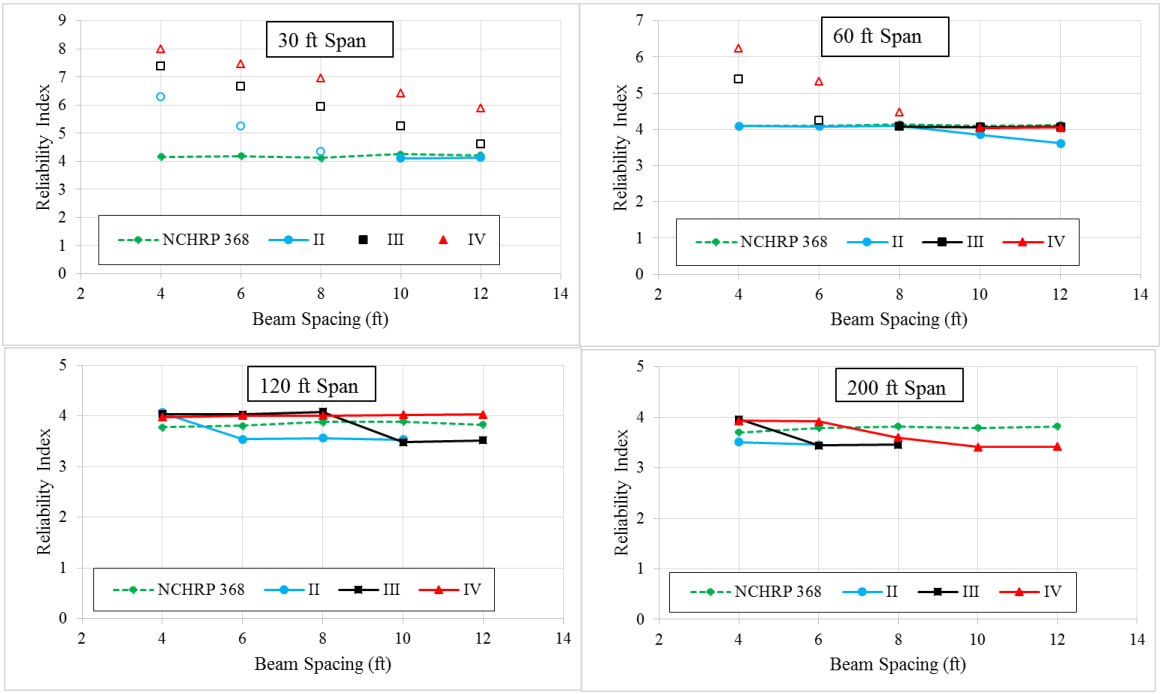

Figure 4.8. Reliability indices as a function of span length and girder spacing

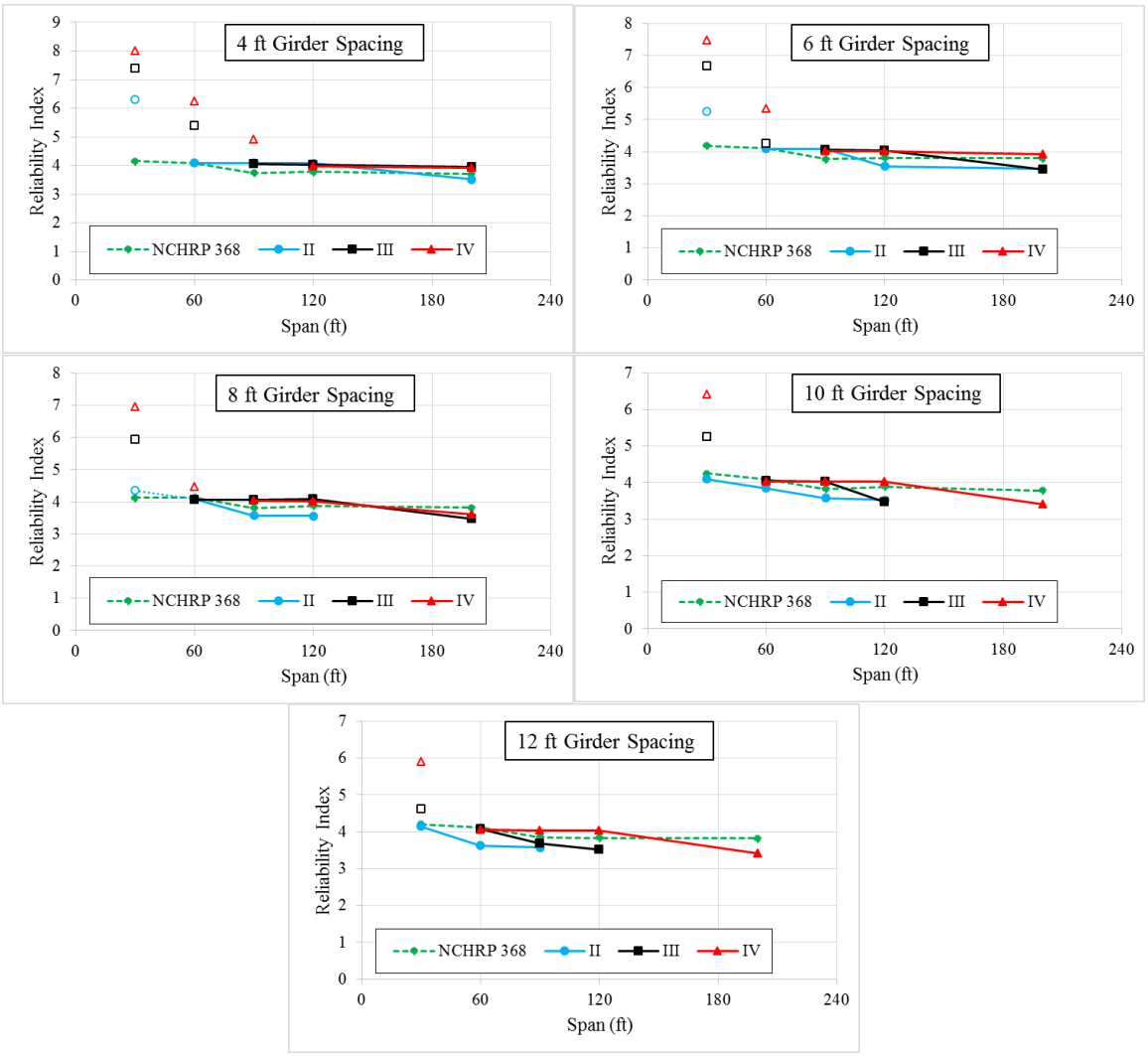

Figure 4.9. Reliability indices as a function of girder spacing and span length

In order to clarify how the change in V_u and M_u affects the calculation of ε_s and the computation of β, a detailed analyses for Type II girder using both methods (original and iterative RF) are shown in Figures 4.10-4.14. These analyses were conducted for 90 ft and 120 ft span cases, and compared the change in ε_s as a function of V_u and M_u, where:

$$\varepsilon_s = \frac{|M_u/d_v| + 0.5N_u + |(V_u - V_p)| - A_{ps}f_{po}}{(E_sA_s + E_pA_{ps})} \tag{4.22}$$

Here, three different V_u and M_u values were compared: LRFD factored values, mean values used in the Original RF Procedure, and mean values at convergence used the Iterative Resistance

Procedure. The comparisons between the reliability indices for the three cases is also shown in Tables 4.6-4.8. By observing the comparisons in the tables, it is clearly shown that as shear and moment forces increased the corresponding reliability indices decreased. Moreover, the resulted ε_s values based on the mean shear and moment used in the Original Resistance Procedure were negative for all of the cases, but positive for the majority of the cases when design or converged values (Iterative Resistance) were used, as shown in Table 4.7. This switch from negative to positive is mainly due to the increase in V_u and M_u used to calculate ε_s in the design and the Iterative Resistance, which as a result, affected the computation of V_n and β. The evaluated value of ε_s is compared between the Original Resistance, design, and Iterative Resistance approaches, respectively, as shown Table 8.

For example, in Table 4.6, column 4 (Original Resistance), notice that when resistance is calculated using the original (non-iterative) resistance method as assumed in design, reliability indices increased as girder spacing increased. This is because Vu and Mu increased as girder spacing increased (Tables 4.7 and 4.8). This in turn caused ε_s to decrease and become negative compared to those computed in design. This decrease caused the mean resistance to increase relative to nominal resistance, and hence the β value to increase.

In column 5 (NCHRP), all reliability indices are nearly the same since a constant bias factor for resistance was used rather than actually calculating resistance for each different case. Note that these values were computed based on mean resistance and mean load values provided in the NCHRP 368 report, rather than computed for Type II girder with separate resistance parameters.

In column 6 (Iterative Resistance), reliability indices are more consistent than the original case and closer to those presented in NCHRP 368. The reason behind this consistency, is because the Iterative Resistance method used to compute β is similar to that presented in the old LRFD

(AASHTO LRFD 1994) code method for shear design (iterative), which required the use of tables for evaluation of β and θ, where β is the longitudinal strain in the concrete.

Table 4.6. Effect of ε_s on the computation of reliability index

			Reliability Index			Longitudinal Strain (εs)		
#	Span (ft)	Spacing (ft)	Original Resistance	NCHRP	Iterative Resistance	Original Resistance	Design	Iterative Resistance
11	90	4	4.44	3.74	4.09	-0.00020	-0.00013	-0.00008
12	90	6	4.42	3.77	4.08	-0.00014	-0.00005	-0.00001
13	90	8	4.84	3.81	3.57	-0.00010	0.00031	0.00078
14	90	10	5.72	3.83	3.58	-0.00007	0.00152	0.00210
15	90	12	6.24	3.85	3.57	-0.00003	0.00271	0.00334
16	120	4	4.41	3.78	4.07	-0.00016	-0.00007	-0.00003
17	120	6	4.70	3.81	3.54	-0.00011	0.00022	0.00068
18	120	8	5.79	3.88	3.56	-0.00006	0.00173	0.00232
19	120	10	6.40	3.89	3.53	-0.00001	0.00321	0.00386
20	120	12	-	3.83	-	-	-	-

Table 4.7. Effect of shear force magnitude on reliability index

			Reliability Index			Vu (kip)		
#	Span (ft)	Spacing (ft)	Original Resistance	NCHRP	Iterative Resistance	Original Resistance	Design	Iterative Resistance
11	90	4	4.44	3.74	4.09	100	153	181
12	90	6	4.42	3.77	4.08	130	198	232
13	90	8	4.84	3.81	3.57	159	242	254
14	90	10	5.72	3.83	3.58	187	285	296
15	90	12	6.24	3.85	3.57	214	326	339
16	120	4	4.41	3.78	4.07	123	185	218
17	120	6	4.70	3.81	3.54	159	239	252
18	120	8	5.79	3.88	3.56	195	292	303
19	120	10	6.40	3.89	3.53	229	343	354
20	120	12	-	3.83	-	-	-	-

Table 4.8. Effect of moment force magnitude on reliability index

			Reliability Index			Mu (kips-ft)		
#	Span (ft)	Spacing (ft)	Original Resistance	NCHRP	Iterative Resistance	Original Resistance	Design	Iterative Resistance
11	90	4	4.44	3.74	4.09	333	508	603
12	90	6	4.42	3.77	4.08	438	668	789
13	90	8	4.84	3.81	3.57	539	822	880
14	90	10	5.72	3.83	3.58	637	970	1044
15	90	12	6.24	3.85	3.57	730	1110	1191
16	120	4	4.41	3.78	4.07	408	612	730
17	120	6	4.70	3.81	3.54	536	805	862
18	120	8	5.79	3.88	3.56	661	991	1067
19	120	10	6.40	3.89	3.53	781	1170	1252
20	120	12	-	3.83	-	-	-	-

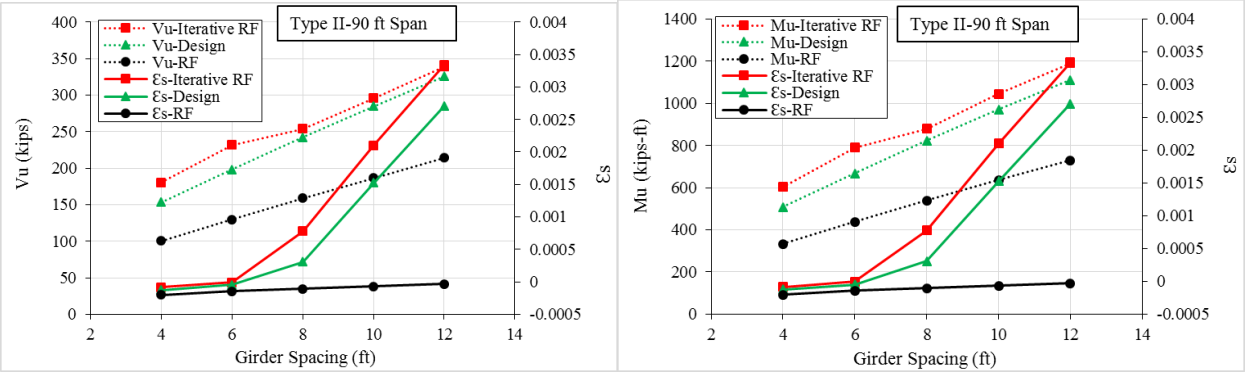

Figure 4.10. Effect of shear and moment on the computation of ε_s (90 ft span-Type II Girder)

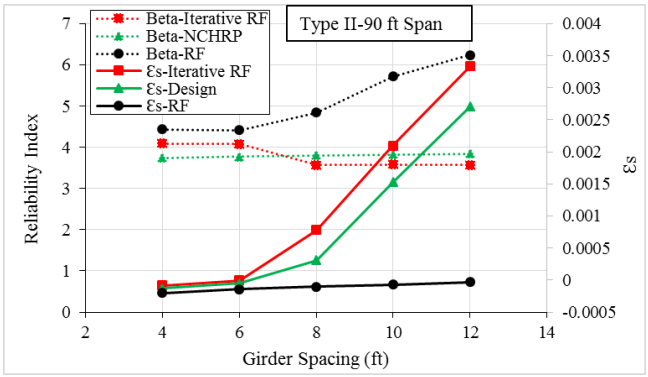

Figure 4.11. Reliability indices as a function of ε_s (90 ft span-Type II Girder)

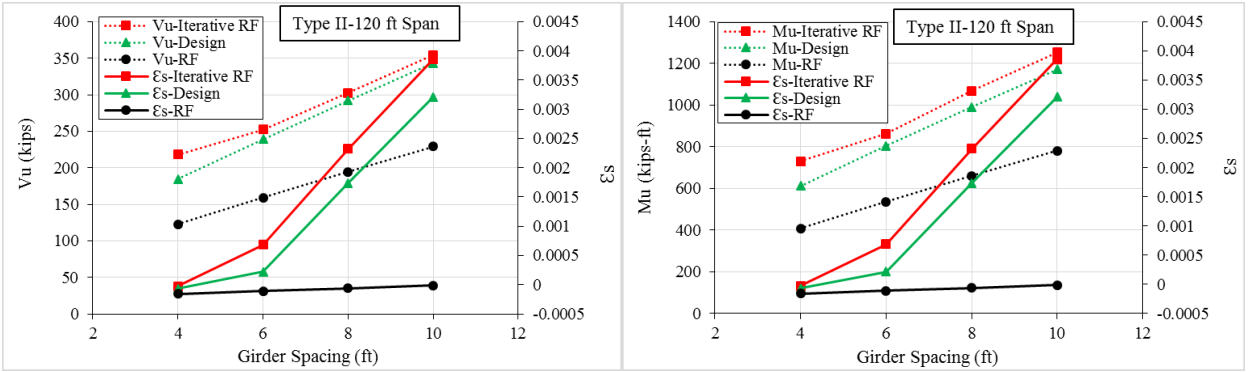

Figure 4.12. Effect of shear and moment on the computation of ε_s (120 ft span-Type II Girder)

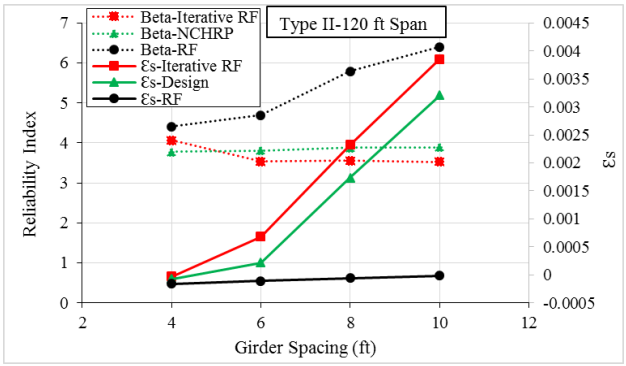

Figure 4.13. Reliability indices as a function of ε_s (120 ft span-Type II girder)

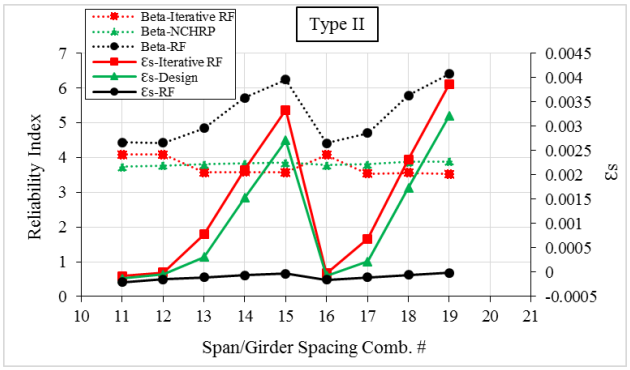

Figure 4.14. Reliability indices as a function of ε_s and span/girder spacing (Type II girder)

4.6 New Shear Capacity Design Method

In the new proposed design procedure, a larger V_u value (V_{u*}) was used for design, and resulted in a more consistent reliability indices compared to those computed using the V_u value specified in the General LRFD Method, especially for cases where the resulted ε_s was positive. Using the new method, increasing the value of V_u by a factor $\gamma_v = 1.06$ reduced the computed V_n value, which as a result required increasing the beam shear capacity. This increase in V_u increased the consistency of the reliability indices for cases when ε_s was positive (cases with long span and large beam spacing), and produced reliability indices with a lower limit of 3.5 for the girder cases considered in this study. This lower limit was chosen based on the target reliability index presented in the NCHRP 368 report. However, the presented reliability indices in the NCHRP 368 had an average of 3.94 with the lowest β as 3.7 for a live load factor of 1.75 and a resistance factor of 0.9. Although a live load factor of 1.75 was not considered in the calculations presented in the NCHRP 368 but used in the 2014 LRFD AASHTO Code strength I limit state, β values for all of the cases presented in NCHRP 368 were recomputed based on a live load factor of 1.70. Using the higher live load factor (1.75) resulted in slightly higher β values (increase average of 0.12) compared to those computed using a factor of 1.70. This new set of β values is based on the current LRFD Code design load factors, and thus considered for comparison with β values computed in this study.

In general, reliability indices showed discrepancy with a significant drop as span length and beam spacing increased, when the original factored LRFD loads (V_u) were used. On the other hand, using the new proposed load (V_{u*}) for design, significant improvements resulted in terms of consistency and level of safety. Thus, more consistent β values with a minimum of 3.5, especially for cases where ε_s is positive, were resulted. The lower limit of 3.5 was achieved by adding a new

factor of 1.05. Thus, $0.9 * 1.05\, V_n = 0.95\, V_n = V_u$, and the new shear and moment values used for design are $V_{u*} = \frac{V_u}{0.9*1.05} = 1.06\, V_u = \gamma_v V_u$ and $M_u = V_{u*}\, d_v$, respectively. Note that V_u is the same factored shear load specified in the LRFD code $= 1.25\big(V_g + V_s + V_b\big) + 1.5(V_{ws}) + 1.75(V_{LT} + V_{LL})$.

Using the new design procedure, β is computed as follows:

1- Design the beam based on the General LRFD Method, but using V_{u*} instead of V_u where, $V_{u*} = \frac{V_u}{0.9*1.05} = 1.06\, V_u$ as follows:

$$V_{u*} = \left[\frac{1.25\big(V_g + V_s + V_b\big) + 1.5(V_{ws}) + 1.75(V_{LT} + V_{LL})}{(0.9 * 1.05)}\right] = V_n \tag{4.23}$$

When $\varepsilon_s > 0$:

$(a)\ V_p = 0$

If $|M_u| < V_{u*} d_v$, take $M_u = V_{u*} d_v$ and:

$$\varepsilon_s = \frac{\left|\frac{M_u}{d_v}\right| + 0.5N_u + \big|(V_{u*} - V_p)\big| - A_{ps} f_{po}}{\big(E_s A_s + E_p A_{ps}\big)} = \frac{2\, V_{u*} - A_{ps} f_{po}}{\big(E_s A_s + E_p A_{ps}\big)} = \frac{2\left(\frac{V_u}{0.9 * 1.05}\right) - A_{ps} f_{po}}{\big(E_s A_s + E_p A_{ps}\big)}$$

$$= \frac{2.116\, V_u - A_{ps} f_{po}}{\big(E_s A_s + E_p A_{ps}\big)} \tag{4.24}$$

Otherwise,

$$\varepsilon_s = \frac{|M_u/d_v| + 1.06\, V_u - A_{ps} f_{po}}{\big(E_s A_s + E_p A_{ps}\big)} \tag{4.25}$$

Where,

$$M_u = 1.25\big(M_g + M_s + M_b\big) + 1.5(M_{ws}) + 1.75(M_{LT} + M_{LL});\ N_u = 0 \tag{4.26}$$

$$V_{u*} = \frac{V_u}{0.9 * 1.05} = 1.06\, V_u$$

$(b)\ V_p > 0$

If $|M_u| < \left|\left(V_{u*} - V_p\right) d_v\right|$, take $M_u = \left|\left(V_{u*} - V_p\right) d_v\right|$ and:

$$\varepsilon_s = \frac{\left|\left(2.116\, V_u - 2V_p\right)\right| - A_{ps} f_{po}}{\left(E_s A_s + E_p A_{ps}\right)} \tag{4.27}$$

Otherwise,

$$\varepsilon_s = \frac{|M_u/d_v| + \left|\left(1.06\, V_u - V_p\right)\right| - A_{ps} f_{po}}{\left(E_s A_s + E_p A_{ps}\right)} \tag{4.28}$$

When $\varepsilon_s < 0$:

Replace the denominator by $\left(E_s A_s + E_p A_{ps} + E_c A_{ct}\right)$

2- Compute β based on the new designed $V_n\ (= V_{u*})$ using the Iterative Resistance Procedure.

Design cases for three different span lengths were considered for design using the new proposed method. As described above, a new resistance factor of $\phi_r = 0.95$ was considered (in place of 0.9) to produce a reliability index with a lower limit of 3.5. Another shear load factor $\gamma_v = 1.06$ was added to produce more consistent β values compared to those computed based on the current LRFD design procedure. Reliability indices computed based on the original and the new design methods for the three girder types (straight and harped strand profile) are summarized in Tables 4.9 and 4.10. More detailed comparisons as a function of span length and girder spacing are presented in Figures 4.15-4.24.

Table 4.9. Comparison between reliability indices using the original and new design method (straight strands)

			Type II	Type II*	Type III	Type III*	Type IV	Type IV*
#	Span (ft)	Girder Spacing (ft)	LRFD	LRFD*	LRFD	LRFD*	LRFD	LRFD*
11	90	4	4.09	3.88	4.05	3.85	4.92	4.92
12	90	6	4.08	3.88	4.06	3.86	4.01	3.80
13	90	8	3.57	3.71	4.05	3.86	4.03	3.83
14	90	10	3.58	3.65	4.04	3.86	4.04	3.84
15	90	12	3.57	3.64	3.69	3.91	4.04	3.84
16	120	4	4.07	3.87	4.04	3.84	3.98	3.76
17	120	6	3.54	3.69	4.03	3.83	4.01	3.80
18	120	8	3.56	3.64	4.08	3.82	4.01	3.79
19	120	10	3.53	3.60	3.48	3.62	4.02	3.80
20	120	12	-	-	3.52	3.60	4.03	3.80
21	200	4	3.51	3.60	3.96	3.77	3.93	3.73
22	200	6	3.46	3.56	3.44	3.56	3.92	3.72
23	200	8	-	-	3.46	3.52	3.60	3.53
24	200	10	-	-	-	-	3.41	3.51
25	200	12	-	-	-	-	3.42	3.50

LRFD= design cases using the General LRFD Method; LRFD*= design cases using the new method

Table 4.10. Comparison between reliability indices using the original and new design method (harped strands)

			Type II	Type II*	Type III	Type III*	Type IV	Type IV*
#	Span (ft)	Girder Spacing (ft)	LRFD	LRFD*	LRFD	LRFD*	LRFD	LRFD*
11	90	4	4.03	3.81	4.53	4.54	5.34	5.34
12	90	6	4.04	3.82	4.00	3.79	3.98	3.72
13	90	8	3.72	3.71	4.02	3.82	4.02	3.77
14	90	10	3.54	3.64	4.03	3.83	4.03	3.80
15	90	12	3.56	3.62	3.97	3.92	4.04	3.82
16	120	4	4.02	3.82	3.98	3.78	3.95	3.69
17	120	6	3.68	3.69	3.99	3.80	4.00	3.76
18	120	8	3.53	3.61	3.98	3.80	4.01	3.78
19	120	10	3.53	3.59	3.58	3.65	4.02	3.78
20	120	12	-	-	3.53	3.61	4.02	3.79
21	200	4	3.48	3.59	3.97	3.75	3.94	3.71
22	200	6	3.48	3.55	3.39	3.53	3.93	3.70
23	200	8	-	-	3.45	3.52	3.71	3.62
24	200	10	-	-	-	-	3.44	3.50
25	200	12	-	-	-	-	3.46	3.50

LRFD= design cases using the General LRFD Method; LRFD*= design cases using the new method

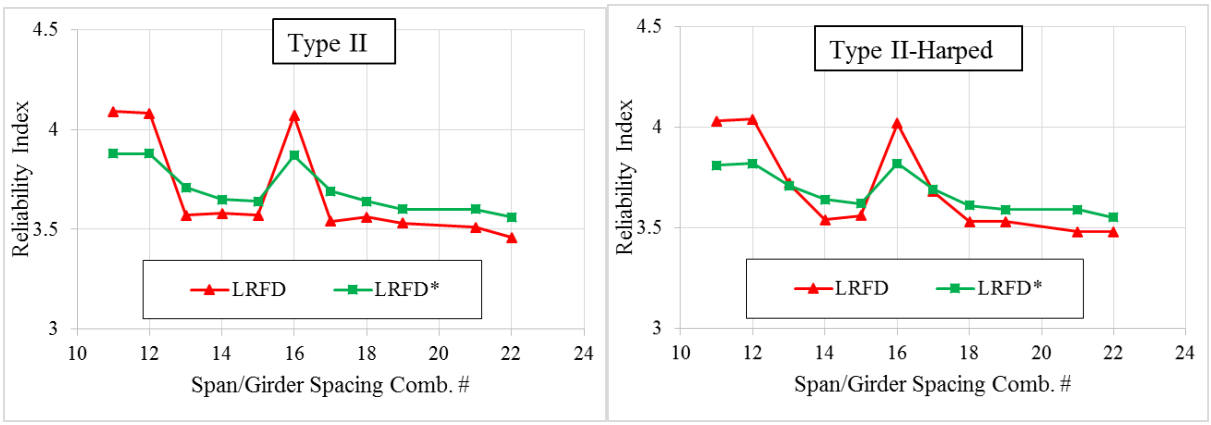

Figure 4.15. Reliability indices for Type II girder using the original and the new LRFD design methods

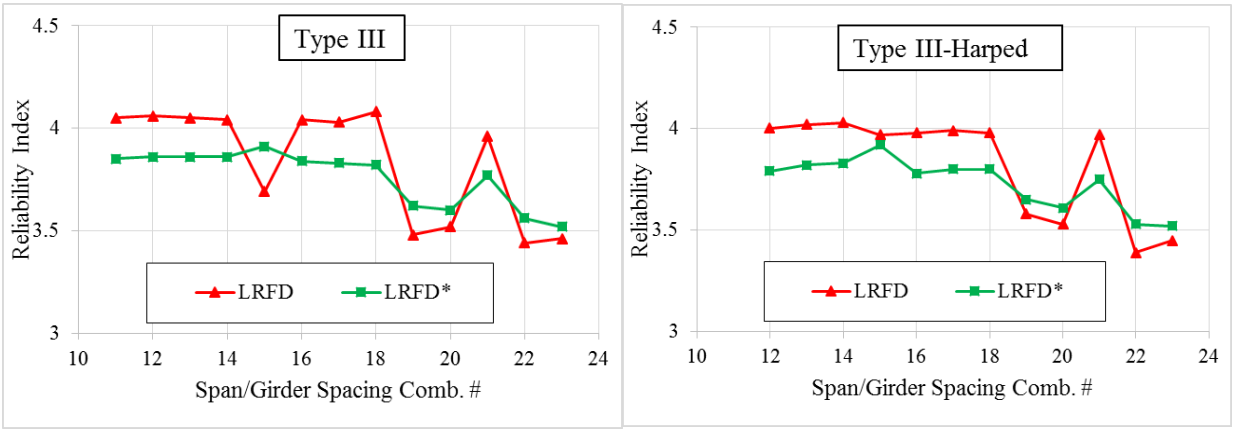

Figure 4.16. Reliability indices for Type III girder using the original and the new LRFD design methods

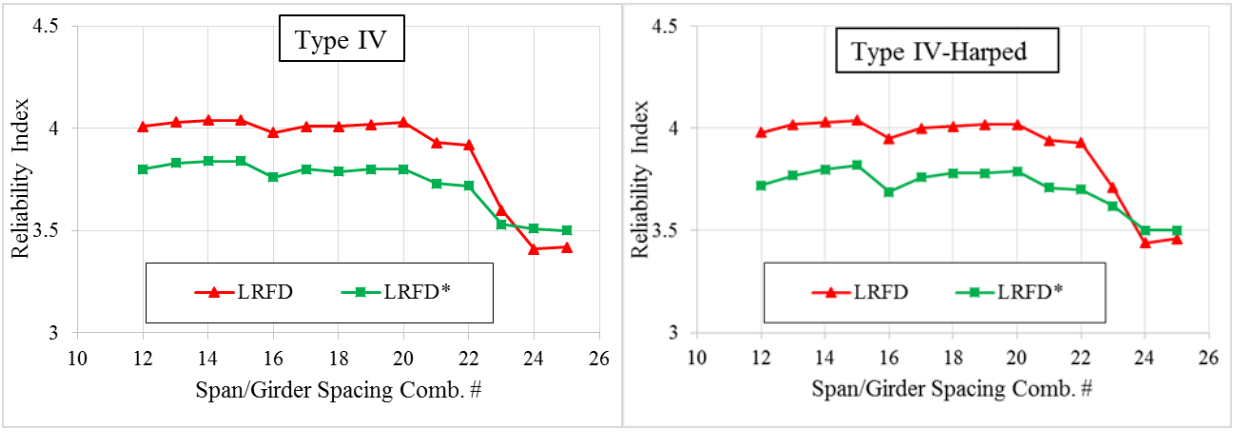

Figure 4.17. Reliability indices for Type IV girder using the original and the new LRFD design methods

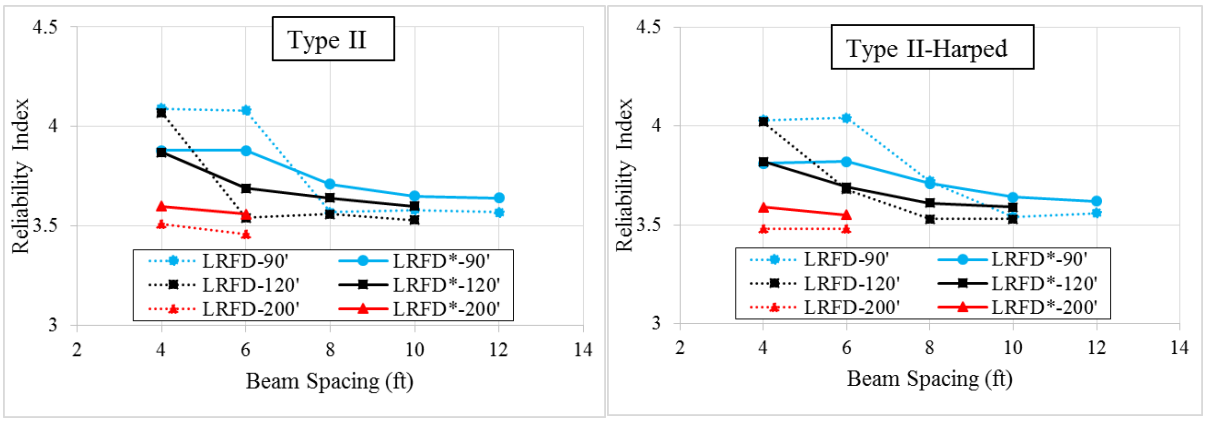

Figure 4.18. Reliability indices for Type II girder using the original and the new LRFD design methods

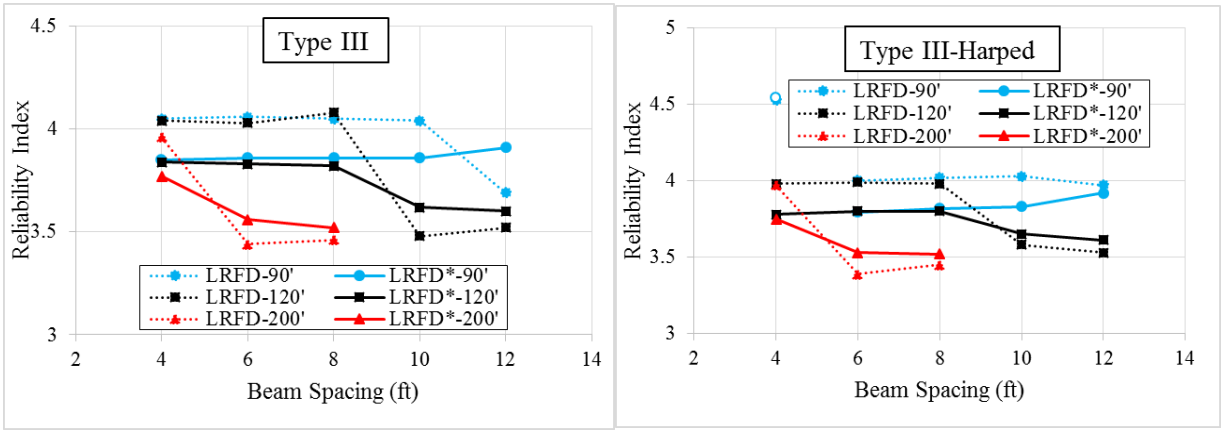

Figure 4.19. Reliability indices for Type III girder using the original and the new LRFD design methods

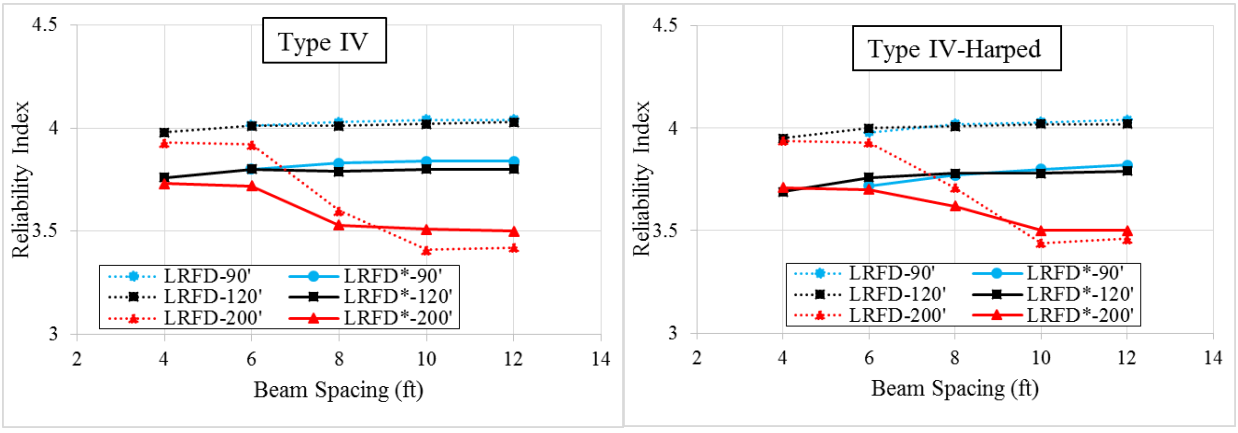

Figure 4.20. Reliability indices for Type IV girder using the original and the new LRFD design methods

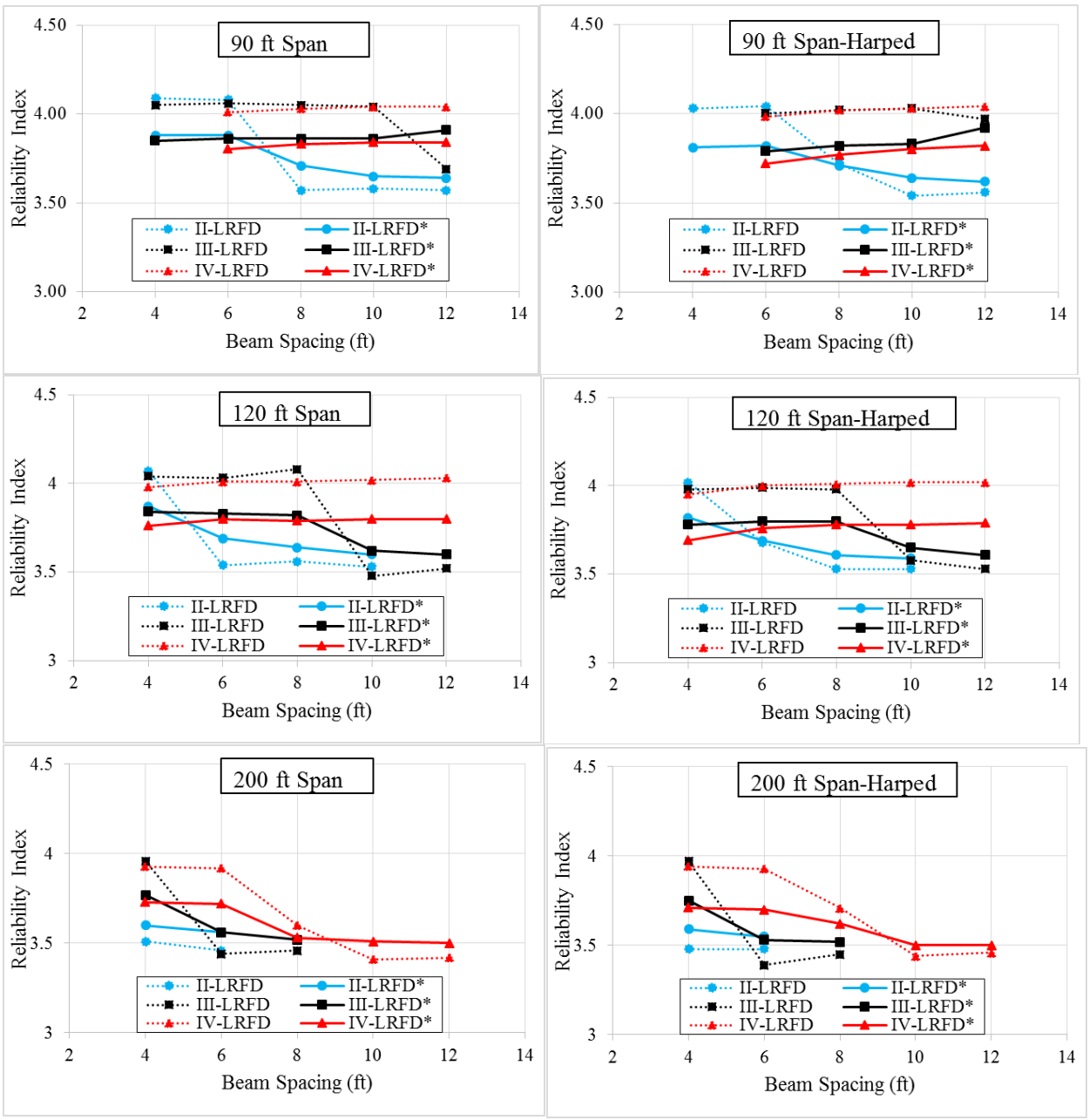

Figure 4.21. Reliability indices comparison between the original and the new LRFD design methods as a function of span length and girder spacing

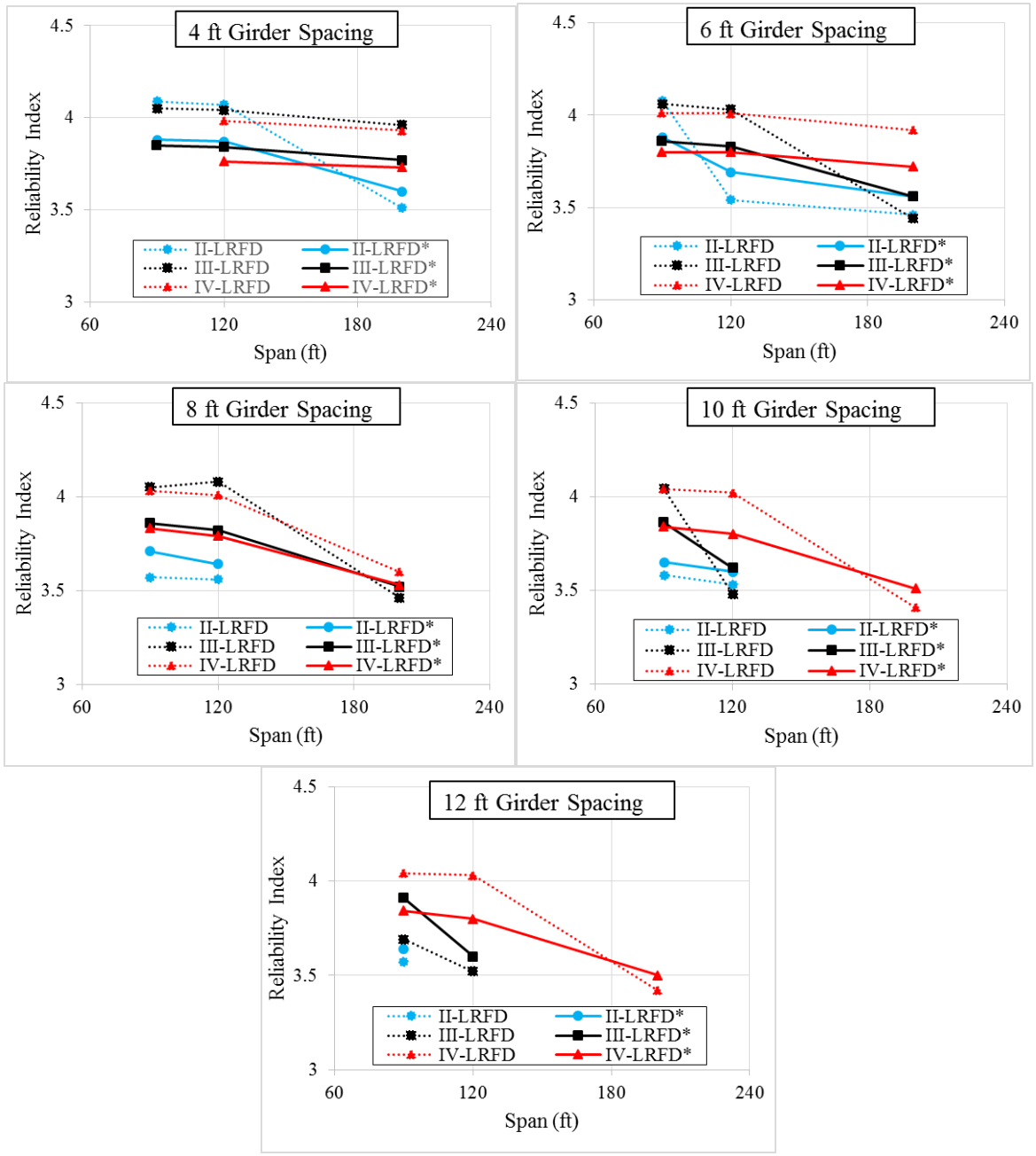

Figure 4.22. Reliability indices comparison between the original and the new LRFD design methods as a function of girder spacing and span length

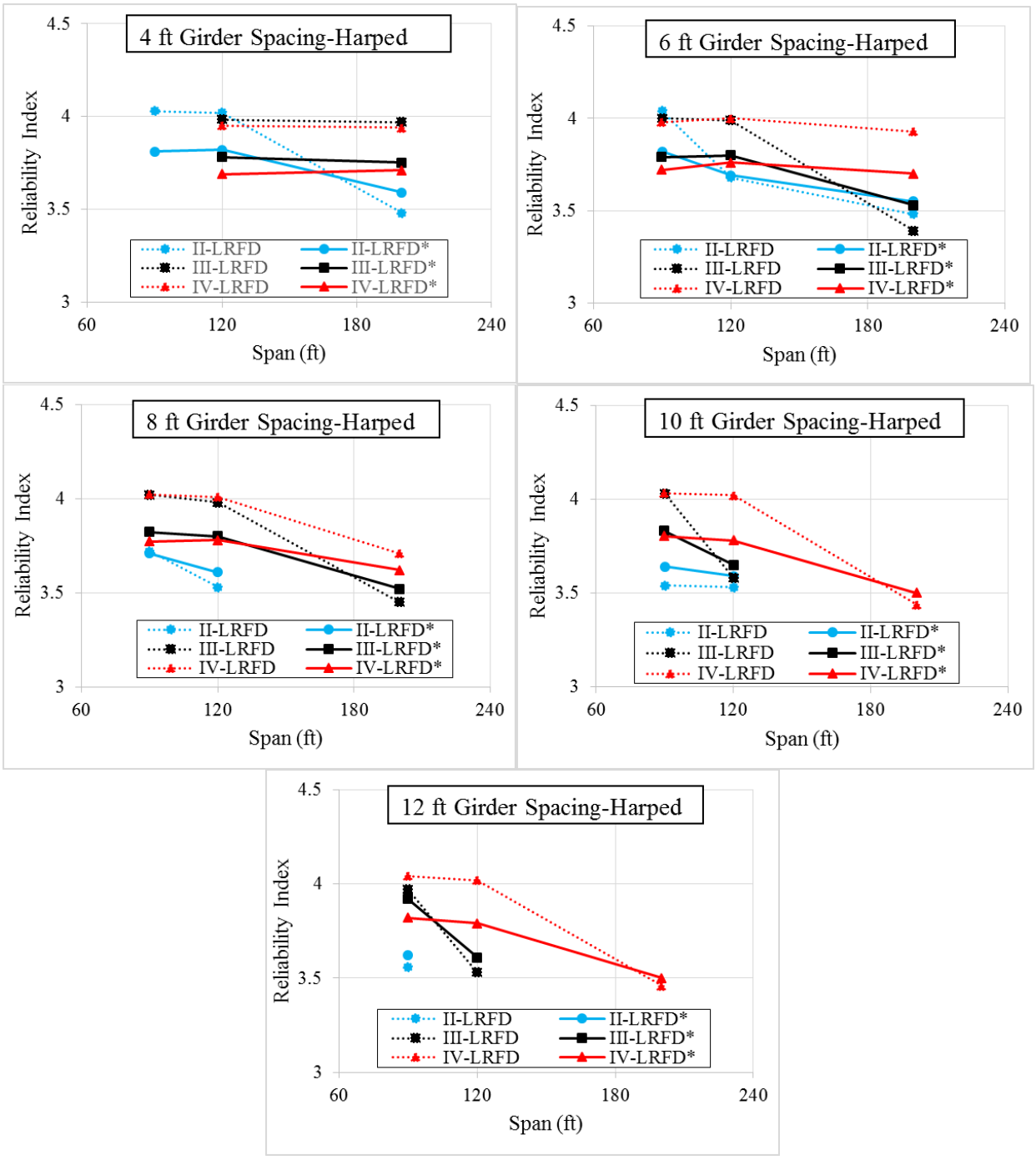

Figure 4.23. Reliability indices comparison between the original and the new LRFD design methods as a function of girder spacing and span length (harped strands)

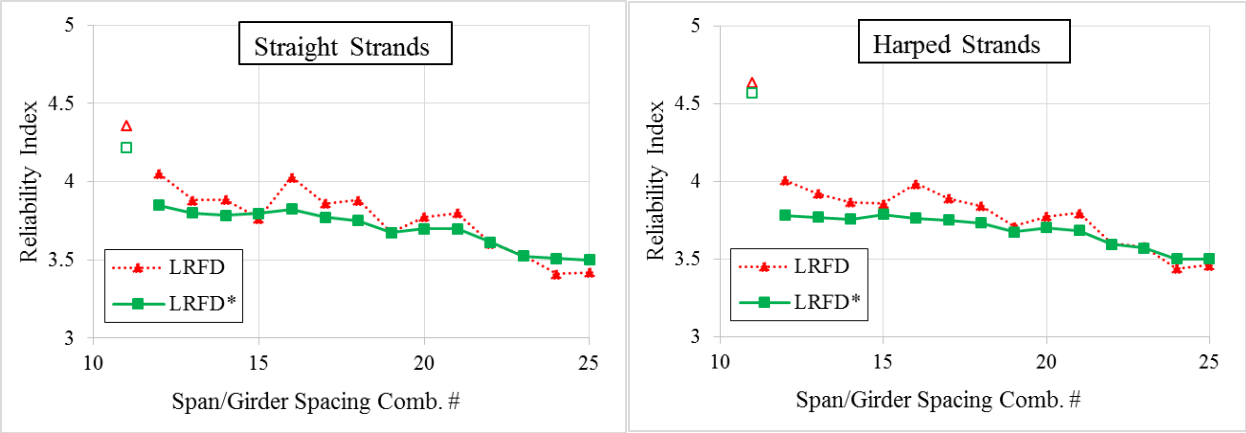

Figure 4.24. Average reliability indices comparison between the original and the new design methods

CHAPTER 5: REGRESSION ANALYSIS AND LOAD RATING

5.1 Development of Regression Equation

Regression analysis based on the computed ratios (FEA/LRFD) for AASHTO girder types II, III and IV was performed. In this regression analysis, the computed ratios (FEA/LRFD) were considered as dependent variables while concrete compressive strength (f_c'), average stress due to prestress force (σ), stirrups spacing (s), and beam height (h) were considered as independent variables. Linear and nonlinear regression analyses were performed on 216 data samples, and two initial regression models were developed, linear and nonlinear. It was found that the linear regression model produced more consistent results than the nonlinear model, and therefore, was considered for this study. Based on the described regression analysis, one regression equation is proposed, as shown below:

$$\left(\frac{FEA}{LRFD}\right)_{Reg.} = r_d = \left(0.009f_c' + 0.2\sigma + 0.035s\left(\frac{0.22}{A_v}\right) + 0.018h + 0.01\right) \quad (5.1)$$

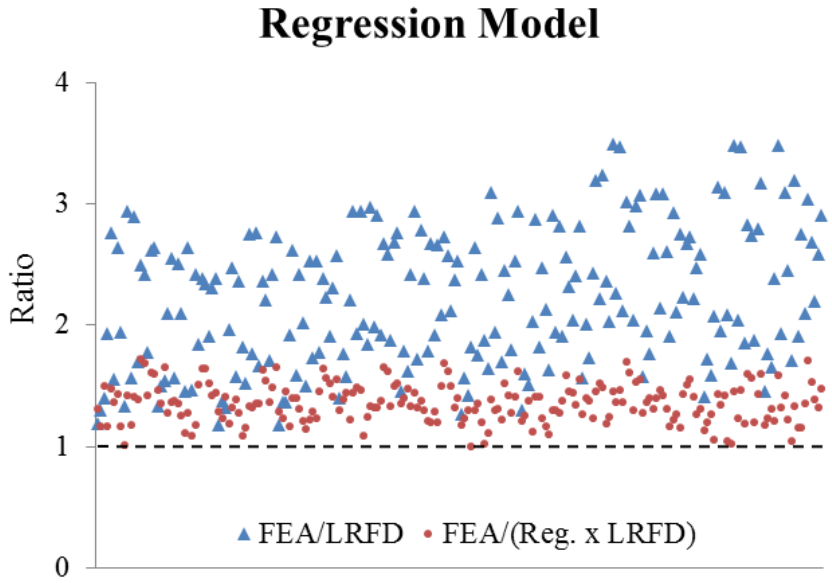

Figure 5.1. Comparison between linear regression model and FEA/LRFD ratios

A comparison between the proposed regression model and the FEA/LRFD ratios is shown in Figure 5.1, and data used to develop this regression model are presented in Appendix C.

As shown in Table 5.1, the developed equation (5.1) provided the lowest deviation (mean ratio of estimation to FEA model predicted capacity = 1.36; COV 0.11) from the expected beam capacities, as determined from the FEA models, with no case unconservatively estimated. Note that if r_d is computed outside of the limit provided (i.e. $1.0 \leq r_d \leq 3.49$), then r_d should be limited to that value; it does not mean that the adjustment is invalid. The upper limit represents the maximum FEA/LRFD ratio found from all of the cases studied, and is imposed for safety.

Table 5.1. Comparisons between the two regression models and the FEA/LRFD ratios

	(FEA/LRFD)	Reg.	FEA/(Reg. x LRFD)
Mean	2.22	1.64	1.36
STDEV.	0.56	0.37	0.16
COV	0.25	0.23	0.11

To best estimate shear capacity V_n of MDOT PC girders, it is recommended that the regression equation (eq. 5.1) is used in conjunction with the modified AASHTO LRFD procedure described in Chapter 2; this procedure is summarized by Eq. 5.2. Specifically, V_n is first computed from the LRFD Sectional Method then an iteration is conducted until $V_n = V_u$, as described in Appendix E, to produce $V_{n\text{-}est}$. This result is then multiplied by the outcome of eq. 5.2, as a function of concrete compressive strength (f'c, ksi), average stress due to prestress force (σ = gross area of concrete beam / total prestress force, ksi), stirrups spacing (s, inches), and beam height (h, inches), to provide the best estimate for V_n.

$$V_n = V_{n-est}\, r_d \tag{5.2}$$

5.2 Development of Regression Equation for Reliability Analysis

In order to compute reliability analysis for the girder design cases presented in Chapter 4, a second regression equation was developed with a mean ratio of estimation $(\frac{\text{FEA}}{\text{Reg. x LRFD}}) = 1$. The developed regression model for reliability is defined in equation 5.3 and shown in Figure 5.2.

$$r_r = \left(0.075 f_c' + 0.2\sigma + 0.038s\left(\frac{0.22}{A_v}\right) + 0.02h + 0.01\right) \quad (5.3)$$

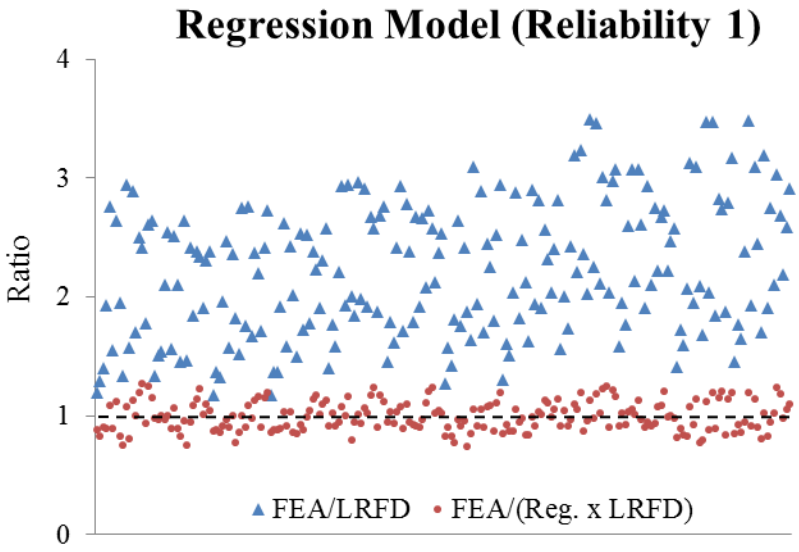

Figure 5.2. Linear regression model for reliability analysis

A second regression model for reliability was developed based a reduced number of FEA/LRFD data, by excluding the cases with highest stress in concrete (2.5 ksi). This modification was made because all the bridge design cases considered for reliability analysis were assumed to have an average stress in concrete of 1 ksi. While the stress level is not included in the calculations of the nominal shear capacity, it is an important parameter for moment design. An average stress level of 1 ksi was considered based on a survey of 31 PC spans in the state of Michigan. The 31 cases had stress levels ranged from 0.24 to 2.11 ksi and 1.09 ksi on average, with the majority of

the cases designed with stress level less than 1.5 ksi. Therefore an average stress in concrete of 1 ksi was assumed for the reliability analysis regression model. The modified regression equation for reliability produced factors lower on average compared to the initial model, and produced more conservative β values. The regression model used for reliability analysis in this study in presented eq. 5.4 and Figure 5.3.

$$r_r = \left(0.088f_c' + 0.2\sigma + 0.01s\left(\frac{0.22}{A_v}\right) + 0.024h + 0.01\right) \tag{5.4}$$

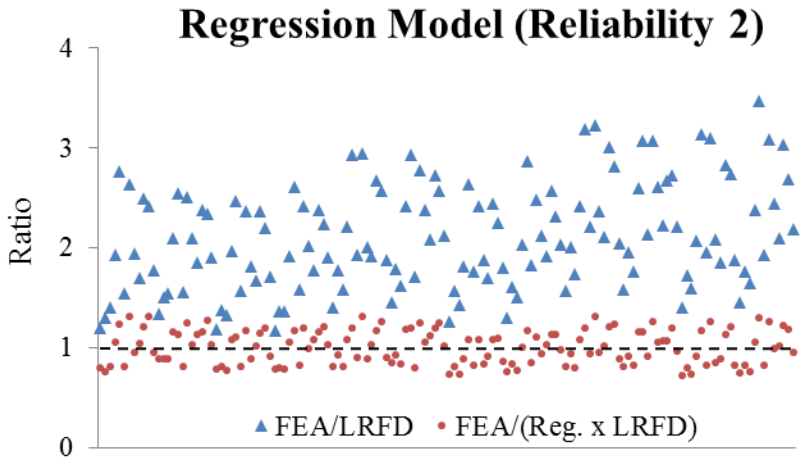

Figure 5.3. Improved linear regression model for reliability analysis

Reliability indices for girder cases designed in accordance to the current LRFD code (HL-93 LL) were computed based on live load data from the state of Michigan (see Appendix H-Table H2). Moreover, the same cases were considered for a second reliability analysis by including the regression factor calculated from equation 5.4. Comparisons between the two sets of results, and the NCHRP 368 β values are shown in Table 5.2 and Figures 5.4-5.8.

Table 5.2. Reliability indices based on live loads from the state on Michigan

				MI LL			MI LL (Regression Factor)		
#	Span (ft)	Spacing (ft)	Beta-NCHRP	Beta-II	Beta-III	Beta-IV	Beta-II	Beta-III	Beta-IV
1	30	4	4.16	4.41	5.85	6.75	7.04	8.14	8.71
2	30	6	4.19	3.61	5.20	6.25	6.51	7.82	8.51
3	30	8	4.12	2.90	4.56	5.72	6.04	7.46	8.28
4	30	10	4.25	2.89	3.94	5.20	6.03	7.11	8.04
5	30	12	4.21	3.04	3.35	4.69	6.21	6.75	7.79
6	60	4	4.09	1.83	3.32	4.48	5.30	6.73	7.69
7	60	6	4.10	2.33	2.48	3.72	5.62	6.21	7.30
8	60	8	4.14	2.64	2.58	3.01	5.99	6.23	6.90
9	60	10	4.10	2.35	2.76	2.71	6.26	6.41	6.88
10	60	12	4.12	2.35	2.90	2.83	6.17	6.60	6.75
11	90	4	3.74	1.66	1.70	2.78	5.19	5.71	6.78
12	90	6	3.77	2.15	2.14	2.14	5.81	5.96	6.49
13	90	8	3.81	1.75	2.42	2.42	5.67	6.22	6.58
14	90	10	3.83	2.02	2.59	2.60	5.70	6.27	6.66
15	90	12	3.85	2.13	2.23	2.71	5.81	6.30	6.83
16	120	4	3.78	1.63	1.70	1.77	5.26	5.69	6.27
17	120	6	3.81	1.36	2.11	2.16	5.25	6.01	6.39
18	120	8	3.88	1.74	2.26	2.58	5.40	6.12	6.61
19	120	10	3.89	1.91	1.87	2.57	5.54	5.98	6.81
20	120	12	3.83	-	2.06	2.71	-	6.04	6.98
21	200	4	3.70	0.83	1.64	1.78	4.73	5.63	6.23
22	200	6	3.79	1.26	1.29	2.10	5.06	5.59	6.37
23	200	8	3.82	-	1.61	1.81	-	5.76	6.45
24	200	10	3.79	-	-	1.80	-	-	6.55
25	200	12	3.82	-	-	1.92	-	-	6.76

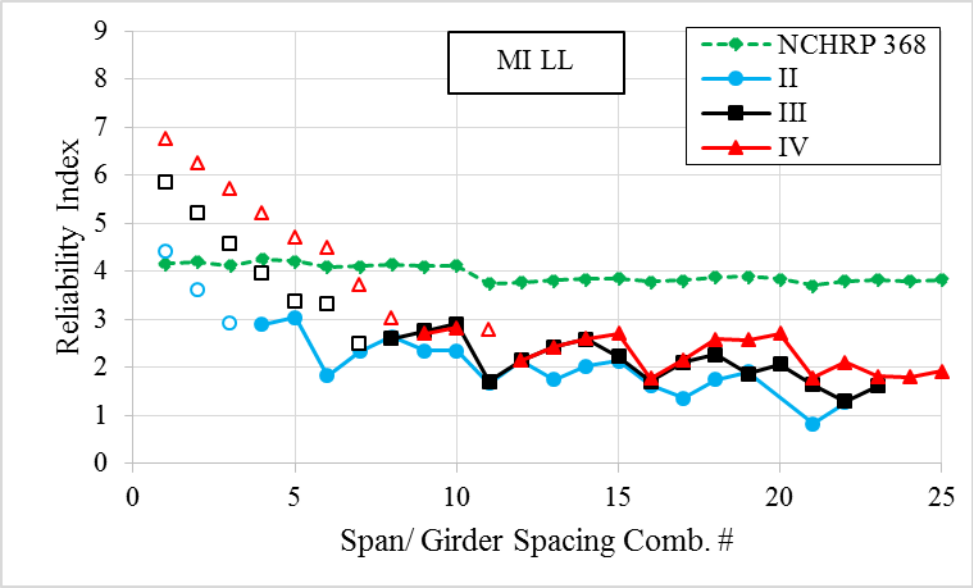

Figure 5.4. Reliability indices based on Michigan live loads compared to NCHRP 368

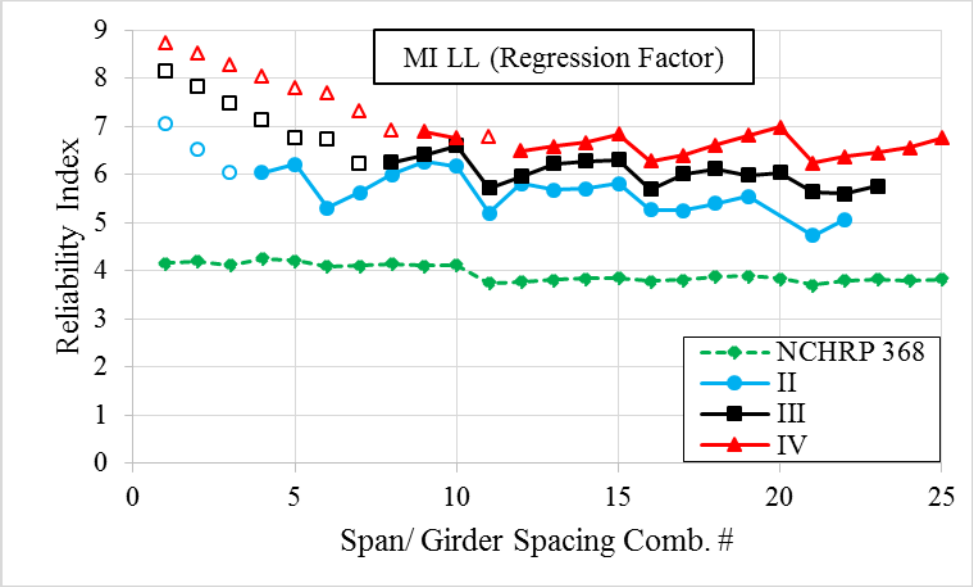

Figure 5.5. Reliability indices based on Michigan live loads and using the regression model

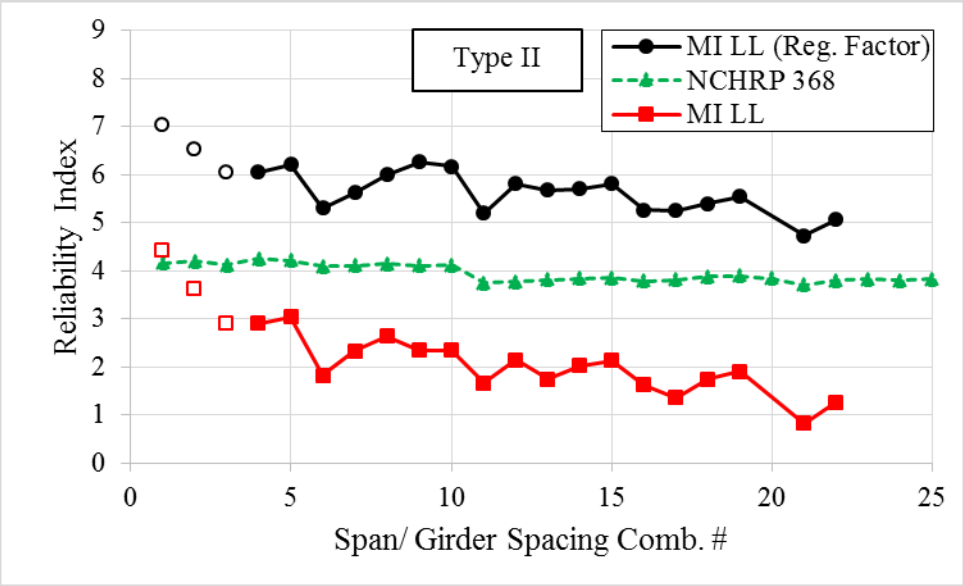

Figure 5.6. Comparison of reliability indices based on Michigan live loads for Type II girder

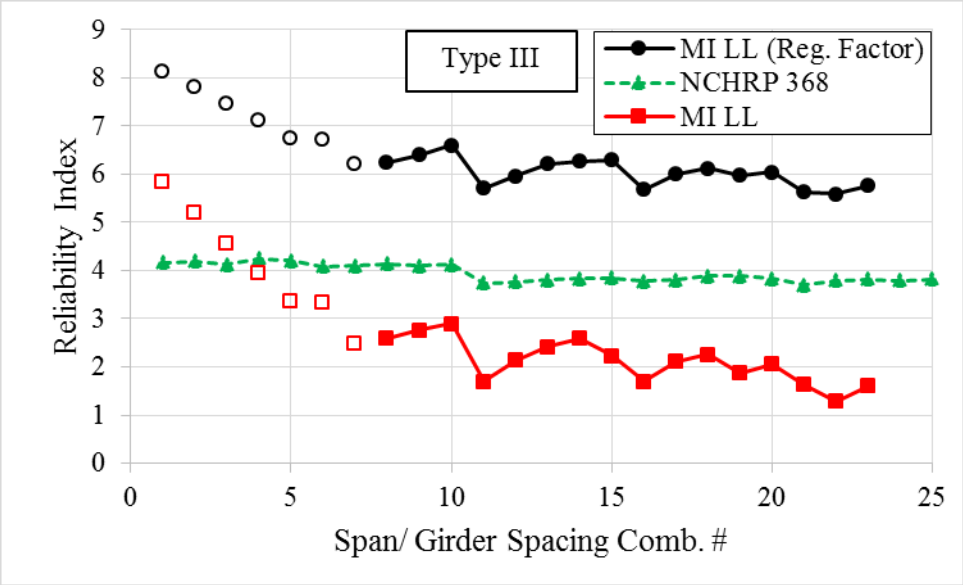

Figure 5.7. Comparison of reliability indices based on Michigan live loads for Type III girder

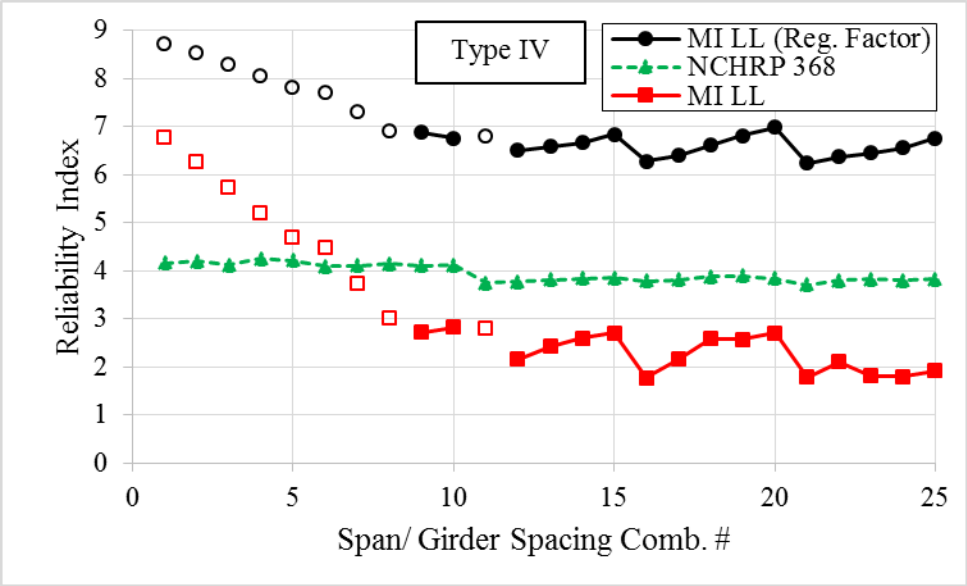

Figure 5.8. Comparison of reliability indices based on Michigan live loads for Type IV girder

By analyzing the results, it is clearly shown that applying the regression factor resulted in significantly higher reliability index values than those computed without the regression factor and values from NCHRP 368. However, low reliability indices resulted (≤3) under MI live loads when the Original LRFD Procedure was used for design. To show an estimation of the actual reliability

indices for the cases considered, the average of the two sets of results (with and without regression factor) was computed and plotted, as shown in Figure 5.9. Moreover, the average of the three girder results is plotted in Figure 5.10 for a simpler comparison with NCHRP 368 values. This estimation does not accurately capture the actual reliability index, since linearity is assumed, but it shows a reasonable approximation based on methods used to compute each set of the results.

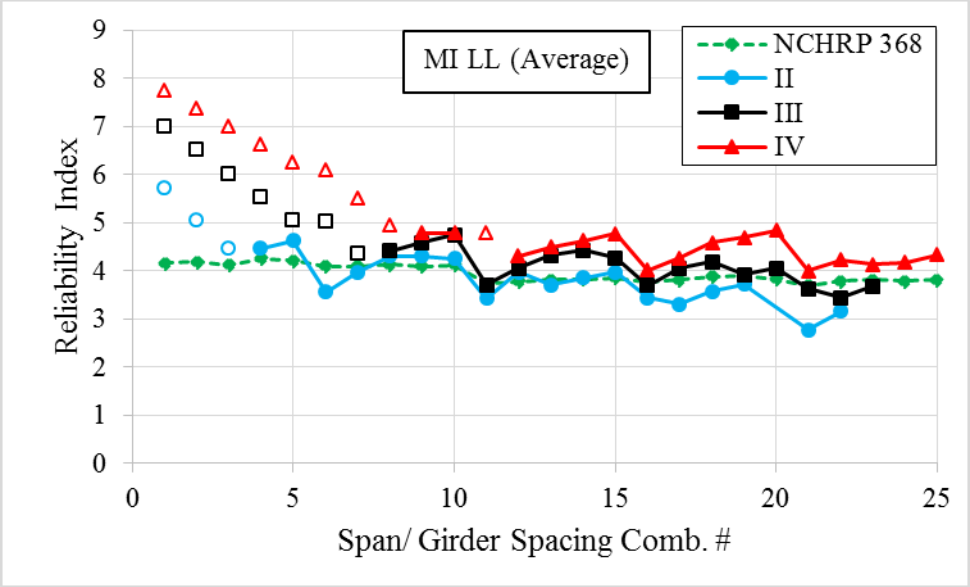

Figure 5.9. Average reliability indices for girders Type II, III and IV based on Michigan live loads

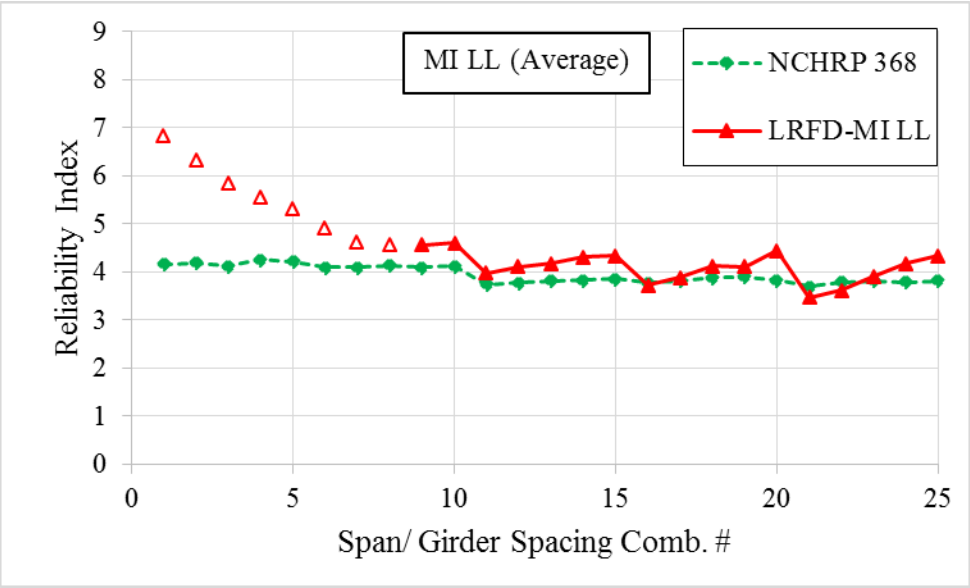

Figure 5.10. Comparison of average reliability indices based on Michigan live loads

Reliability indices based on the mean values of the initial two sets of results showed to have an adequate level of safety on average (>4), and thus the MI live load traffic used for analysis are acceptable for PC bridges designed in accordance to the General LRFD Procedure.

5.3 Load Rating

The procedure of load rating is used to identify the need for bridge strengthening, load postings, and issuing overweight vehicle permits. The focus of this section is on the load rating for prestressed concrete bridges under traffic live loads in the state of Michigan.

In design, a conservative reliability index may be imposed to insure serviceability and durability requirements without adding a significant cost. However, the cost of increasing the strength of existing structures, or to restrict traffic on these structures (to the user) can be substantial. Therefore, a lower target reliability index is chosen for load rating at the strength limit state. In the NCHRP 368 report, a target reliability index of 3.5 was adopted based on a severe traffic loading (5000 ADTT), while the LRFR procedures reduced the target reliability index to approximately 2.5, calibrated to past AASHTO operating level load rating (AASHTO 2011).

The procedure for the load and resistance factor rating (LRFR) of bridges is consisted of three different procedures: 1) Design load rating, 2) legal load rating, and 3) permit load rating. In this study, the design load rating is considered for analysis. As a first level assessment and a measure of the performance of PC bridges, design load rating is based on the HL-93 and LRFD design specifications. Bridges that pass the design load check at the Inventory level, have satisfactory load rating for all legal loads that comply with the LRFD limits, and have a rating factor (RF) ≥ 1. Otherwise, bridges that do not pass the load check at the inventory level have a RF ≤ 1. The determination of the rating factor for each component subjected to a single force effect is represented in the general expression below:

$$RF = \frac{C - (\gamma_{DC})(DC) - (\gamma_{DW})(DW) \pm (\gamma_P)(P)}{(\gamma_{LL})(LL + IM)} \tag{5.5}$$

Where $C = \varphi_c \varphi_s \varphi R_n;\ \ \varphi_c \varphi_s \geq 0.85$

Where RF is the rating factor, C is the capacity, R_n is the nominal resistance, φ_c is the condition factor, φ_s is the system factor, φ is the LRFD resistance factor, DC is the dead load effect due to structural components and attachments, DW is the dead load effect due to wearing surface and utilities, P represents permanent loads other than dead loads, LL is the live load effect, IM is the dynamic load allowance, $\gamma_{DC}, \gamma_{DW}, \gamma_P$ are LRFD load factors for structural components, wearing surfaces and permanent loads, respectively, and γ_{LL} is the evaluation live load factor.

Using the appropriate factors for the PC girders considered in this study, the resulted RF equations for inventory and operating are presented below:

$$RF = \frac{(0.9)R_n - (1.25)(DC) - (1.5)(DW)}{(1.75)(LL + IM)}\ ; Inventory \tag{5.6}$$

$$RF = \frac{(0.9)R_n - (1.25)(DC) - (1.5)(DW)}{(1.35)(LL + IM)}\ ; Operating \tag{5.7}$$

Projected live load data for traffic in the state of Michigan (Eamon et al., 2014) were computed and considered for load rating (see Appendix H-Table H2). PC girder Types II, III, and IV designed in accordance to the LRFD General Method were considered for evaluation under the MDOT live loads, and compared to the ideal load rating factors. Rating factors were conducted for both inventory and operating levels using equations 5.6 and 5.7, respectively. The regression factor resulted from equation 5.4 was also applied for rating, and comparisons of the resulted rating factors are presented in Figures 5.11-5.16.

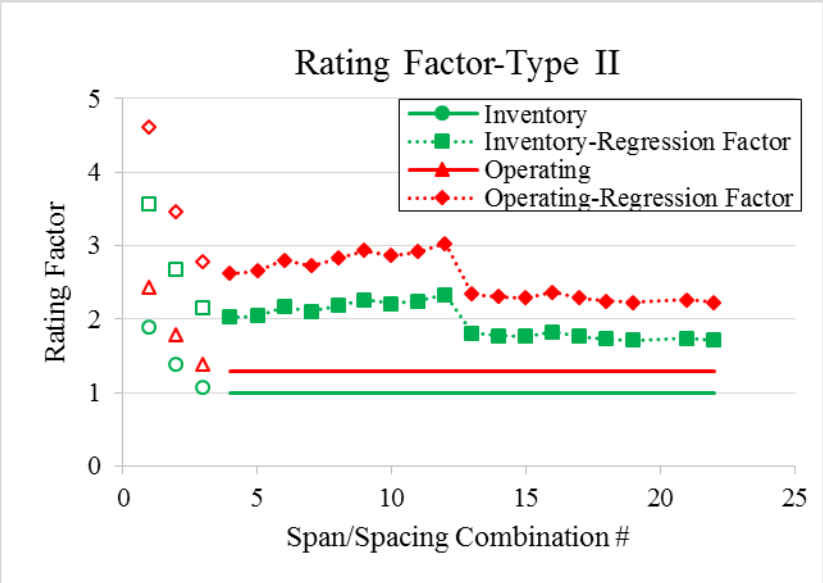

Figure 5.11. Rating factors for Type II girder

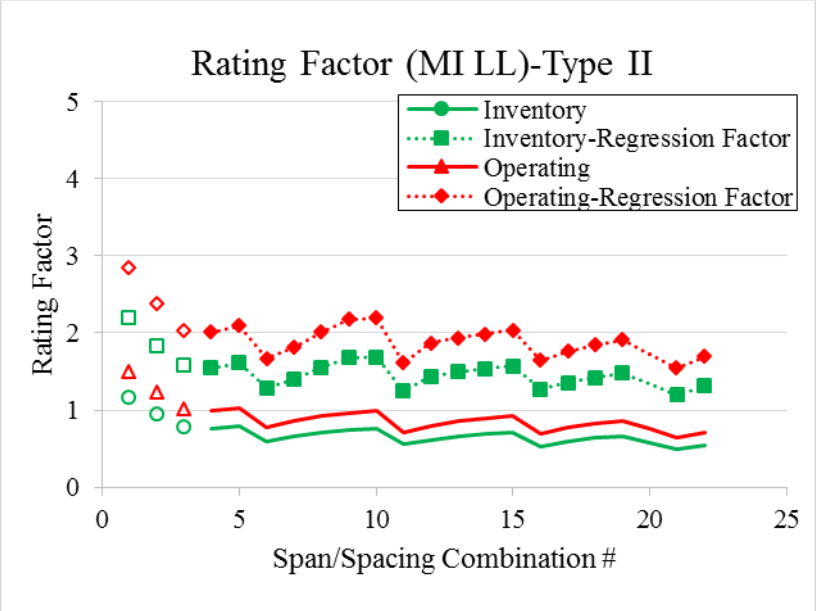

Figure 5.12. Rating factors for Type II girder based on Michigan LL

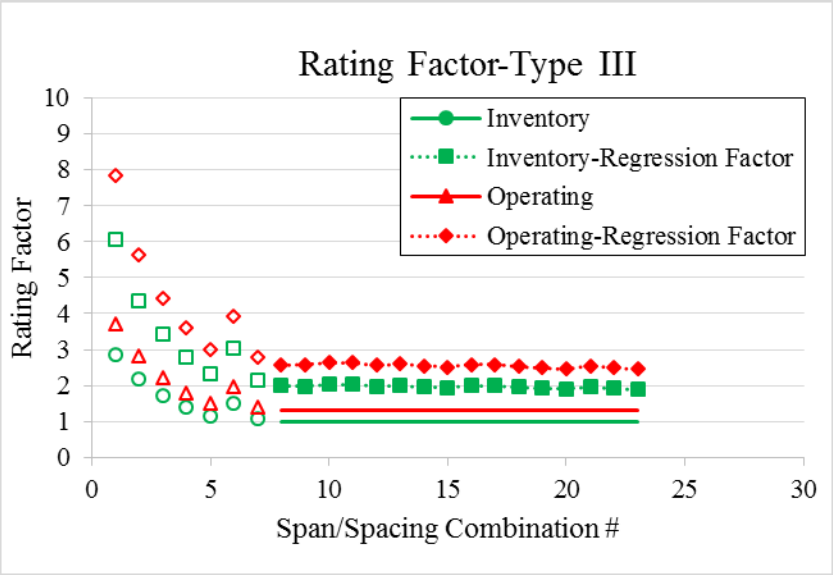

Figure 5.13. Rating factors for Type III girder

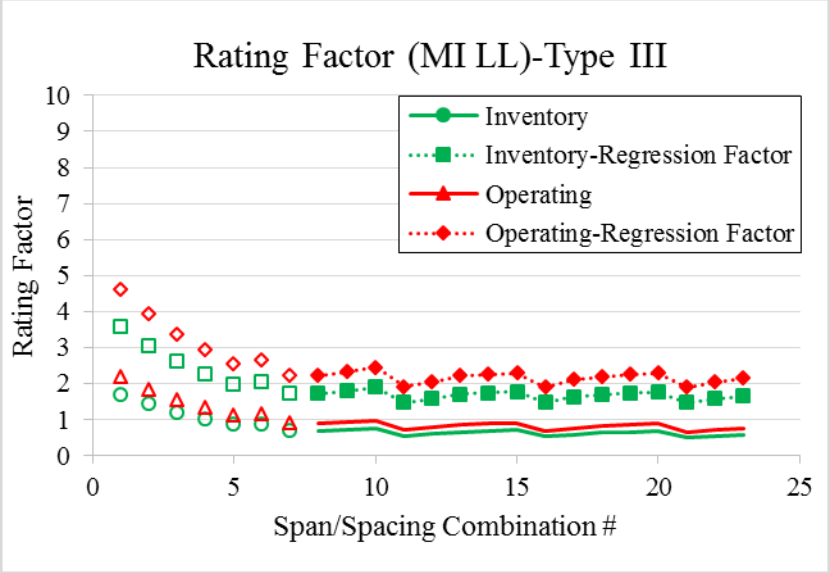

Figure 5.14. Rating factors for Type III girder based on Michigan LL

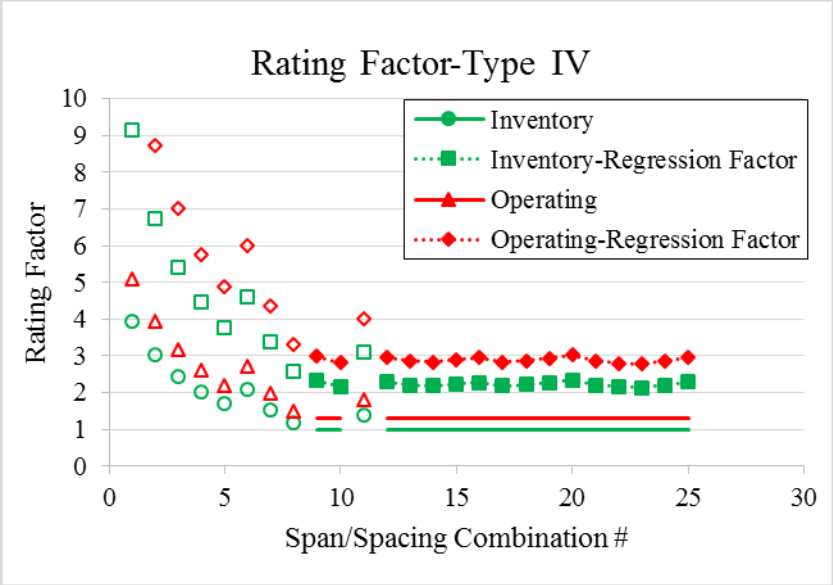

Figure 5.15. Rating factors for Type IV girder

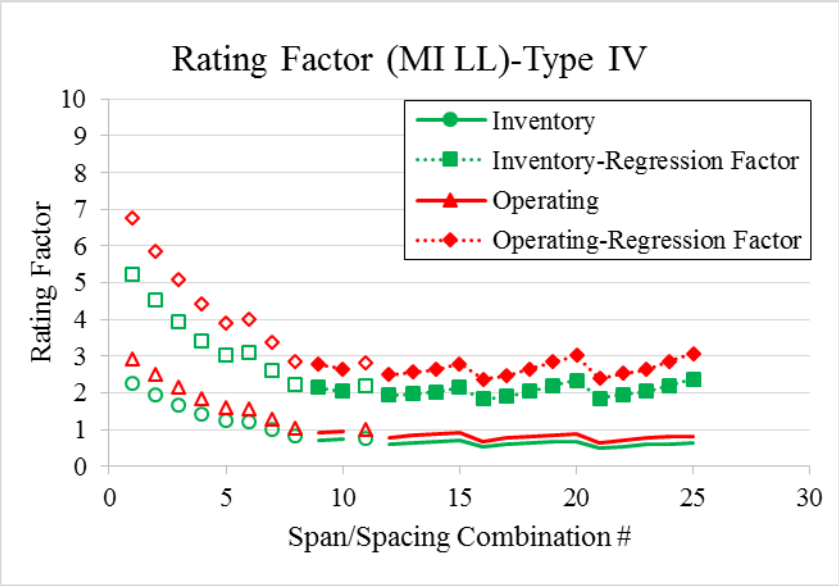

Figure 5.16. Rating factors for Type IV girder based on Michigan LL

In general, the resulted RF for all the design cases was ≥1 when the HL-93 live load was used for evaluation. Conversely, rating factors < 1 resulted when the MI live loads were considered for evaluation, while all RFs evaluated based on the regression factor were > 1.

CHAPTER 6: SUMMARY, CONCLUSIONS AND RECOMMENDATIONS

6.1 Summary

The main research objectives of this study were to assess the adequacy of the current AASHTO PC shear design methods; determine the reliability of PC bridge girders in shear based on the current LRFD General Procedure; determine the most accurate and consistent method for predicting shear capacity of AASHTO "I" shape PC bridge girders; recalibrate the AASHTO LRFD code for shear as necessary, such that PC bridge girders will have more consistent and a minimum target of reliability for shear; and compute load rating analysis based on the HL-93 and MI live loads for PC bridges designed in accordance to the General LRFD Procedure for shear. These objectives were achieved through:

1) Detailed literature review of the existing methods for design and rating of PC girders. In particular, the AASHTO Standard Code, the AASHTO LRFD Code, and the 1979 AASHTO Interim Specifications, as well as the supporting technical literature, were reviewed as summarized in Chapter 1.
2) Experimental study on two 36 feet long AASHTO Type II PC girders, tested under various point load and span configurations. Each girder was tested three times in different regions of the span by adjusting support locations to generate data for different critical shear span-to-depth (a/d) ratios and stirrup spacings. Stirrup spacings ranged from 8 to 12 in and shear span/depth ratios from 2.0 to 3.5. The purpose of the testing was to gather reliable experimental data that could be used to validate numerical (FEA) models.
3) Development of a reliable FEA model based on the experimental testing results was performed. The developed FEA model could well-match the majority of the experimental results, as well as the seven PC beam shear tests found in the technical literature that were

chosen for validation. The developed numerical model, in combination with the design code predictions, were used to generate necessary data for parametric analysis.

4) Parametric analysis on three PC bridge girder configurations (Types II, III, and IV) was conducted using the developed FEA model. Three code procedures (AASHTO LRFD, 1979 Interim, and AASHTO Standard) were considered for comparison with the FEA results. The AASHTO Standard code could best predict the shear capacity of the FEA cases considered in terms of accuracy as well as consistency. Parameters considered for the parametric analysis included beam type, load position, strand profile, concrete strength, prestress level, stirrup spacing, and longitudinal prestressed steel reinforcement ratio, for a total of 324 analyses.

5) Formulation of a linear regression equation to modify the LRFD calculated shear capacity to best fit the FEA results was performed and shown in equation 6.1 below.

$$\left(\frac{FEA}{LRFD}\right)_{Reg.} = r_d = \left(0.009f_c' + 0.2\sigma + 0.035s\left(\frac{0.22}{A_v}\right) + 0.018h + 0.01\right) \qquad (6.1)$$

The proposed regression equation produced a better estimate of shear capacity, compared to those computed using the General LRFD Procedure.

6) A second regression equation for reliability analysis was developed with a mean ratio of estimation $=\left(\frac{\text{FEA}}{\text{Reg. x LRFD}}\right) = 1$. The developed regression model (r_r) for reliability is defined in equation 6.2 below.

$$r_r = \left(0.088f_c' + 0.2\sigma + 0.01s\left(\frac{0.22}{A_v}\right) + 0.024h + 0.01\right) \qquad (6.2)$$

7) Reliability indices of 175 different PC bridge girders were computed using the RF procedure. Girder cases were designed in accordance to the LRFD General Procedure.

8) Modification to the current LRFD General Procedure was proposed. Where the original code method produced reliability indices less than 3.5 for several cases, the proposed modification produced more consistent reliability indices with a minimum value of 3.5 for the design cases considered. The lower limit of 3.5 was achieved by adding a new design factor of 1.05. Thus, $0.9 * 1.05\ V_n = 0.95\ V_n = V_u$, and the new shear and moment values used for design are $V_{u*} = \frac{V_u}{0.9*1.05} = 1.06\ V_u = \gamma_v V_u$ and $M_u = V_{u*}\ d_v$, respectively. In the proposed design procedure, a larger V_u value (V_{u*}) was used for design. Increasing the value of V_u (used to compute ε_s) by a factor of 1.06, or ($\frac{1}{0.95}$), reduced the computed V_n value which, as a result, required increasing the design shear capacity. In total, two factors are proposed, one factor ($\gamma_v = 1.06$) for the design shear load and the other ($\phi_r = 0.95$) for the nominal shear resistance in place of the original resistance factor ($\phi = 0.9$) specified by the current LRFD code. Thus, $\phi_r\ V_n = V_u$ and $V_{u*} = \gamma_v\ V_u$, where V_n is the nominal shear capacity, V_u is the factored shear load specified by the LRFD code, and V_{u*} is the new shear load value used to compute ε_s.

9) Reliability indices for girder cases designed in accordance to the current LRFD code (HL-93 LL) were computed based on live load data from the state of Michigan. This reliability analysis was based on the original code method for calculating V_n, and considered the regression factor (r_r) resulted from the proposed equation 6.2. Applying the regression factor resulted in significantly higher reliability indices than those for the original cases (without the regression factor) and from those reported in NCHRP 368. In contrast, low reliability indices resulted (≤3) under MI live loads when the Original LRFD Procedure was used for design.

10) Rating factors (RF) at inventory and operating levels were computed for ASSHTO Types II, III, and IV bridge girders under both HL-93 and MI live loads. The rating was based on the original code method for calculating V_n, and on the regression factor resulted from the proposed equation 6.1. When the regression factor was included, the resulted RFs for all the design cases were ≥1 when the HL-93 or MI live loads were used for evaluation. Conversely, when no regression factor was used, rating factors less than 1 resulted only when the MI live loads were considered for evaluation.

6.2 Conclusions

1) The developed FEA model proved to be a reliable and slightly conservative tool in predicting the shear capacity of PC concrete girders.
2) Reliability indices tend to increase as the girder size increases, and to decrease as the span length and girder spacing increase.
3) The current LRFD General Procedure for shear design produced inconsistent reliability indices with several values less than 3.5.
4) Low reliability indices (≤3) resulted using the Original LRFD Procedure for design when MI live loads were considered for analysis.
5) The proposed modification to the current LRFD General Procedure produced more consistent reliability indices. In particular, the proposed increase in shear and moment values used to compute the longitudinal strain.
6) The application of the proposed design factor resulted in a lower design capacity in general, but with a minimum reliability index of 3.5, which does not fall below the target reliability index of 3.5 specified in the NCHRP 368 report.

6.3 Recommendations

For evaluation, to best estimate the shear capacity of MDOT PC girders within the range of beam parameters considered in this study, it is recommended that the developed linear regression function is used in conjunction with the modified AASHTO LRFD procedure as described in Chapter 2 and Appendix E.

For design, it is recommended to use the modified LRFD method described in Chapter 5 which produced more consistent reliability indices with a lower limit of 3.5 compared to those computed based on current General LRFD Procedure for shear design.

For further verification of PC girder shear capacity, it is recommended that a field load test, in the form of monitoring, is considered. Several existing MDOT reports include details on the load testing of bridges.

Finally, for MDOT PC bridges, it is recommended to evaluate and load rate the existing bridges in the state of Michigan based on the MI live loads used in this study (Eamon et al., 2014).

APPENDIX A: GIRDER TEST RESULTS AND CASTING DATA

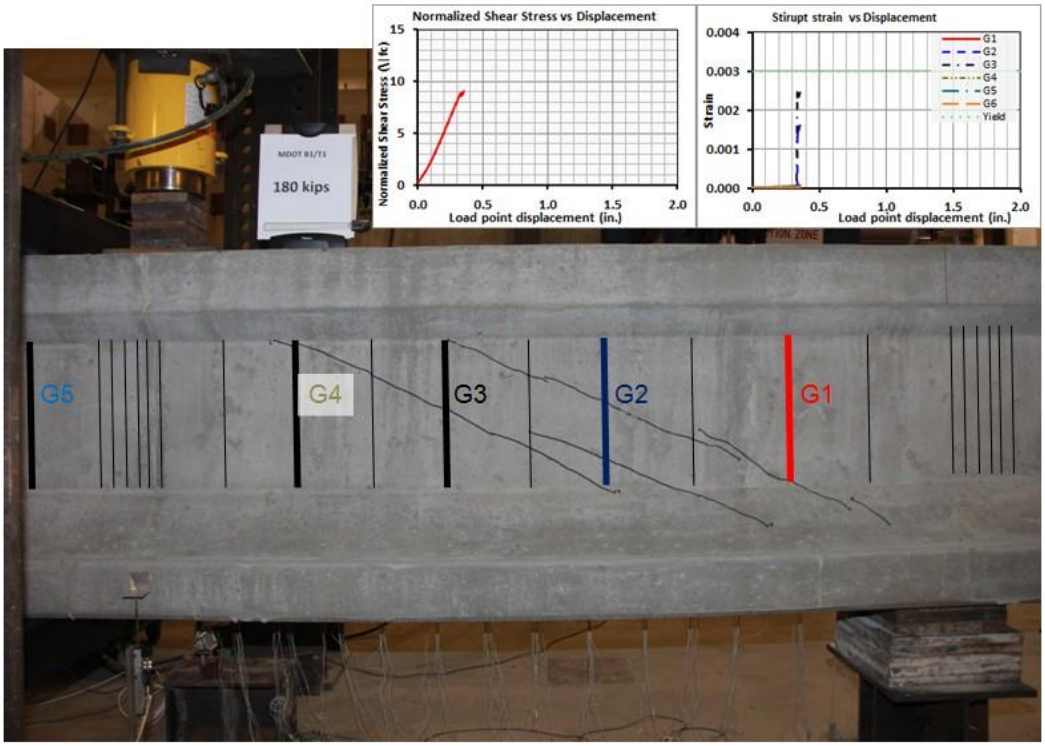

Figure A1. Girder 1-Test 1 first cracking load

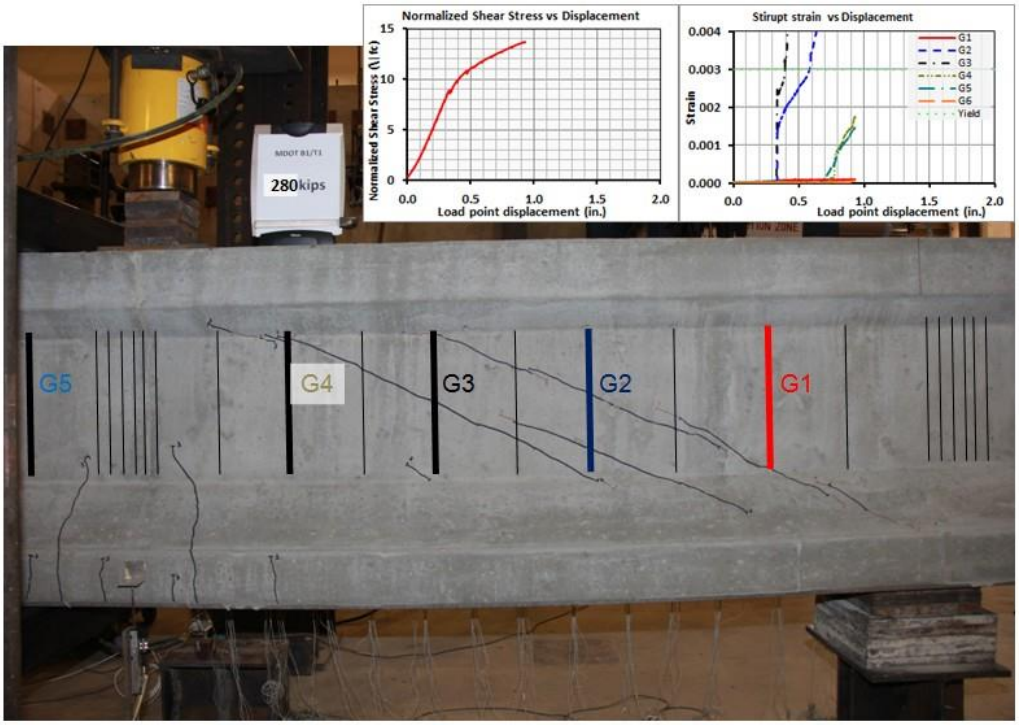

Figure A2. Girder 1-Test 1 flexural cracks

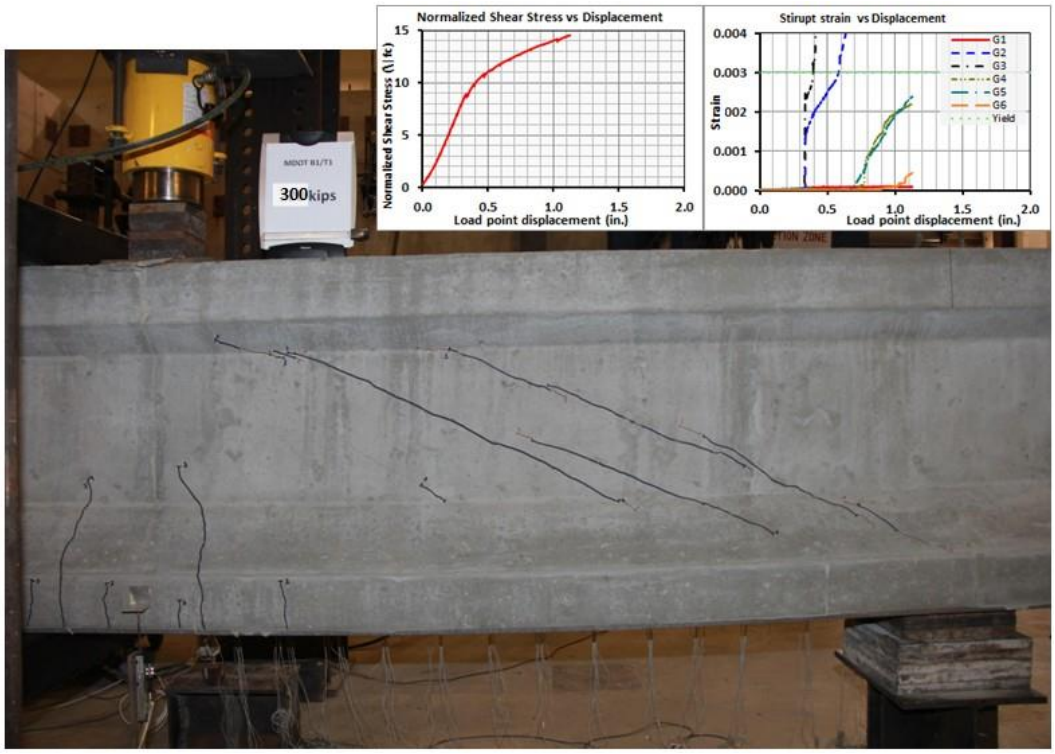

Figure A3. Girder 1-Test 1 peak load prior to failure

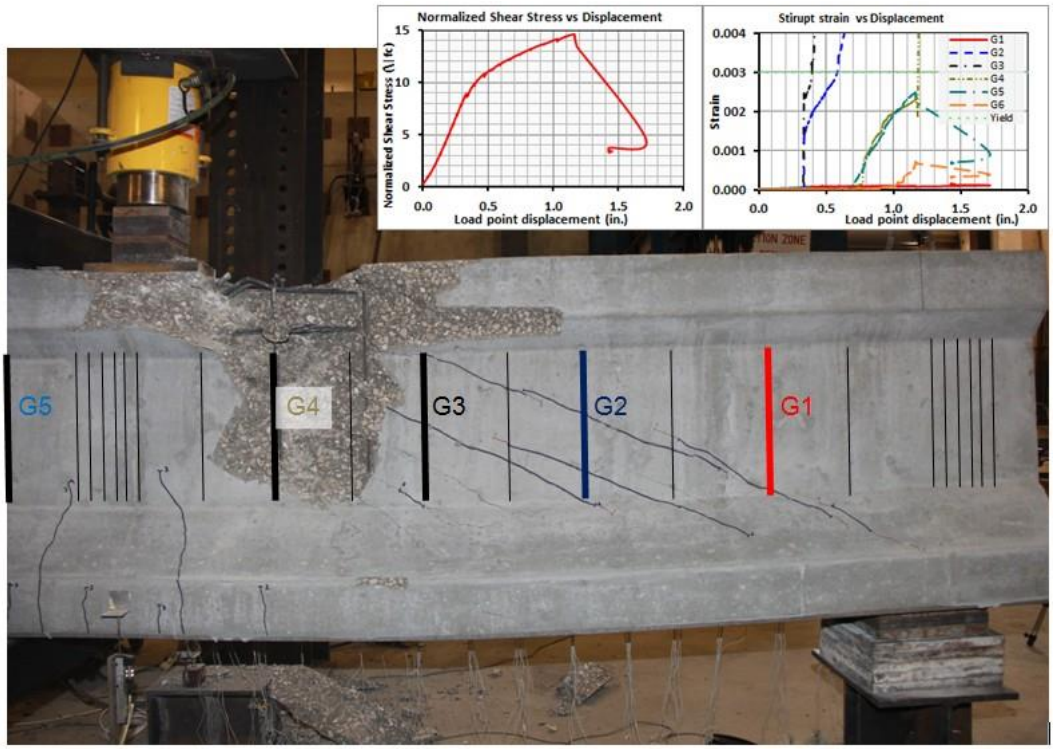

Figure A4. Girder 1-Test 1 failure

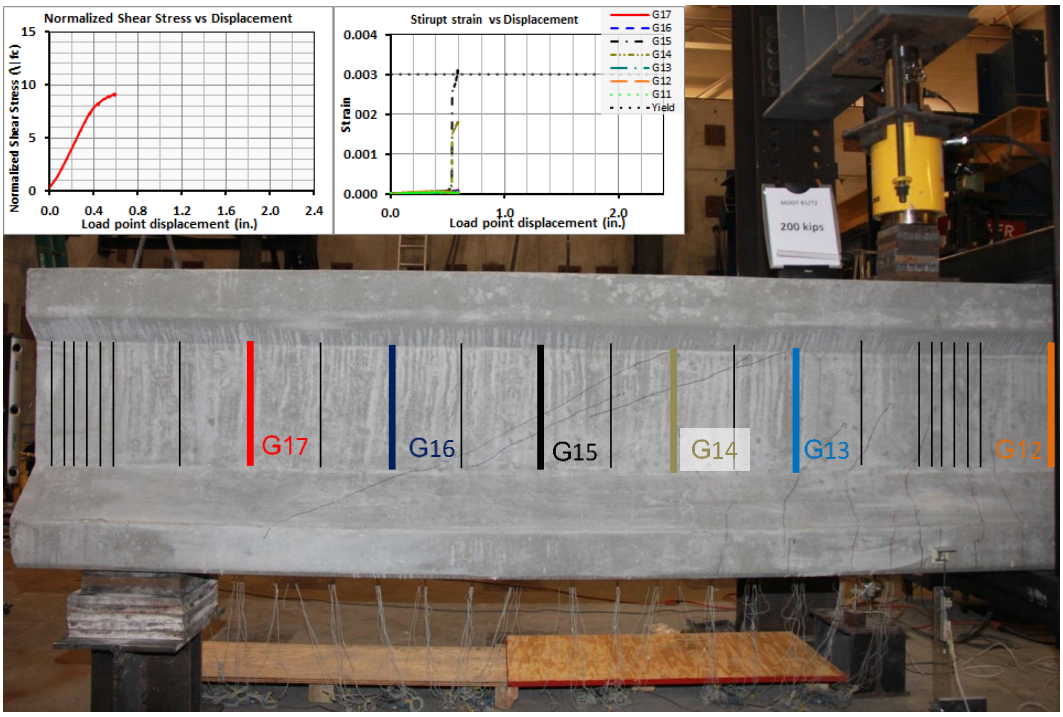

Figure A5. Girder 1-Test 2 first cracking load

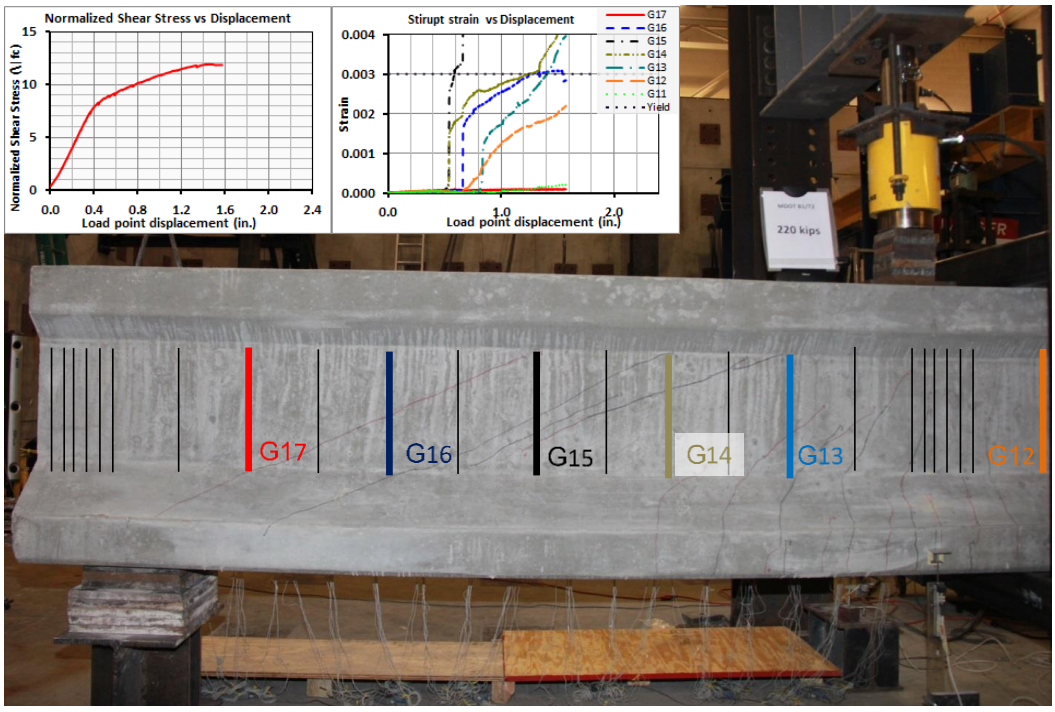

Figure A6. Girder 1-Test 2 at 260 kips

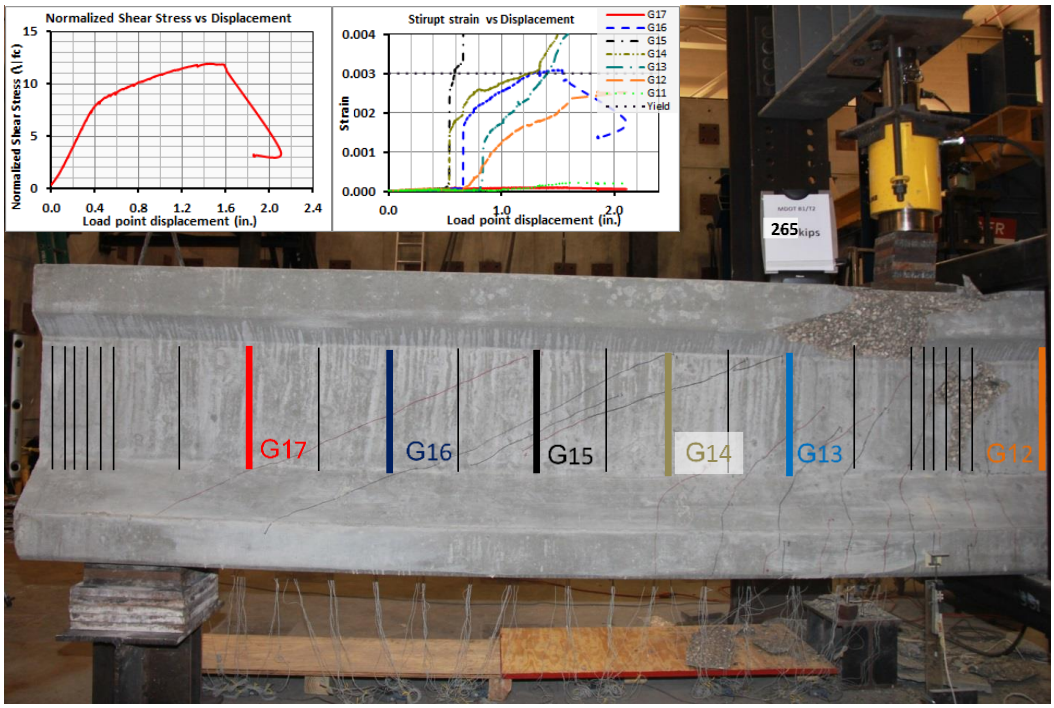

Figure A7. Girder 1-Test 2 failure

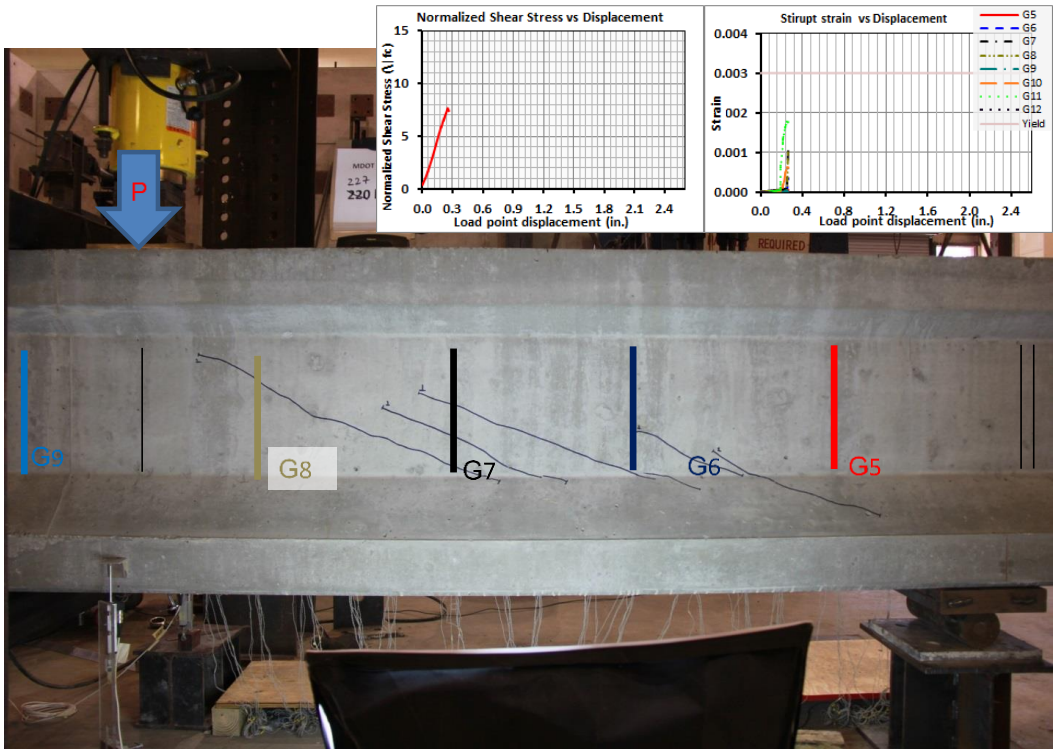

Figure A8. Girder 1-Test 3 first cracking load

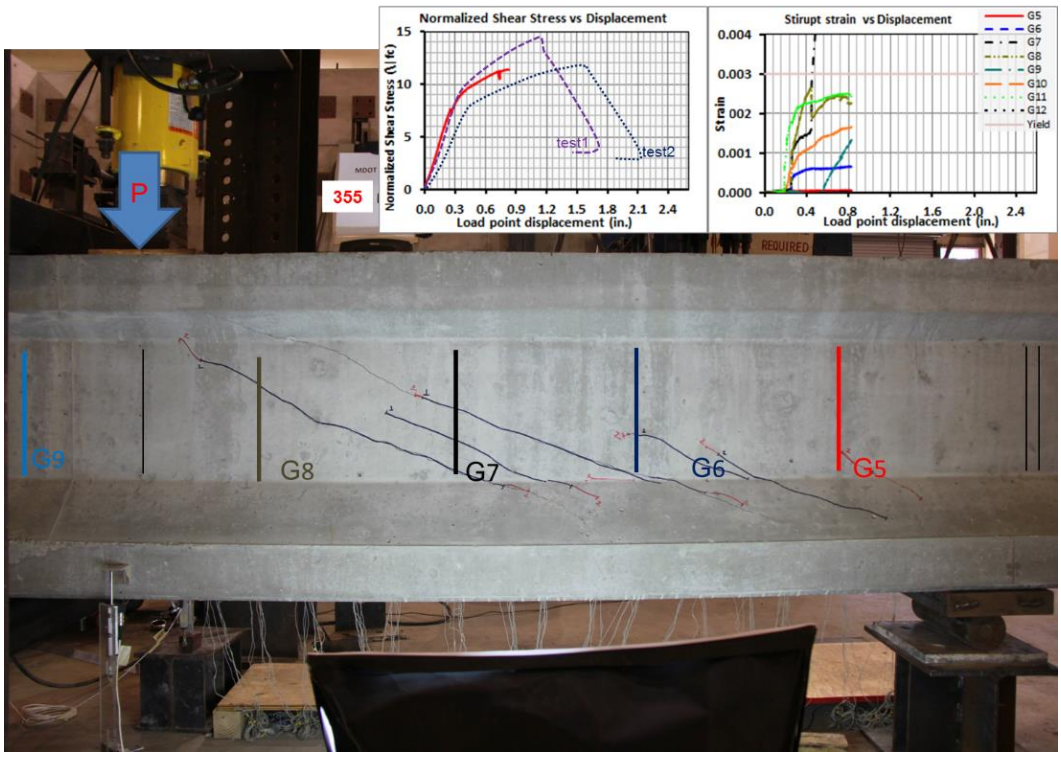

Figure A9. Girder 1-Test 3 peak load prior to failure

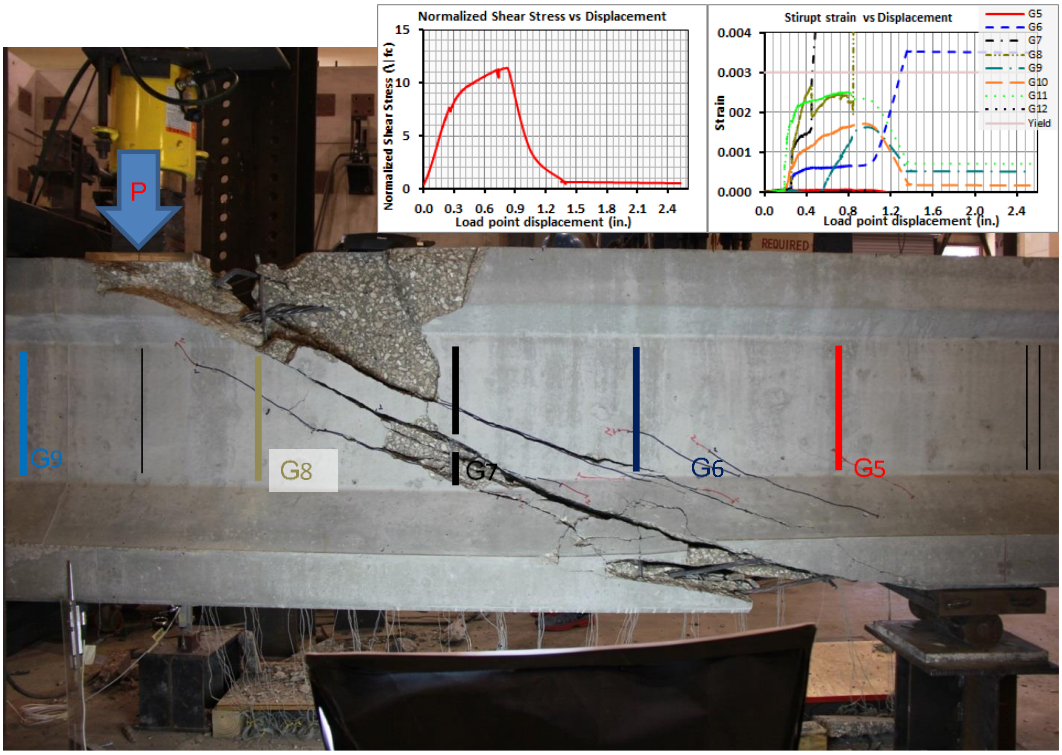

Figure A10. Girder 1-Test 3 failure

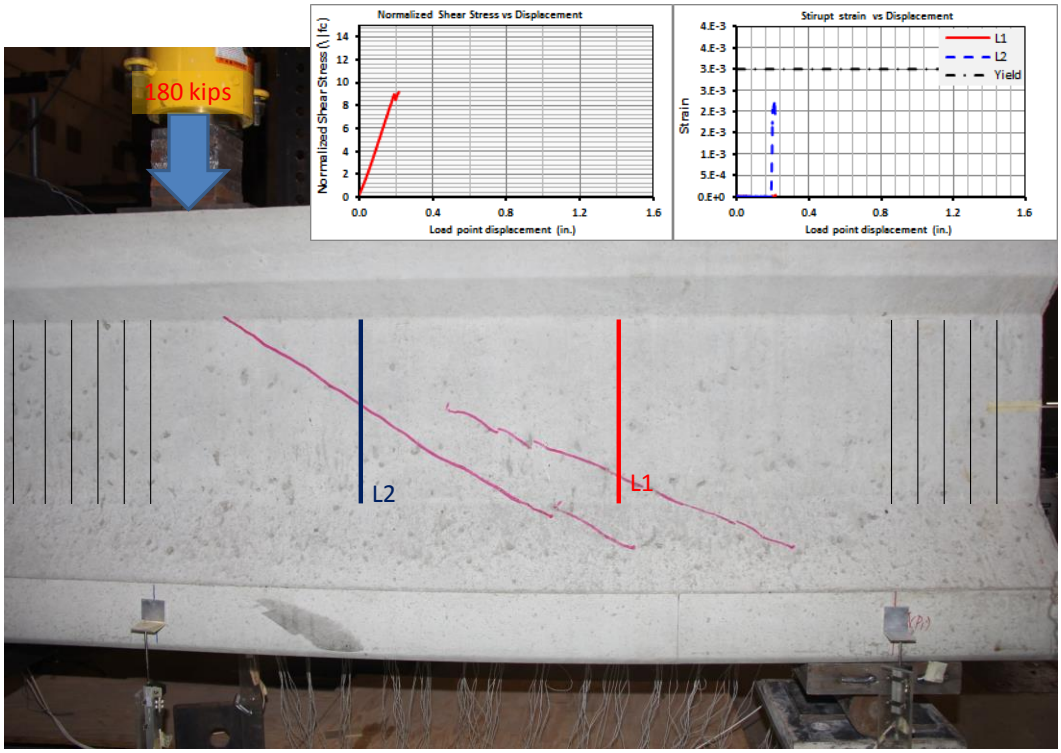

Figure A11. Girder 2-Test 1 first cracking load

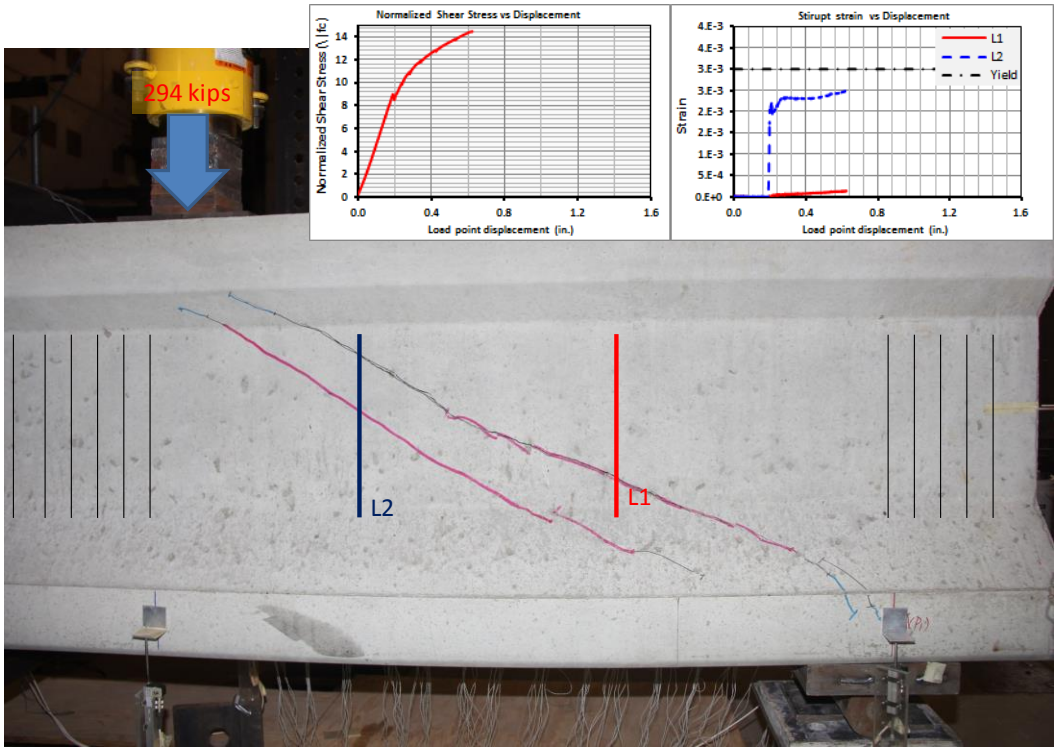

Figure A12. Girder 2-Test 1 peak load prior to failure

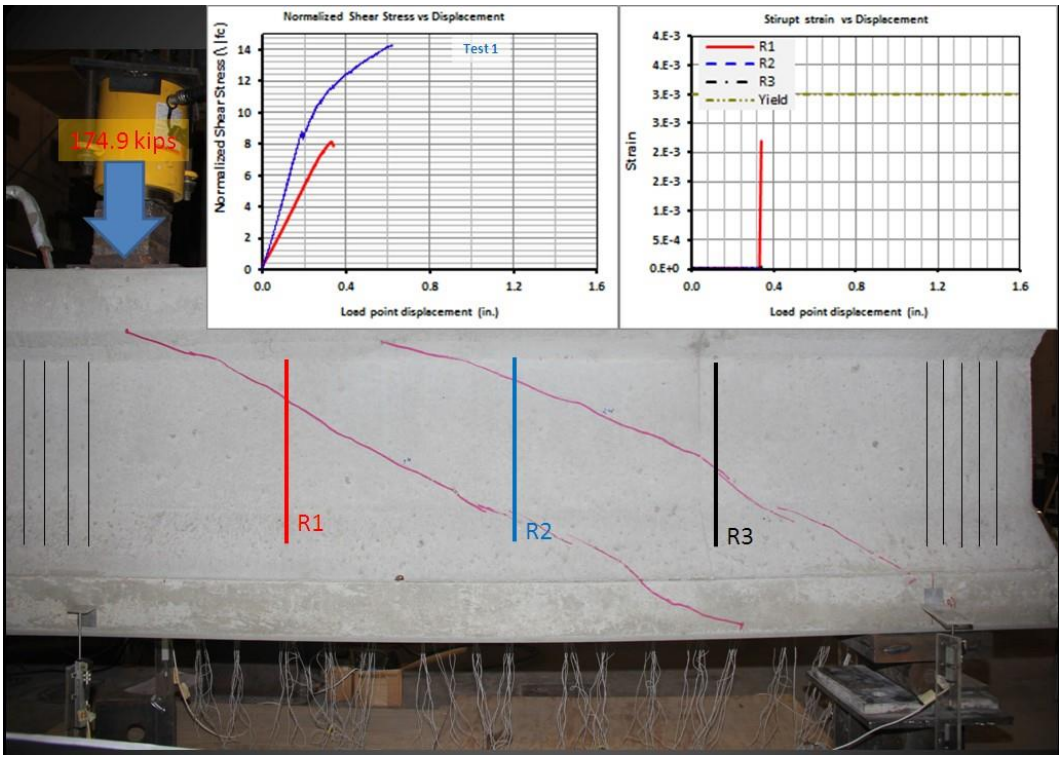

Figure A13. Girder 2-Test 2 first cracking load

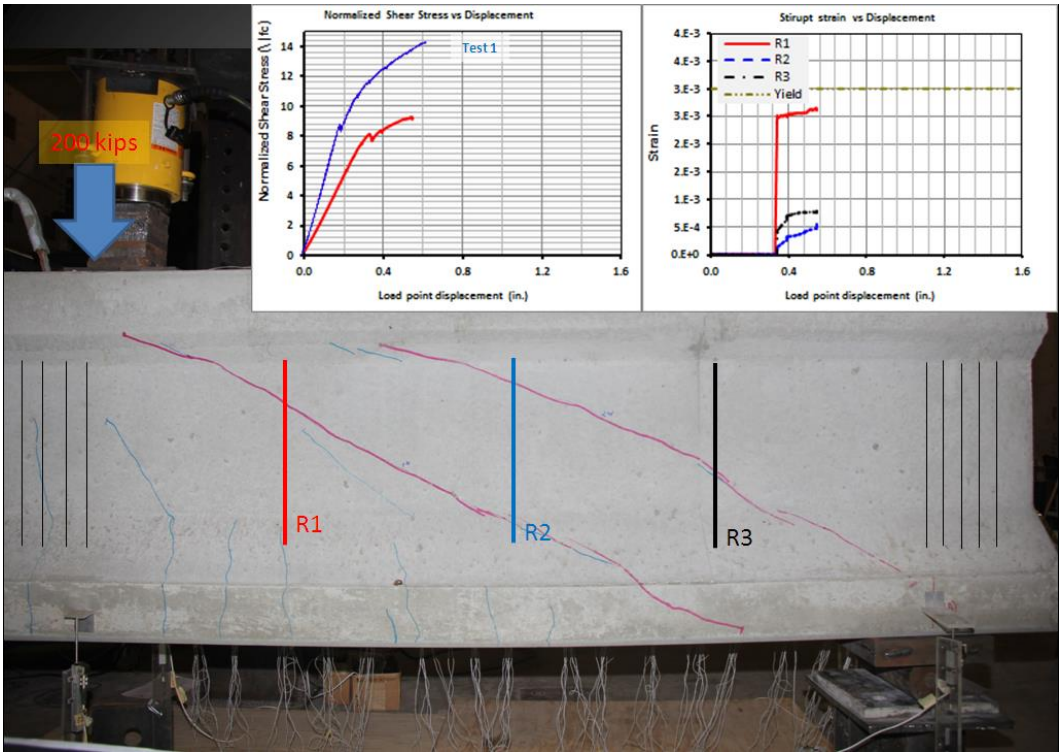

Figure A14. Girder 2-Test 2 flexural cracks

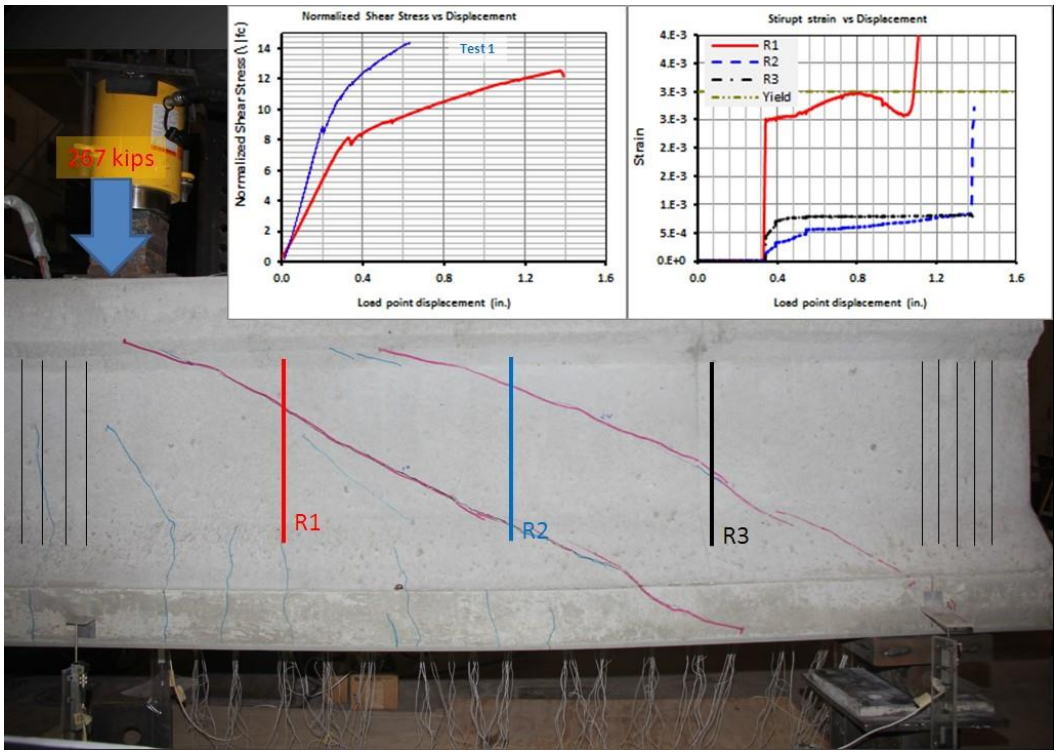

Figure A15. Girder 2-Test 2 peak load prior to failure

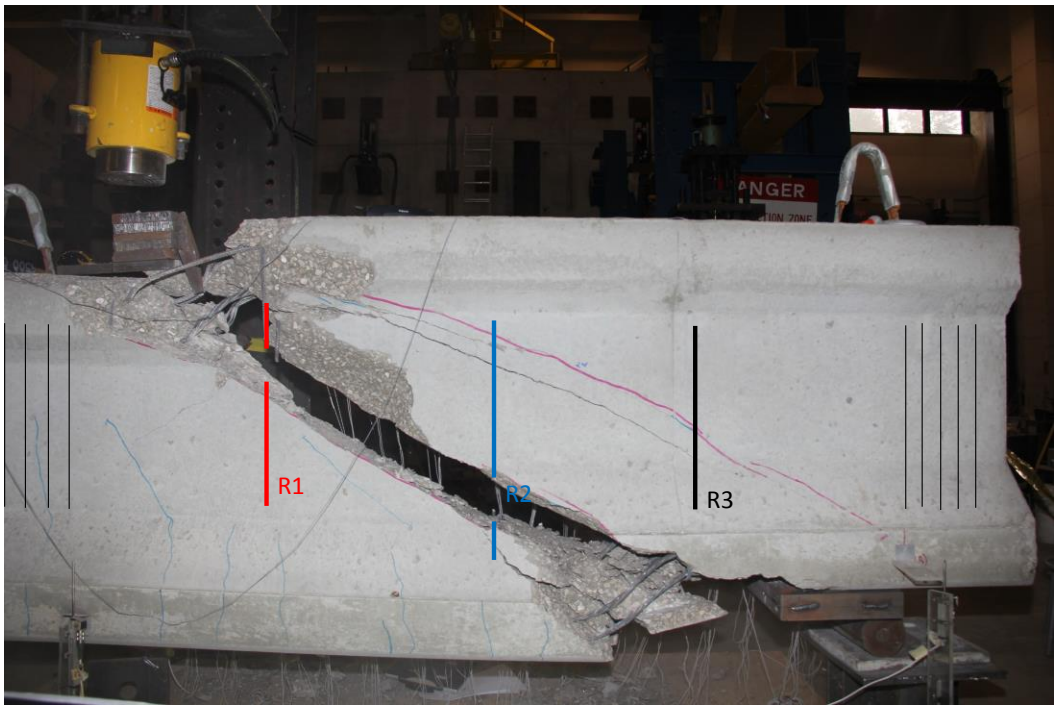

Figure A16. Girder 2-Test 2 failure

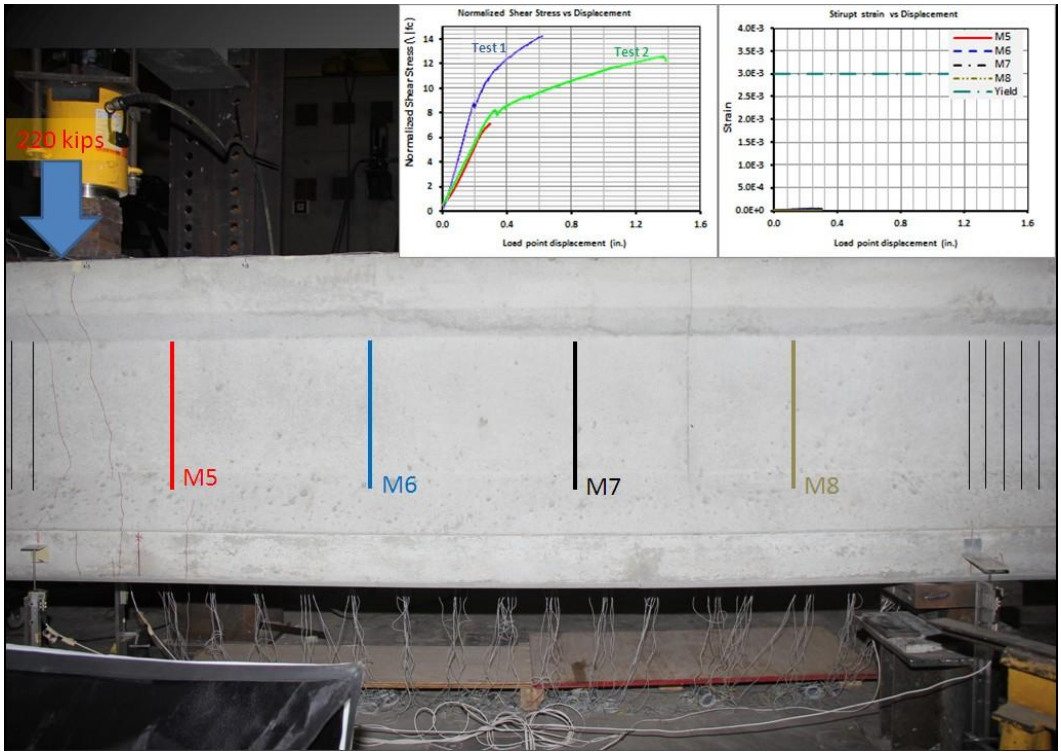

Figure A17. Girder 2-Test 3 first cracking load

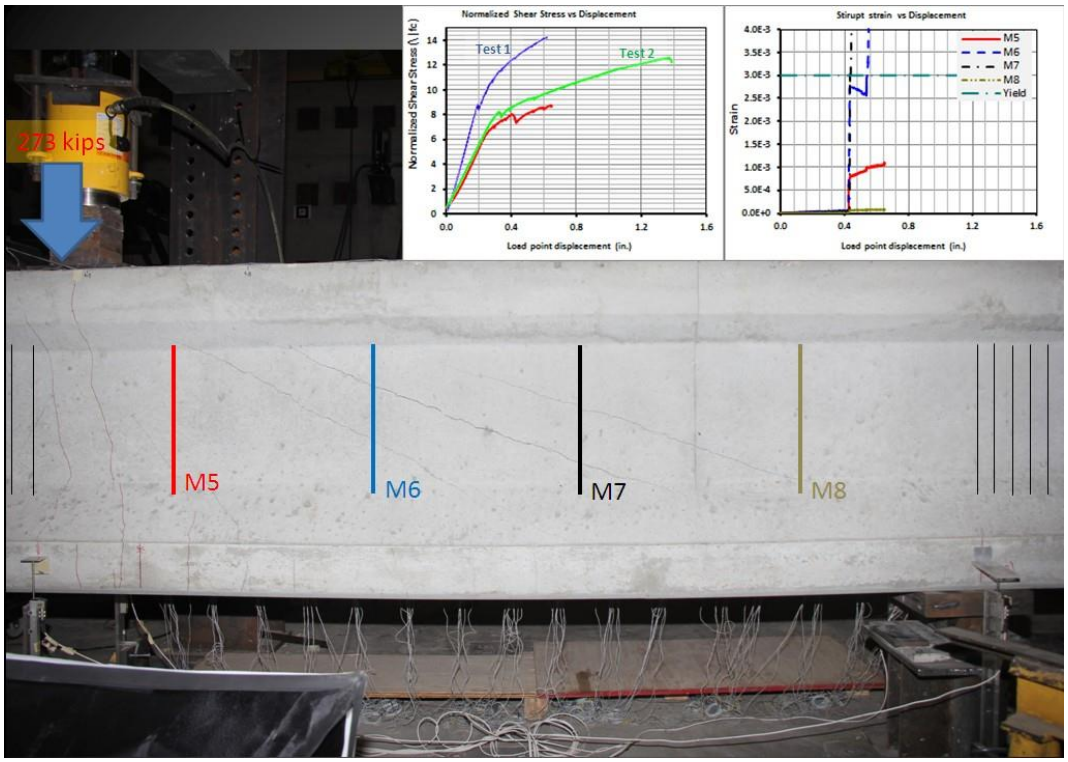

Figure A18. Girder 2-Test 3 peak load prior to failure

Girder 1 Casting Specification Sheet

Stress-con Pour Report

Job Name: US-31 NB OVER ELMER SELTENRIGHT DITCH

Pour Date: 1-28-13 | Bed ID: C-Floor | Job Number: 12080 | Q.C. Inspector: Brian C

Pour Number: 1 | County: | Lead Man:

Piece Number	Piece Length
Test Beam	

Mix Design: 775 | Foreman:

Heat o Steam o Heaters o Ambient Heat o | Inspector:

Required Cylinder Strengths

Release Strength: 5000 psi

28-Day Strength: 7000 psi

Cylinder Strength Results

	1st Set	2nd Set	3rd Set
Release	7369	7434	
28-Day			
Early Ship			

Test Results

	1st	2nd	3rd
Time:	10:15	:	:
Slump:	7 3/4"	"	"
Temp:	60 °F	°F	°F
Air %	6.0 %	%	%
Vsi	0		
Temp: 40	Condi: Rain (light)		

Reel Numbers: 12014027826 4

Hercules o Simms 12980 | Calibration Date: 10-3-12

Strand Size: 1/2"	Initial Force	Net Elongation	Total Force	
Strand Usage:	4000	5 13/16"	31,446 lbs	Time 11 : 15 am Temp: 40 °F
Actual Usage:	(+5%)	6 2/16"	33,019 lbs	Time : Temp: °F
Waste:	(-5%)	5 8/16"	29,874 lbs	Time : Temp: °F

Measured Elongation & Gauge Pressure Witnessed

Strand Diagram

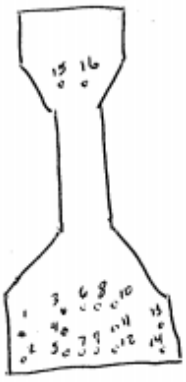

1	6"	32000	24	"	
2	6"	32100	25	"	
3	6"	32100	26	"	
4	5 7/8"	32100	27	"	
5	6"	32000	28	"	
6	6 1/16"	32400	29	"	
7	5 7/8"	32000	30	"	
8	6"	32400	31	"	
9	6"	32000	32	"	
10	6 1/16"	32400	33	"	
11	5 15/16"	32100	34	"	
12	6 1/16"	32100	35	"	
13	6"	32100	36	"	
14	5 7/8"	32000	37	"	
15	6 1/8"	32400	38	"	
16	6 1/16"	32400	39	"	
17	"		40	"	
18	"		41	"	
19	"		42	"	
20	"		43	"	
21	"		44	"	
22	"		45	"	
23	"		46	"	

Comments: Pour Inside

Girder 2 Casting Specification Sheet

STRESS-CON POUR REPORT

Pour Date: 8/30/13 | Pour # 1
Bed ID: C-floor
Piece Number | Piece Length
Test beam #2

Job Name: U of M
Job Number: 13063
County:
Mix Design: 775
Heat o Steam o Heaters o Ambient Heat

Q.C Inspector: Brian
Lead Man:
Foreman:
3rd Party Inspector

Required Cylinder Strengths		
Release Strength:	4000	PSI
28-Day Strength	5500	PSI

Cylinder Strength Results	1st Set	2nd Set	3rd Set
Release			
28-Day			
Early Ship			

Test Results	1st Test	2nd Test	Extra
Time:	1 : 10	:	:
Slump:	8 "	"	"
Temperature	81 °F	°F	°F
Air %	5.4 %	%	%
VSI	0		
Temp and Cond:			

Reel #: 120140389764

Strand Size:	1/2"
Strand Usage:	
Actual Usage:	
Waste:	

	Initial Force:	Net Elongation	Total Force
	4000 lbs	4 1/2"	25586 lbs
	(+5%)	4 3/4"	26865 lbs
	(-5%)	4 5/16"	24307 lbs

o Hercules
o Simms

Date of Calibration			
Time:	8 : 45	Temp:	68 °F
Time:	:	Temp:	°F
Time:	:	Temp:	°F

Measured Elongation Pull and Gauge Pressure Witnessed

1	9 3/8"	25600 lbs	11	9 1/2"	lb	21	"	lb	31	"	lb	51	"	lb
2	9 1/2"	lbs	12	9 1/2"	lb	22	"	lb	32	"	lb	52	"	lb
3	9 1/2"	lbs	13	9 3/8"	lb	23	"	lb	33	"	lb	53	"	lb
4	9 1/2"	lbs	14	9 1/2"	lb	24	"	lb	34	"	lb	54	"	lb
5	9 3/8"	lbs	15	9 5/8"	lb	25	"	lb	35	"	lb	55	"	lb
6	9 1/2"	lbs	16	9 5/8"	lb	26	"	lb	36	"	lb	56	"	lb
7	9 1/2"	lbs	17	"	lb	27	"	lb	37	"	lb	57	"	lb
8	9 1/2"	lbs	18	"	lb	28	"	lb	38	"	lb	58	"	lb
9	9 1/2"	lbs	19	"	lb	29	"	lb	39	"	lb	59	"	lb
10	9 3/8"	lbs	20	"	lb	30	"	lb	40	"	lb	60	"	lb
									41	"	lb	61	"	lb
									42	"	lb	62	"	lb
									43	"	lb	63	"	lb
									44	"	lb	64	"	lb
									45	"	lb	65	"	lb
									46	"	lb	66	"	lb
									47	"	lb	67	"	lb
									48	"	lb	68	"	lb
									49	"	lb	69	"	lb
									50	"	lb	70	"	lb

Strand Diagram

15 16

13 11 12 14

9 7 8 10

5 3 1 2 4 6

Strand Location

( ) @

( ) @

Comments:

APPENDIX B: FEA MODEL VERIFICATION DATA

Verification Data Set 1: Saqan and Frosch Tests

The following dimensions and reinforcement details were used in the FEA models.

Geometric Properties

	Gross Conc.	Trans (n=0.00)
Area (mm^2) x 10^3	253.4	252.9
nertia (mm^4) x 10^6	10347.2	10313.9
y_t (mm)	350	349
y_b (mm)	350	351
S_t (mm^3) x 10^3	29563.3	29512.6
S_b (mm^3) x 10^3	29563.3	29424.2

Crack Spacing

2 x dist + 0.1 d_b /ρ

Loading (N,M,V + dN,dM,dV)

0.0 , -0.0 , 0.0 + 0.0 , -1.0 , 0.0

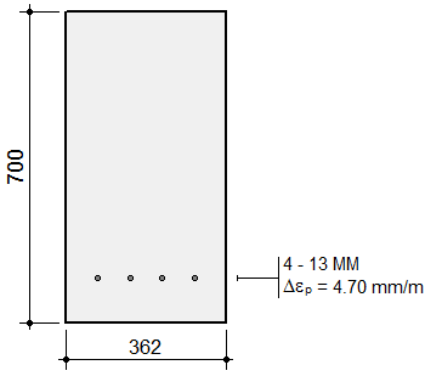

All dimensions in millimetres
Clear cover to reinforcement = 93 mm

Figure B1. Beam V-4-0 cross section; 1 in=25.4 mm

Geometric Properties

	Gross Conc.	Trans (n=0.00)
Area (mm^2) x 10^3	257.6	256.5
Inertia (mm^4) x 10^6	10518.7	10430.8
y_t (mm)	350	349
y_b (mm)	350	351
S_t (mm^3) x 10^3	30053.3	29906.9
S_b (mm^3) x 10^3	30053.3	29698.6

Crack Spacing

2 x dist + 0.1 d_b /ρ

Loading (N,M,V + dN,dM,dV)

0.0 , -0.0 , 0.0 + 0.0 , -1.0 , 0.0

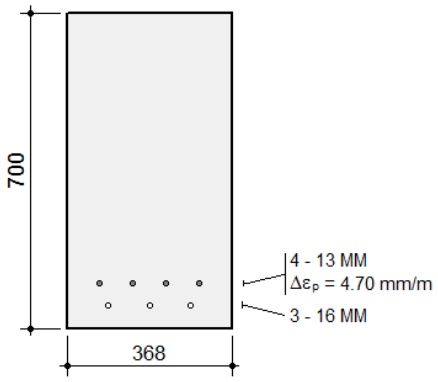

All dimensions in millimetres
Clear cover to reinforcement = 42 mm

Figure B2. Beam V-4-0.93 cross section; 1 in=25.4 mm

Geometric Properties

	Gross Conc.	Trans (n=0.00)
Area (mm^2) x 10^3	261.1	259.0
nertia (mm^4) x 10^6	10661.6	10490.3
y_t (mm)	350	348
y_b (mm)	350	352
S_t (mm^3) x 10^3	30461.7	30168.1
S_b (mm^3) x 10^3	30461.7	29778.8

Crack Spacing

2 x dist + 0.1 d_b /ρ

Loading (N,M,V + dN,dM,dV)

0.0 , -0.0 , 0.0 + 0.0 , -1.0 , 0.0

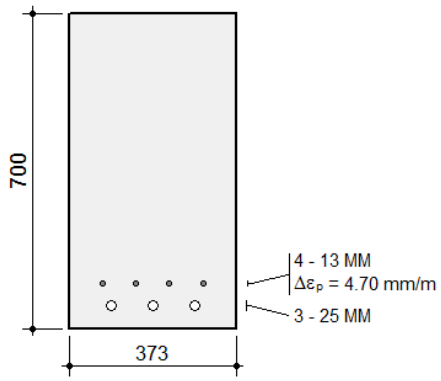

All dimensions in millimetres
Clear cover to reinforcement = 37 mm

Figure B3. Beam V-4-2.37 cross section; 1 in=25.4 mm

The truss reinforcement is perfectly bonded over the entire beam length and a prestress force of 480 kN was applied as a prestrain to the prestressing truss elements.

- Reinforcement material properties:
  - Prestressing steel:
    - Yield Strength, $F_y = 1517\ MPa$
    - Ultimate Strength, $F_u = 1862\ MPa$
    - Elastic modulus, $E_s = 193000\ MPa$
    - Strain hardening Strain, $esh = 10\ me$
    - Prestrain, $Dep = 4.7\ me$
  - Mild steel:
    - Yield Strength, $F_y = 413\ MPa$
    - Ultimate Strength, $F_u = 620\ MPa$
    - Elastic modulus, $E_s = 200000\ MPa$

- Strain hardening Strain, $esh = 10\ me$

- Concrete model properties:
  - Cylinder compressive strength, $f_c' = 41.8\ MPa$
  - Tensile strength, $f_t' = 2950\ MPa$
  - Cylinder strain at $f_c', eo = 2.1\ me$
  - Poisson's ratio, $Mu = 0.15$
  - Thermal expansion coefficient, $Cc = 1e-5\ /\mathrm{C}^{\circ}$
  - Maximum aggregate size, $a = 20\ mm$
  - Density= 2400 $^{kg}/_{m^3}$
  - Thermal diffusivity, $= Kc = 1.2\ ^{mm^2}/_{s}$

Table B1. FEA model mesh details

Beam ID	Beam V-4-0	Beam V-4-0.93	Beam V-4-2.37
Number of concrete materials	1	1	1
Number of steel materials	1	1	1
Structure type	Plane	Plane membrane	Plane membrane
Rectangular elements	2800	2604	2604
Truss elements	25	186	186
Nodes	2929	2726	2726
Restrained nodes	30	30	30
Total number of elements	2825	2790	2790
Mesh density	581.25	625	625

Verification Data Set 3: Girder Lab Testing

Beam 1 Dimensions and Materials Properties

The following dimensions and reinforcement details were used for modeling Girder 1 in VecTor2 (Original Model).

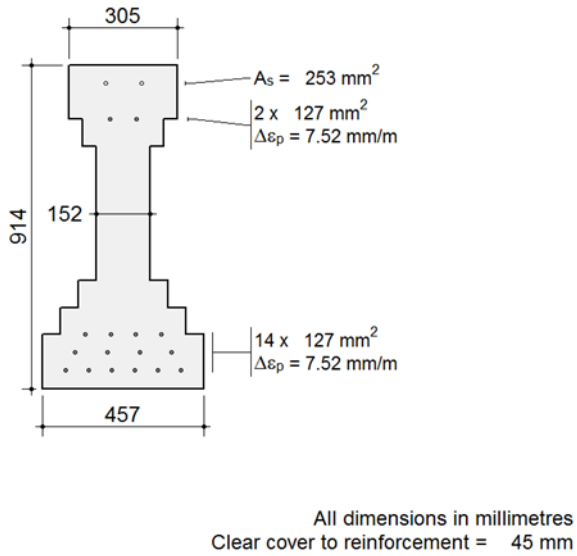

Figure B4. Type II girder initial cross section model; 1 in=25.4 mm

The truss reinforcement is perfectly bonded over the entire beam length and a prestress force of 32.15 kips (143 KN) was applied as a prestrain (7.52 *me*) to each strand. Mesh and element information for each test are summarized in Table B2.

- Reinforcement material properties:
    - Prestressing Steel:
        - Yield Strength, $F_y = 1676\ MPa\ (243\ ksi)$
        - Ultimate Strength, $F_u = 1862\ MPa\ (270\ ksi)$
        - Elastic modulus, $E_s = 196500\ MPa\ (28500\ ksi)$
        - Strain hardening Strain, $esh = 10\ me$
        - Prestrain, $Dep = 7.52\ me$

- Mild steel:
  - Yield Strength, $F_y = 413\ MPa$ (60 ksi)
  - Ultimate Strength, $F_u = 620\ MPa$ (90 ksi)
  - Elastic modulus, $E_s = 200000\ MPa$ (29000 ksi)
  - Strain hardening Strain, $esh = 10\ me$

- Concrete model properties:
  - Cylinder compressive strength, $f_c' = 42 - 63\ MPa$ $(6100 - 9200\ psi)$
  - Tensile strength, $f_t' = 2.3 - 2.7\ MPa$ $(310 - 392\ psi)$
  - Cylinder strain at $f_c', eo = 2.55\ me$
  - Poisson's ratio, $Mu = 0.15$
  - Thermal expansion coefficient, $Cc = 1e - 5\ /\mathrm{C}^{\circ}$
  - Maximum aggregate size, $a = 25\ mm$ $(1\ in)$
  - Concrete Density= 2400 $^{kg}/_{m^3}$ (150 $^{lb}/_{ft^3}$)
  - Thermal diffusivity, $= Kc = 1.2\ ^{mm^2}/_{s}$ (0.00186 $^{in^2}/_{s}$)

Table B2. FEA models details for Girder 1

Test ID	Test 1	Test 2	Test 3
Number of concrete materials	1	1	2
Number of steel materials	2	2	2
Element type	Plane membrane	Plane membrane	Plane membrane
Rectangular elements	4328	4608	3816
Triangular elements	144	156	126
Truss elements	685	730	530
Nodes	4574	4869	3959
Restrained nodes	5	5	5
Total number of elements	5157	5494	4472
Mesh density $(mm^2/\ element)$	625	625	625

Table B2. Summary of Girder 1 test parameters

Design	Stirrups spacing (in)	a/d ratio
Test 1	8	2.8
Test 2	8	3.4
Test 3	21	3.4

Girder 1 Original FEA Model Results Summary

Girder 1- Test 1

- Test 1 set up:

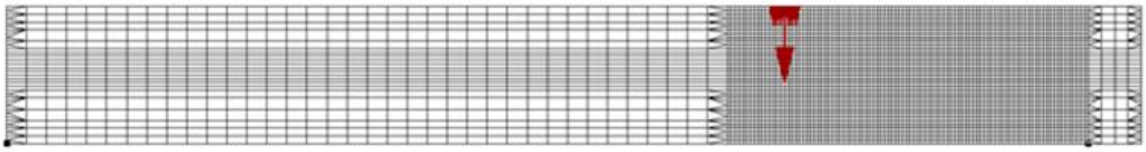

- Cracks propagation started at approximately 156 kips:

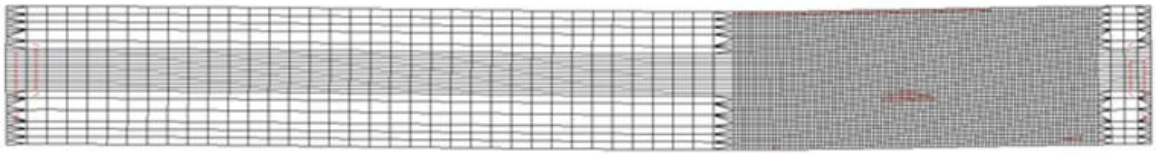

- Beam deformation at 240 kips:

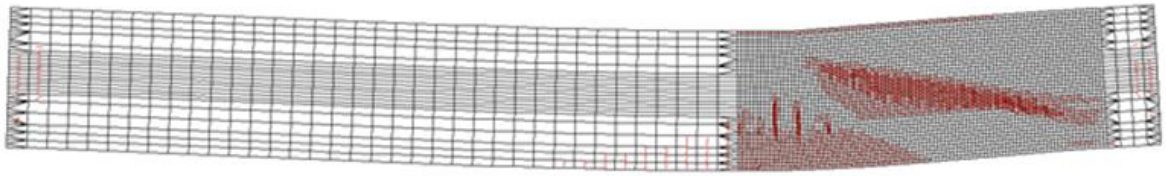

- Beam reached ultimate capacity at 265.3 kips:

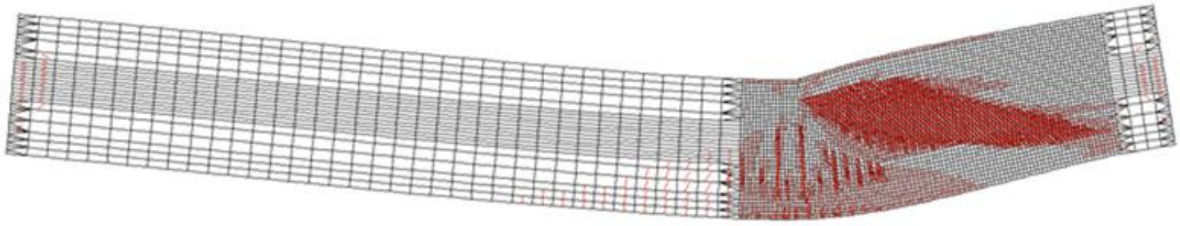

Figure B5. Girder 1-Test 1 model results (f'c=7.5 ksi)

Table B3. Girder 1-Test 1 model results

f'_c (ksi)	Shear cracking load (kips)	Ultimate failure load (kips)
Test	180	299
6.1	147	248
7.5	156	265
9.2	166	278

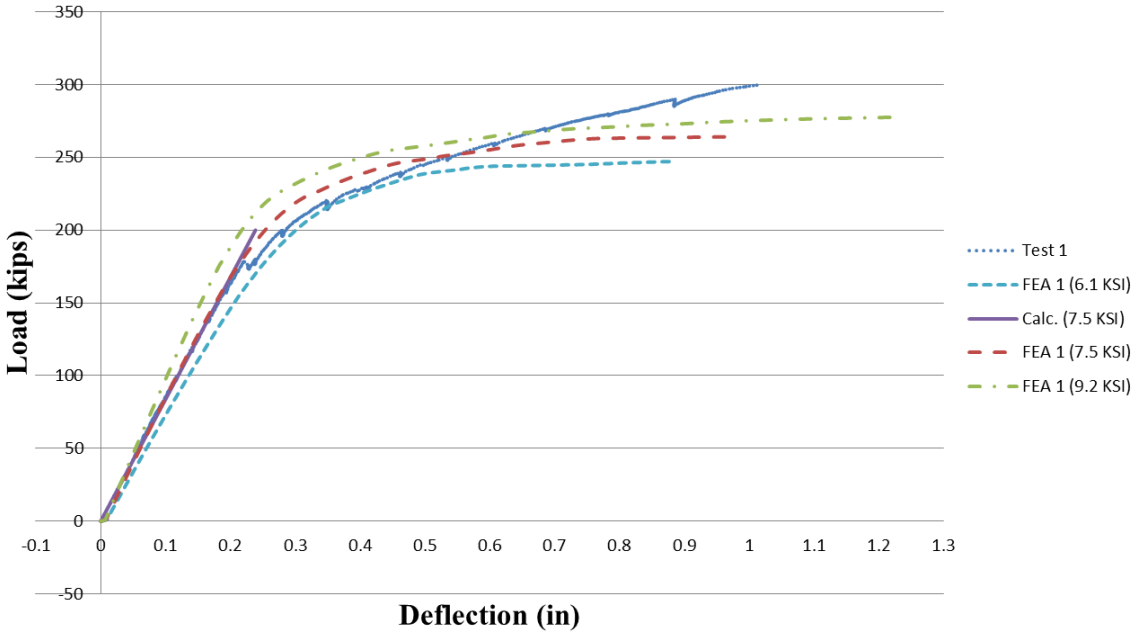

Figure B6. Load versus deflection results (Girder 1-Test 1)

Girder 1- Test 2

- Test 2 set up:

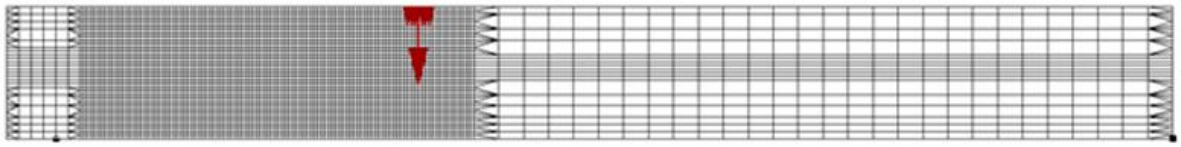

- Cracks propagation started approximately at 167 kips:

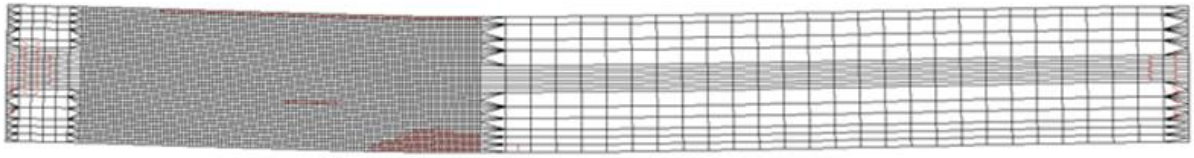

- Beam deformation at 225 kips:

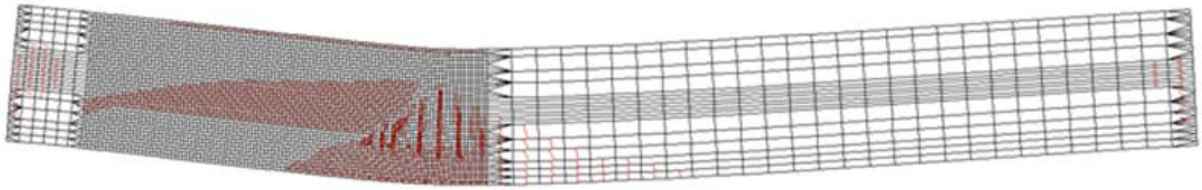

- Beam reached ultimate capacity at 239.4 kips:

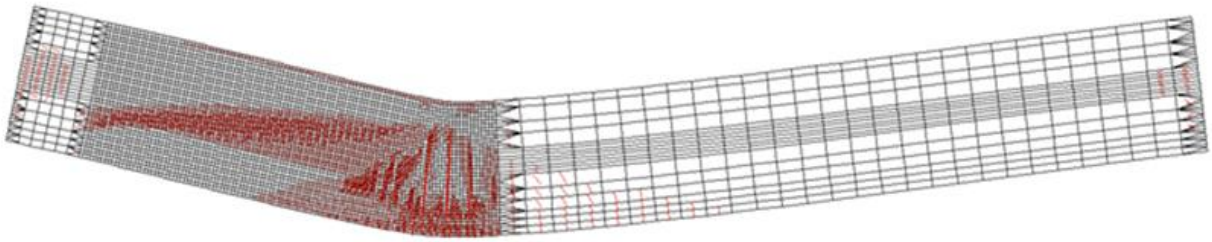

Figure B7. Girder 1-Test 2 model results (f'c=7.8 ksi)

Table B4. Girder 1-Test 2 model results

f'_c (ksi)	Shear cracking load (kips)	Ultimate failure load (kips)
Test	190	262
6.5	157	232
7.8	167	239
9.5	175	245

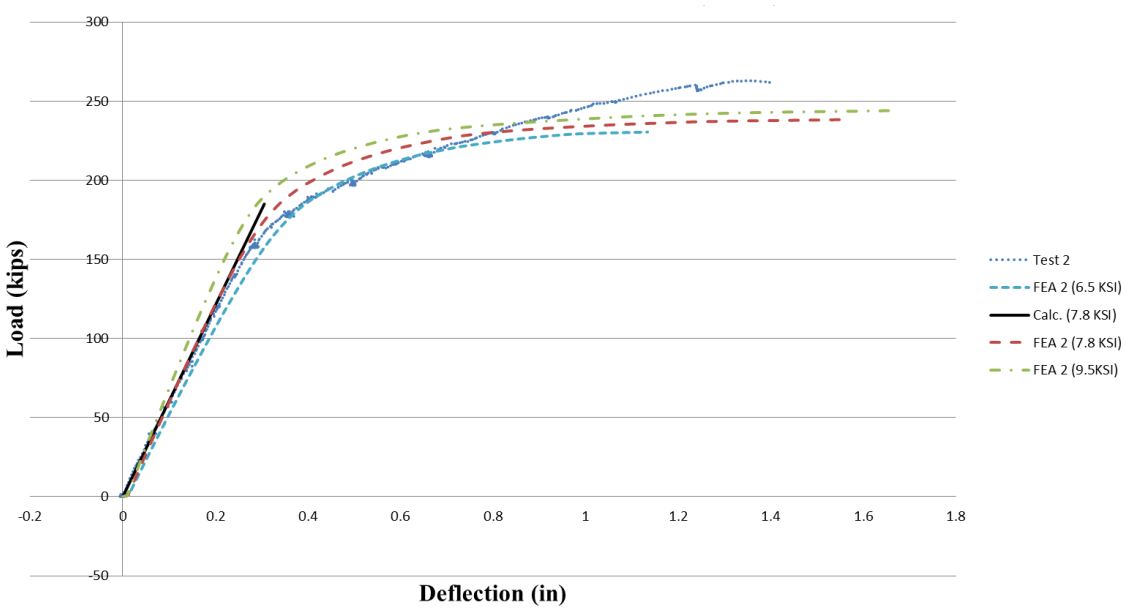

Figure B8. Load versus deflection results (Girder 1-Test 2)

Girder 1- Test 3

- Test 3 set up:

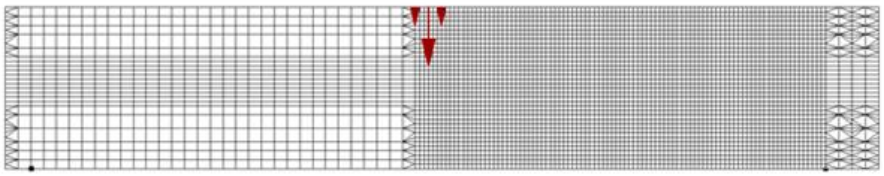

- Cracks propagation started approximately at 226 kips:

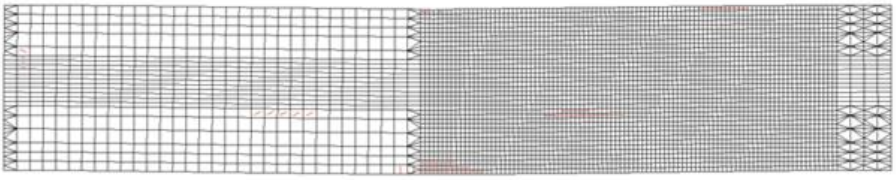

- Beam deformation at 263 kips:

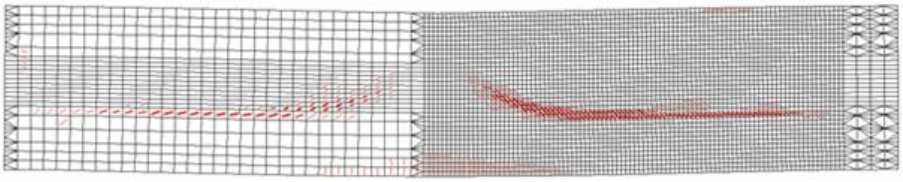

- Beam reached ultimate capacity at 279.9 kips.

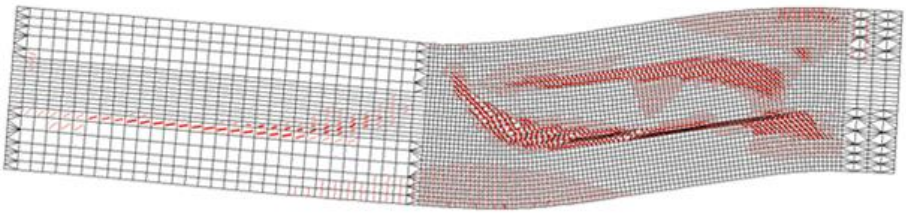

Figure B9. Girder 1-Test 3 model results (f'c=8.6 ksi)

Table B5. Girder 1-Test 3 model results

f'_c (ksi)	Shear cracking load (kips)*	Ultimate failure load (kips)
Test	227	356
7.5	225	264
8.6	226	280
8.6 Modified Model	245	337
10.0	242	299

*Shear cracking load in Test 3 was less than the FEA model results due to the existing cracks in the beam from Test 1 and Test 2.

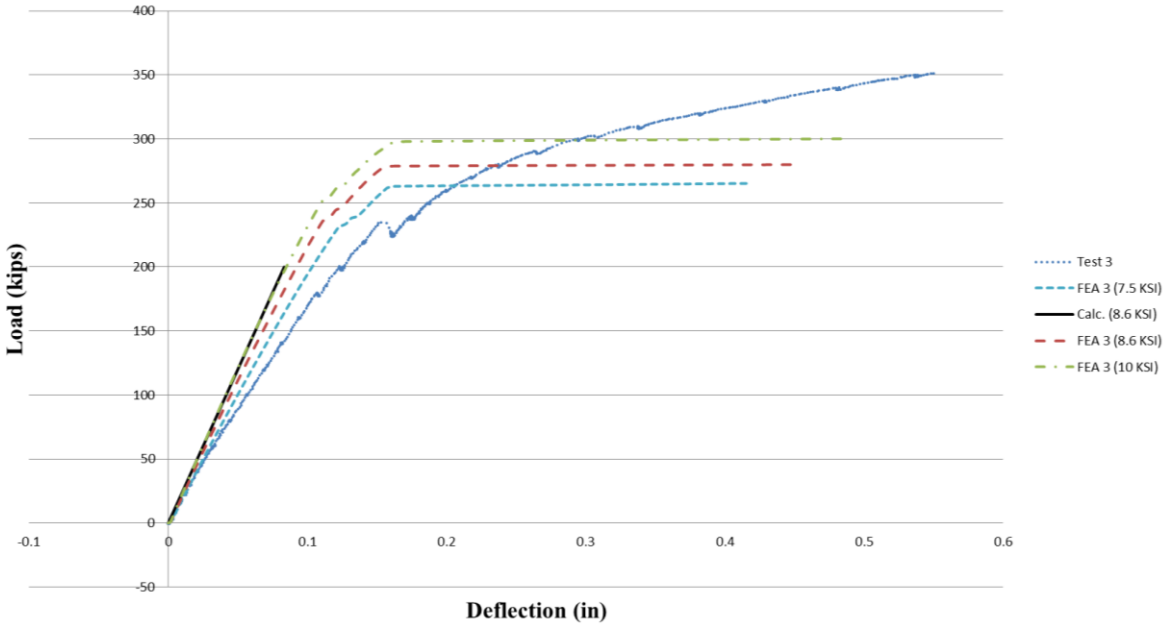

Figure B10. Load versus deflection results (Girder 1-Test 3)

Load vs. Deflection (Girder 1- Modified Model)

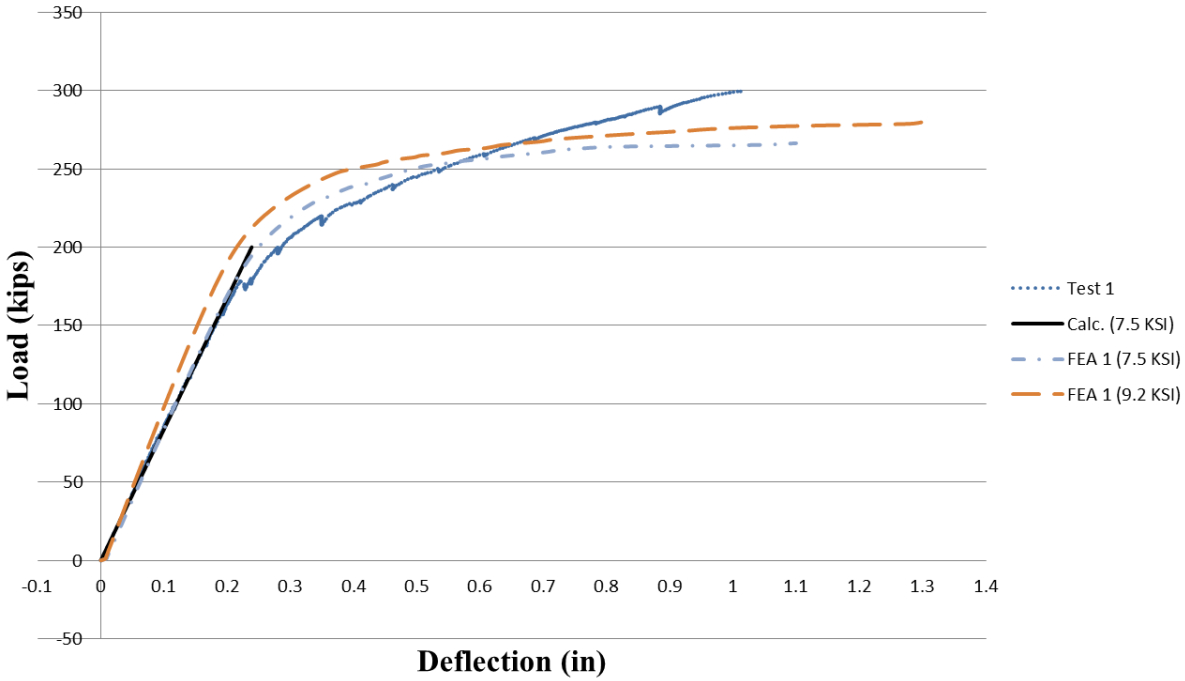

Figure B11. Load versus deflection results (Girder 1-Test 1)

Table B6. Modified model results for Girder 1-Test 1

	Ultimate failure load (Kips)
Test 1	299
f'_c = 7.5 ksi	266
f'_c = 9.2 ksi	279

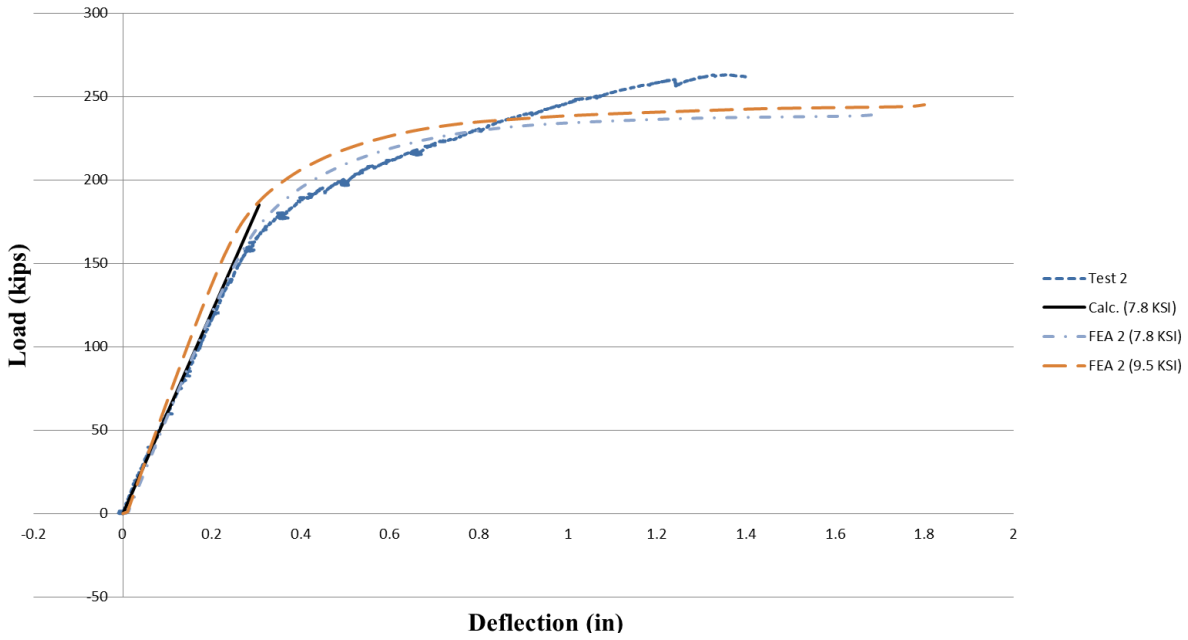

Figure B12. Load versus deflection results (Girder 1 -Test 2)

Table B7. Modified model results for Girder 1-Test 2

	Ultimate failure load (Kips)
Test 2	262
f'_c = 7.8 ksi	239
f'_c = 9.5 ksi	244

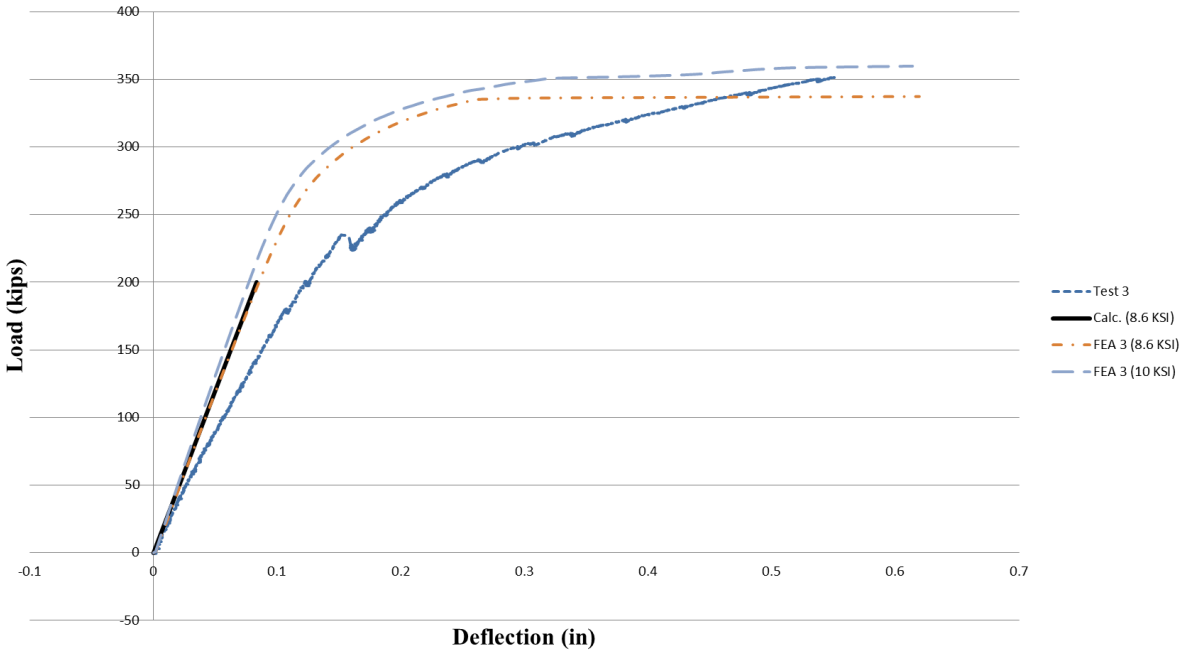

Figure B13. Load versus deflection results (Girder 1-Test 3)

Table B8. Modified model results for Girder 1-Test 3

	Ultimate failure load (Kips)
Test 3	356
f'_c = 8.6 ksi	337
f'_c = 10.0 ksi	353

Stirrups Strain Data (Girder 1)

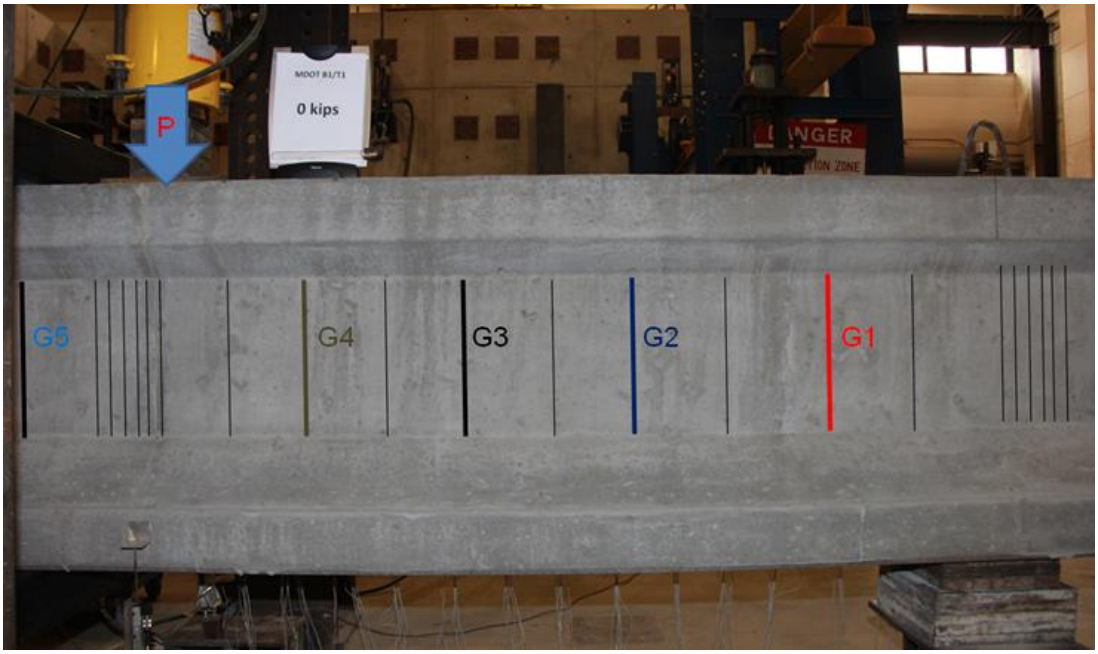

Figure B14. Girder 1- Test 1 stirrups strain gauges locations

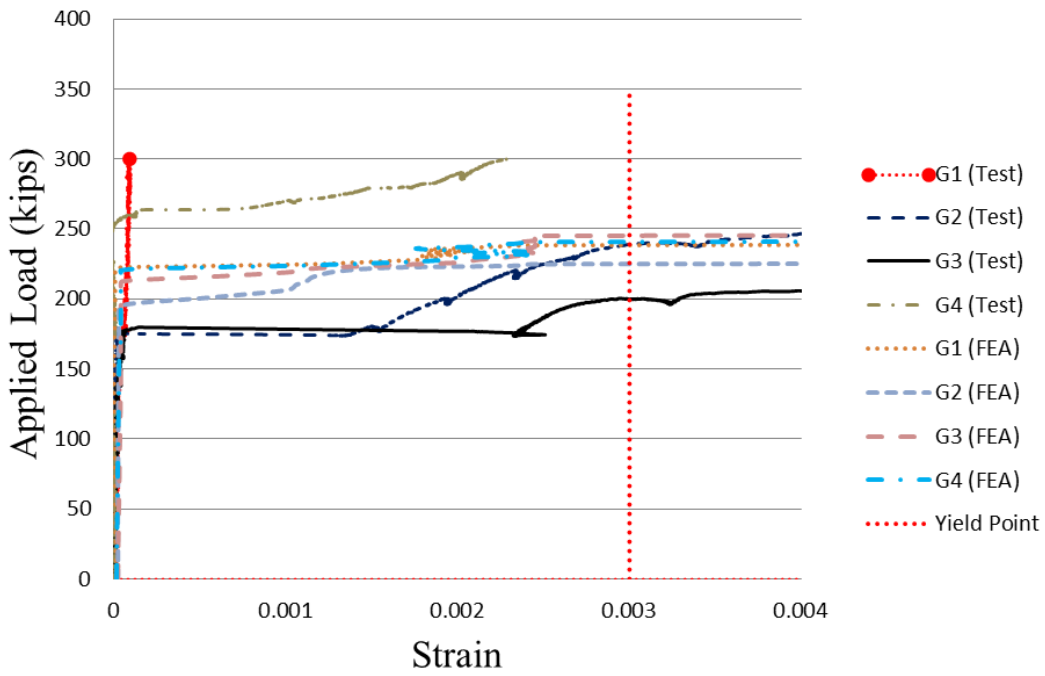

Figure B15. Girder 1- Test 1 (7.5 ksi) stirrups strains comparison with FEA results

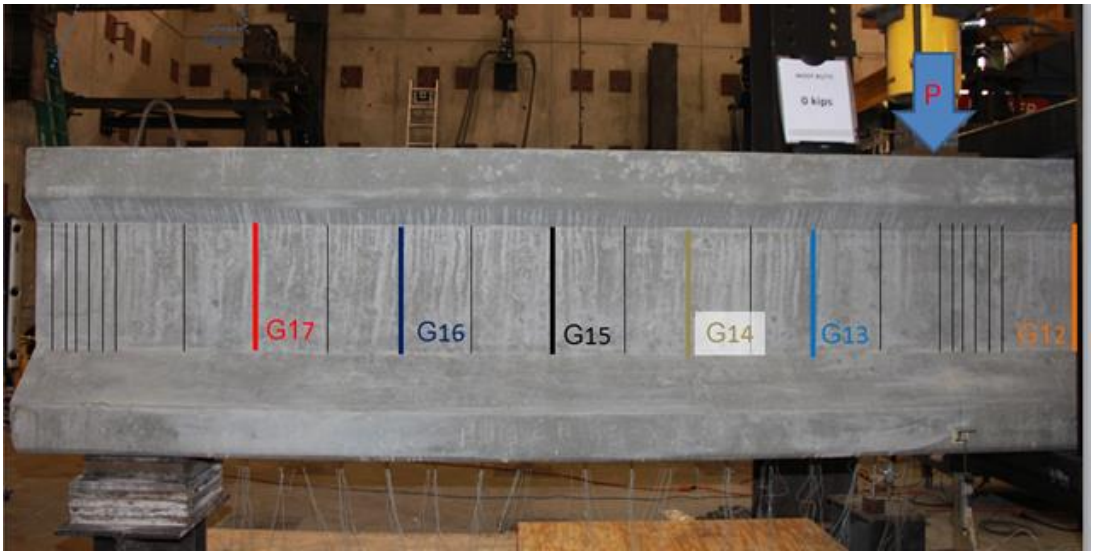

Figure B16. Girder 1- Test 2 stirrups strain gauges locations

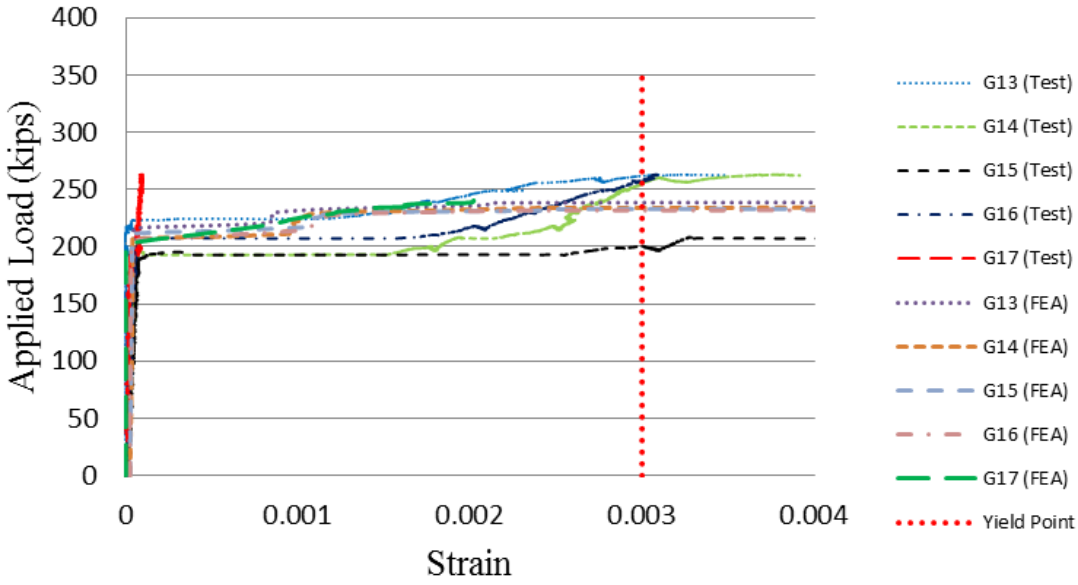

Figure B17. Girder 1- Test 2 (7.8 ksi) stirrups strains comparison with FEA results

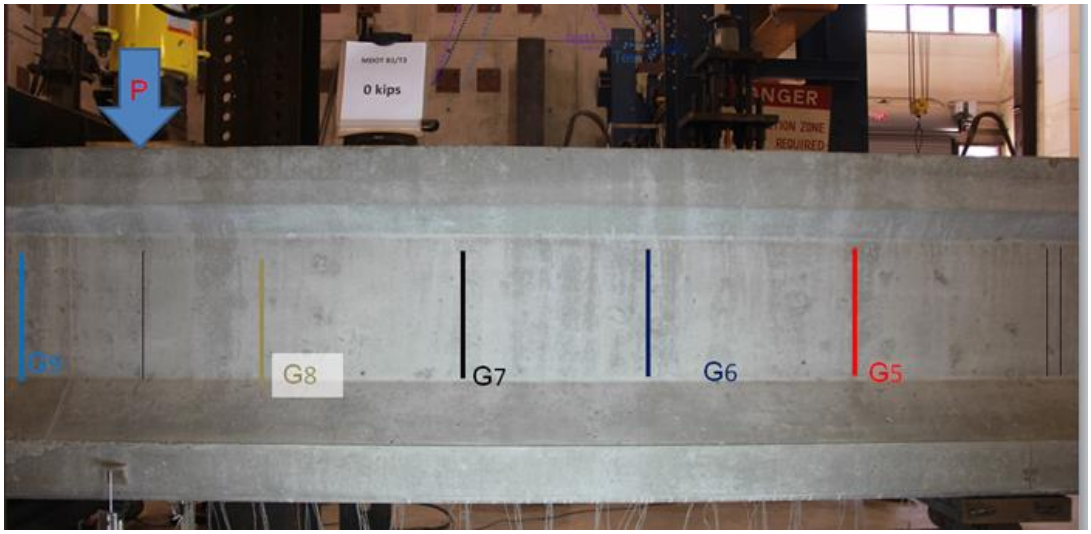

Figure B18. Girder 1- Test 3 stirrups strain gauges locations

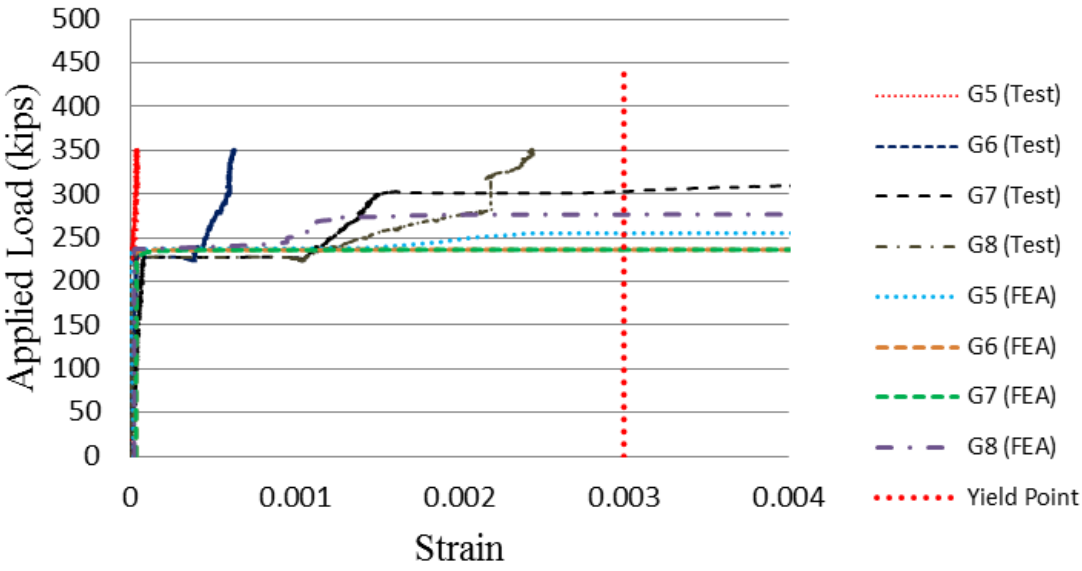

Figure B19. Girder 1- Test 3 (8.6 ksi) stirrups strains comparison with FEA results

Girder 2 Dimensions and Materials Properties

Similarly to Girder 1 testing, three tested were performed on Girder 2 considering three different loading (P1, P2 and P3) and three different sets of boundary conditions. The layout for Girder 2 is shown in Figure B20. The modeling technique, mesh density and loading type for Girder 1 FEA model were used in modeling Girder 2.

- Reinforcement material properties:
    - Prestressing Steel: same as Girder 1 (except that Prestrain, $Dep = 5.43\ me$)
    - Mild Steel: same as Girder 1
- Concrete Model Properties:
    - Cylinder compressive strength, $f_c' = 63\ MPa$ ($9200\ psi$)
    - Tensile strength, $f_t' = 2.6\ MPa$ ($381\ psi$)
    - Cylinder strain at $f_c', eo = 2.70\ me$
    - Poisson's ratio, $Mu = 0.15$
    - Thermal expansion coefficient, $Cc = 1e-5\ /\mathrm{C}^{\circ}$
    - Maximum aggregate size, $a = 25\ mm$ ($1\ in$)
    - Concrete Density= 2400 $^{kg}/_{m^3}$ (150 $^{lb}/_{ft^3}$)
    - Thermal diffusivity, $= Kc = 1.2$ $^{mm^2}/_{s}$ (0.00186 $^{in^2}/_{s}$)

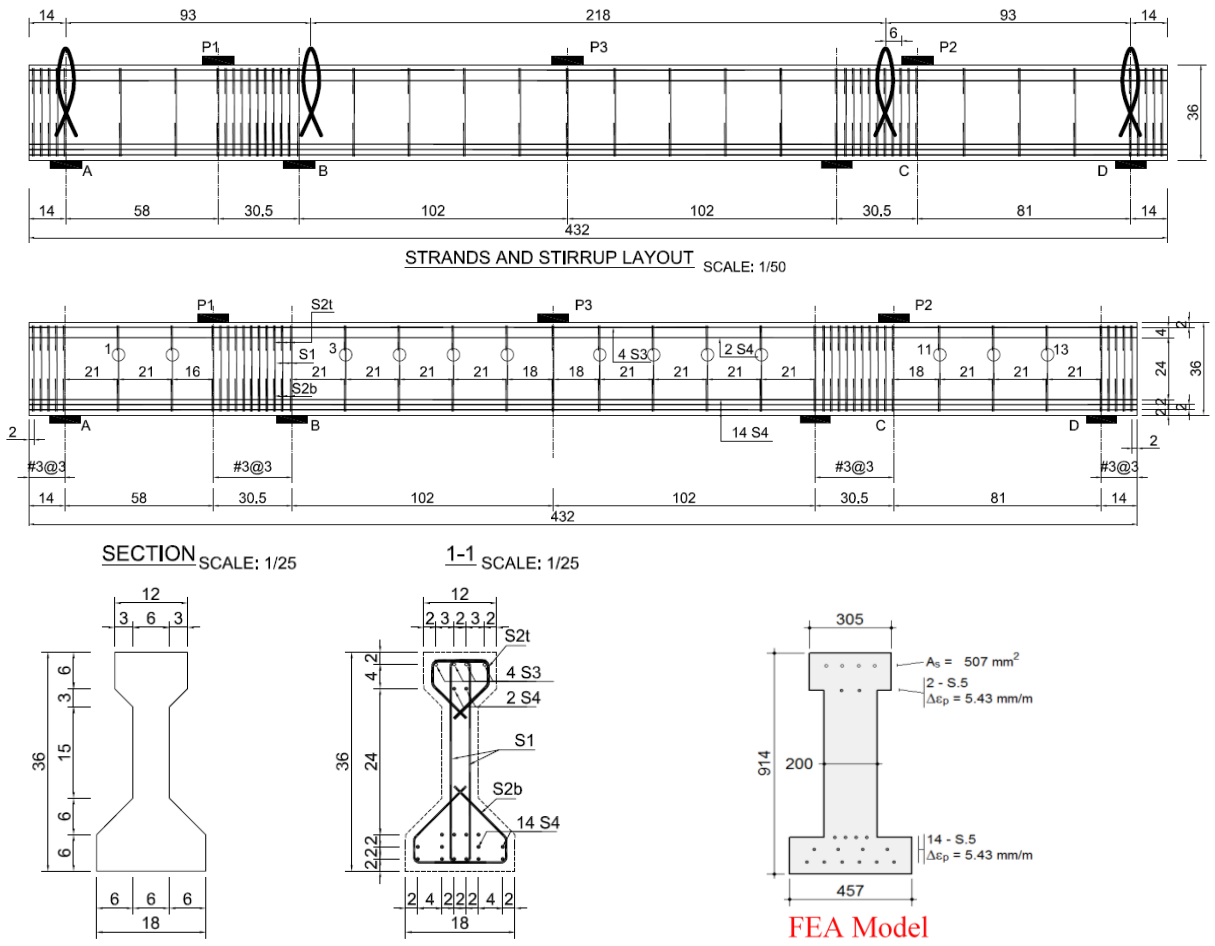

Figure B20. Girder 2 test setup and cross section details

Girder 2 FEA Model (Modified) Results Summary

Girder 2-Test 1

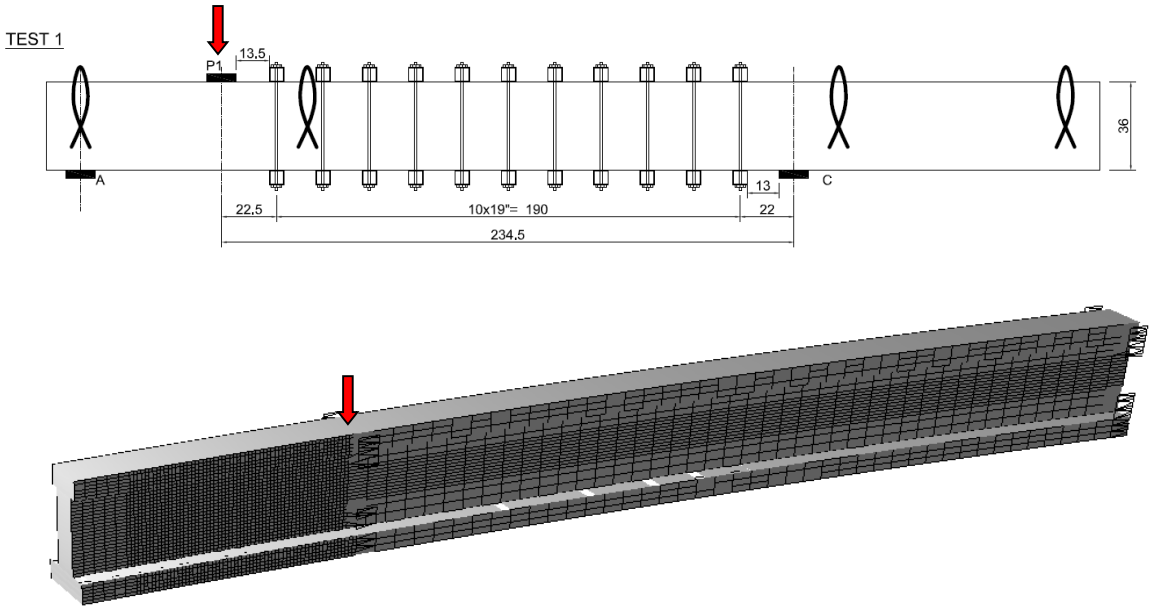

Figure 2. Girder 2-Test 1 model set up

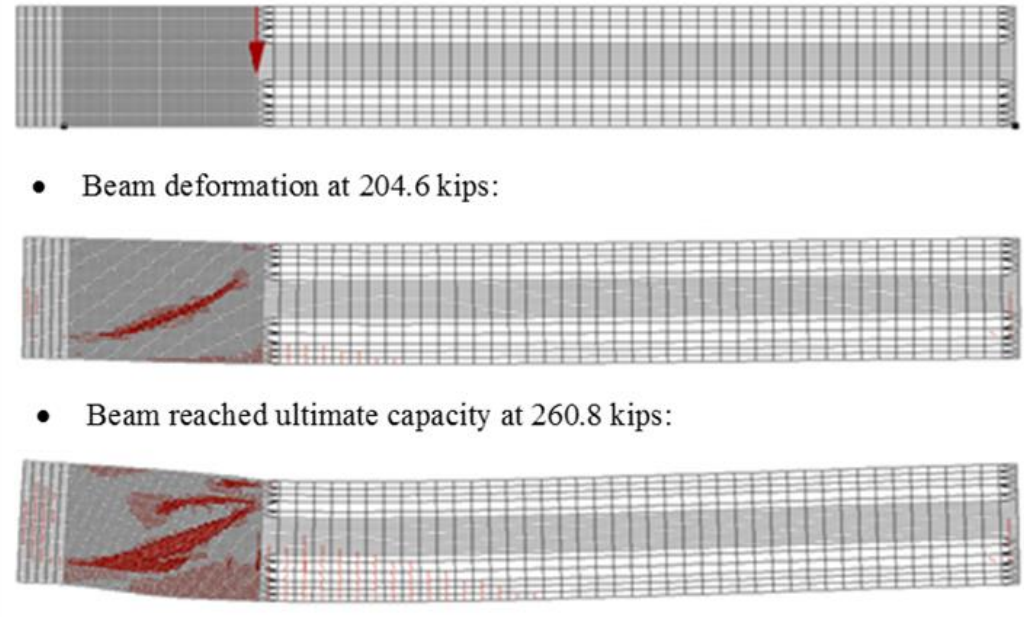

- Beam deformation at 204.6 kips:

- Beam reached ultimate capacity at 260.8 kips:

Figure B20. Girder 2-Test 1 model results (f'c=9.2 ksi)

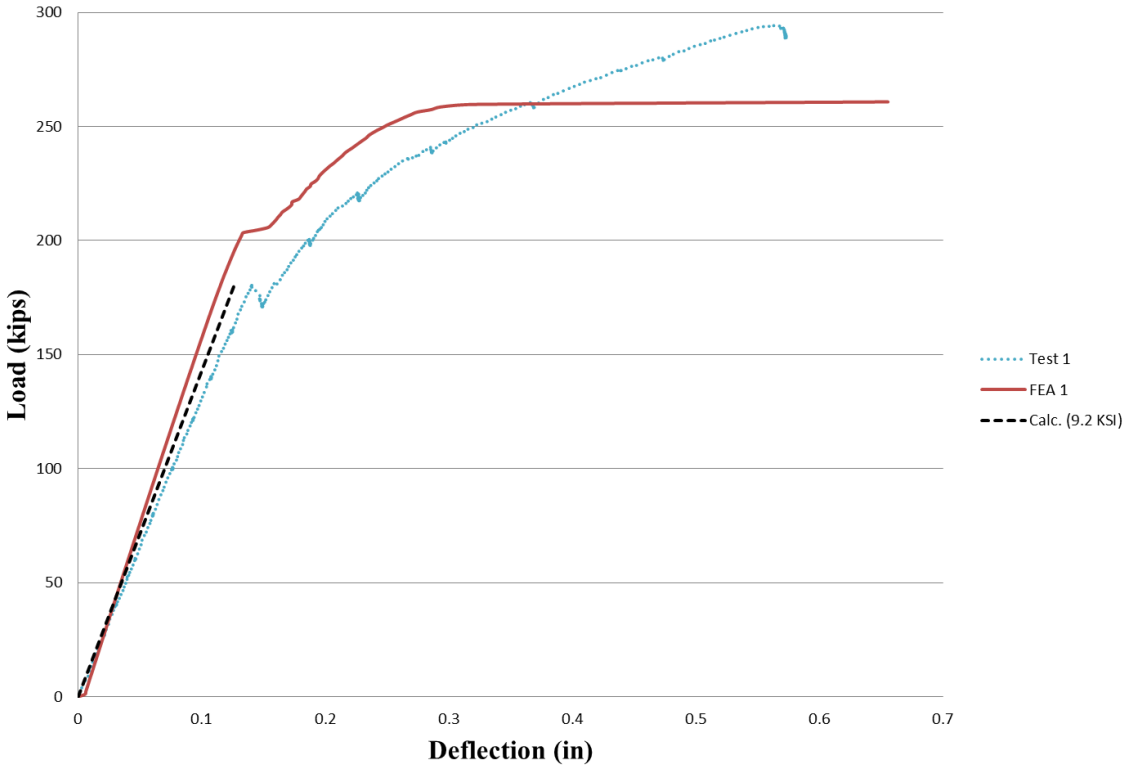

Figure B21. Load versus deflection results (Girder 2-Test 1)

Girder 2-Test 2

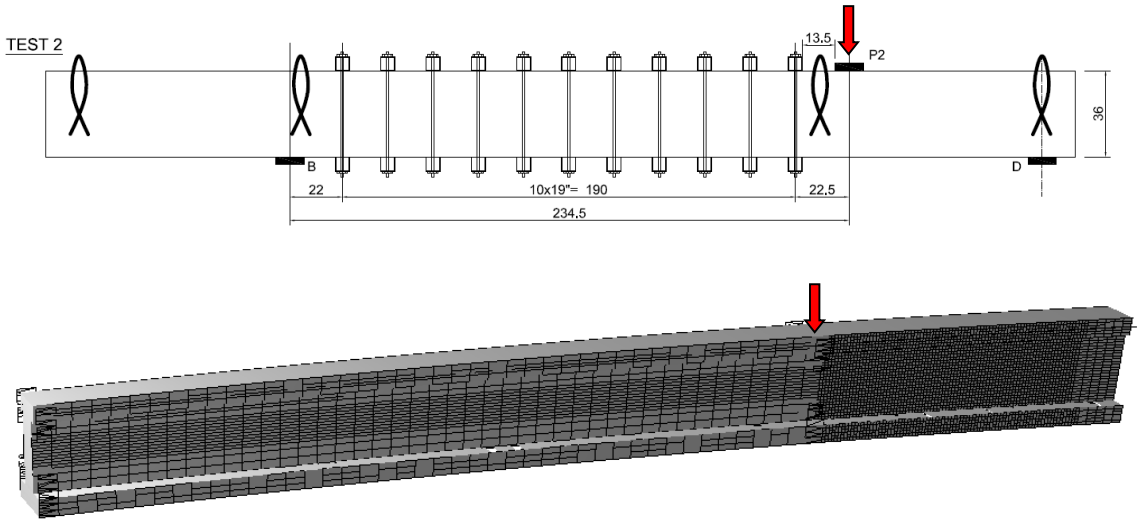

Figure B22. Girder 2-Test 2 model set up

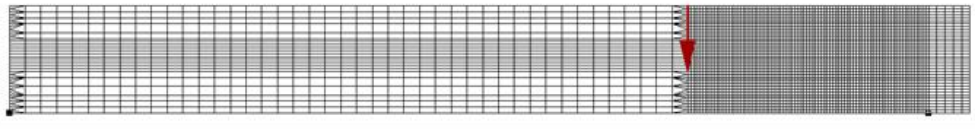

- Beam deformation at 202.3 kips:

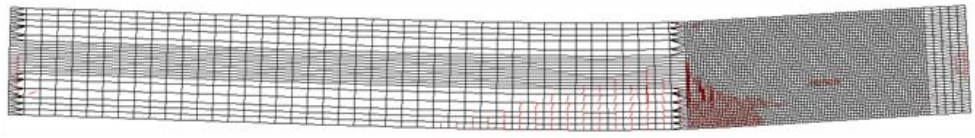

- Beam reached ultimate capacity at 213.6 kips:

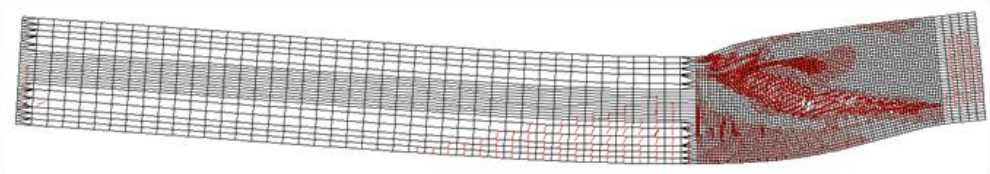

Figure B23. Girder 2-Test 2 model results (f'c=9.2 ksi)

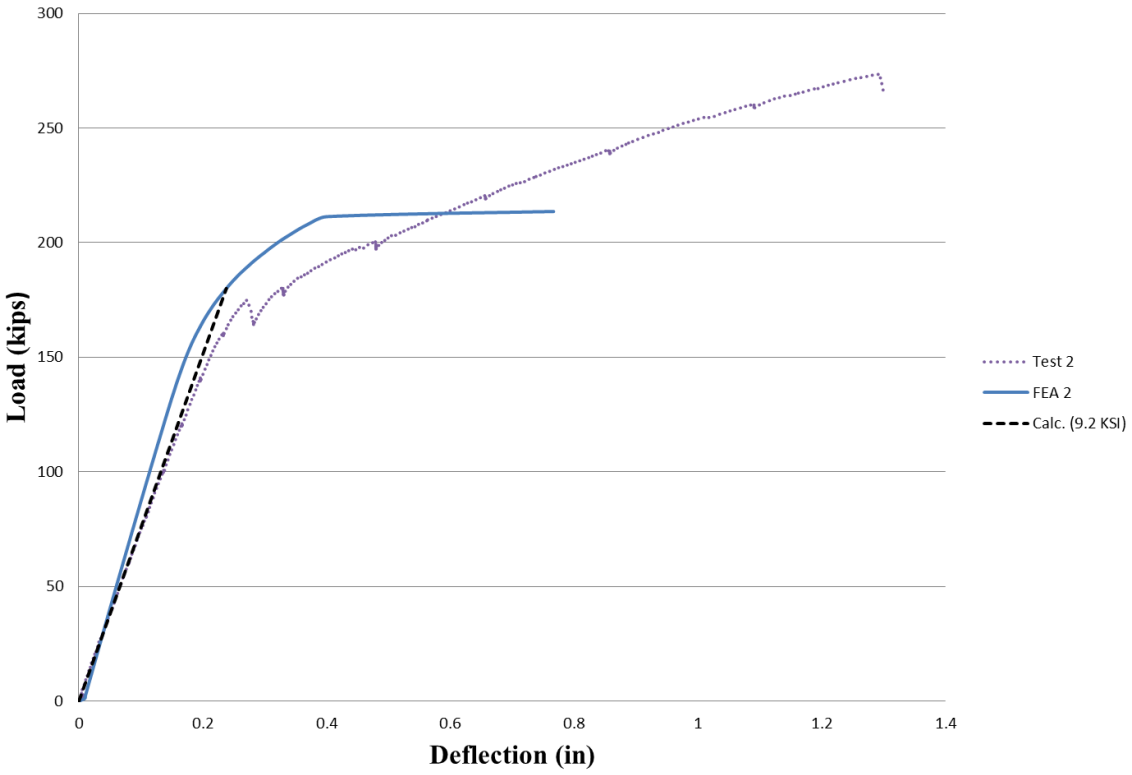

Figure B24. Load versus deflection results (Girder 2-Test 2)

Girder 2-Test 3

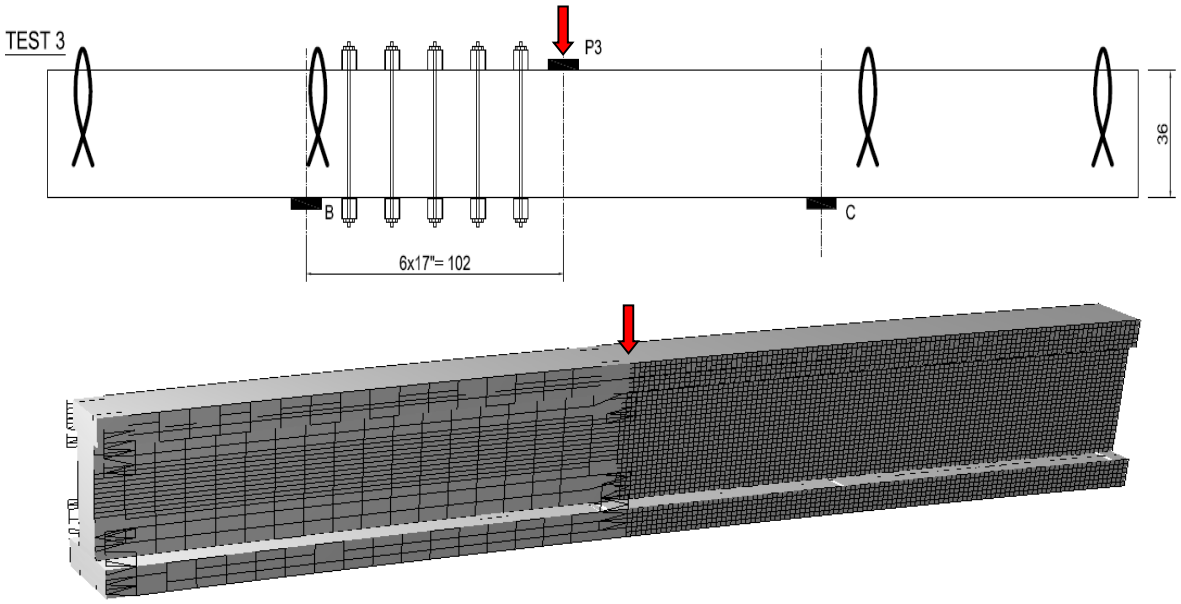

Figure B25. Girder 2-Test 3 model set up

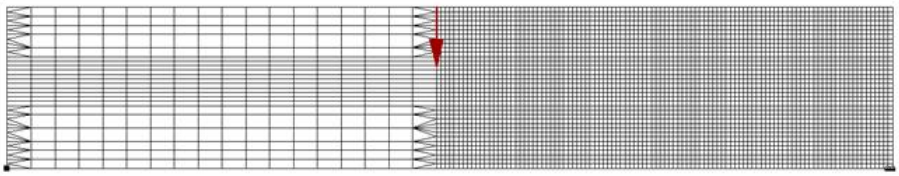

- Beam deformation at 258.5 kips:

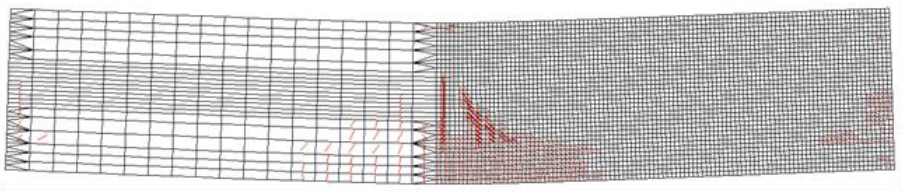

- Beam reached ultimate capacity at 275.4 kips:

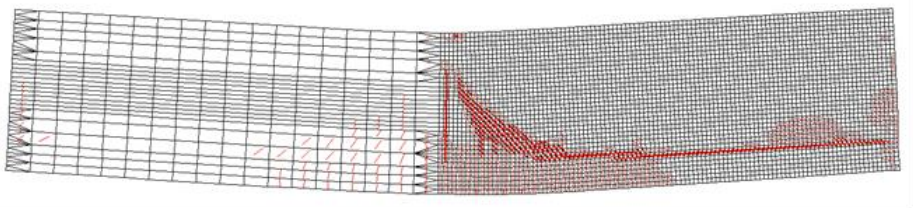

Figure B26. Girder 2-Test 3 model results (f'c=9.2 ksi)

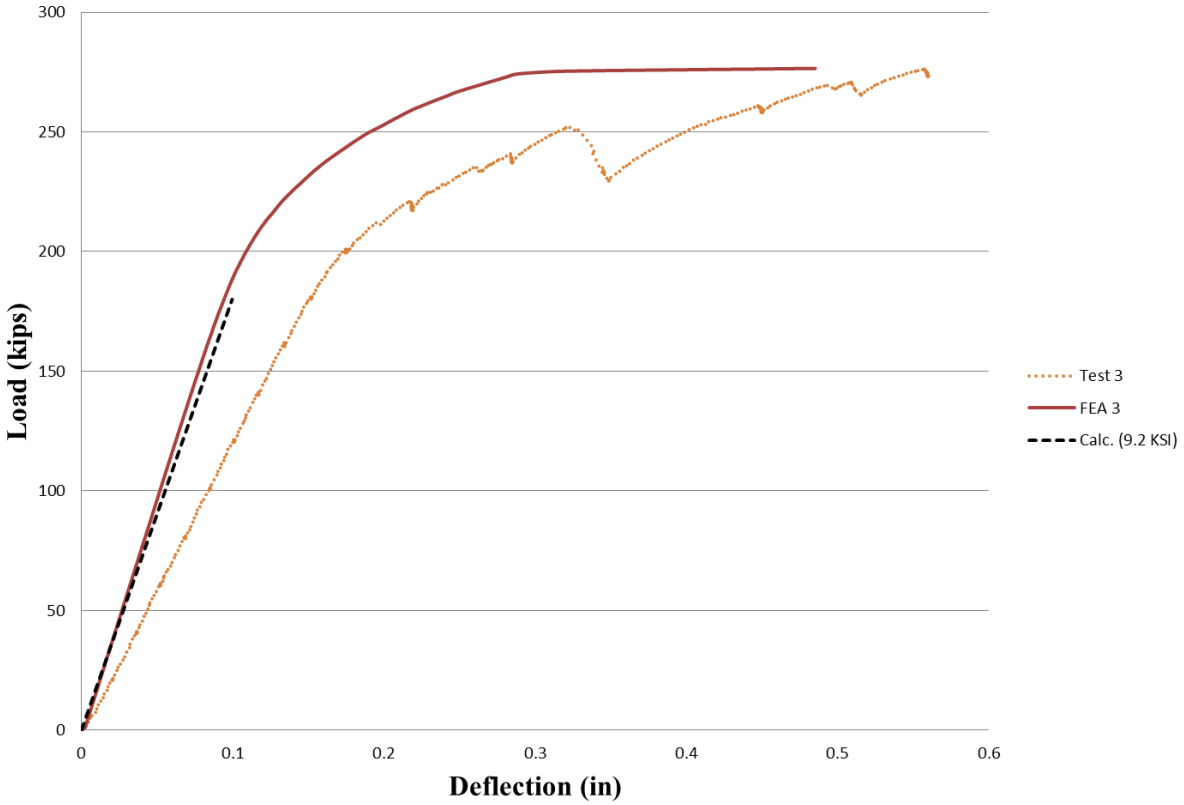

Figure B27. Load versus deflection results (Girder 2-Test 3)

APPENDIX C: PARAMETRIC ANALYSIS RESULTS

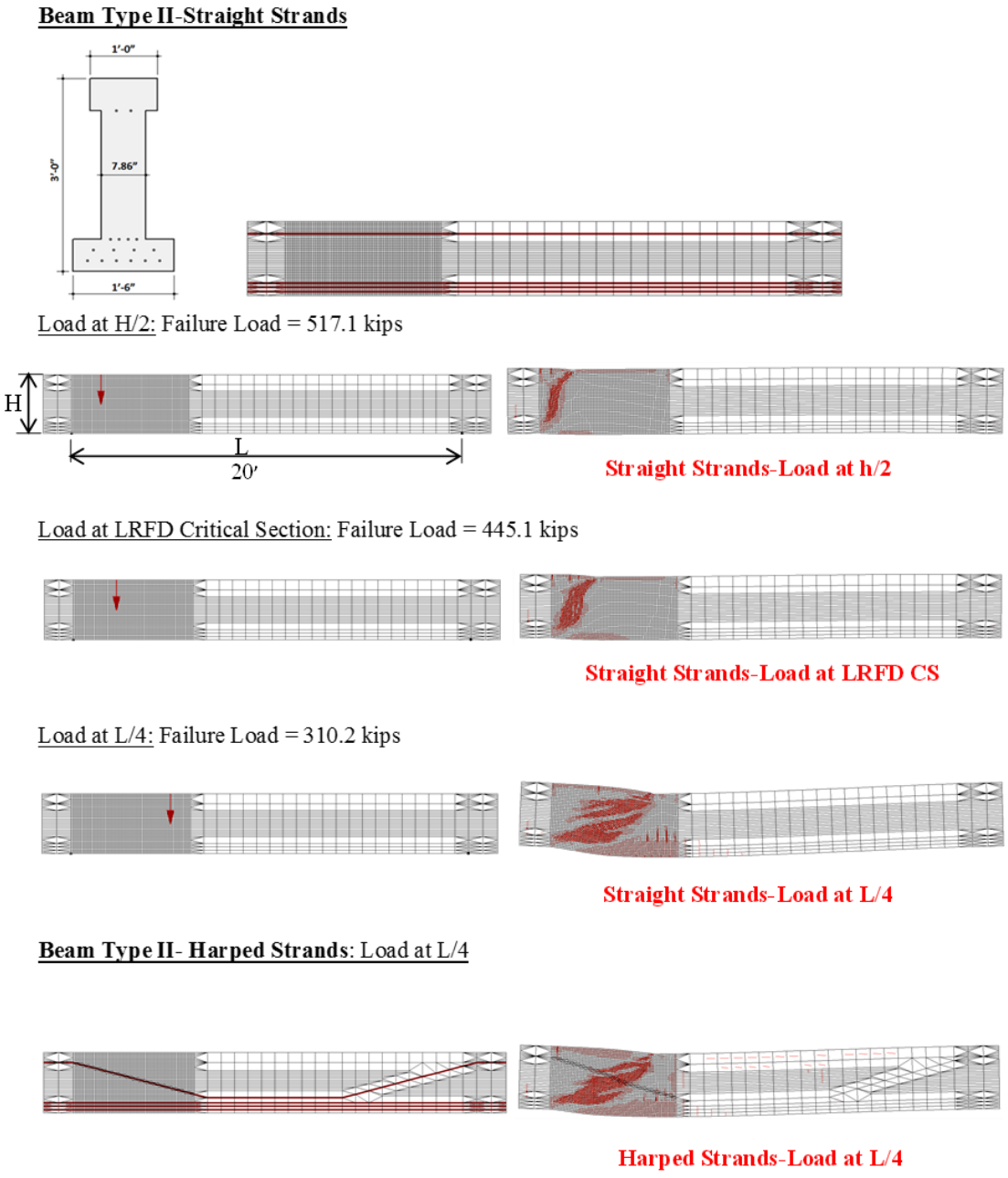

Figure C1. Example of girder Type II failure at different load locations (parametric analysis)

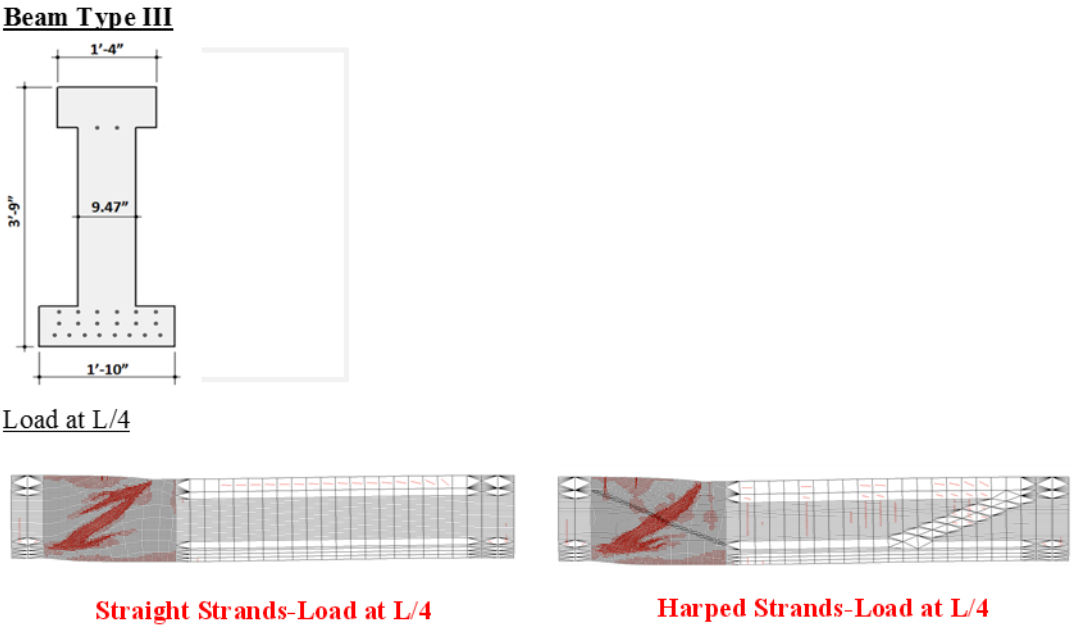

Figure F6. Example of girder Type III failure (parametric analysis)

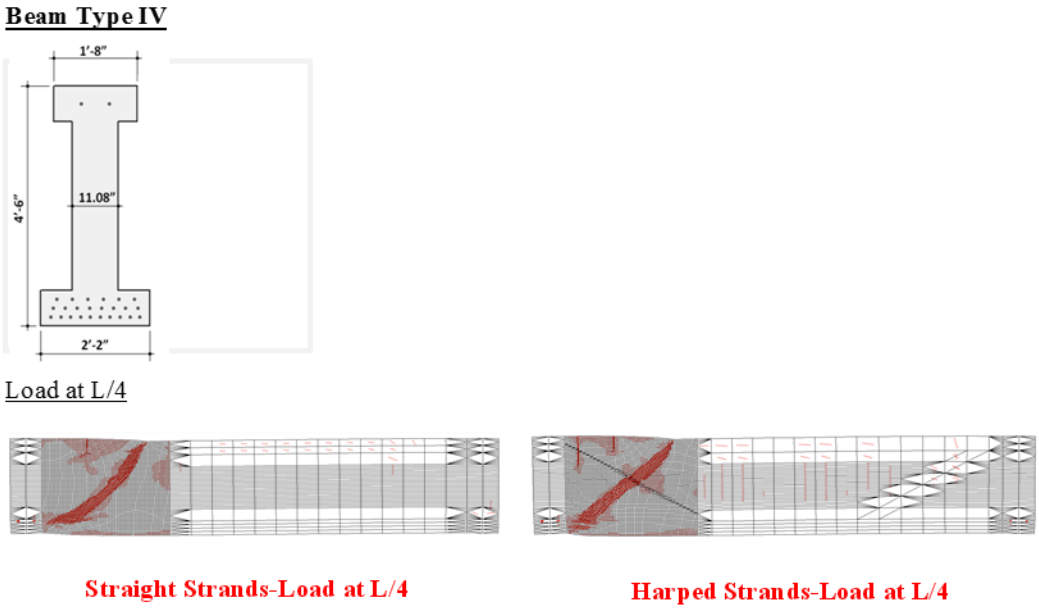

Figure C2. Example of girder Type IV failure (parametric analysis)

Table C1. FEA models parameters

Variable	Avg. Stress (ksi)	Concrete f'c (psi)	Strands Profile	Load Location	Stirrups Spacing (in)
1	0.5	5500	Straight/Harped	h/2 (Standard)	3 (min)
2	1.5	8000	Straight/Harped	LRFD	24 (max)
3	2.5	-	-	L/4 (1979)	12 (avg)

Table C2. Models combinations for girder Types II, III, and IV

Combination #	Girder Type	Avg. Stress	Concrete f'c	Load Location	Stirrups Spacing	Strands Profile
1	II, III, IV	1	1	1	1	S, H
2	II, III, IV	2	1	1	1	S, H
3	II, III, IV	1	2	1	1	S, H
4	II, III, IV	1	1	1	2	S, H
5	II, III, IV	2	2	1	2	S, H
6	II, III, IV	2	2	1	1	S, H
7	II, III, IV	2	1	1	2	S, H
8	II, III, IV	1	2	1	2	S, H
9	II, III, IV	3	1	1	1	S, H
10	II, III, IV	3	2	1	2	S, H
11	II, III, IV	3	2	1	1	S, H
12	II, III, IV	3	1	1	2	S, H
13	II, III, IV	1	1	1	3	S, H
14	II, III, IV	2	2	1	3	S, H
15	II, III, IV	2	1	1	3	S, H
16	II, III, IV	1	2	1	3	S, H
17	II, III, IV	3	1	1	3	S, H
18	II, III, IV	3	2	1	3	S, H
19	II, III, IV	1	1	2	1	S, H
20	II, III, IV	2	1	2	1	S, H
21	II, III, IV	1	2	2	1	S, H
22	II, III, IV	1	1	2	2	S, H
23	II, III, IV	2	2	2	2	S, H
24	II, III, IV	2	2	2	1	S, H
25	II, III, IV	2	1	2	2	S, H
26	II, III, IV	1	2	2	2	S, H
27	II, III, IV	3	1	2	1	S, H
28	II, III, IV	3	2	2	2	S, H
29	II, III, IV	3	2	2	1	S, H
30	II, III, IV	3	1	2	2	S, H
31	II, III, IV	1	1	2	3	S, H
32	II, III, IV	2	2	2	3	S, H
33	II, III, IV	2	1	2	3	S, H
34	II, III, IV	1	2	2	3	S, H
35	II, III, IV	3	1	2	3	S, H
36	II, III, IV	3	2	2	3	S, H
37	II, III, IV	1	1	3	1	S, H
38	II, III, IV	2	1	3	1	S, H
39	II, III, IV	1	2	3	1	S, H
40	II, III, IV	1	1	3	2	S, H
41	II, III, IV	2	2	3	2	S, H
42	II, III, IV	2	2	3	1	S, H
43	II, III, IV	2	1	3	2	S, H
44	II, III, IV	1	2	3	2	S, H
45	II, III, IV	3	1	3	1	S, H
46	II, III, IV	3	2	3	2	S, H
47	II, III, IV	3	2	3	1	S, H
48	II, III, IV	3	1	3	2	S, H
49	II, III, IV	1	1	3	3	S, H
50	II, III, IV	2	2	3	3	S, H
51	II, III, IV	2	1	3	3	S, H
52	II, III, IV	1	2	3	3	S, H
53	II, III, IV	3	1	3	3	S, H
54	II, III, IV	3	2	3	3	S, H

Table C3. Results for Girder Type II, Straight Strands, Aps at Tension Controlled Limit

	FEA, kips			Code (Vn), kips				
Type II	1	2	3	4	5	6	7	8
Combination #	h/2	LRFD	L/4	Standard	LRFD	Interim 1979	LRFD (Ɛx_max)	LRFD (HL-93)
1	346.2	323.7	310.2	243.3	260.1	282.2	106.8	270.9
2	404.7	427.1	337.2	243.3	260.1	282.2	106.8	270.9
3	431.6	400.2	328.2	252.6	235.0	305.7	108.9	281.8
4	314.7	274.3	170.9	131.3	88.6	80.5	24.3	86.4
5	490.1	445.1	274.3	140.6	99.3	104.0	24.3	86.4
6	508.1	517.1	364.2	252.6	235.0	305.7	108.9	281.8
7	391.2	364.2	233.8	131.3	88.6	80.5	24.3	86.4
8	355.2	305.7	193.3	140.6	99.3	104.0	24.3	86.4
9	463.1	458.6	346.2	243.3	260.1	282.2	106.8	270.9
10	521.6	454.1	292.3	140.6	99.3	104.0	24.3	86.4
11	526.1	530.5	368.7	252.6	235.0	305.7	108.9	281.8
12	418.1	386.7	256.3	131.3	88.6	80.5	24.3	86.4
13	319.2	287.8	193.3	147.3	113.6	109.3	34.3	112.7
14	517.1	445.1	310.2	156.6	124.2	132.8	36.4	124.1
15	404.7	382.2	274.3	147.3	113.6	109.3	34.3	112.7
16	355.2	332.7	220.3	156.6	124.2	132.8	36.4	124.1
17	436.1	395.7	296.7	147.3	113.6	109.3	34.3	112.7
18	521.6	467.6	328.2	156.6	124.2	132.8	36.4	124.1
Comparison #	(1/4)	(2/5)	(3/6)	(3/4)	(3/5)	(3/7)	(2/8)	(3/8)
1	1.42	1.24	1.10	1.27	1.19	2.90	1.20	1.15
2	1.66	1.64	1.20	1.39	1.30	3.16	1.58	1.24
3	1.71	1.70	1.07	1.30	1.40	3.01	1.42	1.16
4	2.40	3.09	2.12	1.30	1.93	7.03	3.17	1.98
5	3.49	4.48	2.64	1.95	2.76	11.29	5.15	3.17
6	2.01	2.20	1.19	1.44	1.55	3.34	1.83	1.29
7	2.98	4.11	2.90	1.78	2.64	9.62	4.22	2.71
8	2.53	3.08	1.86	1.38	1.95	7.96	3.54	2.24
9	1.90	1.76	1.23	1.42	1.33	3.24	1.69	1.28
10	3.71	4.57	2.81	2.08	2.94	12.03	5.26	3.38
11	2.08	2.26	1.21	1.46	1.57	3.38	1.88	1.31
12	3.18	4.36	3.18	1.95	2.89	10.55	4.48	2.97
13	2.17	2.53	1.77	1.31	1.70	5.64	2.55	1.71
14	3.30	3.58	2.34	1.98	2.50	8.53	3.59	2.50
15	2.75	3.37	2.51	1.86	2.42	8.00	3.39	2.43
16	2.27	2.68	1.66	1.41	1.77	6.05	2.68	1.78
17	2.96	3.48	2.71	2.01	2.61	8.65	3.51	2.63
18	3.33	3.76	2.47	2.10	2.64	9.02	3.77	2.65
Mean	2.55	3.00	2.00	1.63	2.06	6.85	3.05	2.09
STDEV.	0.69	1.05	0.72	0.32	0.61	3.11	1.27	0.75
COV	0.27	0.35	0.36	0.19	0.30	0.45	0.42	0.36

Table C4. Results for girder Type III, Straight Strands, Aps at Tension Controlled Limit

	FEA, kips			Code (Vn), kips			
Type III	1	2	3	4	5	6	7
Combination #	h/2	LRFD	L/4	Standard	LRFD	Interim 1979	LRFD (Ɛx_max)
1	499.1	499.1	458.6	334.8	327.7	381.9	142.5
2	589.0	616.0	580.0	334.8	327.7	381.9	142.5
3	589.0	593.5	526.1	349.0	332.8	417.9	145.7
4	422.6	373.2	296.7	187.6	134.5	117.0	31.4
5	660.9	607.0	467.6	201.9	159.2	153.0	34.6
6	737.4	714.9	643.0	349.0	332.8	417.9	145.7
7	562.0	499.1	395.7	187.6	134.5	117.0	31.4
8	512.6	422.6	319.2	201.9	159.2	153.0	34.6
9	625.0	629.5	602.5	334.8	327.7	381.9	142.5
10	705.9	602.5	472.1	201.9	159.2	153.0	34.6
11	714.9	737.4	660.9	349.0	332.8	417.9	145.7
12	589.0	539.5	391.2	187.6	134.5	117.0	31.4
13	440.6	391.2	328.2	208.6	170.9	154.9	47.3
14	674.4	616.0	499.1	222.9	186.9	190.9	50.5
15	566.5	508.1	440.6	208.6	170.9	154.9	47.3
16	481.1	449.6	350.7	222.9	186.9	190.9	50.5
17	580.0	539.5	458.6	208.6	170.9	154.9	47.3
18	687.9	620.5	517.1	222.9	186.9	190.9	50.5

Comparison #	(1/4)	(2/5)	(3/6)	(3/4)	(3/5)	(3/7)
1	1.49	1.52	1.20	1.37	1.40	3.22
2	1.76	1.88	1.52	1.73	1.77	4.07
3	1.69	1.78	1.26	1.51	1.58	3.61
4	2.25	2.78	2.54	1.58	2.21	9.45
5	3.27	3.81	3.06	2.32	2.94	13.52
6	2.11	2.15	1.54	1.84	1.93	4.41
7	3.00	3.71	3.38	2.11	2.94	12.60
8	2.54	2.66	2.09	1.58	2.01	9.23
9	1.87	1.92	1.58	1.80	1.84	4.23
10	3.50	3.79	3.08	2.34	2.97	13.65
11	2.05	2.22	1.58	1.89	1.99	4.54
12	3.14	4.01	3.34	2.09	2.91	12.46
13	2.11	2.29	2.12	1.57	1.92	6.94
14	3.03	3.29	2.61	2.24	2.67	9.89
15	2.72	2.97	2.84	2.11	2.58	9.32
16	2.16	2.41	1.84	1.57	1.88	6.95
17	2.78	3.16	2.96	2.20	2.68	9.70
18	3.09	3.32	2.71	2.32	2.77	10.24
Mean	2.47	2.76	2.29	1.90	2.28	8.22
STDEV.	0.61	0.78	0.74	0.32	0.52	3.58
COV	0.25	0.28	0.32	0.17	0.23	0.44

Table C5. Results for girder Type IV, Straight Strands, Aps at Tension Controlled Limit

	FEA, kips			Code (Vn), kips			
Type IV	1	2	3	4	5	6	7
Combination #	h/2	LRFD	L/4	Standard	LRFD	Interim 1979	LRFD (Ɛx_max)
1	634.0	638.5	634.0	418.2	405.4	482.9	177.7
2	728.4	800.3	813.8	418.2	405.4	482.9	177.7
3	737.4	741.9	714.9	438.2	412.0	533.4	182.2
4	535.0	445.1	418.1	237.5	172.5	157.6	41.3
5	827.3	723.9	625.0	257.5	195.7	208.1	45.8
6	908.2	926.2	912.7	438.2	412.0	533.4	182.2
7	683.4	643.0	557.5	237.5	172.5	157.6	41.3
8	607.0	535.0	463.1	257.5	195.7	208.1	45.8
9	782.3	791.3	822.8	418.2	405.4	482.9	177.7
10	867.8	741.9	683.4	257.5	195.7	208.1	45.8
11	939.7	935.2	930.7	438.2	412.0	533.4	182.2
12	741.9	651.9	598.0	237.5	172.5	157.6	41.3
13	526.1	508.1	449.6	263.3	212.7	204.1	60.8
14	863.3	750.9	710.4	283.4	235.8	254.6	65.3
15	687.9	643.0	598.0	263.3	212.7	204.1	60.8
16	616.0	580.0	481.1	283.4	235.8	254.6	65.3
17	741.9	669.9	634.0	263.3	212.7	204.1	60.8
18	876.8	800.3	723.9	283.4	235.8	254.6	65.3

Comparison #	(1/4)	(2/5)	(3/6)	(3/4)	(3/5)	(3/7)
1	1.52	1.57	1.31	1.52	1.56	3.57
2	1.74	1.97	1.69	1.95	2.01	4.58
3	1.68	1.80	1.34	1.63	1.74	3.92
4	2.25	2.58	2.65	1.76	2.42	10.13
5	3.21	3.70	3.00	2.43	3.19	13.66
6	2.07	2.25	1.71	2.08	2.22	5.01
7	2.88	3.73	3.54	2.35	3.23	13.51
8	2.36	2.73	2.23	1.80	2.37	10.12
9	1.87	1.95	1.70	1.97	2.03	4.63
10	3.37	3.79	3.28	2.65	3.49	14.93
11	2.14	2.27	1.74	2.12	2.26	5.11
12	3.12	3.78	3.79	2.52	3.47	14.49
13	2.00	2.39	2.20	1.71	2.11	7.40
14	3.05	3.18	2.79	2.51	3.01	10.89
15	2.61	3.02	2.93	2.27	2.81	9.84
16	2.17	2.46	1.89	1.70	2.04	7.37
17	2.82	3.15	3.11	2.41	2.98	10.43
18	3.09	3.39	2.84	2.55	3.07	11.09
Mean	2.44	2.76	2.43	2.11	2.56	8.93
STDEV.	0.59	0.73	0.77	0.37	0.61	3.84
COV	0.24	0.26	0.32	0.17	0.24	0.43

Table C6. Summary of results for girder Types II-IV, straight strands, Aps at tension controlled limit

Mean Comparison	(1/4)	(2/5)	(3/6)	(3/4)	(3/5)	(3/7)
II	2.55	3.00	2.00	1.63	2.06	6.85
III	2.47	2.76	2.29	1.90	2.28	8.22
IV	2.44	2.76	2.43	2.11	2.56	8.93
Mean	2.49	2.84	2.24	1.88	2.30	8.00

COV Comparison	(1/4)	(2/5)	(3/6)	(3/4)	(3/5)	(3/7)
II	0.27	0.35	0.36	0.19	0.30	0.45
III	0.25	0.28	0.32	0.17	0.23	0.44
IV	0.24	0.26	0.32	0.17	0.24	0.43
Mean	0.25	0.30	0.33	0.18	0.25	0.44
STDEV.	0.02	0.04	0.02	0.01	0.04	0.01
COV	0.07	0.15	0.07	0.07	0.14	0.03

Table C7. Results for girder Type II, harped strands, Aps at tension controlled limit

	FEA, kips			Code (Vn), kips			
Type II (Harped)	1	2	3	4	5	6	7
Combination #	h/2	LRFD	L/4	Standard	LRFD	Interim 1979	LRFD (Ɛx_max)
1	368.7	-	314.7	255.1	236.1	288.0	112.7
2	463.1	-	355.2	278.5	236.1	299.7	124.4
3	431.6	-	368.7	264.4	239.0	311.5	114.8
4	332.7	-	197.8	143.0	94.3	86.3	28.1
5	512.6	-	296.7	175.7	116.4	121.5	41.9
6	553.0	-	386.7	287.8	247.5	323.2	126.5
7	436.1	-	265.3	166.4	105.7	98.1	39.8
8	386.7	-	220.3	152.3	105.0	109.8	30.2
9	467.6	-	368.7	301.9	253.0	311.5	136.1
10	539.5	-	337.2	199.2	127.9	133.3	53.6
11	566.5	-	395.7	311.2	270.8	334.9	138.2
12	445.1	-	283.3	189.9	117.1	109.8	51.5
13	373.2	-	220.3	159.0	119.2	115.2	40.2
14	526.1	-	337.2	191.7	141.3	150.4	54.0
15	454.1	-	305.7	182.4	130.6	126.9	51.9
16	368.7	-	247.3	168.3	129.9	138.6	42.2
17	476.6	-	328.2	205.9	142.0	138.6	63.6
18	548.5	-	364.2	215.2	152.7	162.1	65.7

Comparison #	(1/4)	(3/6)	(3/4)	(3/5)	(3/7)
1	1.45	1.09	1.23	1.33	2.79
2	1.66	1.19	1.28	1.50	2.86
3	1.63	1.18	1.39	1.54	3.21
4	2.33	2.29	1.38	2.10	7.05
5	2.92	2.44	1.69	2.55	7.09
6	1.92	1.20	1.34	1.56	3.06
7	2.62	2.71	1.59	2.51	6.67
8	2.54	2.01	1.45	2.10	7.31
9	1.55	1.18	1.22	1.46	2.71
10	2.71	2.53	1.69	2.64	6.29
11	1.82	1.18	1.27	1.46	2.86
12	2.34	2.58	1.49	2.42	5.50
13	2.35	1.91	1.39	1.85	5.49
14	2.74	2.24	1.76	2.39	6.25
15	2.49	2.41	1.68	2.34	5.89
16	2.19	1.78	1.47	1.90	5.85
17	2.32	2.37	1.59	2.31	5.16
18	2.55	2.25	1.69	2.38	5.55
Mean	2.23	1.92	1.48	2.02	5.09
STDEV.	0.45	0.59	0.18	0.45	1.69
COV	0.20	0.31	0.12	0.22	0.33

Table C8. Results for girder Type III, harped strands, Aps at tension controlled limit

	FEA, kips			Code (Vn), kips			
Type III (Harped)	1	2	3	4	5	6	7
Combination #	h/2	LRFD	L/4	Standard	LRFD	Interim 1979	LRFD (Ɛx_max)
1	517.1	-	485.6	343.7	334.1	390.9	151.5
2	629.5	-	620.5	361.6	346.8	408.8	169.4
3	616.0	-	548.5	358.0	339.2	426.9	154.7
4	449.6	-	346.2	196.5	143.0	126.0	40.3
5	696.9	-	517.1	228.7	176.0	179.8	61.4
6	755.4	-	678.9	375.8	395.8	444.8	172.6
7	607.0	-	445.1	214.4	160.2	143.8	58.2
8	512.6	-	377.7	210.8	158.7	162.0	43.5
9	634.0	-	643.0	379.5	359.8	426.6	187.2
10	746.4	-	517.1	246.5	193.2	197.7	79.3
11	777.8	-	701.4	393.7	364.7	462.6	190.4
12	625.0	-	472.1	232.3	177.3	161.7	76.1
13	445.1	-	364.2	217.6	174.9	163.8	56.2
14	705.9	-	566.5	249.7	207.9	217.7	77.3
15	593.5	-	494.6	235.4	192.1	181.7	74.1
16	526.1	-	404.7	217.6	190.7	163.8	59.4
17	584.5	-	512.6	253.3	215.8	199.6	92.0
18	741.9	-	584.5	267.6	230.6	235.6	95.2

Comparison #	(1/4)	(3/6)	(3/4)	(3/5)	(3/7)
1	1.50	1.24	1.41	1.45	3.21
2	1.74	1.52	1.72	1.79	3.66
3	1.72	1.28	1.53	1.62	3.55
4	2.29	2.75	1.76	2.42	8.58
5	3.05	2.88	2.26	2.94	8.42
6	2.01	1.53	1.81	1.72	3.93
7	2.83	3.09	2.08	2.78	7.65
8	2.43	2.33	1.79	2.38	8.68
9	1.67	1.51	1.69	1.79	3.43
10	3.03	2.62	2.10	2.68	6.52
11	1.98	1.52	1.78	1.92	3.68
12	2.69	2.92	2.03	2.66	6.20
13	2.05	2.22	1.67	2.08	6.48
14	2.83	2.60	2.27	2.73	7.33
15	2.52	2.72	2.10	2.58	6.68
16	2.42	2.47	1.86	2.12	6.81
17	2.31	2.57	2.02	2.37	5.57
18	2.77	2.48	2.18	2.53	6.14
Mean	2.32	2.24	1.89	2.25	5.92
STDEV.	0.49	0.62	0.25	0.45	1.90
COV	0.21	0.28	0.13	0.20	0.32

Table C9. Results for girder Type IV, harped strands, Aps at tension controlled limit

	FEA, kips			Code (Vn), kips			
Type IV (Harped)	1	2	3	4	5	6	7
Combination #	h/2	LRFD	L/4	Standard	LRFD	Interim 1979	LRFD (Ɛx_max)
1	669.9	-	660.9	432.3	418.5	497.0	191.8
2	719.4	-	858.8	460.6	439.0	525.2	220.1
3	782.3	-	750.9	452.3	425.1	547.5	196.3
4	557.5	-	485.6	251.6	187.2	171.7	55.4
5	858.8	-	732.9	299.9	238.0	250.4	88.1
6	867.8	-	953.2	480.6	445.5	575.7	224.5
7	701.4	-	660.9	279.8	214.8	199.9	83.6
8	710.4	-	548.5	271.6	210.5	222.2	59.9
9	791.3	-	876.8	488.8	459.7	553.4	248.3
10	881.3	-	777.8	328.1	265.6	278.6	116.3
11	944.2	-	980.2	508.8	466.1	603.9	252.8
12	741.9	-	665.4	308.1	242.3	228.1	111.8
13	602.5	-	508.1	277.5	228.4	218.2	74.9
14	890.2	-	746.4	325.7	279.2	296.9	107.6
15	773.3	-	696.9	305.7	255.9	246.4	103.1
16	705.9	-	557.5	297.5	251.6	268.7	79.4
17	795.8	-	701.4	333.9	283.5	274.6	131.3
18	894.7	-	791.3	353.9	306.7	325.1	135.8

Comparison #	(1/4)	(3/6)	(3/4)	(3/5)	(3/7)
1	1.55	1.33	1.53	1.58	3.45
2	1.56	1.64	1.86	1.96	3.90
3	1.73	1.37	1.66	1.77	3.82
4	2.22	2.83	1.93	2.59	8.77
5	2.86	2.93	2.44	3.08	8.32
6	1.81	1.66	1.98	2.14	4.25
7	2.51	3.31	2.36	3.08	7.91
8	2.62	2.47	2.02	2.61	9.16
9	1.62	1.58	1.79	1.91	3.53
10	2.69	2.79	2.37	2.93	6.69
11	1.86	1.62	1.93	2.10	3.88
12	2.41	2.92	2.16	2.75	5.95
13	2.17	2.33	1.83	2.22	6.79
14	2.73	2.51	2.29	2.67	6.94
15	2.53	2.83	2.28	2.72	6.76
16	2.37	2.08	1.87	2.22	7.03
17	2.38	2.55	2.10	2.47	5.34
18	2.53	2.43	2.24	2.58	5.83
Mean	2.23	2.29	2.04	2.41	6.02
STDEV.	0.43	0.61	0.26	0.44	1.88
COV	0.19	0.27	0.13	0.18	0.31

Table C10. Summary of results for girder Types II-IV, harped Strands, Aps at tension controlled limit

Mean Comparison	(1/4)	(3/6)	(3/4)	(3/5)	(3/7)
II	2.23	1.92	1.48	2.02	5.09
III	2.32	2.24	1.89	2.25	5.92
IV	2.23	2.29	2.04	2.41	6.02
Mean	2.26	2.15	1.80	2.23	5.67

COV Comparison	(1/4)	(3/6)	(3/4)	(3/5)	(3/7)
II	0.20	0.31	0.12	0.22	0.33
III	0.21	0.28	0.13	0.20	0.32
IV	0.19	0.27	0.13	0.18	0.31
Mean	0.20	0.28	0.13	0.20	0.32
STDEV.	0.01	0.02	0.01	0.02	0.01
COV	0.04	0.07	0.04	0.09	0.03

Table C11. Results for girder Type II, straight strands, high Aps

	FEA, kips	Code (Vn), kips				
Type II	3	4	5	6	7	8
Combination #	L/4	Standard	LRFD	Interim 1979	LRFD (Ɛx_max)	LRFD (HL-93)
1	328.2	286.5	278.3	289.9	109.7	285.1
2	382.2	286.5	278.3	289.9	109.7	285.1
3	382.2	296.0	288.8	314.0	111.9	295.8
4	197.8	171.4	100.8	82.7	22.8	93.3
5	274.3	180.9	111.1	106.8	25.0	104.9
6	454.1	296.0	288.8	314.0	111.9	295.8
7	238.3	171.4	100.8	82.7	22.8	93.3
8	202.3	180.9	111.1	106.8	25.0	104.9
9	422.6	286.5	278.3	289.9	109.7	285.1
10	305.7	180.9	111.1	106.8	25.0	104.9
11	508.1	296.0	288.8	314.0	111.9	295.8
12	278.8	171.4	100.8	82.7	22.8	93.3
13	211.3	187.8	126.5	112.3	35.2	120.7
14	323.7	197.4	136.8	136.4	37.4	132.2
15	278.8	187.8	126.5	112.3	35.2	120.7
16	233.8	197.4	136.8	136.4	37.4	132.2
17	305.7	187.8	126.5	112.3	35.2	120.7
18	373.2	197.4	136.8	136.4	37.4	132.2

Comparison #	(3/6)	(3/4)	(3/5)	(3/7)	(3/8)
1	1.13	1.15	1.18	2.99	1.15
2	1.32	1.33	1.37	3.48	1.34
3	1.22	1.29	1.32	3.42	1.29
4	2.39	1.15	1.96	8.67	2.12
5	2.57	1.52	2.47	10.99	2.61
6	1.45	1.53	1.57	4.06	1.54
7	2.88	1.39	2.36	10.44	2.55
8	1.89	1.12	1.82	8.10	1.93
9	1.46	1.48	1.52	3.85	1.48
10	2.86	1.69	2.75	12.25	2.91
11	1.62	1.72	1.76	4.54	1.72
12	3.37	1.63	2.77	12.22	2.99
13	1.88	1.13	1.67	6.00	1.75
14	2.37	1.64	2.37	8.66	2.45
15	2.48	1.48	2.20	7.91	2.31
16	1.71	1.18	1.71	6.25	1.77
17	2.72	1.63	2.42	8.68	2.53
18	2.74	1.89	2.73	9.98	2.82
Mean	2.12	1.44	2.00	7.36	2.07
STDEV.	0.68	0.24	0.52	3.13	0.59
COV	0.32	0.16	0.26	0.43	0.29

Table C12. Results for girder Type III, straight strands, high Aps

	FEA, kips	Code (Vn), kips			
Type III	3	4	5	6	7
Combination #	L/4	Standard	LRFD	Interim 1979	LRFD (Ɛx_max)
1	490.1	419.9	386.7	388.2	144.9
2	607.0	419.9	386.7	388.2	144.9
3	571.0	434.4	401.4	424.8	148.1
4	296.7	270.3	163.5	119.0	31.9
5	467.6	284.8	177.1	155.5	35.2
6	705.9	434.4	401.4	424.8	148.1
7	395.7	270.3	163.5	119.0	31.9
8	332.7	284.8	177.1	155.5	35.2
9	634.0	419.9	386.7	388.2	144.9
10	548.5	284.8	177.1	155.5	35.2
11	777.8	434.4	401.4	424.8	148.1
12	472.1	270.3	163.5	119.0	31.9
13	332.7	291.7	195.6	157.4	48.0
14	512.6	306.2	209.4	194.0	51.3
15	440.6	291.7	195.6	157.4	48.0
16	377.7	306.2	209.4	194.0	51.3
17	494.6	291.7	195.6	157.4	48.0
18	616.0	306.2	209.4	194.0	51.3

Comparison #	(3/6)	(3/4)	(3/5)	(3/7)
1	1.26	1.17	1.27	3.38
2	1.56	1.45	1.57	4.19
3	1.34	1.31	1.42	3.86
4	2.49	1.10	1.82	9.30
5	3.01	1.64	2.64	13.30
6	1.66	1.62	1.76	4.77
7	3.33	1.46	2.42	12.40
8	2.14	1.17	1.88	9.46
9	1.63	1.51	1.64	4.38
10	3.53	1.93	3.10	15.60
11	1.83	1.79	1.94	5.25
12	3.97	1.75	2.89	14.79
13	2.11	1.14	1.70	6.92
14	2.64	1.67	2.45	9.99
15	2.80	1.51	2.25	9.17
16	1.95	1.23	1.80	7.36
17	3.14	1.70	2.53	10.29
18	3.18	2.01	2.94	12.01
Mean	2.42	1.51	2.11	8.69
STDEV.	0.81	0.28	0.55	3.90
COV	0.34	0.18	0.26	0.45

Table C13. Results for girder Type IV, straight strands, high Aps

	FEA, kips	Code (Vn), kips			
Type IV	3	4	5	6	7
Combination #	L/4	Standard	LRFD	Interim 1979	LRFD (Ɛx_max)
1	687.9	553.0	489.0	493.4	181.6
2	840.8	553.0	489.0	493.4	181.6
3	813.8	573.4	511.1	545.0	186.2
4	418.1	368.4	201.8	161.0	42.2
5	701.4	388.8	223.9	212.6	46.8
6	998.2	573.4	511.1	545.0	186.2
7	625.0	368.4	201.8	161.0	42.2
8	467.6	388.8	223.9	212.6	46.8
9	822.8	553.0	489.0	493.4	181.6
10	778.6	388.8	223.9	212.6	46.8
11	1043.1	573.4	511.1	545.0	186.2
12	700.5	368.4	201.8	161.0	42.2
13	449.6	394.7	243.2	208.5	62.1
14	750.9	415.2	265.3	260.1	66.7
15	665.4	394.7	243.2	208.5	62.1
16	499.1	415.2	265.3	260.1	66.7
17	680.1	394.7	243.2	208.5	62.1
18	840.1	415.2	265.3	260.1	66.7

Comparison #	(3/6)	(3/4)	(3/5)	(3/7)
1	1.39	1.24	1.41	3.79
2	1.70	1.52	1.72	4.63
3	1.49	1.42	1.59	4.37
4	2.60	1.14	2.07	9.91
5	3.30	1.80	3.13	15.00
6	1.83	1.74	1.95	5.36
7	3.88	1.70	3.10	14.82
8	2.20	1.20	2.09	10.00
9	1.67	1.49	1.68	4.53
10	3.66	2.00	3.48	16.65
11	1.91	1.82	2.04	5.60
12	4.35	1.90	3.47	16.61
13	2.16	1.14	1.85	7.24
14	2.89	1.81	2.83	11.26
15	3.19	1.69	2.74	10.72
16	1.92	1.20	1.88	7.48
17	3.26	1.72	2.80	10.95
18	3.23	2.02	3.17	12.60
Mean	2.59	1.59	2.39	9.53
STDEV.	0.90	0.30	0.69	4.38
COV	0.35	0.19	0.29	0.46

Table C14. Summary of results for girder Types II-IV, straight strands, high Aps

Mean Comparison	(3/6)	(3/4)	(3/5)	(3/7)
II	2.12	1.44	2.00	7.36
III	2.42	1.51	2.11	8.69
IV	2.59	1.59	2.39	9.53
Mean	2.38	1.51	2.17	8.53

COV Comparison	(3/6)	(3/4)	(3/5)	(3/7)
II	0.32	0.16	0.26	0.43
III	0.34	0.18	0.26	0.45
IV	0.35	0.19	0.29	0.46
Mean	0.33	0.18	0.27	0.44
STDEV	0.01	0.01	0.02	0.02
COV	0.04	0.08	0.06	0.04

Table C15. Results for girder Type II, harped strands, high Aps

	FEA, kips	Code (Vn), kips			
Type II (Harped)	3	4	5	6	7
Combination #	L/4	Standard	LRFD	Interim 1979	LRFD (Ɛx_max)
1	332.7	309.1	283.1	294.8	114.7
2	400.2	328.8	292.6	304.6	124.5
3	400.2	318.7	293.5	318.9	116.8
4	202.3	194.0	105.5	87.6	27.8
5	328.2	223.3	125.4	121.6	39.8
6	481.1	338.4	303.1	328.8	126.7
7	278.8	213.7	115.1	97.5	37.6
8	233.8	203.6	115.9	111.7	29.9
9	454.1	348.6	302.1	314.5	134.4
10	341.7	243.0	135.0	131.5	49.6
11	539.5	358.1	312.6	338.6	136.5
12	314.7	233.5	124.6	107.3	47.5
13	233.8	210.5	131.3	117.2	40.2
14	359.7	239.7	151.1	151.2	52.2
15	314.7	230.2	140.8	127.1	50.0
16	269.8	220.0	141.6	141.3	42.3
17	346.2	249.9	150.3	136.9	59.9
18	413.6	259.5	160.7	161.1	62.0

Comparison #	(3/6)	(3/4)	(3/5)	(3/7)
1	1.13	1.08	1.18	2.90
2	1.31	1.22	1.37	3.21
3	1.25	1.26	1.36	3.43
4	2.31	1.04	1.92	7.29
5	2.70	1.47	2.62	8.26
6	1.46	1.42	1.59	3.80
7	2.86	1.30	2.42	7.41
8	2.09	1.15	2.02	7.82
9	1.44	1.30	1.50	3.38
10	2.60	1.41	2.53	6.89
11	1.59	1.51	1.73	3.95
12	2.93	1.35	2.53	6.63
13	1.99	1.11	1.78	5.82
14	2.38	1.50	2.38	6.89
15	2.48	1.37	2.24	6.29
16	1.91	1.23	1.91	6.38
17	2.53	1.39	2.30	5.78
18	2.57	1.59	2.57	6.67
Mean	2.09	1.32	2.00	5.71
STDEV.	0.59	0.16	0.47	1.77
COV	0.28	0.12	0.24	0.31

Table C16. Results for girder Type III, harped strands, high Aps

	FEA, kips	Code (Vn), kips			
Type III (Harped)	3	4	5	6	7
Combination #	L/4	Standard	LRFD	Interim 1979	LRFD (Ɛx_max)
1	512.6	426.9	393.4	395.2	151.9
2	651.9	441.0	406.6	409.3	165.9
3	616.0	441.4	408.1	431.8	155.1
4	346.2	277.4	170.1	126.0	38.9
5	566.5	305.9	197.1	176.6	56.2
6	768.8	455.5	421.4	445.8	169.2
7	454.1	291.4	183.3	140.0	53.0
8	391.2	291.9	183.8	162.6	42.2
9	683.4	455.0	420.0	423.3	180.0
10	611.5	319.9	210.4	190.6	70.3
11	845.3	469.5	434.8	459.9	183.2
12	553.0	305.4	196.5	154.1	67.0
13	386.7	298.7	202.2	164.4	55.1
14	589.0	327.3	229.4	215.1	72.4
15	499.1	312.8	215.5	178.5	69.1
16	440.6	313.2	216.1	201.0	58.3
17	549.8	326.8	228.7	192.5	83.2
18	683.4	341.3	242.8	229.1	86.4

Comparison #	(3/6)	(3/4)	(3/5)	(3/7)
1	1.30	1.20	1.30	3.37
2	1.59	1.48	1.60	3.93
3	1.43	1.40	1.51	3.97
4	2.75	1.25	2.04	8.89
5	3.21	1.85	2.87	10.08
6	1.72	1.69	1.82	4.54
7	3.24	1.56	2.48	8.57
8	2.41	1.34	2.13	9.27
9	1.61	1.50	1.63	3.80
10	3.21	1.91	2.91	8.70
11	1.84	1.80	1.94	4.61
12	3.59	1.81	2.81	8.25
13	2.35	1.29	1.91	7.02
14	2.74	1.80	2.57	8.14
15	2.80	1.60	2.32	7.22
16	2.19	1.41	2.04	7.56
17	2.86	1.68	2.40	6.61
18	2.98	2.00	2.81	7.91
Mean	2.43	1.59	2.17	6.80
STDEV.	0.71	0.24	0.50	2.18
COV	0.29	0.15	0.23	0.32

Table C17. Results for girder Type IV, harped strands, high Aps

	FEA, kips	Code (Vn), kips			
Type IV (Harped)	3	4	5	6	7
Combination #	L/4	Standard	LRFD	Interim 1979	LRFD (Ɛx_max)
1	723.9	562.6	498.3	503.0	191.3
2	912.7	581.9	517.0	522.3	210.6
3	858.8	583.1	520.4	554.6	195.9
4	503.6	378.0	211.1	170.7	51.8
5	876.8	417.8	252.0	241.6	75.7
6	1043.1	602.4	539.1	574.0	215.2
7	710.4	397.3	229.8	190.0	71.1
8	571.0	398.4	233.3	222.3	56.4
9	912.7	601.2	535.6	541.6	229.9
10	863.3	437.1	270.8	260.9	95.0
11	1065.6	621.7	557.8	593.3	234.5
12	683.4	416.6	248.5	209.3	90.4
13	530.5	404.4	252.6	218.2	71.7
14	890.2	444.1	293.4	289.1	95.6
15	728.4	423.7	271.3	237.5	91.0
16	602.5	424.8	274.7	269.8	76.3
17	749.0	443.0	289.9	256.8	110.4
18	908.2	463.4	312.2	308.4	114.9

Comparison #	(3/6)	(3/4)	(3/5)	(3/7)
1	1.44	1.29	1.45	3.78
2	1.75	1.57	1.77	4.33
3	1.55	1.47	1.65	4.38
4	2.95	1.33	2.39	9.72
5	3.63	2.10	3.48	11.58
6	1.82	1.73	1.93	4.85
7	3.74	1.79	3.09	9.99
8	2.57	1.43	2.45	10.12
9	1.69	1.52	1.70	3.97
10	3.31	1.98	3.19	9.09
11	1.80	1.71	1.91	4.54
12	3.27	1.64	2.75	7.56
13	2.43	1.31	2.10	7.39
14	3.08	2.00	3.03	9.31
15	3.07	1.72	2.69	8.00
16	2.23	1.42	2.19	7.89
17	2.92	1.69	2.58	6.79
18	2.95	1.96	2.91	7.90
Mean	2.56	1.65	2.40	7.29
STDEV.	0.75	0.25	0.60	2.45
COV	0.29	0.15	0.25	0.34

Table C18. Summary of results for girder Types II-IV, harped strands, high Aps

Mean Comparison	(3/6)	(3/4)	(3/5)	(3/7)
II	2.09	1.32	2.00	5.71
III	2.43	1.59	2.17	6.80
IV	2.56	1.65	2.40	7.29
Mean	2.36	1.52	2.19	6.60

COV Comparison #	(3/6)	(3/4)	(3/5)	(3/7)
II	0.28	0.12	0.24	0.31
III	0.29	0.15	0.23	0.32
IV	0.29	0.15	0.25	0.34
Mean	0.29	0.14	0.24	0.32
STDEV	0.00	0.02	0.01	0.01
COV	0.02	0.13	0.04	0.04

APPENDIX D: LRFD CALCULATIONS EXAMPLE

This design example demonstrates the calculations of the nominal shear capacity using the General LRFD Procedure (AASHTO LRFD 2014) for one of the existing simple span AASHTO Type IV PC bridge girders in the state of Michigan (I-696 and Coolidge Road-7933). The bridge has two 77' simple spans with a total width of 82'-8". Bridge configurations are shown in Figures D1 and D2.

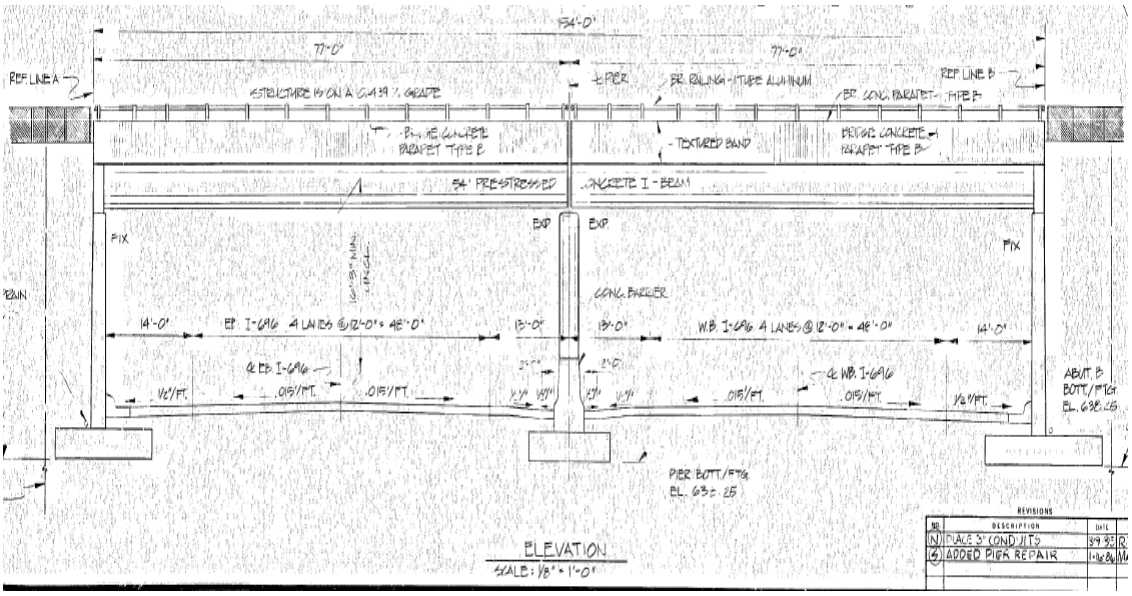

Figure D1. Bridge Dimensions

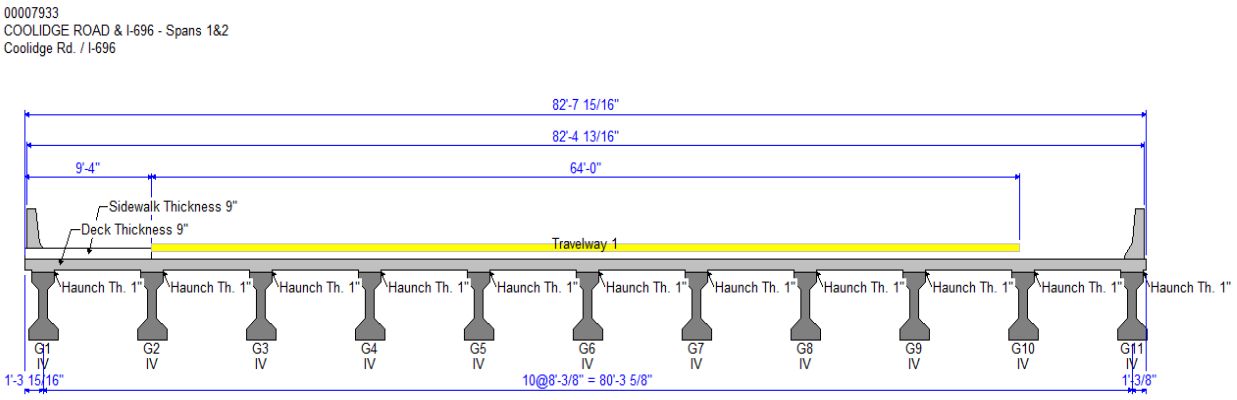

Figure D2. Span cross section details and girder spacings

1- Materials:

- Slab:
  - Slab thickness= 9 in
  - Concrete strength at 28 days, $f'_c = 4$ ksi
- AASHTO Type IV girder:
  - Concrete strength at release, $f'_{ci} = 3.5$ ksi
  - Concrete strength at 28 days, $f'_c = 5$ ksi
  - Concrete unit weight, $w_c = 150$ pcf
  - Overall girder length (spans 1&2) $= 78.167$ ft
    - Girder clear length = 77 ft
- Pre-tensioning strands (1/2 in dia.):
  - Area of one tendon, A_{ps}= 0.153 in^2
  - Ultimate stress, $f_{pu} = 270$ ksi
  - Yield strength, f_{py}= 0.9 $f_{pu} = 243$ ksi
  - Initial pre-tensioning, $f_{pi} = 0.75 f_{pu} = 202.5$ ksi
    - At service limit state, $f_{pe} = 0.8 f_{py} = 194.4$ ksi
  - Modulus of elasticity, $E_p = 28500$ ksi
- Transverse reinforcement bars:
  - Yield strength, $f_y = 60$ ksi
  - Modulus of elasticity, $E_s = 29000$ ksi

2- AASHTO- Type IV girder construction specifications:

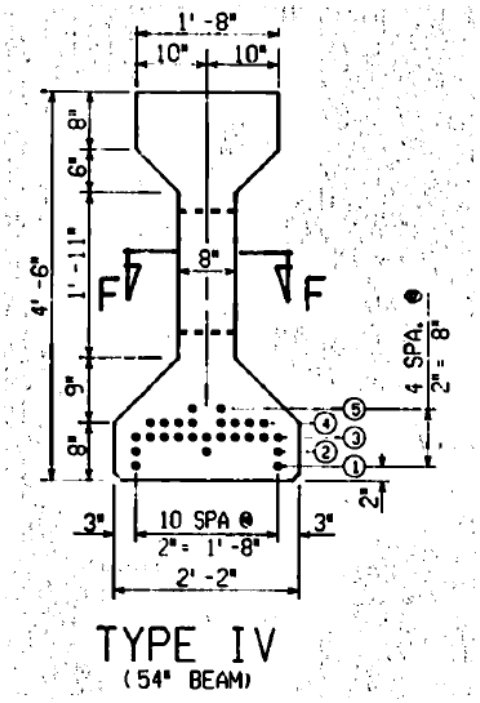

Figure D3. AASHTO Type IV girder dimensions and reinforcement details

A = area of cross section of precast girder= 789 in^2

h = overall depth of precast girder = 54 in^2

I = moment of inertia about the centroid of non-composite precast girder = 261000 in^2

y_b = distance from centroid to the extreme bottom fiber of the non-composite precast girder = 24.73 in

y_t = distance from centroid to the extreme top fiber of the non-composite precast girder = 29.27 in

Y_{bs}= distance from the center of gravity of strands to the bottom fiber of the girder

$$= \frac{(2)\,(2") + (3)\,(4") + (11)(6") + (8)\,(8") + (2)\,(10")}{26} = 6.38 \text{ in}$$

S_b = section modulus for the extreme bottom fiber of the non-composite precast girder = $\frac{I}{y_b} = 10550\ in^3$

S_t = section modulus for the extreme top fiber of the non-composite precast girder

$= \frac{I}{y_t} = 8910 \text{ in}^3$

$W_t = 0.822 \ {}^{k}/_{ft}$

E_c = modulus of elasticity of concrete = $(w_c)^{1.5} \ (33)\sqrt{f'_c}/1000$

- Cast-in-place slab $f'_c = 4000$ psi:

$$E_c = (150)^{1.5} \ (33)\sqrt{4000}/1000 = 3834.2 \text{ ksi}$$

- Girder at release, $f'_{ci} = 3500$ psi

$$E_{ci} = (150)^{1.5} \ (33)\sqrt{3500}/1000 = 3586.6 \text{ ksi}$$

- Girder at service loads, $f'_c = 5000$ psi:

$$E_{ci} = (150)^{1.5} \ (33)\sqrt{5000}/1000 = 4286.8 \text{ ksi}$$

3- Composite section properties:

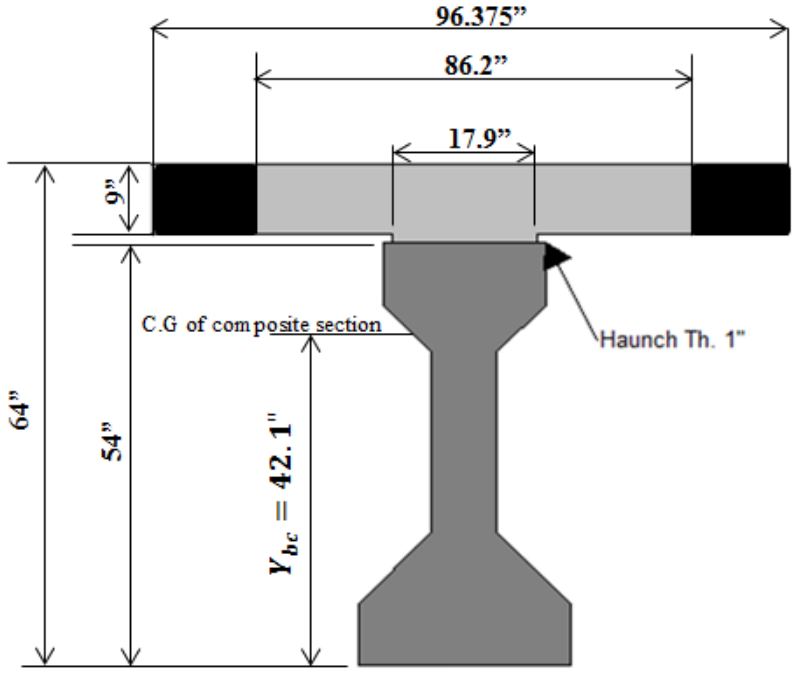

Figure 4: Composite section dimensions

Table D1. Properties of the Composite Section

	Transformed Area ($\boldsymbol{A}$) , $\boldsymbol{in^2}$	$\boldsymbol{y_b, in}$	$\boldsymbol{Ay_b, in^3}$	$\boldsymbol{A(y_{bc} - y_b)^2}$	I, $\boldsymbol{in^4}$	I + $\boldsymbol{A(Y_b - y_b)^2}$, $\boldsymbol{in^4}$
Girder	789.00	24.73	19511.97	238054.63	26100.00	499054.63
Haunch	17.89	54.50	975.0	2750.77	1.49	2752.26
Slab	775.78	59.50	46158.91	234875.15	5236.68	240111.83
Σ	1582.67	-	66646.00	-	-	$I_c = 741925.5$

Y_{bc}= distance from the centroid of composite section to extreme bottom fiber of girder =

$$\frac{\Sigma Ay_b}{\Sigma A} = \frac{66646}{1582.67} = 42.10 \text{ in}$$

h_c= total height of the composite section = 64 in

S_{bc}= composite section modulus for extreme bottom fiber of the girder

$$= \frac{I_c}{Y_{bc}} = \frac{741926}{42.1} = 17618.7 \text{ in}^3$$

- <u>Effective Flange Width:</u>

  The effective flange width is the lesser of:

  - ¼ span length= $\frac{77(12)}{4} = 231"$
  - Distance center-to-center of girders= <u>96.375"</u> ……Controls
  - 12 * effective slab thickness + greater of web thickness or ½ girder top flange width= $(12)\ (9) + (\frac{20}{2}) = 118"$

- <u>Modular Ratio:</u>

  - $n = \frac{E_c(\text{slab})}{E_c(\text{beam})} = \frac{3834.2}{4286.8} = 0.894$

- Transformed Section Properties:

  - Transformed flange width = n(effective flange width)
    $= (0.894)(96.375) = 86.20 \text{ in}$
  - Transformed flange area $=$ n(effective flange width) (t_s)
    $= (86.2)(9) = 775.78 \text{ in}^2$
  - Transformed haunch width $=$ n(top flange width)
    $= (0.894)(20) = 17.89 \text{ in}$
  - Transformed haunch area $=$ n(top flange width)(haunch height)
    $= (17.89)(1") = 17.89 \text{ in}$

4- Shear forces and bending moments:

- Critical Section Location:
  - The critical section is located at the larger of d_v or $0.5\, d_v \cot\theta$ from the face of the support (LRFD 3rd edition).

*note: in the revised LRFD specifications (4th edition) only d_v is considered.

  - The effective shear depth $\mathbf{d_v}$ is calculated as $d_e - a/2$ when strands are straight and compression stays in the top flange.
  - d_v should not be less than the greater of $0.9d_e$ or $0.72h$
  - d_e= effective depth from the extreme compression fiber to the centroid of the tensile force in the tension reinforcement = $h_c - Y_{bs} = 64 - 6.846 = 57.615"$
  - a = depth of the equivalent rectangular stress block = $\beta_1 c$
  - $C = \dfrac{A_{ps}f_{pu} + A_s f_y - A'_s f'_y}{0.85 f'_c \beta_1 b + k A_{ps}\left(\frac{f_{pu}}{d_p}\right)}$
  - Where:

$C =$ distance between the neutral axis and the compressive face, in

$A_{ps} =$ area of prestresing steel $= 26X0.153 = 3.98 \text{ in}^2$

$f_{pu} =$ tensile strength of prestressing steel $= 270$ ksi

$A_s =$ area of mild steel tension reinforcement $= 0$

$A'_s =$ area of compression reinforcement $= 0$

$f'_c = 28-\text{day compressive stress of slab concrete} = 4$ ksi

$f_y =$ yield strength of tension reinforcemen, ksi

$f'_y =$ yield strength of compresion reinforcemeny, ksi

$d_p =$ distance from extreme compression fiber to the strands centroid

$$= h_c - y_{bs} = 57.615 \text{ in}$$

$b =$ effective width of compression flange $= 96.375$ in

$k =$ factor related to type of strand $= 0.28$ (for low relaxation strands)

$\beta_1 =$ stress factor of compression block $= 0.85$ for $f'_c \leq 4.0$ ksi

- $C = \frac{(3.98)(270)}{(0.85)(4)(0.85)(9.375)+(0.28)(398)(\frac{270}{57.615})} = 3.785$ in
- $a = \beta_1 C = (0.85)(3.785) = 3.218$ in
- $d_v = d_e - \frac{a}{2} = 57.615 - \left(\frac{3.218}{2}\right) = 56.01 \text{ in} = 4.67 \text{ ft}$ ……..…….Controls
- $0.9d_e = (0.9)(57.615) = 51.85 \text{ in} < d_v$
- $0.72h = (0.72)(64) = 46.08 \text{ in} < d_v$

- <u>Dead Loads:</u>
  - Girder self-weight $= 0.822$ k/ft
  - 9” slab weight $= (0.15)\left(\frac{9"}{12}\right)(8.03125) = 0.9035$ k/ft
  - 1” haunch weight $= (0.15)(1"/12)\ (20"/12) = 0.0208$ k/ft
  - Barriers weight* $= (2 \text{ barriers})\left(\frac{0.3\frac{k}{ft}}{11 \text{ beams}}\right) = 0.0545\ \frac{k}{ft}$/beam

    *New Jersey- type barrier: Unit weight $= 0.30$ k/ft
  - 2” Future wearing surface unit weight $= (2"/12)(0.15) = 0.025$ ksf
  - Future wearing surface weight/girder* $= \frac{(82.66)(0.025)}{11 \text{ beams}} = 0.188\frac{k}{ft}$/beam

    *Ignore the side walk distributed weight since the wearing surface width was taken as the total bridge width.

- <u>Un-factored Shear Forces and Bending Moments:</u>
  - $V_x = w(0.5L - X)$
  - $M_x = 0.5wX(L - X)$

- Due to girder self-weight:
  - $V_g = 0.822(0.5(77) - 4.67) = (0822)(33.83) = 27.81$ kip
  - $M_g = 0.5(0.822)(4.67)(77 - 4.67) = 138.75$ kip. ft
- Due to slab and haunch weight:
  - $V_s = (0.9243)(33.83) = 31.27$ kip
  - $M_s = 0.5(0.9243)(4.67)(77 - 4.67) = 156.02$ kip. ft
- Due to barrier and future wearing surface weight:
  - $V_b = 0.0545(33.83) = 1.84$ kip
  - $V_{ws} = 0.188(33.83) = 6.36$ kip
  - $M_b = 0.5(0.0545)(4.67)(77 - 4.67) = 9.20$ kip. ft
  - $M_{ws} = 0.5(0.188)(4.67)(77 - 4.67) = 31.73$ kip. ft

- Distribution Factor for Bending Moment (DFM):

  For two or more lanes loaded:

  - $\text{DFM} = 0.075 + \left(\frac{S}{9.5}\right)^{0.6}\left(\frac{S}{L}\right)^{0.2}\left(\frac{K_g}{12Lt_s^3}\right)^{0.1}$
  - where,

    DFM= distribution factor for moment for interior beam

    S= beam spacing = 8.0125 ft

    L= beam span, = 77ft

    t_s = depth of concrete slab = 9 in

    K_g = longitodinal stiffness parameter, $\text{in}^4 = n\left(I + A\, e_g^2\right)$

    $n = \frac{E_{ci}(\text{beam})}{E_{ci}(\text{slab})} = \frac{4286.8}{3834.2} = 1.118$

    e_g = distance between the centers of gravity of the beam and slab, in

    $e_g = \left(\frac{9}{2}\right) + 1 + (54 - 24.73) = 34.77$ in

    $K_g = 1.118(26100 + 789(34.77)^2 = 1{,}358{,}259.0\ \text{in}^4$

    - Check limits:

    $3.5 \le S \le 16$ O.K.

    $4.5 \le t_s \le 12$ O.K.

$20 \leq L \leq 240$ O.K.

$N_b \geq 4$ O.K.

$10{,}000 \leq K_g \leq 7{,}000{,}000$ O.K.

$$DFM = 0.075 + \left(\frac{8.03125}{9.5}\right)^{0.6}\left(\frac{8.03125}{77}\right)^{0.2}\left(\frac{1358259}{(12)(77)(9)^3}\right)^{0.1} = 0.692 \text{ lane/beam}$$

For one design lane loaded:

- $DFM = 0.06 + \left(\frac{S}{14}\right)^{0.4}\left(\frac{S}{L}\right)^{0.3}\left(\frac{K_g}{12Lt_s^3}\right)^{0.1}$

$$DFM = 0.06 + \left(\frac{8.03125}{14}\right)^{0.4}\left(\frac{8.03125}{77}\right)^{0.3}\left(\frac{1358259}{(12)(77)(9)^3}\right)^{0.1} = 0.496 \text{ lane/beam}$$

- $DFM = 0.692$ lane/beam……...……Controls

- Distribution Factor for Shear Force (DFV):

  For two or more lanes loaded:

  - $DFV = 0.2 + \left(\frac{S}{12}\right) - \left(\frac{S}{35}\right)^2$

  $$DFV = 0.2 + \left(\frac{8.03125}{12}\right) - \left(\frac{8.03125}{35}\right)^2 = 0.817 \text{ lane/beam}$$……Controls

  For one design lane loaded:

  - $DFV = 0.36 + \frac{S}{25} = 0.36 + \frac{8.03125}{25} = 0.681$ lane/beam

- Dynamic Allowance: IM= 33%
- Un-factored Shear Forces and Bending Moments Due To Truck load:
  - $V_{LT} = (\text{maximum shear force per lane})(DFV)(1 + IM)$
  - $M_{LT} = (\text{maximum bending moment per lane})(DFM)(1 + IM)$
  - Where: $(\text{at } X_{min} = 0)$
    - $V_x = \frac{72[(L-X)-9.33]}{L}$, maximum shear force per lane
    - $M_x = \frac{72(X)[(L-X)-9.33]}{L}$, maximum bending moment per lane

- $V_{LT} = (\frac{72[(77-4.67)-9.33]}{77})(0.817)(1+0.33) = 63.98 \text{ kip}$
- $M_{LT} = \left(\frac{72(4.67)[(77-4.67)-9.33]}{77}\right)(0.692)(1+0.33) = 253.09 \text{ kip.ft}$

- Un-factored Shear Forces and Bending Moments Due To Design Lane Loading:
  - $V_{LL} = \frac{0.32(L-X)^2}{L}(DFV)$ for $(X \leq 0.5L)$
    - $V_{LL} = \frac{0.32(77-4.67)^2}{77}(0.817) = 17.76 \text{ kip}$
  - $M_{LL} = 0.32(X)(L-X)(DFM)$
    - $M_{LL} = 0.32(4.67)(77-4.67)(0.692) = 74.77 \text{ kip.ft}$

- Total Factored Shear Force and Bending Moment at Critical Section:

  - $V_u = 1.25(V_g + V_s + V_b) + 1.5(V_{ws}) + 1.75(V_{LT} + V_{LL})$
    $= 1.25(2.81 + 31.27 + 1.84) + 1.5(6.36) + 1.75(63.98 + 17.76)$
    $= 228.74 \text{ kip}$

  - $M_u = 1.25(M_g + M_s + M_b) + 1.5(M_{ws}) + 1.75(M_{LT} + M_{LL})$
    $= 1.25(138.75 + 156.02 + 9.2) + 1.5(31.73) + 1.75(253.09 + 74.77)$
    $= 1001.31 \text{ kip.ft}$

5- Nominal Shear resistance:

- Contribution of Concrete to Nominal Shear Resistance:
  - $V_c = 0.0316\,\beta\sqrt{f'_c}\,b_v d_v$
    where β is a factor indicating the ability of diagonally cracked concrete to transmit tension.
  - $\varepsilon_s = \frac{|M_u/d_v| + 0.5N_u + |(V_u - V_p)| - A_{ps}f_{po}}{(E_s A_s + E_p A_{ps})}$
    - $f_{po} = 0.7f_{pu} = 0.7(270) = 189 \text{ ksi}$
    - $N_u = 0$ (no axial force is applied)
    - $V_p = 0$ (no harped strands)

- $\varepsilon_s = \frac{|1001.31/4.67\,|+(0)+|(228.74-0)|-(3.978)(189)}{(0+(28500)(3.978))} = -0.0015976$
- $\varepsilon_s < 0$, use $\varepsilon_s = 0$

- Values of β and θ:
  - $\beta = \frac{4.8}{(1+750\varepsilon_s)} = \frac{4.8}{1+0} = 4.8$
  - $\theta = 29 + 3500\varepsilon_s = 29 + 3500(0) = 29^0$

  - $V_c = 0.0316\,(4.8)\frac{\sqrt{5000}}{1000}(8)(56.01) = 173.65$ kip

- Contribution of Reinforcement to Nominal Shear Resistance:
  - $V_s = \frac{A_v f_y d_v(\cot\theta+\cot\alpha)\sin\alpha}{S} = \frac{(0.6136)(60)(\cot 29)}{9} = 423.41$ kip
  - $V_n = V_c + V_s + V_p = 173.65 + 423.41 + 0 = 597.06$ kip
  - $\phi V_n = 0.9(597.06) = 537.36$ kip

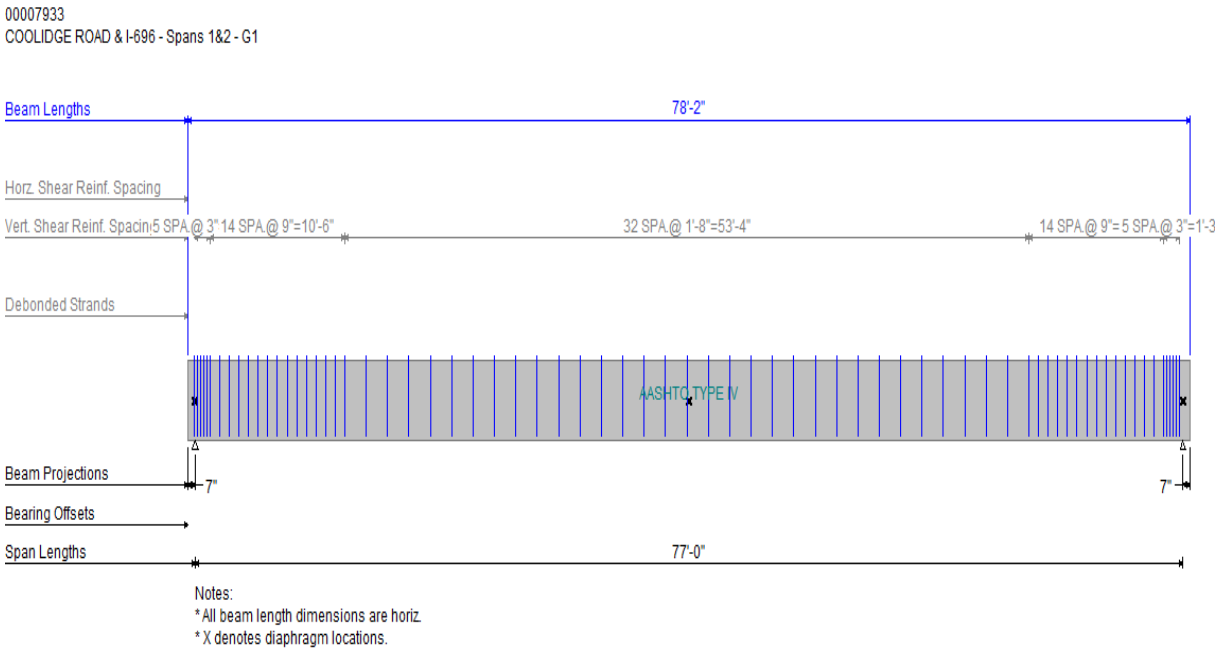

Figure D5. Stirrups layout

6- Prestress Losses:

- Total Prestress Loss: $\Delta f_{pT} = \Delta f_{pES} + \Delta f_{pSR} + \Delta f_{pCR} + \Delta f_{pR2}$
  - $\Delta f_{pES} = \frac{E_p}{E_{ci}} f_{cgp}$ (loss due to elastic shortening)

    where,
    - f_{cgp} = sum of concrete stresses at the center of gravity of prestressing tendons due to prestressing force at transfer and self weight of the member at sections of maximum moment.
    - $f_{cgp} = \frac{p_i}{A} + \frac{p_i e_c^2}{I} - \frac{M_g e_c}{I}$
    - $p_i = (26 \text{ strands})(0.153)(202.5)(0.95) = 765.27$ kip (assuming 5% initial loss)
    - M_g at midspan $= 609.2$ kip. ft
    - $e_c = Y_b - Y_{bs} = 18.345$ in
    - $f_{cgp} = \frac{765.27}{789} + \frac{(765.27)(18.345)^2}{261000} - \frac{(609.2)((18.345)(12)}{261000} = 1.44$ ksi
    - $\Delta f_{pES} = \frac{28500}{3586.616}(1.44) = 11.47$ ksi
    - Percent of actual loss due to elastic shortening $= \frac{11.47}{202.5}(100\%) = 5.66\%$ (very close to the assumed 5%) O.K.

  - $\Delta f_{pSR} = (17 - 0.15H)$ (loss due to shrinkage)
    - $H = 75\%$ (relative humidity)
    - $\Delta f_{pSR} = (17 - 0.15(75)) = 5.75$ ksi

  - $\Delta f_{pCR} = 12 f_{cgp} - 7\Delta f_{cdp}$ (loss due to creep)
    - $\Delta f_{cdp} = \frac{M_s e_c}{I} + \frac{(M_{ws}+M_b)(Y_{bc}-Y_{bs})}{I_c}$
    - $\Delta f_{cdp} = \frac{(685.06)(12)(18.345)}{261000} + \frac{(217.12)(12)(42.1-6.385)}{741995.5} = 0.703$
    - $\Delta f_{pCR} = 12(1.44) - 7(0.703) = 12.39$ ksi

  - $\Delta f_{pR2} = 0.3[20 - 0.4\Delta f_{pES} - 0.2(\Delta f_{pSR} + \Delta f_{pCR})]$ (loss due to relaxation)

- $\Delta f_{pR2} = 0.3[20 - 0.4(11.47) - 0.2(5.75 + 12.39)] = 3.54$ ksi

- Total Losses Δf_{pT}:
  - $\Delta f_{pT} = 11.74 + 5.75 + 12.39 + 3.54 = 33.1$ ksi

- Total prestressing force after all losses P_{pe}:
  - $f_{pe} = f_{pi} - \Delta f_{pT} = 202.5 - 33.1 = 169.4$ ksi
  - $P_{pe} = (169.4)(26 \text{ strands})(0.153) = 673.8$ kip

APPENDIX E: ITERATIVE LRFD METHOD EXAMPLE

This example demonstrates the calculations of the nominal shear capacity (V_n) of AASHTO Type II Girder (Girder 1- Test 2 in Chapter 2) using the general LRFD Procedure based on the assumption that $V_u = V_n$, where V_u is the service load applied at the LRFD critical section. The span and girder details are shown in Figure E1.

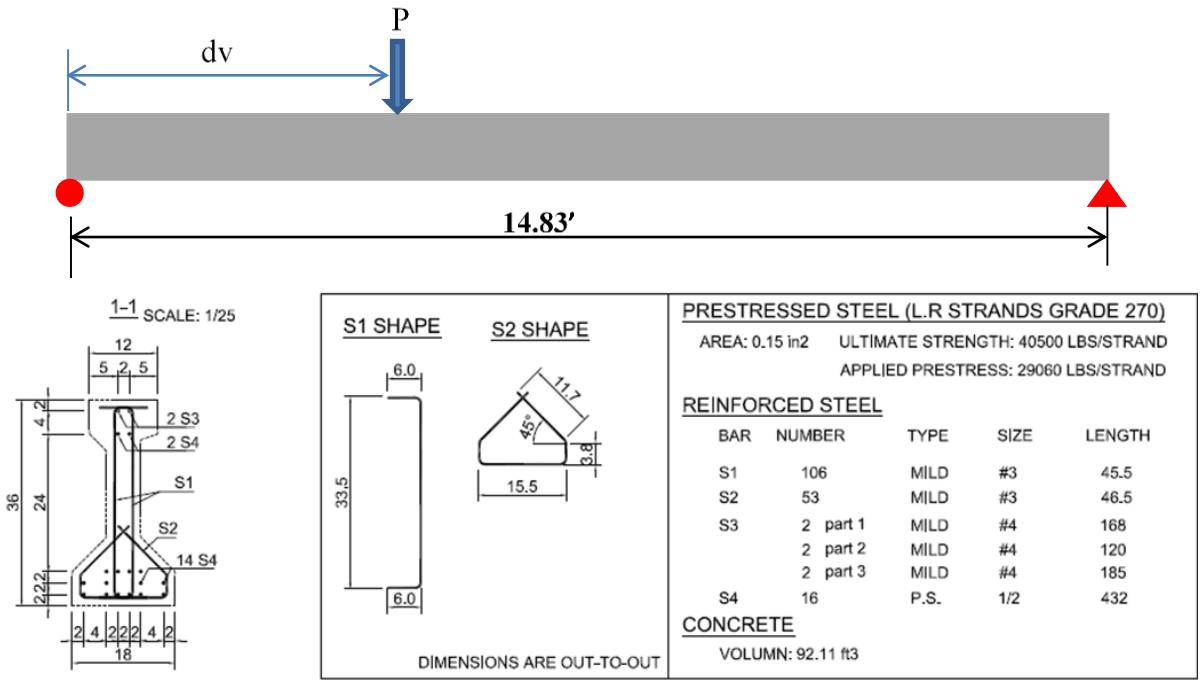

Figure E1. Type II girder design and span configuration

Properties of the girder used to evaluate the shear capacity are shown in Table E1.

Table E1. Girder details

Variable	Value	Unit(s)	Variable	Value	Unit(s)
Beam type	AASHTO II	-	Total # of strands	16	-
Area (Ac)	369	in^2	Ybs	7.000	in
Clear span	25.8	ft	# of rows	4	-
Weight	384	lb/ft	row 1	6	-
Flange width (be)	12	in	row 2	4	-
Web Thicknes (bv)	6	in	row 3	4	-
Yt	20.17	in	row 4	2	-
Yb	15.83	in	row 1	2	in
St	2530	in^3	row 2	4	in
Sb	3220	in^3	row 3	6	in
I	51000	in^4	row 4	30	in
Height (in)	36	in	Harped strands	0	-
f'c (28)	8.6	ksi	k	0.28	-
Ec beam	5814.93	ksi	dp	29.00	in
f's (ksi)	270	ksi	c	8.53	in
# of Strands	16	#	Aps	2.10	in^2
Diameter	0.5	in	fpu	270	ksi
Nominal area	0.15	in^2	fpo	189	ksi
fpe	23.25	kips/strand	f'c slab	8.6	ksi
fpc	1.01	ksi	beta β1	0.65	f'c>8 ksi
Bar size	3	#	be	12	in
# beams	1	#	a	5.54	in
Ep	28500	ksi	de	29.00	in
Av	0.221	in^2	de-a/2	26.23	in
fy	60	ksi	0.9de	26.10	in
Stirrups spacing	21	in	0.72h	25.92	in
vu	0.756	ksi	theta	0.50	radians
vu/f'c	0.008	<0.125	dv	26.23	in
S_max	21.0	in (<24 in)	Crt section (dv)	2.19	ft

Iterative LRFD Procedure:

1- Start the iteration process by assuming a random value for V_u.

2- Calculate M_u based on the assumed V_u ($M_u = V_u dv$).

3- Calculate ε_s using equation E1

4- If ε_s is negative, recalculate ε_s using equation E2.

5- Calculate θ using equation E5.

6- Calculate β using equation E6.

7- Calculate V_c using equation E7.

8- Calculate V_s using equation E8.

9- Calculate V_n using equation E9.

10- If the resulted V_n is less than the assumed V_u value, repeat steps 1-9 by assuming a smaller value of V_u.

11- If the resulted V_n is larger than the assumed V_u value, assume a larger or an equal value of V_u in the next iteration.

12- Repeat steps 1-11 until convergence is achieved.

Calculations:

1- For this girder example, start the iteration process by assuming that V_u=200 kips.

2- Since the calculated V_n (100.0 kips) at the first iteration is smaller than the assumed V_u (200 kips), a smaller V_u value (150 kips) is assumed in the second iteration.

3- In the second iteration, the resulted V_n (102.7 kips) is still smaller than the assumed V_u (150 kips). Thus, a third iteration is required.

4- In the third iteration, using a smaller V_u value of 100 kips resulted in a V_n value of 105.5 kips.

5- The previous prosses was repeated until convergrence has been achieved after the fifth iteration ($V_u = V_n = 105.2\ kips$), as shown in Table E2.

Calculations for the first iteration:

- $\varepsilon_s = \frac{|M_u| + 0.5N_u + |(V_u - V_p)| - A_{ps}f_{po}}{(E_s A_s + E_p A_{ps})}$ (E1)
- When ε_x is negative, it is taken as either zero or recalculated as the following:
- $\varepsilon_s = \frac{|M_u| + 0.5N_u + |(V_u - V_p)| - A_{ps}f_{po}}{(E_s A_s + E_p A_{ps} + E_c A_{ct})}$ (E2)
- $S_{xe} = \frac{1.38\,S_x}{0.63 + a_g}$ (for members having less than the minimum shear reinforcement) (E3)
- $S_{xe} = S_{ze} = 12$ (for members having at least the minimum shear reinforcement) (E4)
- $\theta = 29 + 3500\varepsilon_s = 29 + 3500(-0.0000115) = 29.0^0$ (E5)
- $\beta = \frac{4.8}{(1 + 750\varepsilon_s)} = \frac{4.8}{1 + 750(-0.0000115)} = 4.8$ (E6)
- $V_c = 0.0316\,\beta\sqrt{f'_c}\,b_v d_v = 0.0316\,(4.8)(6)(\sqrt{8.6})(26.23) = 70.3$ kips (E7)
- $V_s = \frac{A_v f_y d_v (\cot\theta + \cot\alpha)\sin\alpha}{S} = \frac{(0.221)(60)(26.23)(\cot 28.96)}{21} = 29.8$ kips (E8)
- $V_n = V_c + V_s + V_p = 70.26 + 29.75 + 0 = 100.0$ kips (E9)

Table E2. LRFD iteration process

Iteraion #	1	2	3	4	5
Vu (kips)	200	150	100	105	105.2
Mu (ft-kips)	376.5	283.7	190.89	200.17	200.55
εs (original)	-0.0003976	-0.0019459	-0.0034943	-0.0033394	-0.0033332
εs (alternative)	-0.0000115	-0.0000561	-0.0001008	-0.0000963	-0.0000962
θ (degrees)	29.0	28.8	28.7	28.7	28.7
β	4.8	5.0	5.2	5.2	5.2
Vc (kips)	70.3	72.7	75.4	75.1	75.1
Vs (kips)	29.8	29.9	30.1	30.1	30.1
Vn (kips)	100.0	102.7	105.5	105.2	105.2

APPENDIX F: NCHRP 368 CALCULATIONS EXAMPLE

In this example, the calculations of the mean load and mean resistance for a 90 ft simple span PC bridge with 6 ft girder spacing is presented. The purpose of this example is to clarify the calculations of the mean load and mean resistance values presented in the NCHRP 368 report that were used in computing reliability analysis. These calculations are based on load data and factors given in the NCHRP 368 report, as presented in Tables F1-F4.

Table F1. Parameters of bridge load components (Table F1-NCHRP 368)

Load Component	Bias Factor	COV
Dead Load (D1)	1.03	0.08
Dead Load (D2)	1.05	0.10
Dead Load (D3)	1.00	0.25
Live Load + Impact	1.1-1.2	0.18

Table F2. Mean maximum shears for simple spans due to multiple trucks in one lane divided by corresponding HS20 shear (Table B7-NCHRP 368)

Span (ft)	1 Day	2 Weeks	1 Month	2 Months	6 Months	1 Year	5 Years	50 Years	75 Years
90	1.48	1.58	1.62	1.64	1.69	1.72	1.76	1.84	1.85

Table F3. Representative load components and resistance for PC girder bridges, shears (Table E9-NCHRP 368)

Span (ft)	Spacing (ft)	D1 (kips)	D2 (kips)	D3 (kips)	LL (kips)	I (%)	mQ	sQ	R(min)
90	4	37	25	5	26	23	129	12	155
90	6	37	34	7	37	23	158	15	200
90	8	37	41	10	49	23	185	18	246
90	10	37	52	12	60	23	215	21	292
90	12	37	64	15	72	23	245	24	342

Table F4. Reliability indices and resistance ratios for LRFD Code simple span shears in PC girder bridges (Table F10-NCHRP 368)

Span (ft)	Spacing (ft)	mQ (kips)	Std. (kips)	R_{HS20} (k-ft)	r	Beta
90	4	129	12	155	1.33	3.69
90	6	158	15	200	1.27	3.71
90	8	185	18	246	1.22	3.72
90	10	215	21	292	1.20	3.73
90	12	245	24	342	1.17	3.72

Mean load calculations:

$mQ = (\lambda 1 \times D1) + (\lambda 2 \times D2) + (\lambda 3 \times D3) + (LL \times (V_{max}/V_{HS20}) \times \lambda_{LL})$

$mQ = (1.03 \times 37) + (1.05 \times 34) + (1.0 \times 7) + (37 \times 1.85 \times 1.1) = 156.1$ kips

where,

mQ = Total mean load

D1= Dead load due to factory made elements, kips (Table F3)

D2= Dead load due to cast in place concrete members, kips (Table F3)

D3= Dead load due to wearing surface (asphalt), kips (Table F3)

LL= Live load due to HS20 load, kips (Table F3)

$\lambda 1$= Bias factor for D1

$\lambda 2$= Bias factor for D2

$\lambda 3$= Bias factor for D3

V_{max}/V_{HS20}= maximum shears for simple spans due to multiple trucks in one lane divided by corresponding HS20 shear (Table F2)

$\lambda_{LL=}$ Bias factor for LL (Table F1)

Mean resistance calculations:

R_{HS20} = 1.3 x (D1 + D2+D3) + 2.17 x (LL x (1+I))

R_{HS20} = 1.3 x (37 + 34 + 7) + 2.17 x (37 x (1+0.23)) = 200.2 kips

mR= R_{HS20} x λ_R x r

mR= 200.2 x 1.15 x 1.27 = 292.4 kips

where,

mR = Mean shear resistance, kips

I= Impact load magnitude (Table F3)

$\lambda_{R=}$ Resistance bias factor=1.15

R_{HS20} = Shear resistance based on HS20 load, kips

r = R_{LRFD}/R_{HS20} (Table F4)

After computing the mean load and mean resistance, compute the standard deviation for each component simply by multiplying the mean value by the appropriate coefficient of variation (0.14 for R). Next, use the mean and standard deviation values to compute the reliability index using the Rackwitz-Fiessler Procedure.

APPENDIX G: DESIGN CASES PARAMETERS

Table G1. Design parameters for Type II girder using the Original LRFD Procedure (30 ft span)

Type II- 30 ft Span					
Comb. #	1	2	3	4	5
Girder Spacing (ft)	4	6	8	10	12
f'c (ksi)	4	4	4	5	6
bv (in)	6	6	6	6	6
de (in)	42	42	42	42	42
Av (in ^2)	0.22	0.22	0.22	0.22	0.22
fy (ksi)	60	60	60	60	60
s (in)	24	24	24	19	14
fpu (ksi)	270	270	270	270	270
Eps (ksi)	28500	28500	28500	28500	28500
Aps (in^2)	2.45	2.45	2.45	2.45	2.45
be (in)	48	72	90	90	90
h (in)	36	36	36	36	36
ts (in)	9	9	9	9	9
f'cs (in)	4	4	4	4	4
Vg (kips)	4	4	4	4	4
Vs (kips)	5	8	11	13	16
Vb (kips)	1	1	1	1	1
Vws (kips)	1	2	3	3	4
Vll-HL93 (kips)	33	42	51	60	68
Vu (kips)	72	93	114	133	152
Vn (kips)	136	134	133	148	169
φVn (kips)	123	121	120	133	152

Table G2. Design parameters for Type II girder using the Modified LRFD Procedure (30 ft span)

Type II- 30 ft Span					
Comb. #	1	2	3	4	5
Girder Spacing (ft)	4	6	8	10	12
f'c (ksi)	4	4	4	4	4
bv (in)	6	6	6	6	6
de (in)	42	42	42	42	42
Av (in ^2)	0.22	0.22	0.22	0.22	0.22
fy (ksi)	60	60	60	60	60
s (in)	24	24	24	18	13
fpu (ksi)	270	270	270	270	270
Eps (ksi)	28500	28500	28500	28500	28500
Aps (in^2)	2.45	2.45	2.45	2.45	2.45
be (in)	48	72	90	90	90
h (in)	36	36	36	36	36
ts (in)	9	9	9	9	9
f'cs (in)	4	4	4	4	4
Vg (kips)	4	4	4	4	4
Vs (kips)	5	8	11	13	16
Vb (kips)	1	1	1	1	1
Vws (kips)	1	2	3	3	4
Vll-HL93 (kips)	33	42	51	60	68
Vu (kips)	72	93	114	133	152
Vn (kips)	142	140	137	148	169
φVn* (kips)	128	126	123	133	152

Table G3. Design parameters for Type II girder using the Original LRFD Procedure (60 ft span)

Type II- 60 ft Span					
Comb. #	6	7	8	9	10
Girder Spacing (ft)	4	6	8	10	12
f'c (ksi)	5	6	7	8	8
bv (in)	6	6	6	6	6
de (in)	42	42	42	42	42
Av (in ^2)	0.22	0.39	0.39	0.39	0.39
fy (ksi)	60	60	60	60	60
s (in)	24	24	17	13	8
fpu (ksi)	270	270	270	270	270
Eps (ksi)	28500	28500	28500	28500	28500
Aps (in^2)	2.45	2.45	2.45	2.45	2.45
be (in)	48	72	96	114	114
h (in)	36	36	36	36	36
ts (in)	9	9	9	9	9
f'cs (in)	4	4	4	4	4
Vg (kips)	10	10	10	10	10
Vs (kips)	12	18	24	30	36
Vb (kips)	1	2	2	3	3
Vws (kips)	3	5	6	8	10
Vll-HL93 (kips)	48	62	75	88	100
Vu (kips)	119	154	187	220	252
Vn (kips)	132	171	208	245	280
φVn (kips)	119	154	187	220	252

Table G4. Design parameters for Type II girder using the Modified LRFD Procedure (60 ft span)

Type II- 60 ft Span					
Comb. #	6	7	8	9	10
Girder Spacing (ft)	4	6	8	10	12
f'c (ksi)	4	5	7	8	8
bv (in)	6	6	6	6	6
de (in)	42	42	42	42	42
Av (in ^2)	0.22	0.39	0.39	0.39	0.39
fy (ksi)	60	60	60	60	60
s (in)	24	24	18	13	7
fpu (ksi)	270	270	270	270	270
Eps (ksi)	28500	28500	28500	28500	28500
Aps (in^2)	2.45	2.45	2.45	2.45	2.45
be (in)	48	72	96	114	114
h (in)	36	36	36	36	36
ts (in)	9	9	9	9	9
f'cs (in)	4	4	4	4	4
Vg (kips)	10	10	10	10	10
Vs (kips)	12	18	24	30	36
Vb (kips)	1	2	2	3	3
Vws (kips)	3	5	6	8	10
Vll-HL93 (kips)	48	62	75	88	100
Vu (kips)	119	154	187	220	252
Vn (kips)	133	171	208	245	280
φVn* (kips)	120	154	187	220	252

Table G5. Design parameters for Type II girder using the Original LRFD Procedure (90 ft span)

Type II- 90 ft Span					
Comb. #	11	12	13	14	15
Girder Spacing (ft)	4	6	8	10	12
f'c (ksi)	6	8	8	8	8
bv (in)	6	6	6	6	6
de (in)	42	42	42	42	42
Av (in ^2)	0.39	0.39	0.39	0.39	0.39
fy (ksi)	60	60	60	60	60
s (in)	24	15	9	5	4
fpu (ksi)	270	270	270	270	270
Eps (ksi)	28500	28500	28500	28500	28500
Aps (in^2)	2.45	2.45	2.45	2.45	2.45
be (in)	48	72	96	114	114
h (in)	36	36	36	36	36
ts (in)	9	9	9	9	9
f'cs (in)	4	4	4	4	4
Vg (kips)	16	16	16	16	16
Vs (kips)	19	29	38	47	57
Vb (kips)	2	3	4	4	5
Vws (kips)	5	7	10	12	15
Vll-HL93 (kips)	57	73	89	104	118
Vu (kips)	153	198	242	285	326
Vn (kips)	170	220	269	316	362
φVn (kips)	153	198	242	284	326

Table G6. Design parameters for Type II girder using the Modified LRFD Procedure (90 ft span)

Type II- 90 ft Span					
Comb. #	11	12	13	14	15
Girder Spacing (ft)	4	6	8	10	12
f'c (ksi)	5	8	8	8	8
bv (in)	6	6	6	6	6
de (in)	42	42	42	42	42
Av (in ^2)	0.39	0.39	0.39	0.39	0.39
fy (ksi)	60	60	60	60	60
s (in)	24	16	8	5	4
fpu (ksi)	270	270	270	270	270
Eps (ksi)	28500	28500	28500	28500	28500
Aps (in^2)	2.45	2.45	2.45	2.45	2.45
be (in)	48	72	96	114	114
h (in)	36	36	36	36	36
ts (in)	9	9	9	9	9
f'cs (in)	4	4	4	4	4
Vg (kips)	16	16	16	16	16
Vs (kips)	19	29	38	47	57
Vb (kips)	2	3	4	4	5
Vws (kips)	5	7	10	12	15
Vll-HL93 (kips)	57	73	89	104	118
Vu (kips)	153	198	242	285	326
Vn (kips)	170	220	269	316	362
φVn* (kips)	153	198	242	285	326

Table G7. Design parameters for Type II girder using the Original LRFD Procedure (120 ft span)

Type II- 120 ft Span				
Comb. #	16	17	18	19
Girder Spacing (ft)	4	6	8	10
f'c (ksi)	7	7	7	7
bv (in)	6	6	6	6
de (in)	42	42	42	42
Av (in ^2)	0.39	0.39	0.39	0.39
fy (ksi)	60	60	60	60
s (in)	16	9	5	3
fpu (ksi)	270	270	270	270
Eps (ksi)	28500	28500	28500	28500
Aps (in^2)	2.45	2.45	2.45	2.45
be (in)	48	72	96	114
h (in)	36	36	36	36
ts (in)	9	9	9	9
f'cs (in)	4	4	4	4
Vg (kips)	22	22	22	22
Vs (kips)	26	39	52	64
Vb (kips)	3	4	5	6
Vws (kips)	7	10	14	17
Vll-HL93 (kips)	63	82	99	116
Vu (kips)	185	239	292	343
Vn (kips)	205	265	324	381
φVn (kips)	185	239	292	343

Table G8. Design parameters for Type II girder using the Modified LRFD Procedure (120 ft span)

Type II- 120 ft Span				
Comb. #	16	17	18	19
Girder Spacing (ft)	4	6	8	10
f'c (ksi)	7	7	7	9
bv (in)	6	6	6	6
de (in)	42	42	42	42
Av (in ^2)	0.39	0.39	0.39	0.39
fy (ksi)	60	60	60	60
s (in)	18	8	5	3
fpu (ksi)	270	270	270	270
Eps (ksi)	28500	28500	28500	28500
Aps (in^2)	2.45	2.45	2.45	2.45
be (in)	48	72	96	114
h (in)	36	36	36	36
ts (in)	9	9	9	9
f'cs (in)	4	4	4	4
Vg (kips)	22	22	22	22
Vs (kips)	26	39	52	64
Vb (kips)	3	4	5	6
Vws (kips)	7	10	14	17
Vll-HL93 (kips)	63	82	99	116
Vu (kips)	185	239	292	343
Vn (kips)	205	266	325	382
φVn* (kips)	185	239	292	344

Table G9. Design parameters for Type II girder using the Original LRFD Procedure (200 ft span)

Type II- 200 ft Span		
Comb. #	21	22
Girder Spacing (ft)	4	6
f'c (ksi)	7	7
bv (in)	6	6
de (in)	42	42
Av (in ^2)	0.39	0.39
fy (ksi)	60	60
s (in)	6	3
fpu (ksi)	270	270
Eps (ksi)	28500	28500
Aps (in^2)	2.45	2.45
be (in)	48	72
h (in)	36	36
ts (in)	9	9
f'cs (in)	4	4
Vg (kips)	37	37
Vs (kips)	45	66
Vb (kips)	4	6
Vws (kips)	12	17
Vll-HL93 (kips)	79	102
Vu (kips)	263	341
Vn (kips)	293	379
φVn (kips)	263	341

Table G10. Design parameters for Type II girder using the Modified LRFD Procedure (200 ft span)

Type II- 200 ft Span		
Comb. #	21	22
Girder Spacing (ft)	4	6
f'c (ksi)	8	9
bv (in)	6	6
de (in)	42	42
Av (in ^2)	0.39	0.39
fy (ksi)	60	60
s (in)	6	3
fpu (ksi)	270	270
Eps (ksi)	28500	28500
Aps (in^2)	2.45	2.45
be (in)	48	72
h (in)	36	36
ts (in)	9	9
f'cs (in)	4	4
Vg (kips)	37	37
Vs (kips)	45	66
Vb (kips)	4	6
Vws (kips)	12	17
Vll-HL93 (kips)	79	102
Vu (kips)	263	341
Vn (kips)	293	380
φVn* (kips)	263	342

Table G11. Design parameters for Type III girder using the Original LRFD Procedure (30 ft span)

Type III- 30 ft Span					
Comb. #	1	2	3	4	5
Girder Spacing (ft)	4	6	8	10	12
f'c (ksi)	4	4	4	4	4
bv (in)	7	7	7	7	7
de (in)	51	51	51	51	51
Av (in ^2)	0.22	0.22	0.22	0.22	0.22
fy (ksi)	60	60	60	60	60
s (in)	24	24	24	24	24
fpu (ksi)	270	270	270	270	270
Eps (ksi)	28500	28500	28500	28500	28500
Aps (in^2)	3.67	3.67	3.67	3.67	3.67
be (in)	48	72	90	90	90
h (in)	45	45	45	45	45
ts (in)	9	9	9	9	9
f'cs (in)	4	4	4	4	4
Vg (kips)	6	6	6	6	6
Vs (kips)	5	8	10	12	15
Vb (kips)	1	1	1	1	1
Vws (kips)	1	2	3	3	4
Vll-HL93 (kips)	31	40	49	57	65
Vu (kips)	72	92	111	130	148
Vn (kips)	193	193	190	186	183
φVn (kips)	174	173	171	168	164

Table G12. Design parameters for Type III girder using the Modified LRFD Procedure (30 ft span)

Type III- 30 ft Span					
Comb. #	1	2	3	4	5
Girder Spacing (ft)	4	6	8	10	12
f'c (ksi)	4	4	4	4	4
bv (in)	7	7	7	7	7
de (in)	51	51	51	51	51
Av (in ^2)	0.22	0.22	0.22	0.22	0.22
fy (ksi)	60	60	60	60	60
s (in)	24	24	24	24	24
fpu (ksi)	270	270	270	270	270
Eps (ksi)	28500	28500	28500	28500	28500
Aps (in^2)	3.67	3.67	3.67	3.67	3.67
be (in)	48	72	90	90	90
h (in)	45	45	45	45	45
ts (in)	9	9	9	9	9
f'cs (in)	4	4	4	4	4
Vg (kips)	6	6	6	6	6
Vs (kips)	5	8	10	12	15
Vb (kips)	1	1	1	1	1
Vws (kips)	1	2	3	3	4
Vll-HL93 (kips)	31	40	49	57	65
Vu (kips)	72	92	111	130	148
Vn (kips)	202	202	199	195	191
φVn* (kips)	182	181	179	176	172

Table G13. Design parameters for Type III girder using the Original LRFD Procedure (60 ft span)

Type III- 60 ft Span					
Comb. #	6	7	8	9	10
Girder Spacing (ft)	4	6	8	10	12
f'c (ksi)	4	4	5	6	7
bv (in)	7	7	7	7	7
de (in)	51	51	51	51	51
Av (in ^2)	0.22	0.22	0.22	0.22	0.22
fy (ksi)	60	60	60	60	60
s (in)	24	24	17	12	9
fpu (ksi)	270	270	270	270	270
Eps (ksi)	28500	28500	28500	28500	28500
Aps (in^2)	3.67	3.67	3.67	3.67	3.67
be (in)	48	72	96	116	116
h (in)	45	45	45	45	45
ts (in)	9	9	9	9	9
f'cs (in)	4	4	4	4	4
Vg (kips)	15	15	15	15	15
Vs (kips)	12	18	24	29	35
Vb (kips)	1	2	2	3	3
Vws (kips)	3	5	6	8	9
Vll-HL93 (kips)	47	61	74	86	98
Vu (kips)	123	157	190	222	253
Vn (kips)	183	182	211	246	280
φVn (kips)	165	164	190	221	252

Table G14. Design parameters for Type III girder using the Modified LRFD Procedure (60 ft span)

Type III- 60 ft Span					
Comb. #	6	7	8	9	10
Girder Spacing (ft)	4	6	8	10	12
f'c (ksi)	4	5	6	6	7
bv (in)	7	7	7	7	7
de (in)	51	51	51	51	51
Av (in ^2)	0.22	0.22	0.22	0.22	0.22
fy (ksi)	60	60	60	60	60
s (in)	24	24	21	14	10
fpu (ksi)	270	270	270	270	270
Eps (ksi)	28500	28500	28500	28500	28500
Aps (in^2)	3.67	3.67	3.67	3.67	3.67
be (in)	48	72	96	116	116
h (in)	45	45	45	45	45
ts (in)	9	9	9	9	9
f'cs (in)	4	4	4	4	4
Vg (kips)	15	15	15	15	15
Vs (kips)	12	18	24	29	35
Vb (kips)	1	2	2	3	3
Vws (kips)	3	5	6	8	9
Vll-HL93 (kips)	47	61	74	86	98
Vu (kips)	123	157	190	222	253
Vn (kips)	191	188	211	247	281
φVn* (kips)	172	169	190	222	253

Table G15. Design parameters for Type III girder using the Original LRFD Procedure (90 ft span)

Type III- 90 ft Span					
Comb. #	11	12	13	14	15
Girder Spacing (ft)	4	6	8	10	12
f'c (ksi)	4	6	7	7	7
bv (in)	7	7	7	7	7
de (in)	51	51	51	51	51
Av (in ^2)	0.22	0.22	0.39	0.39	0.39
fy (ksi)	60	60	60	60	60
s (in)	24	14	16	12	9
fpu (ksi)	270	270	270	270	270
Eps (ksi)	28500	28500	28500	28500	28500
Aps (in^2)	3.67	3.67	3.67	3.67	3.67
be (in)	48	72	96	116	116
h (in)	45	45	45	45	45
ts (in)	9	9	9	9	9
f'cs (in)	4	4	4	4	4
Vg (kips)	24	24	24	24	24
Vs (kips)	19	28	37	47	56
Vb (kips)	2	3	4	4	5
Vws (kips)	5	7	10	12	15
Vll-HL93 (kips)	56	72	88	102	116
Vu (kips)	162	206	249	291	332
Vn (kips)	180	229	277	323	368
φVn (kips)	162	206	249	291	332

Table G16. Design parameters for Type III girder using the Modified LRFD Procedure (90 ft span)

Type III- 90 ft Span					
Comb. #	11	12	13	14	15
Girder Spacing (ft)	4	6	8	10	12
f'c (ksi)	4	7	8	9	10
bv (in)	7	7	7	7	7
de (in)	51	51	51	51	51
Av (in ^2)	0.22	0.22	0.39	0.39	0.39
fy (ksi)	60	60	60	60	60
s (in)	24	17	20	14	11
fpu (ksi)	270	270	270	270	270
Eps (ksi)	28500	28500	28500	28500	28500
Aps (in^2)	3.67	3.67	3.67	3.67	3.67
be (in)	48	72	96	116	116
h (in)	45	45	45	45	45
ts (in)	9	9	9	9	9
f'cs (in)	4	4	4	4	4
Vg (kips)	24	24	24	24	24
Vs (kips)	19	28	37	47	56
Vb (kips)	2	3	4	4	5
Vws (kips)	5	7	10	12	15
Vll-HL93 (kips)	56	72	88	102	116
Vu (kips)	162	206	249	291	332
Vn (kips)	180	229	277	323	368
φVn* (kips)	162	206	249	291	332

Table G17. Design parameters for Type III girder using the Original LRFD Procedure (120 ft span)

Type III- 120 ft Span					
Comb. #	16	17	18	19	20
Girder Spacing (ft)	4	6	8	10	12
f'c (ksi)	6	7	7	7	7
bv (in)	7	7	7	7	7
de (in)	51	51	51	51	51
Av (in ^2)	0.22	0.39	0.39	0.39	0.39
fy (ksi)	60	60	60	60	60
s (in)	15	16	11	8	5
fpu (ksi)	270	270	270	270	270
Eps (ksi)	28500	28500	28500	28500	28500
Aps (in^2)	3.67	3.67	3.67	3.67	3.67
be (in)	48	72	96	116	116
h (in)	45	45	45	45	45
ts (in)	9	9	9	9	9
f'cs (in)	4	4	4	4	4
Vg (kips)	33	33	33	33	33
Vs (kips)	26	39	51	64	76
Vb (kips)	3	4	5	6	7
Vws (kips)	7	10	13	17	20
Vll-HL93 (kips)	63	81	98	115	131
Vu (kips)	197	251	303	354	403
Vn (kips)	219	279	337	393	448
φVn (kips)	197	251	303	354	403

Table G18. Design parameters for Type III girder using the Modified LRFD Procedure (120 ft span)

Type III- 120 ft Span					
Comb. #	16	17	18	19	20
Girder Spacing (ft)	4	6	8	10	12
f'c (ksi)	6	8	8	8	9
bv (in)	7	7	7	7	7
de (in)	51	51	51	51	51
Av (in ^2)	0.22	0.39	0.39	0.39	0.39
fy (ksi)	60	60	60	60	60
s (in)	18	20	13	7	5
fpu (ksi)	270	270	270	270	270
Eps (ksi)	28500	28500	28500	28500	28500
Aps (in^2)	3.67	3.67	3.67	3.67	3.67
be (in)	48	72	96	116	116
h (in)	45	45	45	45	45
ts (in)	9	9	9	9	9
f'cs (in)	4	4	4	4	4
Vg (kips)	33	33	33	33	33
Vs (kips)	26	39	51	64	76
Vb (kips)	3	4	5	6	7
Vws (kips)	7	10	13	17	20
Vll-HL93 (kips)	63	81	98	115	131
Vu (kips)	197	251	303	354	403
Vn (kips)	219	279	337	393	448
φVn* (kips)	197	251	303	354	404

Table G19. Design parameters for Type III girder using the Original LRFD Procedure (200 ft span)

Type III- 200 ft Span			
Comb. #	21	22	23
Girder Spacing (ft)	4	6	8
f'c (ksi)	7	7	7
bv (in)	7	7	7
de (in)	51	51	51
Av (in ^2)	0.39	0.39	0.39
fy (ksi)	60	60	60
s (in)	11	7	4
fpu (ksi)	270	270	270
Eps (ksi)	28500	28500	28500
Aps (in^2)	3.67	3.67	3.67
be (in)	48	72	96
h (in)	45	45	45
ts (in)	9	9	9
f'cs (in)	4	4	4
Vg (kips)	56	56	56
Vs (kips)	45	66	88
Vb (kips)	4	6	8
Vws (kips)	12	17	23
Vll-HL93 (kips)	78	101	123
Vu (kips)	286	364	439
Vn (kips)	318	404	488
φVn (kips)	286	364	439

Table G20. Design parameters for Type III girder using the Modified LRFD Procedure (200 ft span)

Type III- 200 ft Span			
Comb. #	21	22	23
Girder Spacing (ft)	4	6	8
f'c (ksi)	7	8	9
bv (in)	7	7	7
de (in)	51	51	51
Av (in ^2)	0.39	0.39	0.39
fy (ksi)	60	60	60
s (in)	13	7	4
fpu (ksi)	270	270	270
Eps (ksi)	28500	28500	28500
Aps (in^2)	3.67	3.67	3.67
be (in)	48	72	96
h (in)	45	45	45
ts (in)	9	9	9
f'cs (in)	4	4	4
Vg (kips)	56	56	56
Vs (kips)	45	66	88
Vb (kips)	4	6	8
Vws (kips)	12	17	23
Vll-HL93 (kips)	78	101	123
Vu (kips)	286	364	439
Vn (kips)	318	404	488
φVn* (kips)	286	364	440

Table G21. Design parameters for Type IV girder using the Original LRFD Procedure (30 ft span)

Type IV- 30 ft Span					
Comb. #	1	2	3	4	5
Girder Spacing (ft)	4	6	8	10	12
f'c (ksi)	4	4	4	4	4
bv (in)	8	8	8	8	8
de (in)	59	59	59	59	59
Av (in ^2)	0.22	0.22	0.22	0.22	0.22
fy (ksi)	60	60	60	60	60
s (in)	24	24	24	24	24
fpu (ksi)	270	270	270	270	270
Eps (ksi)	28500	28500	28500	28500	28500
Aps (in^2)	5.20	5.20	5.20	5.20	5.20
be (in)	48	72	90	90	90
h (in)	54	54	54	54	54
ts (in)	9	9	9	9	9
f'cs (in)	4	4	4	4	4
Vg (kips)	9	8	8	8	8
Vs (kips)	5	7	9	12	14
Vb (kips)	0	1	1	1	1
Vws (kips)	1	2	2	3	4
Vll-HL93 (kips)	30	39	47	55	62
Vu (kips)	72	91	109	127	144
Vn (kips)	252	254	252	248	244
φVn (kips)	227	228	227	223	220

Table G22. Design parameters for Type IV girder using the Modified LRFD Procedure (30 ft span)

Type IV- 30 ft Span					
Comb. #	1	2	3	4	5
Girder Spacing (ft)	4	6	8	10	12
f'c (ksi)	4	4	4	4	4
bv (in)	8	8	8	8	8
de (in)	59	59	59	59	59
Av (in ^2)	0.22	0.22	0.22	0.22	0.22
fy (ksi)	60	60	60	60	60
s (in)	24	24	24	24	24
fpu (ksi)	270	270	270	270	270
Eps (ksi)	28500	28500	28500	28500	28500
Aps (in^2)	5.20	5.20	5.20	5.20	5.20
be (in)	48	72	90	90	90
h (in)	54	54	54	54	54
ts (in)	9	9	9	9	9
f'cs (in)	4	4	4	4	4
Vg (kips)	9	8	8	8	8
Vs (kips)	5	7	9	12	14
Vb (kips)	0	1	1	1	1
Vws (kips)	1	2	2	3	4
Vll-HL93 (kips)	30	39	47	55	62
Vu (kips)	72	91	109	127	144
Vn (kips)	265	267	265	261	257
φVn* (kips)	238	240	238	235	231

Table G23. Design parameters for Type IV girder using the Original LRFD Procedure (60 ft span)

Type IV- 60 ft Span					
Comb. #	6	7	8	9	10
Girder Spacing (ft)	4	6	8	10	12
f'c (ksi)	4	4	4	5	5
bv (in)	8	8	8	8	8
de (in)	59	59	59	59	59
Av (in ^2)	0.22	0.22	0.22	0.22	0.22
fy (ksi)	60	60	60	60	60
s (in)	24	24	24	24	15
fpu (ksi)	270	270	270	270	270
Eps (ksi)	28500	28500	28500	28500	28500
Aps (in^2)	5.20	5.20	5.20	5.20	5.20
be (in)	48	72	96	118	118
h (in)	54	54	54	54	54
ts (in)	9	9	9	9	9
f'cs (in)	4	4	4	4	4
Vg (kips)	21	21	21	21	21
Vs (kips)	12	18	23	29	35
Vb (kips)	1	2	2	3	3
Vws (kips)	3	5	6	8	9
Vll-HL93 (kips)	47	60	73	85	97
Vu (kips)	129	162	194	226	256
Vn (kips)	241	240	237	250	284
φVn (kips)	217	216	214	225	256

Table G24. Design parameters for Type IV girder using the Modified LRFD Procedure (60 ft span)

Type IV- 60 ft Span					
Comb. #	6	7	8	9	10
Girder Spacing (ft)	4	6	8	10	12
f'c (ksi)	4	4	4	5	6
bv (in)	8	8	8	8	8
de (in)	59	59	59	59	59
Av (in ^2)	0.22	0.22	0.22	0.22	0.22
fy (ksi)	60	60	60	60	60
s (in)	24	24	24	24	17
fpu (ksi)	270	270	270	270	270
Eps (ksi)	28500	28500	28500	28500	28500
Aps (in^2)	5.20	5.20	5.20	5.20	5.20
be (in)	48	72	96	118	118
h (in)	54	54	54	54	54
ts (in)	9	9	9	9	9
f'cs (in)	4	4	4	4	4
Vg (kips)	21	21	21	21	21
Vs (kips)	12	18	23	29	35
Vb (kips)	1	2	2	3	3
Vws (kips)	3	5	6	8	9
Vll-HL93 (kips)	47	60	73	85	97
Vu (kips)	129	162	194	226	256
Vn (kips)	252	251	250	251	285
φVn* (kips)	227	226	225	226	256

Table G25. Design parameters for Type IV girder using the Original LRFD Procedure (90 ft span)

Type IV- 90 ft Span					
Comb. #	11	12	13	14	15
Girder Spacing (ft)	4	6	8	10	12
f'c (ksi)	4	5	6	6	7
bv (in)	8	8	8	8	8
de (in)	59	59	59	59	59
Av (in ^2)	0.22	0.22	0.22	0.22	0.22
fy (ksi)	60	60	60	60	60
s (in)	24	24	15	10	8
fpu (ksi)	270	270	270	270	270
Eps (ksi)	28500	28500	28500	28500	28500
Aps (in^2)	5.20	5.20	5.20	5.20	5.20
be (in)	48	72	96	118	118
h (in)	54	54	54	54	54
ts (in)	9	9	9	9	9
f'cs (in)	4	4	4	4	4
Vg (kips)	33	33	33	33	33
Vs (kips)	19	28	37	46	55
Vb (kips)	2	3	3	4	5
Vws (kips)	5	7	10	12	14
Vll-HL93 (kips)	56	72	87	101	115
Vu (kips)	172	216	258	300	340
Vn (kips)	233	240	287	333	377
φVn (kips)	210	216	258	300	340

Table G26. Design parameters for Type IV girder using the Modified LRFD Procedure (90 ft span)

Type IV- 90 ft Span					
Comb. #	11	12	13	14	15
Girder Spacing (ft)	4	6	8	10	12
f'c (ksi)	4	4	6	7	8
bv (in)	8	8	8	8	8
de (in)	59	59	59	59	59
Av (in ^2)	0.22	0.22	0.22	0.22	0.22
fy (ksi)	60	60	60	60	60
s (in)	24	24	17	12	9
fpu (ksi)	270	270	270	270	270
Eps (ksi)	28500	28500	28500	28500	28500
Aps (in^2)	5.20	5.20	5.20	5.20	5.20
be (in)	48	72	96	118	118
h (in)	54	54	54	54	54
ts (in)	9	9	9	9	9
f'cs (in)	4	4	4	4	4
Vg (kips)	33	33	33	33	33
Vs (kips)	19	28	37	46	55
Vb (kips)	2	3	3	4	5
Vws (kips)	5	7	10	12	14
Vll-HL93 (kips)	56	72	87	101	115
Vu (kips)	172	216	258	300	340
Vn (kips)	243	240	287	333	378
φVn* (kips)	218	216	258	300	340

Table G27. Design parameters for Type IV girder using the Original LRFD Procedure (120 ft span)

Type IV- 120 ft Span					
Comb. #	16	17	18	19	20
Girder Spacing (ft)	4	6	8	10	
f'c (ksi)	5	6	7	8	9
bv (in)	8	8	8	8	8
de (in)	59	59	59	59	59
Av (in ^2)	0.22	0.22	0.22	0.22	0.22
fy (ksi)	60	60	60	60	60
s (in)	24	13	9	7	5
fpu (ksi)	270	270	270	270	270
Eps (ksi)	28500	28500	28500	28500	28500
Aps (in^2)	5.20	5.20	5.20	5.20	5.20
be (in)	48	72	96	118	118
h (in)	54	54	54	54	54
ts (in)	9	9	9	9	9
f'cs (in)	4	4	4	4	4
Vg (kips)	46	45	45	45	45
Vs (kips)	26	38	51	63	76
Vb (kips)	3	4	5	6	7
Vws (kips)	7	10	13	17	20
Vll-HL93 (kips)	63	80	98	114	130
Vu (kips)	212	265	317	368	417
Vn (kips)	236	295	352	408	463
φVn (kips)	212	265	317	368	417

Table G28. Design parameters for Type IV girder using the Modified LRFD Procedure (120 ft span)

Type IV- 120 ft Span					
Comb. #	16	17	18	19	20
Girder Spacing (ft)	4	6	8	10	12
f'c (ksi)	4	6	7	8	8
bv (in)	8	8	8	8	8
de (in)	59	59	59	59	59
Av (in ^2)	0.22	0.22	0.39	0.39	0.39
fy (ksi)	60	60	60	60	60
s (in)	24	16	18	14	10
fpu (ksi)	270	270	270	270	270
Eps (ksi)	28500	28500	28500	28500	28500
Aps (in^2)	5.20	5.20	5.20	5.20	5.20
be (in)	48	72	96	118	118
h (in)	54	54	54	54	54
ts (in)	9	9	9	9	9
f'cs (in)	4	4	4	4	4
Vg (kips)	46	45	45	45	45
Vs (kips)	26	38	51	63	76
Vb (kips)	3	4	5	6	7
Vws (kips)	7	10	13	17	20
Vll-HL93 (kips)	63	80	98	114	130
Vu (kips)	212	265	317	368	417
Vn (kips)	236	295	352	409	463
φVn* (kips)	212	265	317	368	417

Table G29. Design parameters for Type IV girder using the Original LRFD Procedure (200 ft span)

Type IV- 200 ft Span					
Comb. #	21	22	23	24	25
Girder Spacing (ft)	4	6	8	10	12
f'c (ksi)	7	7	7	8	9
bv (in)	8	8	8	8	8
de (in)	59	59	59	59	59
Av (in ^2)	0.39	0.39	0.39	0.39	0.39
fy (ksi)	60	60	60	60	60
s (in)	15	10	7	5	3
fpu (ksi)	270	270	270	270	270
Eps (ksi)	28500	28500	28500	28500	28500
Aps (in^2)	5.20	5.20	5.20	5.20	5.20
be (in)	48	72	96	118	118
h (in)	54	54	54	54	54
ts (in)	9	9	9	9	9
f'cs (in)	4	4	4	4	4
Vg (kips)	78	78	78	78	78
Vs (kips)	45	66	88	109	131
Vb (kips)	4	6	8	10	11
Vws (kips)	11	17	23	29	34
Vll-HL93 (kips)	78	101	122	143	162
Vu (kips)	314	391	466	539	611
Vn (kips)	349	434	518	599	679
φVn (kips)	314	391	466	539	611

Table G30. Design parameters for Type IV girder using the Modified LRFD Procedure (200 ft span)

Type IV- 200 ft Span					
Comb. #	21	22	23	24	25
Girder Spacing (ft)	4	6	8	10	12
f'c (ksi)	7	7	8	9	9
bv (in)	8	8	8	8	8
de (in)	59	59	59	59	59
Av (in ^2)	0.39	0.39	0.39	0.39	0.39
fy (ksi)	60	60	60	60	60
s (in)	17	11	8	5	3
fpu (ksi)	270	270	270	270	270
Eps (ksi)	28500	28500	28500	28500	28500
Aps (in^2)	5.20	5.20	5.20	5.20	5.20
be (in)	48	72	96	118	118
h (in)	54	54	54	54	54
ts (in)	9	9	9	9	9
f'cs (in)	4	4	4	4	4
Vg (kips)	78	78	78	78	78
Vs (kips)	45	66	88	109	131
Vb (kips)	4	6	8	10	11
Vws (kips)	11	17	23	29	34
Vll-HL93 (kips)	78	101	122	143	162
Vu (kips)	314	391	466	539	611
Vn (kips)	349	434	518	599	679
φVn* (kips)	314	391	466	539	611

APPENDIX H: REGRESSION ANALYSIS DATA

Table H1. LRFD regression analysis results for 216 data samples

#	f'c (ksi)	Stress (ksi)	Stirrups Spacing (in)	h (in)	(FEA/LRFD)	Reg.	FEA/(Reg. x LRFD)
1	5.5	0.5	3	36	1.19	0.91	1.31
2	5.5	1.5	3	36	1.30	1.11	1.17
3	8	0.5	3	36	1.40	0.94	1.49
4	5.5	0.5	24	36	1.93	1.65	1.17
5	8	1.5	24	36	2.76	1.87	1.48
6	8	1.5	3	36	1.55	1.14	1.37
7	5.5	1.5	24	36	2.64	1.85	1.43
8	8	0.5	24	36	1.95	1.67	1.17
9	5.5	2.5	3	36	1.33	1.31	1.01
10	8	2.5	24	36	2.94	2.07	1.42
11	8	2.5	3	36	1.57	1.34	1.18
12	5.5	2.5	24	36	2.89	2.05	1.41
13	5.5	0.5	12	36	1.70	1.23	1.39
14	8	1.5	12	36	2.50	1.45	1.72
15	5.5	1.5	12	36	2.42	1.43	1.69
16	8	0.5	12	36	1.77	1.25	1.42
17	5.5	2.5	12	36	2.61	1.63	1.61
18	8	2.5	12	36	2.64	1.65	1.60
19	5.5	0.5	3	36	1.33	0.91	1.46
20	5.5	1.5	3	36	1.50	1.11	1.35
21	8	0.5	3	36	1.54	0.94	1.65
22	5.5	0.5	24	36	2.10	1.65	1.27
23	8	1.5	24	36	2.55	1.87	1.36
24	8	1.5	3	36	1.56	1.14	1.38
25	5.5	1.5	24	36	2.51	1.85	1.36
26	8	0.5	24	36	2.10	1.67	1.26
27	5.5	2.5	3	36	1.46	1.31	1.11
28	8	2.5	24	36	2.64	2.07	1.27
29	8	2.5	3	36	1.46	1.34	1.09
30	5.5	2.5	24	36	2.42	2.05	1.18
31	5.5	0.5	12	36	1.85	1.23	1.51
32	8	1.5	12	36	2.39	1.45	1.65
33	5.5	1.5	12	36	2.34	1.43	1.64
34	8	0.5	12	36	1.90	1.25	1.52
35	5.5	2.5	12	36	2.31	1.63	1.42
36	8	2.5	12	36	2.38	1.65	1.45
37	5.5	0.5	3	36	1.18	0.91	1.29
38	5.5	1.5	3	36	1.37	1.11	1.23
39	8	0.5	3	36	1.32	0.94	1.42
40	5.5	0.5	24	36	1.96	1.65	1.19
41	8	1.5	24	36	2.47	1.87	1.32
42	8	1.5	3	36	1.57	1.14	1.39
43	5.5	1.5	24	36	2.36	1.85	1.28
44	8	0.5	24	36	1.82	1.67	1.09
45	5.5	2.5	3	36	1.52	1.31	1.16
46	8	2.5	24	36	2.75	2.07	1.33
47	8	2.5	3	36	1.76	1.34	1.32
48	5.5	2.5	24	36	2.77	2.05	1.35
49	5.5	0.5	12	36	1.67	1.23	1.36
50	8	1.5	12	36	2.37	1.45	1.63

Table H1 (cont.). LRFD regression analysis results for 216 data samples

#	f'c (ksi)	Stress (ksi)	Stirrups Spacing (in)	h (in)	(FEA/LRFD)	Reg.	FEA/(Reg. x LRFD)
51	5.5	1.5	12	36	2.20	1.43	1.54
52	8	0.5	12	36	1.71	1.25	1.37
53	5.5	2.5	12	36	2.42	1.63	1.48
54	8	2.5	12	36	2.73	1.65	1.65
55	5.5	0.5	3	36	1.18	0.91	1.29
56	5.5	1.5	3	36	1.37	1.11	1.23
57	8	0.5	3	36	1.36	0.94	1.46
58	5.5	0.5	24	36	1.92	1.65	1.16
59	8	1.5	24	36	2.62	1.87	1.40
60	8	1.5	3	36	1.59	1.14	1.40
61	5.5	1.5	24	36	2.42	1.85	1.31
62	8	0.5	24	36	2.02	1.67	1.21
63	5.5	2.5	3	36	1.50	1.31	1.15
64	8	2.5	24	36	2.53	2.07	1.22
65	8	2.5	3	36	1.73	1.34	1.29
66	5.5	2.5	24	36	2.53	2.05	1.23
67	5.5	0.5	12	36	1.78	1.23	1.45
68	8	1.5	12	36	2.38	1.45	1.64
69	5.5	1.5	12	36	2.24	1.43	1.57
70	8	0.5	12	36	1.91	1.25	1.52
71	5.5	2.5	12	36	2.30	1.63	1.42
72	8	2.5	12	36	2.57	1.65	1.56
73	5.5	0.5	3	45	1.40	1.07	1.30
74	5.5	1.5	3	45	1.77	1.27	1.39
75	8	0.5	3	45	1.58	1.10	1.44
76	5.5	0.5	24	45	2.21	1.81	1.22
77	8	1.5	24	45	2.94	2.03	1.45
78	8	1.5	3	45	1.93	1.30	1.49
79	5.5	1.5	24	45	2.94	2.01	1.46
80	8	0.5	24	45	2.01	1.83	1.09
81	5.5	2.5	3	45	1.84	1.47	1.25
82	8	2.5	24	45	2.97	2.23	1.33
83	8	2.5	3	45	1.99	1.50	1.33
84	5.5	2.5	24	45	2.91	2.21	1.32
85	5.5	0.5	12	45	1.92	1.39	1.38
86	8	1.5	12	45	2.67	1.61	1.66
87	5.5	1.5	12	45	2.58	1.59	1.62
88	8	0.5	12	45	1.88	1.41	1.33
89	5.5	2.5	12	45	2.68	1.79	1.50
90	8	2.5	12	45	2.77	1.81	1.53
91	5.5	0.5	3	45	1.45	1.07	1.35
92	5.5	1.5	3	45	1.79	1.27	1.40
93	8	0.5	3	45	1.62	1.10	1.47
94	5.5	0.5	24	45	2.42	1.81	1.34
95	8	1.5	24	45	2.94	2.03	1.45
96	8	1.5	3	45	1.72	1.30	1.32
97	5.5	1.5	24	45	2.78	2.01	1.38
98	8	0.5	24	45	2.38	1.83	1.30
99	5.5	2.5	3	45	1.79	1.47	1.21
100	8	2.5	24	45	2.68	2.23	1.20

Table H1 (cont.). LRFD regression analysis results for 216 data samples

#	f'c (ksi)	Stress (ksi)	Stirrups Spacing (in)	h (in)	(FEA/LRFD)	Reg.	FEA/(Reg. x LRFD)
101	8	2.5	3	45	1.92	1.50	1.28
102	5.5	2.5	24	45	2.66	2.21	1.20
103	5.5	0.5	12	45	2.08	1.39	1.50
104	8	1.5	12	45	2.73	1.61	1.69
105	5.5	1.5	12	45	2.58	1.59	1.62
106	8	0.5	12	45	2.12	1.41	1.50
107	5.5	2.5	12	45	2.37	1.79	1.33
108	8	2.5	12	45	2.53	1.81	1.40
109	5.5	0.5	3	45	1.27	1.07	1.18
110	5.5	1.5	3	45	1.57	1.27	1.23
111	8	0.5	3	45	1.42	1.10	1.30
112	5.5	0.5	24	45	1.82	1.81	1.00
113	8	1.5	24	45	2.64	2.03	1.30
114	8	1.5	3	45	1.76	1.30	1.36
115	5.5	1.5	24	45	2.42	2.01	1.20
116	8	0.5	24	45	1.88	1.83	1.03
117	5.5	2.5	3	45	1.64	1.47	1.11
118	8	2.5	24	45	3.10	2.23	1.39
119	8	2.5	3	45	1.94	1.50	1.29
120	5.5	2.5	24	45	2.89	2.21	1.31
121	5.5	0.5	12	45	1.70	1.39	1.22
122	8	1.5	12	45	2.45	1.61	1.52
123	5.5	1.5	12	45	2.25	1.59	1.42
124	8	0.5	12	45	1.80	1.41	1.28
125	5.5	2.5	12	45	2.53	1.79	1.41
126	8	2.5	12	45	2.94	1.81	1.62
127	5.5	0.5	3	45	1.30	1.07	1.21
128	5.5	1.5	3	45	1.60	1.27	1.26
129	8	0.5	3	45	1.51	1.10	1.38
130	5.5	0.5	24	45	2.04	1.81	1.13
131	8	1.5	24	45	2.87	2.03	1.41
132	8	1.5	3	45	1.82	1.30	1.41
133	5.5	1.5	24	45	2.48	2.01	1.23
134	8	0.5	24	45	2.13	1.83	1.16
135	5.5	2.5	3	45	1.63	1.47	1.10
136	8	2.5	24	45	2.91	2.23	1.30
137	8	2.5	3	45	1.94	1.50	1.30
138	5.5	2.5	24	45	2.81	2.21	1.27
139	5.5	0.5	12	45	1.91	1.39	1.38
140	8	1.5	12	45	2.57	1.61	1.59
141	5.5	1.5	12	45	2.32	1.59	1.46
142	8	0.5	12	45	2.04	1.41	1.44
143	5.5	2.5	12	45	2.40	1.79	1.34
144	8	2.5	12	45	2.81	1.81	1.55
145	5.5	0.5	3	54	1.56	1.24	1.26
146	5.5	1.5	3	54	2.01	1.44	1.40
147	8	0.5	3	54	1.74	1.26	1.38
148	5.5	0.5	24	54	2.42	1.97	1.23
149	8	1.5	24	54	3.19	2.19	1.46
150	8	1.5	3	54	2.22	1.46	1.52

Table H1 (cont.). LRFD regression analysis results for 216 data samples

#	f'c (ksi)	Stress (ksi)	Stirrups Spacing (in)	h (in)	(FEA/LRFD)	Reg.	FEA/(Reg. x LRFD)
151	5.5	1.5	24	54	3.23	2.17	1.49
152	8	0.5	24	54	2.37	1.99	1.19
153	5.5	2.5	3	54	2.03	1.64	1.24
154	8	2.5	24	54	3.49	2.39	1.46
155	8	2.5	3	54	2.26	1.66	1.36
156	5.5	2.5	24	54	3.47	2.37	1.46
157	5.5	0.5	12	54	2.11	1.55	1.36
158	8	1.5	12	54	3.01	1.77	1.70
159	5.5	1.5	12	54	2.81	1.75	1.61
160	8	0.5	12	54	2.04	1.57	1.30
161	5.5	2.5	12	54	2.98	1.95	1.53
162	8	2.5	12	54	3.07	1.97	1.55
163	5.5	0.5	3	54	1.58	1.24	1.28
164	5.5	1.5	3	54	1.96	1.44	1.36
165	8	0.5	3	54	1.77	1.26	1.40
166	5.5	0.5	24	54	2.59	1.97	1.32
167	8	1.5	24	54	3.08	2.19	1.40
168	8	1.5	3	54	2.14	1.46	1.47
169	5.5	1.5	24	54	3.08	2.17	1.42
170	8	0.5	24	54	2.61	1.99	1.31
171	5.5	2.5	3	54	1.91	1.64	1.17
172	8	2.5	24	54	2.93	2.39	1.22
173	8	2.5	3	54	2.10	1.66	1.27
174	5.5	2.5	24	54	2.75	2.37	1.16
175	5.5	0.5	12	54	2.22	1.55	1.43
176	8	1.5	12	54	2.67	1.77	1.51
177	5.5	1.5	12	54	2.72	1.75	1.55
178	8	0.5	12	54	2.22	1.57	1.41
179	5.5	2.5	12	54	2.47	1.95	1.27
180	8	2.5	12	54	2.58	1.97	1.31
181	5.5	0.5	3	54	1.41	1.24	1.14
182	5.5	1.5	3	54	1.72	1.44	1.20
183	8	0.5	3	54	1.59	1.26	1.26
184	5.5	0.5	24	54	2.07	1.97	1.05
185	8	1.5	24	54	3.13	2.19	1.43
186	8	1.5	3	54	1.95	1.46	1.34
187	5.5	1.5	24	54	3.10	2.17	1.43
188	8	0.5	24	54	2.09	1.99	1.05
189	5.5	2.5	3	54	1.68	1.64	1.03
190	8	2.5	24	54	3.48	2.39	1.45
191	8	2.5	3	54	2.04	1.66	1.23
192	5.5	2.5	24	54	3.47	2.37	1.46
193	5.5	0.5	12	54	1.85	1.55	1.19
194	8	1.5	12	54	2.83	1.77	1.60
195	5.5	1.5	12	54	2.74	1.75	1.56
196	8	0.5	12	54	1.88	1.57	1.19
197	5.5	2.5	12	54	2.80	1.95	1.43
198	8	2.5	12	54	3.17	1.97	1.60
199	5.5	0.5	3	54	1.45	1.24	1.17
200	5.5	1.5	3	54	1.77	1.44	1.23

Table H1 (cont.). LRFD regression analysis results for 216 data samples

#	f'c (ksi)	Stress (ksi)	Stirrups Spacing (in)	h (in)	(FEA/LRFD)	Reg.	FEA/(Reg. x LRFD)
201	8	0.5	3	54	1.65	1.26	1.31
202	5.5	0.5	24	54	2.39	1.97	1.21
203	8	1.5	24	54	3.48	2.19	1.59
204	8	1.5	3	54	1.93	1.46	1.33
205	5.5	1.5	24	54	3.09	2.17	1.42
206	8	0.5	24	54	2.45	1.99	1.23
207	5.5	2.5	3	54	1.70	1.64	1.04
208	8	2.5	24	54	3.19	2.39	1.33
209	8	2.5	3	54	1.91	1.66	1.15
210	5.5	2.5	24	54	2.75	2.37	1.16
211	5.5	0.5	12	54	2.10	1.55	1.35
212	8	1.5	12	54	3.03	1.77	1.71
213	5.5	1.5	12	54	2.69	1.75	1.53
214	8	0.5	12	54	2.19	1.57	1.39
215	5.5	2.5	12	54	2.58	1.95	1.32
216	8	2.5	12	54	2.91	1.97	1.47
				Mean	2.22	1.64	1.36
				STDEV.	0.56	0.37	0.16
				COV	0.25	0.23	0.11

Table H2. Mean live load data from the state of Michigan based on one lane loading (Eamon et al., 2014)

Span (ft)	Spacing (ft)	mLL (kips)	COV
30	4	53	0.176
30	6	61	0.176
30	8	70	0.176
30	10	78	0.176
30	12	86	0.176
60	4	81	0.187
60	6	94	0.187
60	8	106	0.187
60	10	118	0.187
60	12	131	0.187
90	4	103	0.191
90	6	118	0.191
90	8	134	0.191
90	10	150	0.191
90	12	166	0.191
120	4	119	0.194
120	6	137	0.194
120	8	156	0.194
120	10	174	0.194
120	12	192	0.194
200	4	160	0.198
200	6	184	0.198
200	8	209	0.198
200	10	233	0.198
200	12	258	0.198

APPENDIX I: FORTRAN CODE

The following FORTRAN algorithm was used to compute reliability indices for Type II girder using Rackwitz-Fiessler Procedure and based on the iterative approach discussed in Chapter 4.

```
PROGRAM RFstep

 !Rackwitz-Fiessler for nonlinear limit states

!! Note although gives good B convergence, MPP does not
!! completely satisfy g(linearized)=0

REAL g, gm, linsum, grad, xn, dgn, V, snpU, toterror
REAL Beta, BetaLast, exIalp, exIu, EIP, EIC, pv, PHI, UPDF, UPCF
INTEGER nrv, d, interlimit, l

REAL, DIMENSION (:), ALLOCATABLE :: x
REAL, DIMENSION (:), ALLOCATABLE :: xm
REAL, DIMENSION (:), ALLOCATABLE :: xb
REAL, DIMENSION (:), ALLOCATABLE :: sd
REAL, DIMENSION (:), ALLOCATABLE :: dg
REAL, DIMENSION (:), ALLOCATABLE :: xpert
REAL, DIMENSION (:), ALLOCATABLE :: gpert
REAL, DIMENSION (:), ALLOCATABLE :: lin
REAL, DIMENSION (:), ALLOCATABLE :: sdlin
INTEGER, DIMENSION (:), ALLOCATABLE :: lrv
INTEGER, DIMENSION (:), ALLOCATABLE :: xd
REAL, DIMENSION (:), ALLOCATABLE :: xurl
REAL, DIMENSION (:), ALLOCATABLE :: xurh
REAL, DIMENSION (:), ALLOCATABLE :: xmb
REAL, DIMENSION (:), ALLOCATABLE :: sdb
REAL, DIMENSION (:), ALLOCATABLE :: xold
REAL, DIMENSION (:), ALLOCATABLE :: totalerror

REAL Mu, Vu, Vinc, balerror, errtol, vdfrac
INTEGER iterlim, iters

!!!!!!!!! ENTER DATA HERE ((5) steps)!!!!!!!!!!!!!!!!!!!!!!!!!!!!!!

! (1) ENTER #RVs:
nrv = 19 !15

ALLOCATE(x(nrv))
ALLOCATE(sd(nrv))
ALLOCATE(xm(nrv))
ALLOCATE(dg(nrv))
```

```
ALLOCATE(xb(nrv))
ALLOCATE(xpert(nrv))
ALLOCATE(gpert(nrv))
ALLOCATE(lrv(nrv))
ALLOCATE(lin(nrv))
ALLOCATE(sdlin(nrv))
ALLOCATE(xd(nrv))
ALLOCATE(xurl(nrv))
ALLOCATE(xurh(nrv))
ALLOCATE(xmb(nrv))
ALLOCATE(sdb(nrv))
ALLOCATE(xold(nrv))
ALLOCATE(totalerror(nrv))

! (2) ENTER RV means (xm(i)), std. dev's (sd(i)), anf distribution types xd(i),
! For distributions, enter 1=normal, 2=lognormal, 3=extreme I/Gumbel, 4 = Uniform
! If Uniform, must enter RV range: xurl(i) (low), xurh(i) (high)

!Mu=663.56

Vinc = 1.0 !Enter increment step up for Vu
errtol = 0.04  !Vu & Rrn error tolerance (fraction; i.e. 1% = 0.01)
iterlim = 5000 ! max. number of balance iterations to allow Vu=Rrn
vdfrac = 0.1 !fraction to reduce Vinc if over/undershoots.

Vu=         150.8
Sp=         720
xm(1)=          9.66
xm(2)=          6.06
xm(3)=          41.75
xm(4)=          0.39
xm(5)=          68.70
xm(6)=          16.66
xm(7)=          280.80
xm(8)=          28500.00
xm(9)=          2.45
xm(10)=         96.00
xm(11)=         36.00
xm(12)=         9.09
xm(13)=         5.52
xm(14)=         10.52
xm(15)=         25.49
xm(16)=         2.39
xm(17)=         6.38
xm(18)=         105.97
xm(19)=         1
```

sd(1)= 1.16
sd(2)= 0.24
sd(3)= 1.04
sd(4)= 0.01
sd(5)= 3.44
sd(6)= 0.67
sd(7)= 7.02
sd(8)= 285.00
sd(9)= 0.04
sd(10)= 3.84
sd(11)= 1.08
sd(12)= 1.09
sd(13)= 0.66
sd(14)= 0.84
sd(15)= 2.55
sd(16)= 0.24
sd(17)= 1.60
sd(18)= 19.82
sd(19)= 0.1

xd(1)=1
xd(2)=1
xd(3)=1
xd(4)=1
xd(5)=1
xd(6)=1
xd(7)=1
xd(8)=1
xd(9)=1
xd(10)=1
xd(11)=1
xd(12)=1
xd(13)=1
xd(14)=1
xd(15)=1
xd(16)=1
xd(17)=1
xd(18)=1
xd(19)=1
! (3) ENTER which RVs are LOAD RVs by: lrv(i) = 1. Do not input anything for
!resistance RVs

lrv(14)=1
lrv(15)=1
lrv(16)=1

```
lrv(17)=1
lrv(18)=1

! (4) ENTER step size for gradient difference (+/- fraction)

grad = 0.01
converge = 0.01 !error fraction for MPP convergence criteria
iterlimit = 20

! (5) NTER G at subroutine  Limitstate below:

open (1,file="RFoutput.txt")

!!!!!!!!!!!!!!!!!!!!!!!!!!!!!!!!!!!!!!!!!!!!!!!!!!!!!!!!!!!!!!!!!!!!!!!!!!

!Save the base means and std. devs:
do i=1,nrv
xmb(i) = xm(i)
sdb(i) = sd(i)
end do

!First assume initial RV values are means

do i=1,nrv
x(i) = xm(i)
end do

!begin Beta Loop

do

d=d+1
!print*, "d=", d

                if (d == iterlimit+1) then
                goto 700
                else
                end if

!!1.5) Determine Equivalent Normal RV parameters at design point

do i=1,nrv
        if (xd(i)==1) then
        goto 90
        else if (xd(i)==2) then
        call Lognormal
```

```
        else if (xd(i)==3) then
        call ExtremeI
        else if (xd(i)==4) then
        call Uniform
        else
        end if

90 rt=0 !dummy
end do


!2nd get derivatives of g:

!gradients dg/dx

        ! g base value

        !save base values
        do i=1,nrv
        xb(i) = x(i)
        end do

        call Limitstate
        gm = g

        print*,"g =",g

        !g perturbed values
        do i=1,nrv

                do l=1,nrv
                x(l)=xb(l)
                end do

                x(i) = xb(i)*(grad+1)
                xpert(i) = x(i)

                call Limitstate
                gpert(i) = g

        !print*,"gpert (i)=",gpert(i)
        print*,"gm =",gm
   print*,"---------- ",gm-g

        end do
```

```
        !set x(i) back to unperturbed values

        do i=1,nrv
        x(i) = xb(i)
        end do

        !calc dg/dx

        do i=1,nrv
        dg(i) = ((gm - gpert(i))/(x(i)-xpert(i)))
!       print*, "dg(i)=", dg(i)
        end do



!end gradient calculation
!!!!!!!!!!!!!!!!!!!!!!!!!!!!!!!!!!!!!!!!!!!!!!!


!3rd create linearized limit state

        linsum = 0
        do i=1,nrv
        lin(i) = (xm(i)-x(i))*dg(i)
        linsum= lin(i) + linsum
   print*,"dg(i) =",dg(i)
        end do


        glin = gm + linsum

   print*,"linsum =",linsum
        print*,"glin =",glin
   print*, " Vu=", Vu


!4th creat linearized std. deviation

        sdsum = 0
        do i=1,nrv
        sdlin(i) = (sd(i)*dg(i))**2
        sdsum = sdlin(i) + sdsum
        end do

        sdsum = sdsum**0.5
```

```
!5th approximate Beta

Beta = glin/sdsum

print*, "glin, sdsum=", glin, sdsum
print*, "beta=", Beta

!6th calculate new design point

print*, "New Design Point (basic coords):"

        do i=1,nrv

        !For Load RVs:

        if(lrv(i) == 1 ) then

        x(i) = xm(i) + (dg(i)*Beta*sd(i)**2)/sdsum

        print*, "x(i)=", i, x(i)

        else
        !For Resistance RVs:

        x(i) = xm(i) - (dg(i)*Beta*sd(i)**2)/sdsum

        print*, "x(i)=", i, x(i)

        end if

        end do

!Convergence Criteria

! by beta
!       if (abs(BetaLast - Beta) <= converge) then
!               goto 500
!               else
!       end if

!Convergence by design point

do i=1,nrv
        if (xold(i) == 0) then
        xold(i) = 2*x(i)
        else
```

```
        end if
        totalerror(i) = (abs(x(i)-xold(i)))/xold(i)
end do

toterror=0
do i=1,nrv
toterror = toterror + totalerror(i)
end do
!print*, "toterror=", toterror

if (toterror < converge) then
goto 500
else
end if

!save current x(i) values for convergence check
do i=1,nrv
xold(i) = x(i)
end do

BetaLast= Beta
end do

400 goto 800
500 print*, "MPP Converged, Beta =", Beta
505 print*, "Total limit state calls, total calls=", lsc, totalcalls
600 goto 800
620 goto 800
700 print*, "MPP not converged after max. iteration ", iterlimit
710 print*, "Total limit state calls, total calls=", lsc, totalcalls
800 w=0 !dummy

CONTAINS

=========================================================================
===
SUBROUTINE Limitstate

ENTER FORM OF G HERE (4)
lsc=lsc+1  !total #of limit state calls
iters = 0
pic = 0
pde = 0

Do
```

```
totalcalls = totalcalls +1
iters = iters +1

!print*, "Iteration, Vu=", iters, Vu
write (1,20000) iters, Vu

20000 format ("Iteration, Vu=", I3, "  ", F8.4)

if (iters .GT. iterlim) then
print*, "Vu=Rrn balance not converged after max. iteration ", iterlim
stop
end if


Beta1=0.85-0.05*((abs(x(13)*1000)-4000)/10000)
c=(x(9)*x(7))/(0.85*abs(x(13))*Beta1*x(10)+0.28*x(9)*(x(7)/x(3)))
a=Beta1*c
dv=x(3)-(a/2)

Mu=Vu*dv

es=((Mu/dv)+Vu-x(9)*0.7*x(7))/(x(8)*x(9))

if (es .LT. 0) then
es=((Mu/dv)+Vu-x(9)*0.7*x(7))/(x(8)*x(9)+(144+x(2)*(((x(11)+x(12)+1)/2)-
6))*((150**1.5)*33*(abs(x(1)*1000)*(1/(abs(x(1)*1000)**0.5)))/1000))
else
dummy=0
end if

Bb=4.8/(1+750*es)
Theta=(29+3500*es)*(3.14/180)


Vc=0.0316*Bb*(abs(x(1))*(1/(abs(x(1))**0.5)))*x(2)*dv

Vs=(x(4)*x(5)*dv*(1/tan(Theta)))/x(6)

Vp=0

Rrn=Vc+Vs+Vp


        !exit if error tolerance satisfied

        balerror = (Vu - Rrn)/Rrn
```

```
        if (abs(balerror) .LE. errtol) then
        print*, "balanced; Vu, Rrn, #iters=", Vu, Rrn, iters
   Print*, "balerror" , balerror
                goto 500 !exit; error tolerance satisfied
        end if

10000 dummy=0

if (Vu .LE. Rrn) then

        pic = pic +1     !# of increase processes

        Vu = Vu + Vinc


else if (Vu .GT. Rrn) then

        pde = pde + 1  !#of decrease processes

        if (pic == 1.0) then

                !process was increasing, now decreasing; means overshot

                print*, "Vu overshot target of Rrn=", Rrn, ". Reduce to Vu=", Vu-Vinc
                print*, "     and restart with new increment of Vinc=", Vinc*Vdfrac

                Vu = Vu - Vinc
                Vinc = Vinc*Vdfrac

                goto 10000

        end if
        Vu = Vu - Vinc

end if

End do

500 Qqn=x(14)+x(15)+x(16)+x(17)+x(18)

!print*, "Qqn=", Qqn
g=Rrn*x(19)-Qqn

print*, "es=", es
print*, "Vu=", Vu
```

```
print*, "Mu=", Mu
print*, "g=", g


END SUBROUTINE
!=====================================================================
====
SUBROUTINE Lognormal

!change xm(i) and sd(i)


        V = sdb(i) / xmb(i)

!print*, "i, sdb(i), xmb(i), V(i) =", i, sdb(i), xmb(i), V

        sd(i) = x(i)*(LOG(V**2+1))**.5    !equiv. norm s.d.


!print*, "equiv. norm sd", i, sd(i)

!equiv norm mean
        xm(i) = x(i)*(1-LOG(x(i)) + LOG(xmb(i)) - 0.5*LOG(V**2+1))

!print*, "equiv. norm mean", i, xm(i)

END SUBROUTINE
!---------------------------------------------------------------------------

SUBROUTINE ExtremeI


exIalp = 1.28254983/sdb(i)

exIu = xmb(i) - 0.5772/exIalp

!pdf:
EIP = exIalp*EXP(-EXP(-exIalp*(x(i)-exIu)))*EXP(-exIalp*(x(i)-exIu))
!cdf:
EIC = EXP(-EXP(-exIalp*(x(i)-exIu)))


!Equiv. s.d. calcluation:

        !computation of inverse standard normal distribution
```

```
        IF (EIC > 0.5) THEN
        EIC = 1-EIC
        condition = 1
        ELSE
        condition = 0
        END IF

        pv = (-LOG(EIC**2))**.5
        PHI = -pv + (2.515517 + 0.802853*pv + 0.010328*pv**2)/(1 + 1.432788*pv +
0.189269*pv**2 + 0.001308*pv**3)

        IF (condition == 1) THEN
        PHI = -PHI
        ELSE
        END IF

!Std Norm PDF(i)=

snpEI = 0.3989422804*EXP(-0.5*(PHI)**2)

!equivalent sd:

sd(i) = (1/EIP)*snpEI

!equivalent mean:

xm(i) = x(i) - sd(i)*(PHI)


END SUBROUTINE
!-------------------------------------------------------------------------------

SUBROUTINE Uniform

!change xm(i) and sd(i)

!pdf:
UPDF = 1/(xurh(i)-xurl(i))
!cdf:
UCDF = UPDF*(x(i) -xurl(i))

!Equiv. s.d. calcluation:

        !computation of inverse standard normal distribution

        IF (UCDF > 0.5) THEN
```

```
        UCDF = 1-UCDF
        condition = 1
        ELSE
        condition = 0
        END IF

        pv = (-LOG(UCDF**2))**.5
        PHI = -pv + (2.515517 + 0.802853*pv + 0.010328*pv**2)/(1 + 1.432788*pv +
0.189269*pv**2 + 0.001308*pv**3)

        IF (condition == 1) THEN
        PHI = -PHI
        ELSE
        END IF

!Std Norm PDF(i)=

snpU = 0.3989422804*EXP(-0.5*(PHI)**2)

!equivalent sd:

sd(i) = (1/UPDF)*snpU

!equivalent mean:

xm(i) = x(i) - sd(i)*(PHI)


END SUBROUTINE
-----------------------------------------------------------------------


END PROGRAM
```

REFERENCES

AASHTO Interim Specifications for Highway Bridges. American Association of State Highway and Transportation Officials, Washington, D.C., 1979.

AASHTO LRFD Bridge Design Specifications, 1st ed. American Association of State Highway and Transportation Officials, Washington, D.C., 1994.

AASHTO LRFD Bridge Design Specifications, 6th ed. American Association of State Highway and Transportation Officials, Washington, D.C., 2014.

AASHTO Manual for Bridge Evaluation, 2nd ed. American Association of State Highway and Transportation Officials, Washington, D.C., 2011.

AASHTO Standard Specifications for Highway Bridges, 12th ed. American Association of State Highway and Transportation Officials, Washington, D.C., 1983.

AASHTO Standard Specifications for Highway Bridges, 17th ed. American Association of State Highway and Transportation Officials, Washington, D.C., 2002.

AASHTO Standard Specifications for Highway Bridges, American Association of State Highway and Transportation Officials, Washington, D.C., 1989.

AASHTO. Standard Specifications for Highway Bridges. 11th. American Association of State Highway and Transportation Officials, Washington, D.C., 1973.

Aboutaha, R., and Burns, N. "Shear Strengthening of Pretensioned Prestressed Concrete Composite Flexural Members". Federal Highway Administration, Austin, Texas. Report CTR-3-5-89/1-1210-2. p 92. March 1991.

ACI 318-11 Building Code and Commentary, American Concrete Institute, Farmington Hills, MI, 2011.

ACI-ASCE Committee 426. “The Shear Strength of Reinforced Concrete Members,” Journal of the Structural Division, Vol. 99, No. ST6, pp. 1091-1187, 1973.

Baker, M., Thompson, P. D. “Bridge Software--Validation Guidelines and Examples”. NCHRP Report 485. Transportation research Board, Washington, D.C., 2003.

Belarbi, A., and Hsu, T. C. “Consecutive laws of RC in Biaxial tension-Compression”. Research report UHCEE 91-2. University of Houston, Texas. 1991.

Belarbi, A., and Hsu, T. C. “Softened Concrete in Biaxial Tension-Compression”. ACI Structural Journal, v 92, n 5, 562-573. Sept-Oct 1995.

Belarbi, A., Bae, S-W., Ayoub, A., Kuchma, D., Mirmiran, A., and Okeil, A. “Design of FRP Systems for Strengthening Concrete Girders in Shear”. NCHRP Report 678. Transportation research Board, Washington, D.C., 2011.

Bennett, E.W. and Mlingwa, G. "Cracking and Shear Strength of Beams with Prestressed Web Reinforcement." Structural Engineering, v 58, n 2, p 25-32.

Bennett, E.W., Abdul-Ahad, H.Y., and Neville, A.M. “ Shear strength of reinforced and prestressed beams subject to moving loads”. Journal of the Prestressed Concrete Institute, v 17, n 6, p 58-69, Nov-Dec 1972.

Bentz, E. C., Vecchio, F. J., and Collins, M. P. “Simplified Modified Compression Field Theory for Calculating Shear Strength of Reinforced Concrete Elements”. ACI Structural Journal,103(4):614– 624, July-August 2006.

Bentz, E.C., 2000. "Sectional Analysis of Reinforced Concrete Members", Ph.D. Thesis, Department of Civil Engineering, University of Toronto, 310 pp.

Bentz, Evan C., and Michael P. Collins. "Development of the 2004 Canadian Standards Association (CSA) A23. 3 shear provisions for reinforced concrete." Canadian Journal of Civil Engineering 33.5 (2006): 521-534.

Bresler, B., and Pister, K.S. “Strength of Concrete under Combined Stresses”. ACI Journal Proceedings, v 55, n 9, 321-345, 1958.

British Standards Institution. Eurocode 2: Design of Concrete Structures: Part 1-1: General Rules and Rules for Buildings. British Standards Institution, 2004.

Brown, M.D. and Bayrak, O. “Design of Deep Beams using Strut-and-Tie Models - Part I: Evaluating U.S. Provisions”. ACI Structural Journal, 105(4):395–404, July-August 2008.

Castrodale, R. W., and White, C. D. “Extending Span Ranges of Precast Prestressed Concrete Girders”. NCHRP Report 517. Transportation Research Board, Washington, D.C., 2004.

Cederwall, K. “Shear Capacity of Composite Prestressed Concrete Beams”. Nordic Concrete Research, n 7, 28-40. December 2006.

Cladera, A., and Marif, A.R. “Shear design of prestressed and reinforced concrete beams”. Magazine of Concrete Research, v 58, n 10, 713-22, Dec. 2006.

Collins, M. P., and Mitchell, D. “Prestressed Concrete Structures”. pp 776. Englewood Cliffs, New Jersey: Prentice-Hall, Inc. 1991.

CSA (Canadian Standards Association). “Design of concrete structures.” CSA A23.3, Mississauga, ON, Canada. 2004.

Cumming, D. A., French, C. E., and Shield, C. K. “Shear Capacity of High-Strength Concrete Prestressed Girders”. Minnesota Department of Transportation. p 396. May 1998.

De Silva, S., Mutsuyoshi, H., and Witchukreangkrai, E. “Evaluation of shear crack width in I-shaped prestressed reinforced concrete beams”. Journal of Advanced Concrete Technology, v 6, n 3, p 443-458, October 2008.

Dei Poli, S., Prisco, M. D., and Gambarova, P. G. “Stress Fields in Web of Reinforced Concrete Thin-Webbed Beams Failing in Shear”. Journal of Structural Engineering, v 116, n 9, 2496-2515. September 1990.

Duthinh, D., and Dat. “Sensitivity of shear strength of reinforced concrete and prestressed concrete beams to shear friction and concrete softening according to modified compression field theory”. ACI Structural Journal, v 96, n 4, p 495-508, July/August 1999.

Eamon, C., Kamjoo, V., and Shinki, K. “Side By Side Probability for Bridge Design and Analysis.” MDOT Research Report RC-1601, 2014.

Eamon, Parra-Montesinos and Chehab, “Evaluation of Prestressed Concrete Beams in Shear", MDOT Report RC-1615, 2014.

Eligehausen, R., Popov, E., and Bertero, V. “Local Bond Stress-Slip relationship of Deformed Bars under Generalized Excitations”, Report No. UCB/EERC-83/23, Earthquake Engineering Center, University of California, Berkeley. 1983.

Esfandiari, A., and Adebar, P. “Shear strength evaluation of concrete bridge girders”. ACI Structural Journal, v 106, n 4, 416-26, July-Aug. 2009.

Fagundo, F. E., Lybas, J. M., Basu, A., Shaw, T. J., White, D. “Effect of Confinement in Transfer Region on the Interaction between Bond and Shear Forces in Prestressed Concrete Girders”. (Florida University, Gainesville. Dept. of Civil Engineering).185p, Dec 1995.

Fenwick, R.C., and Paulay, T. “Mechanisms of shear resistance of concrete beams “. American Society of Civil Engineers Proceedings, Journal of the Structural Division, v 94, n ST10, p 2325-2350, Oct, 1968.

Gustafson, D. P., and Bruce, R. N. “Investigation of Shear Behavior of Prestressed Concrete Bridge Girders”. Tulane Univ., New Orleans, La. Dept. of Civil Engineering. Report: TR-101, 188p, Oct 1966.

Hanson, J. M., and Hulsbos, C. L. “Shear Fatigue Tests of Prestressed Concrete I-Beams with Web Reinforcement”. Lehigh Univ., Bethlehem, Pa. Fritz Engineering Lab. Report: 223.29, 114p, Jan 1969.

Hartmann, D. L., Breen, J. E., and Kreger, M. E. “Shear Capacity of High Strength Prestressed Concrete Girders”. (Texas University at Austin. Center for Transportation Research). Report: CTR-3-5-84-381-2, 271p, Jan 1988.

Hawkins, N. M., and D. A. Kuchma. Application of LRFD Bridge Design Specifications to High Strength Structural Concrete: Shear Provisions, NCHRP Report 579, Transportation Research Board, National Research Council, Washington, DC, 2007.

Hawkins, N. M., and Kuchma, D. A. “Simplified Shear Design of Structural Concrete Members”. NCHRP Report 549. Transportation Research Board, Washington, D.C., 2005.

Hegger, J., Sherif, A., and Görtz, S. “Investigation of Pre- and Postcracking Shear Behavior of Prestressed Concrete Beams Using Innovative Measuring Techniques”. ACI Structural Journal, v 101, n 2, p 183-192, March/April 2004.

Hsu, T.C. "Softened Truss Model Theory for Shear and Torsion." ACI Structural Journal, Nov/Dec 1988.

Idriss, Rola L., and Liang, Zhiyong. “In-service shear and moment girder distribution factors in simple-span prestressed concrete girder bridge: Measured with built-in optical fiber sensor system”. Transportation Research Record, n 2172, p 142-150, January 12, 2010.

Kollegger, J., and Melhorn, G. “Material Model for Analysis of Reinforced Concrete Surface Structures”. Computational Mechanics, n 6, 341-357. 1990.

Kollegger, J., and Melhorn, G. “Material Model for Cracked Reinforced Concrete”. IABSE Colloquium on Computational Mechanics of Concrete Structures: Advances and Applications, Delft, n 54, 63-74. 1987.

Kuchma, D. A., and Hawkins, N. M. “Application of LRFD Bridge Design Specifications to High-Strength Structural Concrete: Shear Provisions”. NCHRP Report 579. Transportation Research Board, Washington, D.C., 2007.

Kuchma, D. A., Hawkins, N. M., et al. “Simplified Shear Provisions of the AASHTO LRFD Bridge Design Specifications”. PCI Journal, 53(3):53–73, May-June 2008.

Kuchma, D., Kang, S. K., Nagle, T. J., and Hawkins, N. M. “Shear Tests on High-Strength Prestressed Bulb-Tee Girders: Strength and Key Observations”. ACI Structural Journal, v 105, n 3, 358-67, May-June 2008.

Kupfer, H. and Bulicek, H. “A Consistent Model for Design of Shear Reinforcement in Slender Beams with I- or Box-Shaped Cross Section”. Proceedings, Symposium on Concrete Shear in Earthquake, 256-265. Houston, Texas. 1992.

Kupfer, H., Hilsdorf, H.K.and Rusch, H. "Behavior of Concrete under Biaxial Stress", ACI Journal, Vol. 87, No. 2, pp. 656-666. 1969.

Kupfer, H., Mang, R., and Karavesyroglou, M. “Ultimate Limit State of Shear Zone of Reinforced and Prestressed Concrete Girders-An Analysis Taking Aggregate Interlock into Account”. Bauingenieur 58, 143-149. 1983.

Kupfer, H.B., and Gerstle, K.H. “Behaviour of Concrete under Biaxial Stresses”, ASCE Journal of Engineering Mechanics, Vol. 99, EM4, pp. 853-866. 1973.

Laskar, A., Hsu, T. C., Mo, Y.L. “Shear strengths of prestressed concrete beams part 1: Experiments and shear design equations”. ACI Structural Journal, v 107, n 3, p 330-339, May-June 2010.

Laskar, A., Howser, R., Mo, Y.L., Hsu, T.T.C. “Modeling of prestressed concrete bridge girders”. Proceedings of the 12th International Conference on Engineering, Science, Construction, and Operations in Challenging Environments - Earth and Space 2010, p 2870-2887, 2010.

Lee, S-C., J-Y Cho, J-Y., Oh, B-H. “Shear Behavior of Large-Scale Post-Tensioned Girders with Small Shear Span-Depth Ratio”. ACI Structural Journal, v 107, n 2, 137-45, March-April 2010.

Libby, J. R., Konczak, L. Z. “Designing for shear in continuous prestressed concrete bridges”. Structural Engineers Assoc of California, p 97-109, 1985; Conference: Proceedings - Convention Structural Engineers Association of California, 1985.

Lin, Chien-Hung, Sung-Tang Chen, and Wei-Chieh Lin. "Shear behaviour of prestressed beams with high-workability concrete." Magazine of Concrete Research 64.5 (2012): 419-432.

Liu, C., Wu, B., and Xu, K.Y. "Parametric Study on Reinforced Concrete Beams with Transversely Prestressed Bars." Applied Mechanics and Materials, v105-107, p 912-917, 2012.

Llanos, G., Ross, B. E., Hamilton, H. R. “Shear Performance of Existing Prestressed Concrete Bridge Girders “. Florida University, Gainesville. Dept. of Civil and Coastal Engineering. Report: BD545-56, 160p, May 2009

Ma, Y., and Hu, J. “Shear Strength of the RPC Prestressed Composite Beam”. Journal of Highway and Transportation Research and Development, v 24, n 12, 85-88. December 2008.

MacGregor, J.G. “Strength and Behavior of Prestressed Concrete Beams with Web Reinforcement,” PhD Thesis, University of Illinois, Urbana, July 1960.

MacGregor, J.G., Sozen, M.A., Siess, C.P. “Strength of Prestressed Concrete Beams with Web Reinforcement,” Journal of the American Concrete Institute, 1503-1518, December 1965.

Mahesh, P., Surinder, D. “Support vector regression based shear strength modeling of deep beams”. Computers and Structures, v 89, p 1430-1439, April 2011.

Maruyama, K., and Rizkalla, S. H. “Shear Design Consideration for Pretensioned Prestressed Beams”. ACI Structural Journal, v 85, n 5, p 492-498, Sep-Oct 1988.

Mast, P.E. “Shortcuts for shear analysis of standard prestressed concrete members”. Prestressed Concrete Institute -- Journal, v 9, n 5, p 15-47, Oct, 1964.

Mau, S. T. and Hsu, T. T. Discussion of paper by Walraven, Frenay, and Pruijssers “Influence of Concrete Strength and Load History on Shear Friction Capacity of Concrete Members”. PCI Journal, v 22, n 1, 166-170. Jan-Feb 1998.

Mikame, A., Uchida, K., and Noguchi, H. “A Study of Compressive Deterioration of Cracked Concrete”. Proceedings, International Workshop on FEA of RC, Columbia University, New York. 1991.

Milynarski, M., Wassef, W. G., and Nowak, A. S. “A Comparison of AASHTO Bridge Load Rating Methods”. NCHRP Project 700. Transportation research Board, Washington, D.C., 2011.

Mindess, S., Young, J. F., and Darwin, D. Concrete. Prentice Hall, 2nd edition, 2003.

Miyahara, T., Kawakami, T., and Maekawa, K. “Nonlinear Behavior of Cracked Reinforced Concrete Plate Element under Uniaxial Compression”. Proceedings, Japan Society of Civil Engineers, v 11, 306-319. 1988

Mörsch, E. Reinforced Concrete Construction Theory and Application. 5th ed. V 1, part 1. Stuttgart, Germany: Konrad Wittwer. 1920.

Mörsch, E. Reinforced Concrete Construction Theory and Application. 5th ed. V 1, part 1. Stuttgart, Germany: Konrad Wittwer. 1922.

Moses, F. “calibration of Load Factors for LRFR Bridge Evaluation”. NCHRP Report 454. Transportation Research Board, Washington, D.C., 2011.

National Swedish Committee on Concrete, Bestimmelser for betongkonstruktioner (Regulations for Concrete Structures) BBK 79, Vol. 1, Design, Stockholm, 1979.

Wilby, C. B., and C. P. Nazir. "Shear strength of uniformly loaded prestressed concrete beams." Civil Engineering & Public Works Review, London 59 (1964): 457-63.

Ning, Z. and Tan, K-H. "Direct Strut-and-Tie Model for Single Span and Continuous Deep Beams." Engineering Structures, Vol. 29, No. 11, pp 2987-3001, Nov 2007.

Nowak, A. S., & Collins, K. R. (2000). Reliability of structures. Boston: McGraw-Hill.

Nowak, A.S. “Calibration of LRFD Bridge Design Code.” NCHRP Report 368. Transportation Research Board, Washington, D.C., 1999.

Nowak, Andrzej S., and Maria M. Szerszen. "Calibration of design code for buildings (ACI 318): Part 1- Statistical models for resistance." ACI Structural Journal 100.3 (2003): 377-382.

Oesterle, R.G., Glikin, J.D., and Larson, S.C. “Design of Precast Prestressed Bridge Girders Made Continuous.” NCHRP Report 322. Transportation Research Board, Washington, D.C., 1989.

Oh, B. H., Kim, Kwang S. “Shear Behavior of Full-Scale Post-Tensioned Prestressed Concrete Bridge Girders”. ACI Structural Journal, v 101, n 2, p 176-182, March/April 2004.

Okamura, H., and Maekawa, K. “Nonlinear Analysis of Reinforced Concrete”. Proceedings of JSCE, n 360, p 1-10. August, 1987.

PCI, Bridge Design Manual, 3th edition, Chicago, IL (2011).

Pei, J. S., Martin, R. D., Sandburg, C. J., and Kang, T. H. “Rating Precast Prestressed Concrete Bridges for Shear”. FHWA-OK-08-08. December 2008.

Prisco, Marco, and Pietro G. Gambarova. "Comprehensive model for study of shear in thin-webbed RC and PC beams." Journal of structural engineering 121.12 (1995): 1822-1831.

Rabbat, B.G., Collins, M.P. “The computer aided design of structural concrete sections subjected to combined loading”. Computers and Structures, v 7, n 2, 229-36, April 1977.

Rackwitz, R. and Fiessler, B., 1978, "Structural Reliability under Combined Random Load Sequences", Computer and Structures, 9, (1978) pp. 489- 494.

Ramirez, J. A., Breen, J. E. “Evaluation of a modified truss-model approach for beams in shear”. ACI Structural Journal, v 88, n 5, p 562-571, Sep-Oct 1991.

Ranasinghe, K., Mutsuyoshi, H., Ashraf, M. “Effect of bond on shear behavior of RC and PC beams: Experiments and FEM analysis”. Transactions of the Japan Concrete Institute, v 23, p 407-412, 2001.

Recupero, A., D'Aveni, A., and Ghersi, A. "Bending Moment-Shear Force Interaction Domains for Prestressed Concrete Beams". Journal of Structural Engineering, v 131, n 9, 1413-1421. September 2005.

Reineck, K. H. "Hintergründe zur Querkraftbemessung in DIN 1045-1 für Bauteile aus Konstruktionsbeton mit Querkraftbewehrung." Bauingenieur 76.4 (2001): 168-179.

Reineck, K. H. "Modeling of Members with Transverse Reinforcement". IABSE Colloquium on Structural Concrete, Stuttgart. IABSE Report, v 62, 481-488. 1991.

Reineck, K. H. "Models for Design of Reinforced and Prestressed Concrete Members". CEB Bulletin d'Information, n 146-Shear in Prestressed Concrete. 1982.

Richart, F.E. "An Investigation of Web Stresses in Reinforced Concrete Beams," Bulletin No. 166, University of Illinois Engineering Experiment Station, 105 p., 1927.

Ritter, W. "Construction Techniques of Hennebique". Schweizerische Bauzeitung, v 33, n 7, 59-61. 1899.

Ross, b. E., Ansley, M., Hamilton, H. R. "Load testing of 30-year-old AASHTO Type III highway bridge girders". PCI Journal, p 152-163, 2011.

Runzell, B., Shield, C. K., French, C. W. "Shear Capacity of Prestressed Concrete Beams". MN/RC 2007-47. March 2008.

Sandburg, C. J. "Shearing Capacity of Prestressed Concrete AASHTO Girders". Master's thesis, University of Oklahoma, School of Civil Engineering and Environmental Science, May 2007.

Saqan, E., Frosch, R. J. "Influence of flexural reinforcement on shear strength of prestressed concrete beams". ACI Structural Journal, v 106, n 1, p 60-68. Jan-Feb 2009.

Schlaich, Jorg, Kurt Schäfer, and Mattias Jennewein. "Toward a consistent design of structural concrete." PCI journal 32.3 (1987): 74-150.

Shahawy, M. A., Cui, C. S. “New approach to shear design of prestressed concrete members”. PCI Journal, v 44, n 4, p 92-117, July/August 1999.

Shirai, S., and Noguchi, H. “Compressive Deterioration of Cracked Concrete”. Proceedings, Structures Congress-Design, Analysis, and Testing, ASCE: New York. p 1-10. 1989.

Standard Specification for Concrete Structures-2007, Japan Society of Civil Engineers (JSCE), Tokyo, Japan, 2007.

Suthinh, D. “Sensitivity of Shear Strength of RC and PC Beams to Shear Friction and Concrete Softening According to the MCFT”. National Institute of Standards and Technology. p 38. Gaithersburg, MD. August 1997.

Tadros, M. K., Badie, S. S., and Tuan, C. Y. “Evaluation and Repair Procedures for Precast/Prestressed Concrete Girders with Longitudinal Cracking in the Web”. NCHRP Report 654. Transportation Research Board, Washington, D.C., 2010.

Thompson, PAUL D., et al. "VIRTIS: AASHTO's New Bridge Load Rating System." Transportation Research Circular 448 (1999).

Tuchscherer, R. G., Birrcher, D. B., and Bayrak , O. “Strut-and-tie model design provisions”. PCI Journal, v 56, n 1, p 155-170, 2011.

Tureyen, A.K., and Frosch, R.J. “Concrete Shear Strength: Another Perspective”. ACI Structural Journal, v 100, n 5, 609-615, 2003.

Ueda, M., Noguchi, H., Shirai, N., and Morita, S. “Introduction to Activity of new Reinforced Concrete”. Proceedings, International Workshop on FEA of reinforced Concrete: Columbia University, New York. 1991.

Vecchio, F. J. "Disturbed stress field model for reinforced concrete: formulation." Journal of Structural Engineering 126.9 (2000): 1070-1077.

Vecchio, F.J. and Collins, M.P. “Compression Response of Cracked reinforced Concrete”. ASCE Journal of Structural Engineering, v 119, n 12, 3590-3610. December 1993.

Vecchio, F.J. and Collins, M.P. “The Modified Compression-Field Theory for Reinforced Concrete Elements Subjected to Shear.” ACI Journal, March-April 1986.

Walraven, J. C. “Fundamental Analysis of Aggregate Interlock”. Journal of Structural Division, ASCE, v 107, n ST11, 2245-2270. 1981.

Walraven, J. C., and Reinhardt, H. W. “Theory and Experiments on Mechanical Behavior of Cracks in Plain and reinforced Concrete Subjected to Shear Loading”. Heron, v 26, n 1A, 68p. 1981.

Wang, G., Meng, S-P. “Modified strut-and-tie model for prestressed concrete deep beams”. Engineering Structures, v 30, n 12, p 3489-3496, December 2008.

Wilby, C.B., Nazir, C.P. “Shear strength of uniformly loaded prestressed concrete beams”. Civil Engineering (London), v 59, n 693, p 457-463, Apr, 1964.

Wong, P., Vecchio, F. J. and Trommels, H., “VecTor2 and FormWorks manual”, 2nd edition, University of Toronto, Toronto, Canada, 2013.

Yang, K.-H., Ashour, A.F., Lee, J.-K. “Shear strength of reinforced concrete dapped-end beams using mechanism analysis”.Magazine of Concrete Research, v 63, n 2, p 81-97, February 1, 2011.

Yoshitake. “Simplified Test of Cracking Strength of Concrete Element Subjected to Pure Shear”. Journal of Materials in Civil Engineering, v 23, n 7, p 999-1006, July, 2011.

Zhang, N. and Tan, K-H. “Direct strut-and-tie model for single span and continuous deep beams”. Engineering Structures, v 29, n 11, p 2987-3001, November 2007.

ABSTRACT

TOWARD A BETTER ESTIMATION OF SHEAR CAPACITY AND STRUCTURAL RELIABILITY OF PRESTRESSED CONCRETE GIRDERS

by

ALAA IBRAHIM CHEHAB

December 2016

Advisor: Dr. Christopher D. Eamon

Major: Civil Engineering (Structural)

Degree: Doctor of Philosophy

The main objectives of this study are to evaluate the adequacy of the current AASHTO methods for shear design of prestressed concrete (PC) bridge girders, determine the reliability of PC bridge girders in shear based on the current LRFD General Procedure, determine the most accurate and consistent method for predicting the shear capacity of AASHTO "I" shape PC bridge girders, and recalibrate the AASHTO LRFD code for shear as necessary. These objectives were achieved through lab testing of two full scale Type II girders, finite element modeling for more than 330 PC girders, parametric analysis, regression analysis, and structural reliability analysis for more than 200 PC bridge cases. As a result of this study, a regression equation and a modification to the current LRFD General Procedure were proposed, and rating factors based on MI live load traffic data were computed and discussed.

AUTOBIOGRAPHICAL STATEMENT

Alaa Ibrahim Chehab has received his B.S. degree in 2010, and his M.S. degree in 2012, both in Civil Engineering from Wayne State University. Alaa was involved with the ASCE student chapter, has participated in regional steel bridge competitions, and has worked as a Graduate Teaching and research Assistant at WSU. He is currently working as an adjunct faculty at the Department of Civil and Environmental Engineering at WSU.